

**REPORT DOCUMENTATION PAGE**

Form Approved  
OMB No. 0704-0188

The public reporting burden for this collection of information is estimated to average 1 hour per response, including the time for reviewing instructions, searching existing data sources, gathering and maintaining the data needed, and completing and reviewing the collection of information. Send comments regarding this burden estimate or any other aspect of this collection of information, including suggestions for reducing the burden, to the Department of Defense, Executive Service Directorate (0704-0188). Respondents should be aware that notwithstanding any other provision of law, no person shall be subject to any penalty for failing to comply with a collection of information if it does not display a currently valid OMB control number.

**PLEASE DO NOT RETURN YOUR FORM TO THE ABOVE ORGANIZATION.**

<b>1. REPORT DATE (DD-MM-YYYY)</b> 10-14-2011		<b>2. REPORT TYPE</b> Final Report		<b>3. DATES COVERED (From - To)</b> 08/01/2008-06/30/2011	
<b>4. TITLE AND SUBTITLE</b> Efficient High-Fidelity, Geometrically Exact, Multiphysics Structural Models				<b>5a. CONTRACT NUMBER</b> FA9550-08-1-0405	
				<b>5b. GRANT NUMBER</b> FA9550-08-1-0405	
				<b>5c. PROGRAM ELEMENT NUMBER</b>	
<b>6. AUTHOR(S)</b> Wenbin Yu				<b>5d. PROJECT NUMBER</b>	
				<b>5e. TASK NUMBER</b>	
				<b>5f. WORK UNIT NUMBER</b>	
<b>7. PERFORMING ORGANIZATION NAME(S) AND ADDRESS(ES)</b> Utah State University				<b>8. PERFORMING ORGANIZATION REPORT NUMBER</b>	
<b>9. SPONSORING/MONITORING AGENCY NAME(S) AND ADDRESS(ES)</b> AFOSR 875 N. Randolph St. Suite 325 Arlington, VA 22203				<b>10. SPONSOR/MONITOR'S ACRONYM(S)</b>	
				<b>11. SPONSOR/MONITOR'S REPORT NUMBER(S)</b> AFRL-OSR-VA-TR-2012-0278	
<b>12. DISTRIBUTION/AVAILABILITY STATEMENT</b> Public release					
<b>13. SUPPLEMENTARY NOTES</b>					
<b>14. ABSTRACT</b> Under the sponsorship of AFOSR, USU carried out a challenging research project to develop efficient high-fidelity, geometrically exact, multiphysics structural models for synergetic exploitations of static or dynamic large nonlinear structural deformations under coupled thermal, electromagnetic, and mechanical loads. The approach uses the concept of decomposition of the rotation tensor to systematically capture all geometrical nonlinearities, and uses the variational asymptotic method to achieve an excellent tradeoff between accuracy and efficiency. In the first year, we have carried out a critical assessment of the proposed approach and developed models for functionally graded plates. In the second year, we developed models for functionally graded smart plates responsive to electromagnetic fields in addition to mechanical fields. We also developed a new classical plate model for heterogeneous plates through simultaneous homogenization and dimensional reduction. In the third year, we initiated the development for a geometrically exact plate analysis, a refined plate model for heterogeneous plates, and used the finite element method to solve the multiphysics plate model and confirmed our analytical solutions.					
<b>15. SUBJECT TERMS</b> Structural Mechanics, Composite Structures, Efficient High-fidelity Modeling, Variational Asymptotic Method					
<b>16. SECURITY CLASSIFICATION OF:</b>			<b>17. LIMITATION OF ABSTRACT</b>	<b>18. NUMBER OF PAGES</b>	<b>19a. NAME OF RESPONSIBLE PERSON</b> Wenbin Yu
a. REPORT	b. ABSTRACT	c. THIS PAGE			<b>19b. TELEPHONE NUMBER (Include area code)</b> 4357978246

Reset

# Efficient High-Fidelity, Geometrically Exact, Multiphysics Structural Models, Final Report: AFOSR Grant FA9550-08-1-0405

Wenbin Yu

Department of Mechanical and Aerospace Engineering  
*Utah State University, Logan, Utah 84332-4130*

## Abstract

Under the sponsorship of AFOSR, USU carried out a challenging research project to develop efficient high-fidelity, geometrically exact, multiphysics structural models for synergetic exploitations of static or dynamic large nonlinear structural deformations under coupled thermal, electromagnetic, and mechanical loads. The approach uses the concept of decomposition of the rotation tensor to systematically capture all geometrical nonlinearities, and uses the variational asymptotic method to achieve an excellent tradeoff between accuracy and efficiency. In the first year, we have carried out a critical assessment of the proposed approach and developed models for functionally graded plates. In the second year, we developed models for functionally graded smart plates responsive to electromagnetic fields in addition to mechanical fields. We also developed a new classical plate model for heterogeneous plates through simultaneous homogenization and dimensional reduction. In the third year, we initiated the development for a geometrically exact plate analysis, a refined plate model for heterogeneous plates, and used the finite element method to solve the multiphysics plate model and confirmed our analytical solutions.

## 1 Introduction

This grant has been active since August 2008. In this final report, all work done will be summarized and papers written under grant sponsorship will be appended to provide the technical details. The goal of this research was to advance our predictive capabilities for aerospace structures undergoing large deformations in coupled multiple fields. The importance of such a research stems from the recent Air Force interest of several novel concepts such as micro air vehicles, sensorcraft, hypersonic vehicles, and adaptive morphing air vehicles to develop future aerospace systems for various missions such as intelligence, surveillance, reconnaissance, and long range strike. These new concepts have three distinctive features:

- These structures are highly flexible and could undergo large nonlinear deformation, which demands the structural models to systematically capture geometrical nonlinearity under quasi-static or dynamic loads.

- These structures will take full advantage of composites and smart materials which are active to thermal and electromagnetic fields in addition to the traditional mechanical field. Behavior of such structures will be multiphysical, for example, a smart wing actuated using piezoelectric materials or shape memory alloys.
- These structures are highly heterogeneous in both material and geometry, such as sandwich structures with woven composites or corrugated cores. The local details will not only affect the global behavior but also the pointwise 3D fields.

These features pose formidable obstacles for theoretical prediction of these structures, which must be overcome before we can reap their full benefits for future air vehicles. Furthermore, to rapidly yet confidently assess the potential and feasibility of these new concepts, the designers must be equipped with a versatile computational design framework to accurately analyze the associated physics while maintaining the speed of conceptual design. This calls for efficient high-fidelity physics-based models to deliver the best possible accuracy within desirable efficiency. Although the ultimate accuracy of multiphysical behavior can be predicted using detailed 3D multiphysics simulation such as those available in ANSYS or COMSOL, they are too time-consuming to be used for effective design space exploration. Timely assessment of future air vehicle concepts presents a pressing need for efficient high-fidelity multiphysics models suitable for geometrically nonlinear quasi-static and dynamic analysis of structures under combined thermal, electromagnetic, and mechanical loads. This project was proposed to meet this need.

There are three main research objectives originally proposed in the proposal:

1. Formulate the exact kinematics to systematically capture all geometrical nonlinearities using the concept of decomposition of the rotation tensor (DRT) [1], a powerful kinematic concept particularly suitable for geometrically nonlinear modeling of beams, plates, and shells.
2. Construct efficient high-fidelity multiphysics plate/shell models using the variational asymptotic method (VAM) [2], the best known method for dimensional reduction, to rigorously split the original three-dimensional (3D) multiphysics problem into a one-dimensional (1D) analysis over the thickness (thickness analysis) and a two-dimensional (2D) analysis over the reference surface (surface analysis) without invoking any a priori assumptions. The thickness analysis will provide a multiphysics constitutive model for the surface analysis.
3. Treat various type of material nonlinearities, such as those inherent in shape memory alloys or electrostrictive materials, by coupling the thickness analysis and the surface analysis into an iterative numerical framework.

We also find out that heterogeneous plates with complex microstructure such as corrugated sandwich panels, woven or braided composites are also extensively used in aerospace systems. Hence, we also started to work on development of models for heterogeneous plates.

## 2 Approach

The proposed approach is founded on two pillars: DRT and VAM. DRT is a powerful kinematic concept for systematically capturing all the geometrical nonlinearities. VAM

is a mathematical method for asymptotical analysis of the governing variational statement. Starting from the 3D multiphysics continuum formulation, we can first use DRT to formulate the kinematics in a geometrically exact manner. Then taking advantage of the small parameters of the structure, say the thickness of a plate/shell, we can use VAM to rigorously reduce the original 3D problem into a lower-dimensional structural analysis. The unique features of the proposed approach are:

- Use VAM to avoid a priori assumptions, which are commonly invoked in other approaches, providing the most mathematical rigor and the best engineering generality.
- Decouple a 3D nonlinear problem into two sets of analyses: a structural modeling analysis of smaller dimensions and a lower-dimensional structural analysis. The synergetic use of DRT and VAM allows the lower-dimensional structural analysis to be formulated exactly as a general continuum and confines all approximations to the structural modeling analysis, whose accuracy is guaranteed to be the best by VAM.
- Maintain the engineering simplicity and legacy by repacking the refined asymptotically correct functionals into common engineering models such as Reissner-Mindlin model for plates/shells [3].

## 3 Work Accomplished-First Year

During the first year, we have made two accomplishments which are summarized as below:

### 3.1 Critical Assessment of the Proposed Approach

We collaborated with Prof. Luciano Demasi of the San Diego State University to assess the performance, including both the accuracy and efficiency, of the proposed approach, against the models constructed based on a priori assumptions. It is found that our proposed approach can achieve an excellent tradeoff between efficiency and accuracy. Our proposed approach is as efficient as first-order shear-deformation theory, yet it is as accurate as higher-order zig-zag and layerwise models. This assessment was documented in [4] and presented on the 50th SDM conference. We have also modified this paper for journal publication and it is now in print with the journal of *Mechanics of Advanced Materials and Structures* [5].

### 3.2 Modeling Plates Made of Functionally Graded Materials

We have also developed efficient high-fidelity models for composite plates made of functionally graded materials. The derivation shows that the theoretical formulation is very similar to the formulation of plates made of layerwise homogeneous materials, although one has to pay attention to the fact that for each layer of functionally graded plates, the material properties are not constant. Several examples have shown that our model can achieve an excellent agreement with the 3D exact solution. We have also shown that it is advantageous to use functionally graded materials to smoothen the discontinuity of in-plane stresses and displacement tangent on the interfaces. This

development was first documented in [6] and presented on the 50th SDM conference. Later, a significantly enhanced version was published in the AIAA Journal [7] in year 2010.

## 4 Work Accomplished-Second Year

During the second year, we have made two accomplishments which are summarized as below:

### 4.1 Modeling Multiphysical Behavior of Smart Plates

We have also developed efficient high-fidelity models for smart plates made of functionally graded materials. By taking advantage of the inherent small parameter characterized by the ratio of the thickness to the in-plane dimension of the plate, we systematically reduced the original multiphysically coupled three-dimensional model to a series of two-dimensional plate models. A companion one-dimensional through-the-thickness analysis provides the necessary constitutive models needed for the plate analysis. For practical uses, we also fit the asymptotically correct second-order electromagnetic enthalpy into a generalized Reissner-Mindlin model. The three-dimensional displacement/strain/stress fields as well as the electric/magnetic potentials and fluxes of the plate are obtained through recovery relations. Without introducing any *a priori* kinematic, electric, or magnetic assumptions in the derivation, the present plate model is rigorously derived to capture geometrical nonlinearity and is valid for large deformations and global rotations. The efficiency and the accuracy of the proposed method has been validated by comparing results with three-dimensional exact solutions for several problems featuring electromagnetic and elastic coupling. This development was first presented on the ASME 2009 Conference on Smart Materials, Adaptive Structures & Intelligent Systems [8] and the 51th SDM conference [9]. We have submitted an updated version for submission for journal publications [10]. We are currently revising this paper.

### 4.2 Modeling Heterogeneous Plates

We have also constructed a classical plate model for heterogeneous plates. We first formulate the original three-dimensional problem in an intrinsic form which is suitable for geometrically nonlinear analysis. Taking advantage of smallness of the plate thickness and heterogeneity, we use the variational asymptotic method to systematically obtain an effective plate model unifying a homogenization process and a dimensional reduction process. This approach is implemented in the computer code VAPAS using the finite element method for the purpose of dealing with real heterogeneous plates in application. A few examples are used to demonstrate the capability of this new model. This development was first documented in [11] and presented on the 16th U.S. National Congress of Theoretical and Applied Mechanics. Later, an updated version was rapidly accepted and quickly published by International Journal of Solids and Structures [12]. Prof. Yu, the PI of this project, also applied this method to model textile composites, a current interest of AFRL/RBSA, through a summer faculty research program.

## 5 Work Accomplished-Third Year

During the third year, we have made several accomplishments which are summarized as below:

### 5.1 Geometrical Exact Plate Analysis

Prof. Hodges of Georgia Tech was initially supported as a consult on this project to work on geometrically exact dynamic analysis of moving plates, which is part of our second objective. On the third year, he hired a graduate student for developing some code for preliminary testing of the theory. Their report entitled “Finite Element Formulation for Dynamics of Moving Plates” is attached in the appendices. Basically, a finite element solution technique, based on a geometrically-exact, fully intrinsic equations is presented and applied to an homogeneous, isotropic cantilevered plate. Right now, the reasons for the deviation of the results compared to the exact solution are being investigated. Future work would involve including the non-linearities and aeroelastic effects and extending the equations to study the dynamics of a flapping wing [13].

### 5.2 Finite Element Formulation for Multiphysics Modeling

The multiphysics plate model developed in the second year was solved analytically with the help of a symbolic manipulator. As shown in our submitted manuscript [10], our model provides accurate predictions for most cases. However, for some cases, the prediction is not that satisfactory. To confirm that we solved the problem correctly, we developed a finite element formulation for the model and find out that the numerical solution reproduces the analytical solution. Thus we are confident to conclude that when some of the multiphysics are truly 3D, they cannot be accurately captured by a plate model. We are preparing a paper to document our findings of the limitation in using a plate theory to model multiphysics behavior.

### 5.3 Refined Modeling Heterogeneous Plates

For heterogeneous plate exhibiting significant transverse shear such as a sandwich structure with a soft core, we find out that the classical plate model we constructed is not sufficient and we extended our work on simultaneous dimensional reduction and homogenization to construct a generalized Reissner-Mindlin model for plates with heterogeneity. The theory has been developed and implemented using the finite element in a numerical code. A paper is in preparation and will be submitted for journal publication shortly. We also applied this approach to model integrated thermal protections which is actively investigated in the AFRL In-House research program entitled “Rapid Insertion and Development of Hypersonic Materials”.

In the third year, we also explored the possibility to treat various type of material nonlinearities, such as those inherent in shape memory alloys or electrostrictive materials. By some preliminary theoretical derivation, we found out that this can be done by coupling the thickness analysis and the surface analysis into an iterative numerical framework, as been demonstrated by our work in micromechanics [14, 15].

## 6 Conclusions

Many progresses have been made in multiphysics modeling of composite structures of Air Force interest. The critical assessment of the proposed approach with many a priori models gives us confidence that we have found an approach that can achieve an excellent tradeoff between efficiency and accuracy for multiphysics modeling of composite/smart plates and shells. We applied this approach to construct models for functionally graded plates and great performance has been achieved for these models. The analytical and numerical modeling of multiphysical behavior of functional graded smart plates provides the right foundation and benchmark for us to develop a general-purpose computational tool for modeling smart structures. Modeling of heterogeneous plates with complex microstructures significantly boosts the application of the ending result of this project. It will not only be applicable to laminated composites, but also textile composites, and sandwich structures and other heterogeneous structures caused by geometry heterogeneity and/or material heterogeneity.

## 7 Personnel Supported

This effort involves two faculty members: Prof. Wenbin Yu (USU) and Prof. Dewey H. Hodges (Georgia Tech), two postdoctoral fellows: Dr. Hui Chen (08/2008-06/2011) and Dr. Chang-Yong Lee (01/2010-07/2011). Several students were also supported during the course of this project including Krishnan Chathadi (Georgia Tech), Nachiket B. Patil (USU).

## 8 Interaction/Transitions

During the course of this project, Prof. Wenbin Yu has a very active interaction with AFRL researchers at WPAFB, particularly the Air Vehicles Directorate and Materials and Manufacturing Directorate. The interaction was initiated with a AFOSR/ASEE summer faculty fellowship in AFRL/RBSD with Dr. Max Blair and Phil Beran to develop efficient high-fidelity structural models for sensorcraft. It was followed by a one-year sabbatical stay with the same branch supported by Chief Scientist Innovative Research Fund. And also in summer 2010, Prof. Yu worked with Dr. Bill Beran (AFRL/RBSA) on efficient high-fidelity modeling of textile composites. In summer 2011, Prof. Yu worked with Dr. Ming Chen (AFRL/RXBC) Dr. Andy Swanson (AFRL/RBSA) on modeling integrated thermal protection systems. All these interactions are focus on applying the theory developed in this project into various applications of Air Force interest.

## Acknowledgements

This research is supported by the Air Force Office of Scientific Research, USAF, under grant FA9550-08-1-0405. The current program manager is Dr. David Stargel (the former program manager was Dr. Victor Giurgiutiu). The views and conclusions contained herein are those of the authors and should not be interpreted as necessarily

representing the official policies or endorsement, either expressed or implied, of AFOSR or the U.S. Government.

## References

- [1] Danielson, D. A. and Hodges, D. H., “Nonlinear Beam Kinematics by Decomposition of the Rotation Tensor,” *Journal of Applied Mechanics*, Vol. 54, No. 2, 1987, pp. 258 – 262.
- [2] Berdichevsky, V. L., “Variational-Asymptotic Method of Constructing a Theory of Shells,” *PMM*, Vol. 43, No. 4, 1979, pp. 664 – 687.
- [3] Yu, W., “Mathematical Construction of a Reissner-Mindlin Plate Theory for Composite Laminates,” *International Journal of Solids and Structures*, Vol. 42, 2005, pp. 6680–6699.
- [4] Demasi, L. and Yu, W., “Assess the Accuracy of the Variational Asymptotic Plate and Shell Analysis (VAPAS) Using the Generalized Unified Formulation (GUF),” *Proceedings of the 50th Structures, Structural Dynamics and Materials Conference*, AIAA, Palm Springs, California, May 4 – 7 2009.
- [5] Demasi, L. and Yu, W., “Assess the Accuracy of the Variational Asymptotic Plate and Shell Analysis (VAPAS) Using the Generalized Unified Formulation (GUF),” *Mechanics of Advanced Materials and Structures*, 2011, in press.
- [6] Chen, H. and Yu, W., “Asymptotical Construction of an Efficient High-Fidelity Model for Functionally Graded Plates,” *Proceedings of the 50th Structures, Structural Dynamics and Materials Conference*, AIAA, Palm Springs, California, May 4 – 7 2009.
- [7] Chen, H. and Yu, W., “Asymptotical Construction of an Efficient High-Fidelity Model for Multilayer Functionally Graded Plates,” *AIAA Journal*, Vol. 48, No. 8, 2010, pp. 1171 – 1183.
- [8] Chen, H. and Yu, W., “Efficient High-Fidelity, Geometrically Exact Plate Model for Electromagnetoelastic Laminates,” *Proceedings of the 2009 ASME Conference on Smart Materials, Adaptive Structures and Intelligent Systems*, ASME, Oxnard, California, Sep. 21 – 23 2009.
- [9] Chen, H. and Yu, W., “Asymptotical Construction of a Geometrically Exact Non-linear Plate Model for Functionally Graded Magneto-Electro-Elastic Laminates,” *Proceedings of the 51th Structures, Structural Dynamics and Materials Conference*, AIAA, Orlando, Florida, Apr. 12– 15 2010.
- [10] Chen, H. and Yu, W., “A Multiphysics Model for Magneto-Electro-Elastic Laminates,” *European Journal of Mechanics A/Solids*, 2011, submitted.
- [11] Lee, C. and Yu, W., “Variational Asymptotic Homogenization and Dimensional Reduction of Heterogeneous Composite Plates,” *Proceedings of the 16th U.S. National Congress of Theoretical and Applied Mechanics*, State College, Pennsylvania, June 25-30, 2010 2010.
- [12] Lee, C. and Yu, W., “Homogenization and Dimensional Reduction of Composite Plates with In-Plane Heterogeneity,” *International Journal of Solids and Structures*, Vol. 48, No. 10, 2011, pp. 1474–1484.

- [13] Chathadi, K. and Hodges, D. H., “Finite Element Formulation for Dynamics of Moving Plates,” Tech. rep., Georgia Institute of Technology, 2011.
- [14] Tang, T. and Yu, W., “Effective Nonlinear Behavior of Electrostrictive Multiphase Composites: A Micromechanical Study,” *International Journal of Engineering Science*, Vol. 48, No. 12, 2010, pp. 1769–1777.
- [15] Tang, T. and Yu, W., “Asymptotical Approach to Initial Yielding Surface and Elastoplasticity of Heterogeneous Materials,” *Mechanics of Advanced Materials and Structures*, Vol. 18, 2011, pp. 244–254.

# Asymptotical Construction of an Efficient High-Fidelity Model for Multilayer Functionally Graded Plates

Hui Chen\*

and

Wenbin Yu†

*Utah State University, Logan, Utah 84322-4130*

An efficient high-fidelity plate model is developed for heterogeneous multilayer laminates made of functionally graded material. Taking advantage of the smallness of the ratio of the thickness to the characteristic wavelength of the deformation of the reference surface, we apply the variational-asymptotic method to rigorously decouple the three-dimensional, anisotropic elasticity problem into a one-dimensional through-the-thickness analysis and a two-dimensional plate analysis. The through-the-thickness analysis provides constitutive relations for the plate analysis as well as the recovery information for the three-dimensional fields, reducing the complex three-dimensional elasticity model to a simple two-dimensional plate model with an excellent tradeoff between efficiency and accuracy. **The present model is valid for large displacements and global rotations and can capture all the geometric nonlinearity of a plate when the strains are small.** A few examples are used to validate this model.

## Nomenclature

$\mathbf{b}_i$	base vectors of the coordinate system before deformation
$\mathbf{B}_i$	base vectors of the coordinate system after deformation
$\mathcal{C}_{ij}$	direction cosine matrix describing the rotation from triad $\mathbf{b}_i$ to triad $\mathbf{B}_i$
$c_{\parallel}$	through-the-thickness average of in-plane warping functions

---

\*Research Engineer, Department of Mechanical and Aerospace Engineering. Member, AIAA and ASME.

†Associate Professor, Department of Mechanical and Aerospace Engineering. Senior Lifetime Member, AIAA; Member, ASME and AHS.

$\varepsilon_{\alpha\beta}, K_{\alpha\beta}, \varepsilon, \kappa$	two-dimensional generalized plate strains
$\mathcal{E}$	a column matrix containing two-dimensional generalized strains $\mathcal{E} = [\varepsilon^T \kappa^T]^T$
$e_{ijk}$	the permutation symbol
$\eta$	a small parameter used to denote the order of strains
$f_i, m_\alpha$	generalized forces and moments, respectively
$F_{ij}$	mixed-basis deformation gradient tensor
$\Gamma_{ij}$	three-dimensional strain tensor
$\mathbf{G}_i$	covariant basis vectors of the deformed configuration
$h$	thickness of the plate
$K^*$	effective bulk modulus estimated by Mori-Tanaka scheme
$\lambda_{\parallel}, \lambda_3, \Lambda_3$	Lagrange multipliers for enforcing in-plane and out-of-plane warping constraints
$\mathcal{K}$	three-dimensional kinetic energy
$\mathcal{K}_{2D}$	two-dimensional kinetic energy
$L_\alpha$	integration constants for determining the relationship between $\mathcal{E}$ and $c_{\parallel}$
$l$	characteristic wavelength of the plate deformation
$\mu$	characteristic magnitude of the elastic constants
$\mu^*$	effective shear modulus estimated by Mori-Tanaka scheme
$\mathcal{M}$	plate moment resultants
$\mathcal{N}$	plate force resultants
$\phi_i$	applied body force
$Q_i$	tractions applied on lateral surfaces
$\mathbf{r}$	position vector of a material point on the undeformed reference surface
$\hat{\mathbf{r}}$	position vector of a material point in the undeformed three-dimensional configuration
$\mathbf{R}$	position vector of a material point on the deformed reference surface
$\mathcal{R}$	generalized strain measures of the Reissner-Mindlin model

$\hat{\mathbf{R}}$	position vector of a material point in the deformed three-dimensional configuration
$\rho$	mass density
$\sigma_{ij}$	three-dimensional stress tensor
$\gamma$	transverse shear strains for the Reissner-Mindlin model
$\tau_i, \beta_i$	tractions applied on top and bottom surfaces
$t_1, t_2$	arbitrary fixed times
$U_i$	three-dimensional displacements
$u_i$	two-dimensional displacements
$\mathcal{U}$	three-dimensional strain energy
$\mathcal{U}_{A0}$	zeroth-order strain energy
$\hat{V}_i$	absolute velocity of a material point in three-dimensional configuration
$V_i$	absolute velocity of a point on the deformed reference surface
$\overline{\delta\mathcal{W}}$	three-dimensional virtual work
$\overline{\delta\mathcal{W}}_{2D}$	two-dimensional virtual work
$\omega$	inertial angular velocity of triad $\mathbf{B}_i$
$\Omega$	the reference surface
$\partial\Omega$	boundary of the reference surface
$w_i$	warping functions
$x_i$	Cartesian coordinates

## Introduction

Functional graded materials (FGM) have received significant attention in recent years. The various functional effects of FGM have been used to address a large variety of application fields, such as graded thermoelectrics and dielectrics, piezoelectrically graded materials for ultrasonic transducers, and tungsten-copper composites for high current connectors and diverter plates, to name but a few.<sup>1,2</sup> One extensively investigated FGM, typically used for constructing panels in aerospace systems, is made of a mixture of

ceramics and metals and characterized by a continuously changing of its mechanical properties using a smooth change in volume fraction of the constituent materials from one surface of the material to the other. The surface with high ceramic constituents can provide superior thermal-resistance for high temperature environments while the surface with high metal constituents offers strong mechanical performance. [This kind of material arrangement](#) reduces the risk of catastrophic fracture under extreme environments. Recently, the concept of FGM is actively explored in the multilayered design of thermal coatings as well as sandwich panels to overcome the mismatch of the thermomechanical properties between the coating and the substrate or between the surface panels and the core.<sup>3-6</sup>

To use FGM effectively, we need to develop efficient yet accurate models for structures made of such materials such as FGM plates and shells. These structures are characterized by one of their dimensions (the thickness) being much smaller than the other two. Although all structures made of FGM can be described using three-dimensional (3D) continuum mechanics, exact solutions exist only for a few specific problems with very idealized material types, geometry, and boundary conditions.<sup>4,5,7-9</sup> For more realistic cases, one often has to rely on 3D numerical simulation tools such as ANSYS and ABAQUS to find approximate solutions. However, this approach is computation intensive and they are usually used in the detailed analysis due to their prohibitive computational cost. In view of the fact that the thickness is small, analysis of such structures can be simplified using two-dimensional (2D) models. Although many 2D models have been developed to analyze FGM plates and shells treating different topics, most of them rely on some *a priori* kinematic assumptions. Examples may be found in the application of classical lamination theory (CLT) in thermal residual stress and free vibration analyses,<sup>3,10</sup> the use of the first-order shear-deformation theory (FSDT) in active control analysis,<sup>11</sup> and the implementation of the third-order shear-deformation theory (TSDT) in bending and buckling analyses.<sup>12</sup> CLT ignores transverse shear effects and provides reasonable results only for very thin plates. Moreover, in CLT, both plane strain and plane stress are assumed [which we know will not be true at the same time for materials having nonzero Poisson's ratios](#). A number of shear deformation theories have been developed to overcome some drawbacks of CLT, with the simplest of which being FSDT (equivalent to Reissner-Mindlin theory for plates made of isotropic homogeneous materials), where a constant distribution of shear strain through the thickness is assumed and a shear correction factor is required to account for the deviation of the real shear strain from the assumed constant one. The dependence of the shear correction

factor on the geometry and material of the plate makes it difficult to guarantee the accuracy of FSDT. By expanding the displacement field of the plate using higher-order polynomials, higher-order shear deformation plate theories are developed, which can account for both transverse normal and shear deformations without relying on shear correction factors. However, as indicated by Bian et. al [13] and Das et. al. [6] for laminated plates and shells, models based on higher-order theories cannot capture the discontinuous slope of in-plane and transverse displacement components in the thickness direction. By extending a generalized refined theory (referred as Soldatos plate theory<sup>14,15</sup>) which incorporates shape functions to guarantee continuity of transverse shear stresses at interfaces, these authors provide analytical solutions for simply- and multiply-spanned functionally graded plates under cylindrical bending.<sup>13</sup> Higher-order shear deformation theories have also been implemented using the finite element method (FEM) to analyze functionally graded plates. As recent examples, Gilhooley et. al.<sup>16</sup> carried out a numerical investigation of a two-constituent metal/ceramics thick plate by combining a meshless local Petrov-Galerkin method and a higher-order shear deformation plate theory; while Zhen and Chen<sup>17</sup> combined the higher-order shear deformation theory with refined three-node triangular element for analyzing multilayer FGMs. Despite of the popularity of the aforementioned methods in analyzing many functionally graded plates and laminated plates, these approaches have two major disadvantages: (1) the *a priori* assumptions which are naturally extended from the analysis of isotropic homogeneous structures cannot be easily justified for heterogeneous and anisotropic structures, such as FGMs; (2) it is difficult for an analyst to determine the accuracy of the result and which assumption should be chosen for efficient yet accurate analysis for a particular plate.

Recently, the variational-asymptotic method (VAM)<sup>18</sup> was used to develop a series of rigorous Reissner-Mindlin plate models for heterogeneous and anisotropic composite plates and smart plates.<sup>19-25</sup> These models have excellent compromise between the efficiency and accuracy. In this paper, we expand this method to construct an [efficient and high-fidelity model which is able to capture the geometric nonlinearity for multilayer functionally graded plates](#), where material properties of each layer can be continuous functions of the thickness coordinate  $x_3$ .

In present work, the 3D displacement field of an arbitrary material point of the plate is expressed [using the deformation of the reference surface along with unknown warping functions, without invoking any \*a priori\* kinematic assumptions](#). The original 3D elasticity problem is cast in an intrinsic form so that the

theory can accommodate arbitrary large deformations and global rotations with the restriction that the strain field is small. Taking advantage of the small parameter  $h/l$ , we apply VAM to systematically reduce the original 3D model to a series of 2D models, so that the original, nonlinear 3D problem is rigorously split into a linear one-dimensional (1D) through-the-thickness analysis and a 2D nonlinear plate analysis. For practical uses, we also transfer the asymptotically correct energy into the Reissner-Mindlin model with the transverse shear stiffness calculated through a least square scheme. To validate this model, we analyzed a couple of examples and excellent agreement with the 3D exact elasticity solution has been achieved using the present model.

### Three-dimensional Formulation

The elastodynamic behavior of a solid is governed by the [extended](#) Hamilton principle:

$$\int_{t_1}^{t_2} [\delta(\mathcal{K} - \mathcal{U}) + \overline{\delta\mathcal{W}}] dt = 0, \quad (1)$$

where the overbar is used to indicate that the virtual work  $\overline{\delta\mathcal{W}}$  [dose not necessarily represent variation of a function, or in other words, there may not exist such a functional  \$\mathcal{W}\$  that its variation is equal to the virtual work done by the applied loads.](#)

A point in the plate can be described by its Cartesian coordinates  $x_i$ , see Figure 1, where  $x_\alpha$  are two orthogonal lines in the reference surface and  $x_3$  is the normal coordinate originating from the middle of the thickness. [Throughout the analysis, Greek indices assume values 1 and 2 while Latin indices assume 1, 2, and 3; repeated indices are summed over their range except where explicitly indicated.](#) Letting  $\mathbf{b}_i$  denote the unit vector along  $x_i$  for the undeformed plate, we can then describe the position of any material point in the undeformed configuration by its position vector  $\hat{\mathbf{r}}$  from a fixed point  $O$ , such that

$$\hat{\mathbf{r}}(x_1, x_2, x_3, t) = \mathbf{r}(x_1, x_2, t) + x_3 \mathbf{b}_3, \quad (2)$$

where  $\mathbf{r}$  is the position vector from a fixed point  $O$  to the point located by  $x_\alpha$  on the reference surface [at a specific time  \$t\$ .](#) When the reference surface of the undeformed plate coincides with its middle surface, we

have

$$\langle \hat{\mathbf{r}}(x_1, x_2, x_3, t) \rangle = h\mathbf{r}(x_1, x_2, t), \quad (3)$$

where the angle brackets denote the definite integral through the thickness of the plate.

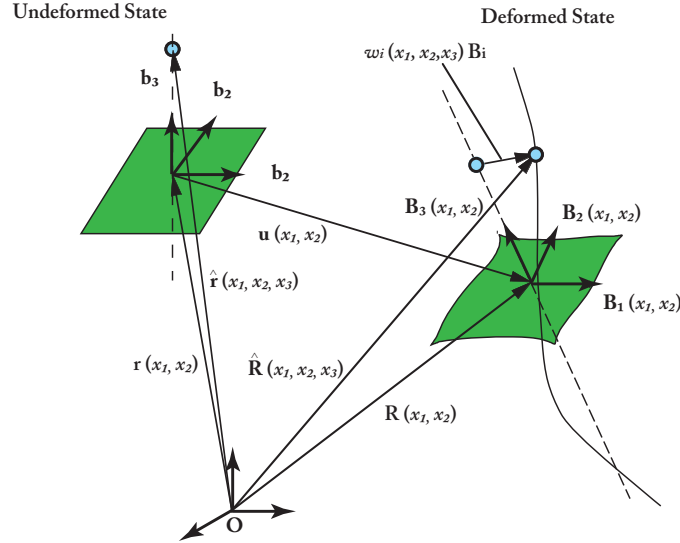


Figure 1. Schematic of plate deformation

When the plate deforms, the particle that had position vector  $\hat{\mathbf{r}}$  in the undeformed state now has position vector  $\hat{\mathbf{R}}$  in the deformed plate, which can be uniquely determined by the deformation of the 3D body. We introduce another orthonormal triad  $\mathbf{B}_i$  for the deformed configuration so that:

$$\mathbf{B}_i = \mathcal{C}_{ij}\mathbf{b}_j, \quad \mathcal{C}_{ij} = \mathbf{B}_i \cdot \mathbf{b}_j, \quad (4)$$

subjecting to the requirement that  $\mathbf{B}_i$  is coincident with  $\mathbf{b}_i$  when the structure is undeformed. The direction cosines matrix  $\mathcal{C}(x_1, x_2)$  represents the possible arbitrary rotation between  $\mathbf{B}_i$  and  $\mathbf{b}_i$ .

After deformation, the position vector  $\hat{\mathbf{R}}$  in the deformed state can be expressed as

$$\hat{\mathbf{R}}(x_1, x_2, x_3, t) = \mathbf{R}(x_1, x_2, t) + x_3\mathbf{B}_3(x_1, x_2, t) + w_i(x_1, x_2, x_3, t)\mathbf{B}_i(x_1, x_2, t), \quad (5)$$

where  $\mathbf{R}$  is the position vector of the reference surface for the deformed plate and  $w_i(x_1, x_2, x_3, t)$  are the warping functions introduced to accommodate all possible deformations. Equation (5) can be considered

as a change of variables for  $\hat{\mathbf{R}}$  in terms of  $\mathbf{R}$ ,  $\mathbf{B}_i$ , and  $w_i$ . Proper definitions of  $\mathbf{R}$  and  $\mathbf{B}_i$  are needed to introduce six constraints to ensure a one-to-one mapping of this change of variables. We can introduce the following three constraints for the warping functions:

$$\langle w_i(x_1, x_2, x_3, t) \rangle = \left\{ \begin{array}{c} c_{\parallel} \\ 0 \end{array} \right\}, \text{ with } c_{\parallel} = \left\{ \begin{array}{c} c_1 \\ c_2 \end{array} \right\}, \quad (6)$$

where  $c_1$  and  $c_2$  are functions of the in-plane coordinates  $x_\alpha$  and time  $t$ , introduced for providing free variables for the construction of an optimal Reissner-Mindlin model which will be described later. Two other constraints can be specified by taking  $\mathbf{B}_3$  as the normal to the reference surface of the deformed plate. It should be noted that this choice has nothing to do with the well-known Kirchhoff hypothesis. In the Kirchhoff assumption, no local deformation of the transverse normal is allowed. However, in present derivation we allow all possible deformation using the warping functions. Because  $\mathbf{B}_\alpha$  can freely rotate around  $\mathbf{B}_3$ , we can introduce the last constraint as

$$\mathbf{B}_1 \cdot \mathbf{R}_{,2} = \mathbf{B}_2 \cdot \mathbf{R}_{,1}, \quad (7)$$

where  $(\cdot)_{,\alpha} = \partial(\cdot)/\partial x_\alpha$ .

Based on the concept of decomposition of rotation tensor,<sup>26,27</sup> the Jauman-Biot-Cauchy strain components for small local rotation are given by

$$\Gamma_{ij} = \frac{1}{2}(F_{ij} + F_{ji}) - \delta_{ij}, \quad (8)$$

with

$$F_{ij} = \mathbf{B}_i \cdot \mathbf{G}_k \mathbf{b}_k \cdot \mathbf{b}_j. \quad (9)$$

Here  $\mathbf{G}_k = \partial \hat{\mathbf{R}} / \partial x_k$  is the covariant basis vector of the deformed configuration. The details for obtaining this concise expression for the Jauman-Biot-Cauchy strain tensor can be found in Ref. [26]. To express the

3D strain field in terms of 2D plate strains, we can define the 2D generalized strains following Ref. [28] as:

$$\mathbf{R}_{,\alpha} = \mathbf{B}_\alpha + \varepsilon_{\alpha\beta}\mathbf{B}_\beta \quad (10)$$

$$\mathbf{B}_{i,\alpha} = (-K_{\alpha\beta}\mathbf{B}_\beta \times \mathbf{B}_3 + K_{\alpha 3}\mathbf{B}_3) \times \mathbf{B}_i \quad (11)$$

Using this definition, one can show that Eq. (7) implies  $\varepsilon_{12} = \varepsilon_{21}$ . The expressions for 2D generalized strains in terms of plate displacements and rotations can be found in Ref. [28].

For geometrically nonlinear analysis, we can assume that both the 3D and 2D strains are small when compared to the unity and from which we can also conclude that warpings are of the order of the strain or smaller. Using Eq. (8) along with Eqs. (9), (5), (2), (10) and (11), we can derive the following expression for the 3D strain field:

$$\begin{aligned} \Gamma_e &= \epsilon + x_3\kappa + I_1 w_{\parallel,1} + I_2 w_{\parallel,2} \\ 2\Gamma_s &= w'_{\parallel} + e_1 w_{3,1} + e_2 w_{3,2} \\ \Gamma_t &= w'_3 \end{aligned} \quad (12)$$

where  $()' = \frac{\partial()}{\partial x_3}$ ,  $()_{\parallel} = [()_1 \quad ()_2]^T$ , and

$$\begin{aligned} \Gamma_e &= [\Gamma_{11}, \quad 2\Gamma_{12} \quad \Gamma_{22}]^T, \quad 2\Gamma_s = [2\Gamma_{13} \quad 2\Gamma_{23}]^T, \quad \Gamma_t = \Gamma_{33}, \\ \epsilon &= [\varepsilon_{11} \quad 2\varepsilon_{12} \quad \varepsilon_{22}]^T, \quad \kappa = [K_{11} \quad K_{12} + K_{21} \quad K_{22}]^T, \end{aligned} \quad (13)$$

$$I_1 = \begin{bmatrix} 1 & 0 \\ 0 & 1 \\ 0 & 0 \end{bmatrix}, \quad I_2 = \begin{bmatrix} 0 & 0 \\ 1 & 0 \\ 0 & 1 \end{bmatrix}, \quad e_1 = \begin{Bmatrix} 1 \\ 0 \end{Bmatrix}, \quad e_2 = \begin{Bmatrix} 0 \\ 1 \end{Bmatrix}. \quad (14)$$

Note in deriving Eq. (12), we have neglected the products between warping and strain because these terms are negligible based on our small strain assumption. With the knowledge of the 3D strain field, we can

express the strain energy as

$$\mathcal{U} = \int_{\Omega} \frac{1}{2} \left\langle \begin{Bmatrix} \Gamma_e \\ 2\Gamma_s \\ \Gamma_t \end{Bmatrix}^T \begin{bmatrix} C_e & C_{es} & C_{et} \\ C_{es}^T & C_s & C_{st} \\ C_{et}^T & C_{st}^T & C_t \end{bmatrix}^T \begin{Bmatrix} \Gamma_e \\ 2\Gamma_s \\ \Gamma_t \end{Bmatrix} \right\rangle d\Omega \equiv \int_{\Omega} \mathcal{U}_{\mathcal{A}} d\Omega \quad (15)$$

where  $C_e, C_{es}, C_{et}, C_s, C_{st}, C_t$  are the corresponding partition matrices of the 3D  $6 \times 6$  material matrix which are functions of  $x_i$  for functionally graded materials. Here for simplicity, we restrict ourselves to FGM plates having material properties as functions of  $x_3$  only.

To calculate the kinetic energy, the absolute velocity of a generic point in the structure is obtained by taking a time derivative of Eq. (5) as

$$\hat{V} = V + \tilde{\omega}(\xi + w) + \dot{w}, \quad (16)$$

where  $\dot{(\ )}$  is the partial derivative with respect to time and the notation  $\tilde{(\ )}$  forms an antisymmetric matrix from a vector according to  $\tilde{(\ )}_{ij} = -e_{ijk}(\ )_k$ . In Eq. (16), the symbols  $\hat{V}, V, \omega, w$  denote column matrices containing the components of corresponding vectors in  $\mathbf{B}_i$  bases, and  $\xi = [0 \ 0 \ x_3]^T$ . The kinetic energy of the plate structure can be obtained by

$$\mathcal{K} = \frac{1}{2} \int_{\mathcal{V}} \rho \hat{V}^T \hat{V} d\mathcal{V} = \mathcal{K}_{2D} + \mathcal{K}^* \quad (17)$$

with

$$\mathcal{K}_{2D} = \frac{1}{2} \int_{\Omega} (\bar{\mu} V^T V + 2\omega^T \tilde{\mu} \xi V + \omega^T j \omega) d\Omega \quad (18)$$

$$\mathcal{K}^* = \frac{1}{2} \int_{\mathcal{V}} \rho [(\tilde{\omega} w + \dot{w})^T (\tilde{\omega} w + \dot{w}) + 2(V + \tilde{\omega} \xi)^T (\tilde{\omega} w + \dot{w})] d\mathcal{V}, \quad (19)$$

where  $\bar{\mu}, \tilde{\mu},$  and  $j$  are inertial constants commonly used in plate dynamics, which can be trivially obtained

by taking integral operations through the thickness:

$$\bar{\boldsymbol{\mu}} = \langle \boldsymbol{\rho} \rangle, \quad \bar{\boldsymbol{\mu}} \bar{\boldsymbol{\xi}} = [0 \ 0 \ \langle x_3 \boldsymbol{\rho} \rangle]^T, \quad \mathbf{j} = \begin{bmatrix} \langle x_3^2 \boldsymbol{\rho} \rangle & 0 & 0 \\ 0 & \langle x_3^2 \boldsymbol{\rho} \rangle & 0 \\ 0 & 0 & 0 \end{bmatrix}. \quad (20)$$

The virtual work of the structure can be calculated as

$$\bar{\delta \mathcal{W}} = \int_{\Omega} \left( \langle \boldsymbol{\phi} \cdot \delta \hat{\mathbf{R}} \rangle + \boldsymbol{\tau} \cdot \delta \hat{\mathbf{R}}^+ + \boldsymbol{\beta} \cdot \delta \hat{\mathbf{R}}^- \right) d\Omega + \int_{\partial\Omega} \langle \mathbf{Q} \cdot \delta \hat{\mathbf{R}} \rangle ds \quad (21)$$

where  $(\ )^{\pm} = (\ )|_{x_3=\pm h/2}$ ;  $\boldsymbol{\phi} = \phi_i \mathbf{B}_i$  is the applied body force;  $\boldsymbol{\tau} = \tau_i \mathbf{B}_i, \boldsymbol{\beta} = \beta_i \mathbf{B}_i$  are tractions applied on the top and bottom surfaces, respectively;  $\mathbf{Q} = Q_i \mathbf{B}_i$  are the applied tractions along the lateral surfaces.  $\delta \hat{\mathbf{R}}$  is the Lagrangian variation of the displacement field which can be expressed as

$$\delta \hat{\mathbf{R}} = \bar{\delta q}_i \mathbf{B}_i + x_3 \delta \mathbf{B}_3 + \delta w_i \mathbf{B}_i + w_j \delta \mathbf{B}_j, \quad (22)$$

in which the virtual displacement and rotation are defined by

$$\bar{\delta q}_i = \delta \mathbf{R} \cdot \mathbf{B}_i, \quad \delta \mathbf{B}_i = (-\bar{\delta \psi}_2 \mathbf{B}_1 + \bar{\delta \psi}_1 \mathbf{B}_2 + \bar{\delta \psi}_3 \mathbf{B}_3) \times \mathbf{B}_i, \quad (23)$$

where  $\bar{\delta q}_i$  and  $\bar{\delta \psi}_i$  contain the components of the virtual displacement and rotation in the  $\mathbf{B}_i$  system, respectively. Since the warping functions are small, one may safely ignore products of the warping functions and the virtual rotations in  $\delta \hat{\mathbf{R}}$  and obtain the virtual work due to applied loads as

$$\bar{\delta \mathcal{W}} = \bar{\delta \mathcal{W}}_{2D} + \bar{\delta \mathcal{W}}^*, \quad (24)$$

where

$$\overline{\delta\mathcal{W}}_{2D} = \int_{\Omega} (f_i \overline{\delta q}_i + m_{\alpha} \overline{\delta \psi}_{\alpha}) d\Omega + \int_{\partial\Omega} (\langle Q_i \rangle \overline{\delta q}_i + \langle x_3 Q_{\alpha} \rangle \overline{\delta \psi}_{\alpha}) ds, \quad (25)$$

$$\overline{\delta\mathcal{W}}^* = \int_{\Omega} (\langle \phi_i \delta w_i \rangle + \tau_i \delta w_i^+ + \beta_i \delta w_i^-) d\Omega + \int_{\partial\Omega} \langle Q_i \delta w_i \rangle ds, \quad (26)$$

with the generalized forces  $f_i$  and moments  $m_{\alpha}$  defined as

$$f_i = \langle \phi_i \rangle + \tau_i + \beta_i, \quad m_{\alpha} = \langle x_3 \phi_{\alpha} \rangle + \frac{h}{2} (\tau_{\alpha} - \beta_{\alpha}). \quad (27)$$

The second integration in Eq. (26) accounts for the virtual work done through warping functions along the lateral boundaries of the plate. This term is necessary for the edge-zone problem, which is an important subject in its own right and beyond the scope of the present paper. For simplicity, we will drop this term hereafter. With the knowledge of Eqs. (17), (15), and (24), the [extended](#) Hamilton's principle in Eq. (1) becomes

$$\int_{t_1}^{t_2} \left[ \delta(\mathcal{K}_{2D} + \mathcal{K}^* - \mathcal{U}) + \overline{\delta\mathcal{W}}_{2D} + \overline{\delta\mathcal{W}}^* \right] dt = 0 \quad (28)$$

So far, we have presented a 3D formulation for the plate structure in terms of 2D displacements (represented by  $\mathbf{R} - \mathbf{r}$ ), 2D rotations (represented by  $\mathbf{b}_i$  and  $\mathbf{B}_i$ ), and 3D warping functions ( $w_i$ ). If we attempt to solve this problem directly, we will meet the same difficulty as solving any full 3D problem with the additional difficulty coming from the anisotropy and heterogeneity of functional graded materials. The main complexity comes from the unknown 3D warping functions  $w_i$ . A common practice in the literature is to use *a priori* assumptions. However, for plates made with general anisotropic and heterogeneous materials such as functionally graded materials, imposition of such assumptions may introduce significant errors. Fortunately, VAM provides a useful technique to obtain  $w_i$  through an asymptotical analysis of the variational statement in Eq. (28) in terms of small parameters inherent in the problem which will be described in the next section.

## Dimensional Reduction

The dimensional reduction from the original 3D formulation to a 2D plate model can only be done approximately. One way to accomplish this is to take advantage of the small parameters in the formulation

to construct a 2D formulation so that the loss of accuracy can be minimized.

In order to apply VAM, we first need to assess the order of quantities in terms of small parameters. As mentioned previously, the ratio of the plate thickness to the characteristic wavelength of the deformation of the reference surface is small, *i.e.*  $h/l \ll 1$ . The strain is also small if we only interest in a geometrically nonlinear but physically linear 2D theory, *i.e.*,  $\epsilon_{\alpha\beta} \sim h\kappa_{\alpha\beta} \sim \eta \ll 1$ . From the plate equations of equilibrium, we can estimate the orders of the following quantities corresponding to the order of strains:

$$\begin{aligned} h\phi_3 \sim \tau_3 \sim \beta_3 \sim \mu(h/l)^2\eta, \quad h\phi_\alpha \sim \tau_\alpha \sim \beta_\alpha \sim \mu(h/l)\eta, \\ Q_\alpha \sim \mu\eta, \quad Q_3 \sim \mu(h/l)\eta, \end{aligned} \quad (29)$$

We can choose the characteristic scale of change of the displacements and warping functions [with respect to time](#) in such a way that  $\mathcal{K}^*$  is much smaller than other terms in Eq. (28). In other words, here we are only interested the accurate description of low frequency dynamic problems.

### Zeroth-order approximation

To clearly illustrate the application of VAM for FGM plates, we first construct a classical FGM plate model. By applying VAM, the zeroth-order approximation of the variational statement in Eq. (28) can be obtained as

$$\int_{t_1}^{t_2} \left[ \delta(\mathcal{K}_{2D} - \int_{\Omega} \mathcal{U}_{A0} d\Omega) + \overline{\delta\mathcal{W}}_{2D} \right] dt = 0 \quad (30)$$

where  $\mathcal{U}_{A0}$  can be obtained from Eq. (15) by dropping the derivatives with respect to  $x_\alpha$  in Equation (12), resulting in

$$\begin{aligned} 2\mathcal{U}_{A0} = & 2 \langle (\epsilon + x_3\kappa)^T (C_{es}w_{\parallel}' + C_{et}w_3') + w_{\parallel}'^T C_{st}w_3' \rangle \\ & + \langle (\epsilon + x_3\kappa)^T C_e(\epsilon + x_3\kappa) + w_{\parallel}'^T C_s w_{\parallel}' + w_3' C_t w_3' \rangle + o\left(\left(\frac{h}{l}\right)^0 \eta^2\right). \end{aligned} \quad (31)$$

It is obvious that the warping functions  $w_i$  can be obtained by solving the following variational statement

$$\delta\mathcal{U}_{A0} = 0, \quad (32)$$

along with the constraint equation expressed in Eq. (6). The corresponding Euler-Lagrange equations are:

$$\begin{aligned} \left[ (\epsilon + x_3 \kappa)^T C_{et}^{(k)} + w_{\parallel}'^{(k)T} C_{st}^{(k)} + w_3'^{(k)} C_t^{(k)} \right]' &= \lambda_3, \\ \left[ (\epsilon + x_3 \kappa)^T C_{es}^{(k)} + w_{\parallel}'^{(k)T} C_s^{(k)} + w_3'^{(k)} C_{st}^{(k)T} \right]' &= \lambda_{\parallel}, \quad k = 1, 2, 3, \dots, N \end{aligned} \quad (33)$$

where  $\lambda_{\parallel}$  and  $\lambda_3$  are Lagrange multipliers corresponding to the in-plane and out-of-plane constraint equations expressed in Eq. (6);  $(\bullet)^{(k)}$  denotes functions  $(\bullet)$  for the  $k$ th layer. The boundary conditions as well as the interlaminar continuous conditions are:

$$\begin{aligned} \left[ (\epsilon + x_3 \kappa)^T C_{et} + w_{\parallel}'^T C_{st} + w_3' C_t \right]^+ &= 0, \\ \left[ (\epsilon + x_3 \kappa)^T C_{es} + w_{\parallel}'^T C_s + w_3' C_{st}^T \right]^- &= 0, \end{aligned} \quad (34)$$

and

$$\begin{aligned} [w_3] &= 0, \quad \left[ (\epsilon + x_3 \kappa)^T C_{et} + w_{\parallel}'^T C_{st} + w_3' C_t \right] = 0, \quad \text{on } \Omega_i, \\ [w_{\parallel}] &= 0, \quad \left[ (\epsilon + x_3 \kappa)^T C_{es} + w_{\parallel}'^T C_s + w_3' C_{st}^T \right] = 0, \quad \text{on } \Omega_i, \end{aligned} \quad (35)$$

respectively. Here,  $\Omega_i$  denotes the interfaces between the  $i$ th layer and  $i + 1$ th layer;  $i = 1 \dots N - 1$  with  $N$  denoting the total number of layers; the bracket  $[\cdot]$  denotes the jump of the enclosed argument on the interface. From these conditions, we can solve  $w_i'$  from Eq. (33):

$$\begin{aligned} w_{\parallel}'^{(k)T} &= -(\epsilon + x_3 \kappa)^T \hat{C}_{es}^{(k)} C_s^{(k)-1}, \\ w_3'^{(k)} &= -(\epsilon + x_3 \kappa)^T \hat{C}_{et}^{(k)} / \hat{C}_t^{(k)}, \end{aligned} \quad (36)$$

with the hatted quantities being expressed as:

$$\begin{aligned} \hat{C}_{es}^{(k)} &= C_{es}^{(k)} - \hat{C}_{et}^{(k)} C_{st}^{(k)T} / C_t^{(k)}, \quad \hat{C}_{et}^{(k)} = C_{et}^{(k)} - C_{es}^{(k)} C_s^{(k)-1} C_{st}^{(k)}, \\ \hat{C}_t^{(k)} &= C_t^{(k)} - C_{st}^{(k)T} C_s^{(k)-1} C_{st}^{(k)}. \end{aligned} \quad (37)$$

Substituting Eq. (36) into Eq. (31), we obtain the zeroth-order strain energy as

$$2\mathcal{U}_{A0} = \begin{Bmatrix} \epsilon \\ \kappa \end{Bmatrix}^T \begin{bmatrix} \hat{A} & \hat{B} \\ \hat{B}^T & \hat{D} \end{bmatrix} \begin{Bmatrix} \epsilon \\ \kappa \end{Bmatrix} + o\left(\left(\frac{h}{l}\right)^0 \eta^2\right), \quad (38)$$

with

$$\hat{A} = \langle \hat{C}_e \rangle, \quad \hat{B} = \langle x_3 \hat{C}_e \rangle, \quad \hat{D} = \langle x_3^2 \hat{C}_e \rangle, \quad \hat{C}_e = C_e - C_{es} C_s^{-1} \hat{C}_{es}^T - C_{et} \hat{C}_{et}^T / \hat{C}_t. \quad (39)$$

With  $\mathcal{U}_{A0}$  expressed in Eq. (38), the original 3D problem in Eq. (1) has been rigorously reduced to a 2D formulation in Eq. (30) which approximates the original problem asymptotically correct to the order of  $\left(\frac{h}{l}\right)^0$ . If we define the force resultants  $\mathcal{N}$  and moment resultants  $\mathcal{M}$  by

$$\mathcal{N} = \frac{\partial \mathcal{U}_{A0}}{\partial \epsilon}, \quad \mathcal{M} = \frac{\partial \mathcal{U}_{A0}}{\partial \kappa} \quad (40)$$

we obtain a 2D constitutive model for the classical plate analysis of FGM plates, expressed as

$$\begin{Bmatrix} \mathcal{N} \\ \mathcal{M} \end{Bmatrix} = \begin{bmatrix} \hat{A} & \hat{B} \\ \hat{B}^T & \hat{D} \end{bmatrix} \begin{Bmatrix} \epsilon \\ \kappa \end{Bmatrix} \quad (41)$$

It is clear that although the plate is made of functionally gradient materials, the 2D plate model of the zeroth-order remains the same. Despite the similarity with CLT, the present model is asymptotically correct and has the following features in contrast with CLT:

1. The normal line of undeformed plate does not remain straight and normal to the deformed plate; rather, it deforms in both the normal and in-plane directions in response to plate deformation ( $\epsilon$  and  $\kappa$ ).
2. This model can handle general functionally gradient materials with full anisotropy.
3. It can be easily observed that neither the normal strain nor the transverse shear strains vanish. The transverse normal and shear stresses can be shown to vanish, which are not assumed *a priori* but can

be concluded from the derivation.

It is worth to emphasize that no *a priori* assumptions, such as setting the transverse normal strain equal to zero, were used in the derivation.

For the zeroth-order approximation, the 3D strain field can be recovered using Eqs. (12) by neglecting those terms of order higher than  $(\frac{h}{l})^0$ :

$$\Gamma_e^0 = \epsilon + x_3 \kappa, \quad 2\Gamma_s^0 = w_{\parallel}', \quad \Gamma_t^0 = w_3'. \quad (42)$$

Up to this point, the **zeroth-order solution**  $w_i$  in Eq. (36) as well as the 2D strain energy in Eq. (38) are valid for FGM plates with fully populated  $6 \times 6$  material matrix  $C$ . As most real materials have at least a monoclinic symmetry about their own mid-plane, hereafter, monoclinic material matrix characterized by 13 independent material properties, implying  $C_{es} = 0$  and  $C_{st} = 0$ , will be used for the rest of derivation. This leads to much simpler expressions for the zeroth-order approximation of warping function:

$$w_{\parallel}^{(k)} = 0, \quad w_3^{(k)} = C_{\perp}^{(k)} \mathcal{E}, \quad k = 1, 2, 3, \dots, N \quad (43)$$

where,

$$C_{\perp}^{(k)} = \begin{bmatrix} -C_{et}^{(k)T} / C_t^{(k)} & -x_3 C_{et}^{(k)T} / C_t^{(k)} \end{bmatrix}, \quad \mathcal{E} = [\epsilon \ \kappa]^T, \quad \langle C_{\perp} \rangle = 0. \quad (44)$$

Note that inter-lamina continuity of  $C_{\perp}^{(k)}$  must be maintained due to the continuity of warping functions to produce a continuous displacement field. It should also be pointed out that we have constrained in-plane warpings to vanish ( $\langle w_{\parallel} \rangle = 0$ ) as the free constants in Eq. (6) will be absorbed in the first-order approximation.

### First-order approximation

To obtain the first-order approximation, we simply perturb the zeroth-order warping functions as

$$w_{\parallel} = v_{\parallel} + o\left(\frac{h}{l}\eta\right), \quad w_3 = v_3 + C_{\perp} \mathcal{E} + o\left(\frac{h}{l}\eta\right). \quad (45)$$

Substituting Eq. (45) back into Eq. (12), and using Eqs. (28), (15) (24) and (26), one can obtain the leading terms for the first-order approximation of the variational statement in Eq. (28) as

$$\delta\Pi_1^* = \left\langle v_{\parallel}'^T C_s \delta v_{\parallel}' + v_3' C_t \delta v_3' + (\epsilon + x_3 \kappa)^T C_{\parallel} I_{\alpha} \delta v_{\parallel, \alpha} + (e_{\alpha} C_{\perp} \mathcal{E}_{, \alpha})^T C_s \delta v_{\parallel}' - \phi_{\parallel}^T \delta v_{\parallel} \right\rangle - \tau_{\parallel}^T \delta v_{\parallel}^+ - \beta_{\parallel}^T \delta v_{\parallel}^- + o\left(\left(\frac{h}{l}\right)^2 \eta^2\right), \quad (46)$$

where  $C_{\parallel} = C_e - C_{et} C_{et}^T / C_t$ .

It can be easily observed that  $v_3$  is decoupled from  $v_{\parallel}$ . Considering the warping constraint in Eq. (6),  $v_3$  only has a trivial solution. The stationary conditions of the functional given in Eq. (46) are

$$\begin{aligned} (C_s^{(k)} v_{\parallel}' + C_s^{(k)} e_{\alpha} C_{\perp}^{(k)} \mathcal{E}_{, \alpha})' &= D_{\alpha}'^{(k)} \mathcal{E}_{, \alpha} + g'^{(k)} + \lambda_{\parallel} \\ (C_s v_{\parallel}' + C_s e_{\alpha} C_{\perp} \mathcal{E}_{, \alpha})^+ &= \tau_{\parallel} \\ (C_s v_{\parallel}' + C_s e_{\alpha} C_{\perp} \mathcal{E}_{, \alpha})^- &= -\beta_{\parallel} \end{aligned} \quad (47)$$

where  $D_{\alpha}'^{(k)} = -I_{\alpha}^T [C_{\parallel}^{(k)} x_3 C_{\parallel}^{(k)}]$ ,  $g'^{(k)} = -\phi_{\parallel}^{(k)}$ , and  $\lambda_{\parallel}$  are Lagrange multipliers to enforce the constraints in Eq. (6). The continuity conditions on the interfaces can be derived as:

$$[v_{\parallel}] = 0, \quad [C_s(v_{\parallel}' + e_{\alpha} C_{\perp} \mathcal{E}_{, \alpha})] = 0 \quad \text{on} \quad \Omega_i, \quad (48)$$

The inter-lamina continuity on  $D_{\alpha}'^{(k)}$  and  $g'^{(k)}$  are maintained by the second condition in Eq. (48). It should be mentioned that since the goal is to obtain an interior solution for the plate without considering edge effects, integration by parts with respect to the in-plane coordinates is used hereafter and throughout the rest of the paper, whenever it is convenient for the derivation.

Integrating the first equation in Eq. (47), one obtains

$$C_s'^{(k)} v_{\parallel} + C_s^{(k)} e_{\alpha} C_{\perp}^{(k)} \mathcal{E}_{, \alpha} = D_{\alpha}^{(k)} \mathcal{E}_{, \alpha} + g^{(k)} + \lambda_{\parallel} x_3 + \text{const}_{\parallel}^{(k)} \quad (49)$$

and the interface continuity condition in the second equation of Eq. (48) becomes

$$\text{const}_{\parallel}^{(k+1)} - \text{const}_{\parallel}^{(k)} = - \int_{z_k}^{z_{k+1}} I_{\alpha}^T [C_{\parallel}^{(k)} x_3 C_{\parallel}^{(k)}] dx_3, \quad (50)$$

where  $const_{\parallel}^{(k)}$  is the integration constant for  $k$ th layer,  $z_k$  is the  $x_3$  coordinate of the bottom of the  $k$ th layer, and  $D_{\alpha}^{(k)}$ ,  $g_{\alpha}^{(k)}$  are defined as:

$$D_{\alpha}^{(k)}(x_3) = \int_{z_k}^{x_3} D_{\alpha}'^{(k)} dz = - \int_{z_k}^{x_3} I_{\alpha}^T [C_{\parallel}^{(k)} z C_{\parallel}^{(k)}] dz, \quad (51)$$

$$g_{\alpha}^{(k)}(x_3) = \int_{z_k}^{x_3} g_{\alpha}'^{(k)} dz = - \int_{z_k}^{x_3} \phi_{\parallel}^{(k)} dz. \quad (52)$$

Solving Eqs. (49), (50), the two boundary equations in Eq. (47) as well as (6), one obtains the following Lagrange multipliers and warping functions:

$$\lambda_{\parallel} = \frac{1}{h} (\tau_{\parallel} + \beta_{\parallel} - \langle D'_{\alpha} \rangle \mathcal{E}_{\alpha} - \langle g' \rangle), \quad (53)$$

$$v_{\parallel}^{(k)} = (\overline{D}_{\alpha}^{(k)} + L_{\alpha}) \mathcal{E}_{,\alpha} + \overline{g}^{(k)}, \quad (54)$$

with

$$\overline{D}_{\alpha}^{(k)'} = C_s^{(k)-1} D_{\alpha}^{(k)*}, \quad \langle \overline{D}_{\alpha} \rangle = 0, \quad \overline{g}^{(k)'} = C_s^{(k)-1} g^{(k)*}, \quad \langle \overline{g} \rangle = 0, \quad L_{\alpha} \mathcal{E}_{,\alpha} = c_{\parallel}/h, \quad (55)$$

where  $D_{\alpha}^{(k)*}$  and  $g^{(k)*}$  can be obtained from Eqs. (49), (50), (53) as well as the boundary conditions in Eq. (47).

Now we are ready to obtain an expression for the total energy that is asymptotically correct through the order of  $\mu(h/l)^2 \eta^2$ , viz.,

$$2\Pi_1 = \mathcal{E}^T A \mathcal{E} + \mathcal{E}_{,1}^T B \mathcal{E}_{,1} + 2\mathcal{E}_{,1}^T C \mathcal{E}_{,2} + \mathcal{E}_{,2}^T D \mathcal{E}_{,2} - 2\mathcal{E}^T F + o\left(\left(\frac{h}{l}\right)^2 \eta^2\right), \quad (56)$$

where

$$\begin{aligned}
A &= \begin{bmatrix} \langle C_{\parallel} \rangle & \langle x_3 C_{\parallel} \rangle \\ \langle x_3 C_{\parallel} \rangle & \langle x_3^2 C_{\parallel} \rangle \end{bmatrix}, \\
B &= \langle C_{s_{11}} C_{\perp}^T C_{\perp} - D_1^{*T} C_s^{-1} D_1^* \rangle + L_1^T \langle D'_1 \rangle + \langle D'_1 \rangle^T L_1, \\
C &= \langle C_{s_{12}} C_{\perp}^T C_{\perp} - D_1^{*T} C_s^{-1} D_2^* \rangle + L_1^T \langle D'_2 \rangle + \langle D'_1 \rangle L_2, \\
D &= \langle C_{s_{22}} C_{\perp}^T C_{\perp} - D_2^{*T} C_s^{-1} D_2^* \rangle + L_2^T \langle D'_2 \rangle + \langle D'_2 \rangle L_2, \\
F &= C_{\perp}^{+T} \tau_3 + C_{\perp}^{-T} \beta_3 + \langle C_{\perp}^T \phi_3 \rangle - \langle D_{\alpha}^{*T} C_s^{-1} g_{,\alpha}^* \rangle - L_{\alpha}^T (\tau_{\parallel} + \beta_{\parallel} + \langle \phi_{\parallel} \rangle)_{,\alpha}. \tag{57}
\end{aligned}$$

Eq. (56) is an energy functional expressed in terms of 2D variables which can asymptotically approximate the original 3D energy. It is noted that quadratic terms of the applied loads are neglected as they will not affect the 2D model.

### Transforming into the Reissner-Mindlin Model

Although Eq. (56) is asymptotically correct through the second order and straightforward use of this strain energy is possible, it involves more complex boundary conditions than necessary since it contains derivatives of the generalized strain measures. To obtain an energy functional that is of practical use, one can transform Eq. (56) into the Reissner-Mindlin model. In the Reissner-Mindlin model, there are two additional degrees of freedom, which are the transverse shear strains incorporated into the rotation of transverse normal. We introduce another triad  $\mathbf{B}_i^*$  for the deformed plate, so that the definition of 2D strains becomes

$$\begin{aligned}
\mathbf{R}_{,\alpha} &= \mathbf{B}_{\alpha}^* + \varepsilon_{\alpha\beta}^* \mathbf{B}_{\beta}^* + 2\gamma_{\alpha 3} \mathbf{B}_3^* \\
\mathbf{B}_{i,\alpha}^* &= (-K_{\alpha\beta}^* \mathbf{B}_{\beta}^* \times \mathbf{B}_3^* + K_{\alpha 3}^* \mathbf{B}_3^*) \times \mathbf{B}_i^* \tag{58}
\end{aligned}$$

where the transverse shear strains are  $\gamma = [2\gamma_{13} \ 2\gamma_{23}]^T$ . Since  $\mathbf{B}_i^*$  is uniquely determined by  $\mathbf{B}_i$  and  $\gamma$ , one can derive the following kinematic identity between the strains measures  $\mathcal{R}$  of Reissner-Mindlin plate and  $\mathcal{E}$ <sup>29</sup>

$$\mathcal{E} = \mathcal{R} - \mathcal{D}_{\alpha} \gamma_{,\alpha} \tag{59}$$

where

$$\begin{aligned}
\mathcal{D}_1 &= \begin{bmatrix} 0 & 0 & 0 & 1 & 0 & 0 \\ 0 & 0 & 0 & 0 & 1 & 0 \end{bmatrix}^T \\
\mathcal{D}_2 &= \begin{bmatrix} 0 & 0 & 0 & 0 & 1 & 0 \\ 0 & 0 & 0 & 0 & 0 & 1 \end{bmatrix}^T \\
\mathcal{R} &= [\varepsilon_{11}^* \quad 2\varepsilon_{12}^* \quad \varepsilon_{22}^* \quad K_{11}^* \quad K_{12}^* + K_{21}^* \quad K_{22}^*]^T
\end{aligned} \tag{60}$$

Now one can express the strain energy asymptotically correct to the second order in terms of strains of the Reissner-Mindlin model as

$$\begin{aligned}
2\Pi_1 &= \mathcal{R}^T A \mathcal{R} - 2\mathcal{R}^T A \mathcal{D}_1 \gamma_{,1} - 2\mathcal{R}^T A \mathcal{D}_2 \gamma_{,2} \\
&\quad + \mathcal{R}_{,1}^T B \mathcal{R}_{,1} + 2\mathcal{R}_{,1}^T C \mathcal{R}_{,2} + \mathcal{R}_{,2}^T D \mathcal{R}_{,2} - 2\mathcal{R}^T F
\end{aligned} \tag{61}$$

The generalized Reissner-Mindlin model is of the form

$$2\Pi_{\mathcal{R}} = \mathcal{R}^T A \mathcal{R} + \gamma^T G \gamma - 2\mathcal{R}^T F_{\mathcal{R}} - 2\gamma^T F_{\gamma} \tag{62}$$

To find an equivalent Reissner-Mindlin model Eq. (62) for Eq. (61), one has to eliminate all partial derivatives of the strain. Here equilibrium equations are used to achieve this purpose. From the two equilibrium equations [relating with the equilibrium of bending moments](#)<sup>30</sup>, one can obtain the following formula

$$G\gamma - F_{\gamma} = \mathcal{D}_{\alpha}^T A \mathcal{R}_{,\alpha} + \begin{Bmatrix} m_1 \\ m_2 \end{Bmatrix}, \tag{63}$$

where  $F_{\mathcal{R},\alpha}$  is dropped because they are high order terms. Substituting Eq. (63) into Eq. (61), one can show that  $F_{\mathcal{R}} = F$  and  $F_{\gamma} = 0$ . Finally one can rewrite Eq. (61) as

$$2\Pi_1 = \mathcal{R}^T A \mathcal{R} + \gamma^T G \gamma - 2\mathcal{R}^T F + U^* \tag{64}$$

where

$$U^* = \mathcal{R}_{,1}^T \bar{B} \mathcal{R}_{,1} + 2\mathcal{R}_{,1}^T \bar{C} \mathcal{R}_{,2} + \mathcal{R}_{,2}^T \bar{D} \mathcal{R}_{,2} \quad (65)$$

and

$$\begin{aligned} \bar{B} &= B + AD_1 G^{-1} \mathcal{D}_1^T A \\ \bar{C} &= C + AD_1 G^{-1} \mathcal{D}_2^T A \\ \bar{D} &= D + AD_2 G^{-1} \mathcal{D}_2^T A \end{aligned} \quad (66)$$

If we can drive  $U^*$  to be zero for any  $\mathcal{R}$ , then we have found an asymptotically correct Reissner-Mindlin plate model. For general anisotropic plates, this term will not be zero; but we can minimize the error to obtain a Reissner-Mindlin model being as asymptotically correct as possible. The accuracy of the Reissner-Mindlin model depends on how close to zero one can drive this term. In other words, one needs to seek an optimal set of the 27 unknowns (3 unknowns for  $G$  and 24 unknowns for  $L_\alpha$ ) so that the value of the quadratic form in Eq. (65) is as close to zero as possible for arbitrary generalized strain measures. We let the distinct 78 terms in the symmetric  $12 \times 12$  coefficient matrix equal to zeros to formulate 78 equations. It is a linear system with 27 unknowns. Then we use a least square technique to solve the overdetermined system for the constants. Mathematically, the overdetermined system (78 equations with 27 unknowns, indicated by  $MX = b$ ) may be singular for some material properties. For example, the rank of  $M^T M$  is only 26 for single-layer isotropic and orthotropic plates. In this situation, singular value decomposing technique can be applied to solve this least square problem. Moreover, for an accurate estimation of the transverse shear matrix, a nondimensional scheme is used to guarantee that each of the 78 equations having the same physical unit.

From the asymptotic point of view, by driving  $U^*$  to zero, we obtain the “best” Reissner-Mindlin model which will be used for 2D plate analysis:

$$2\Pi_{\mathcal{R}} = \mathcal{R}^T A \mathcal{R} + \gamma^T G \gamma + 2\mathcal{R}^T F, \quad (67)$$

where  $A$ ,  $G$ ,  $F$  capture the necessary material and geometric information obtained from the dimensional reduction process. It is worthy to emphasize that although the 2D constitutive model is constructed in a

way dramatically different from traditional Reissner-Mindlin models, the plate analysis remains the same, with no changes in the governing equations and boundary conditions except that the strain measures are now defined using Eqs. (58).

## Recovery 3D Fields

Thus far, we have obtained a generalized Reissner-Mindlin model [based on the asymptotically correct second-order energy](#) for FGM plates. This model can be used for various analyses of FGM plates, spanning from static, dynamic, buckling, to aeroelastic analyses. In many applications, however, the capability of predicting accurate 2D displacement fields of FGM plates is not sufficient. Ultimately, the fidelity of a reduced-order model should be evaluated based on how well it can predict the 3D displacement/strain/stress fields for the original 3D problem. Therefore, it is necessary to provide recovery relations to [express the 3D displacement, strain, and stress fields in terms of 2D quantities and  \$x\_3\$](#) .

Using Eqs. (2), (4) and (5), one can recover the 3D displacement field through the first order as

$$U_i = u_i + x_3(\mathcal{C}_{3i} - \delta_{3i}) + \mathcal{C}_{ji}w_j, \quad (68)$$

where  $w_\alpha = v_\alpha$ ,  $w_3 = C_\perp \mathcal{E}$ . From Eq. (12), the 3D strain field can be recovered up to the first order as

$$\Gamma_e = \epsilon + x_3\kappa, \quad 2\Gamma_s = v'_\parallel + e_\alpha C_\perp \mathcal{E}_{,\alpha}, \quad \Gamma_t = C'_\perp \mathcal{E}. \quad (69)$$

Consequently, 3D stresses  $\sigma_{ij}$  can be obtained by applying the 3D constitutive relations. Since we have obtained an optimal estimation of the shear stiffness matrix  $G$ , the recovered 3D results up to the first order are better than CLT and FSDT. However, the transverse normal stress ( $\sigma_{33}$ ) is a second-order quantity and cannot be estimated within the first-order approximation. Despite that it is usually much smaller than other stress components,  $\sigma_{33}$  is critical for predicting some structural failure mechanisms such as delamination. In order to obtain a reasonable recovery for the transverse normal stress, VAM procedure is applied once more

to find the warping functions of second-order accuracy. Similarly, we perturb the warping functions as

$$w_{\parallel} = v_{\parallel} + y_{\parallel} + o\left(\left(\frac{h}{l}\right)^2\eta\right), \quad w_3 = C_{\perp}\mathcal{E} + y_3 + o\left(\left(\frac{h}{l}\right)^2\eta\right), \quad (70)$$

where  $y_{\parallel}$  and  $y_3$  are the second-order warping functions. It can be shown that the in-plane components  $y_{\parallel}$  vanish and the equations governing  $y_3$  are

$$\begin{aligned} (C_t^{(k)}y_3'^{(k)} + C_{et}^{(k)T}I_{\alpha}v_{\parallel,\alpha}^{(k)})' + e_{\beta}^T C_s^{(k)}(v_{\parallel}^{(k)} + e_{\alpha}C_{\perp}^{(k)}\mathcal{E}_{,\alpha})_{,\beta} + \phi_3 &= \Lambda_3, \\ (C_t y_3' + C_{et}^T I_{\alpha} v_{\parallel,\alpha})^+ &= \tau_3, \\ (C_t y_3' + C_{et}^T I_{\alpha} v_{\parallel,\alpha})^- &= -\beta_3, \\ [y_3] = 0 \quad [C_t y_3' + C_{et}^T I_{\alpha} v_{\parallel,\alpha}] &= 0, \quad \text{on } \Omega_i \end{aligned} \quad (71)$$

where  $\Lambda_3$  is the Lagrange multiplier to enforce the constraint  $\langle y_3 \rangle = 0$ . The Euler-Lagrange equation and the inter-surface continuity equation in (71) can be expressed as:

$$C_t^{(k)}y_3'^{(k)} + C_{et}^{(k)T}I_{\alpha}v_{\parallel,\alpha}^{(k)} = E_{\alpha\beta}^{(k)}\mathcal{E}_{\alpha\beta} + S^{(k)} + \Lambda_3 x_3 + const_{y_3}^{(k)}, \quad k = 1, 2, 3, \dots, N. \quad (72)$$

$$const_{y_3}^{(k+1)} - const_{y_3}^{(k)} = E_{\alpha\beta}^{(k)}\mathcal{E}_{\alpha\beta}(z_{k+1}) + S^{(k)}(z_{k+1}), \quad (73)$$

with

$$E_{\alpha\beta}^{(k)}(x_3) = - \int_{z_k}^{x_3} (e_{\alpha}^T D_{\beta}^{*(k)} + C_{s_{\alpha\beta}}^{(k)} C_{\perp}^{(k)}) dz, \quad (74)$$

$$S^{(k)}(x_3) = - \int_{z_k}^{x_3} (e_{\alpha}^T g_{,\alpha}^{*(k)} + \phi_3^{(k)}) dz. \quad (75)$$

The Lagrange multiplier  $\Lambda_3$  and the solution of  $y_3$  are given by

$$\Lambda_3 = \frac{1}{h}(\tau_3 + \beta_3 - \langle E'_{\alpha\beta} \rangle \mathcal{E}_{,\alpha\beta} - \langle S' \rangle), \quad (76)$$

$$y_3^{(k)} = \overline{E}_{,\alpha\beta}^{(k)} \mathcal{E}_{,\alpha\beta} + \overline{S}^{(k)}, \quad (77)$$

with

$$\overline{E}_{\alpha\beta}^{(k)} = C_t^{(k)-1} E_{\alpha\beta}^{(k)*}, \quad \langle \overline{E}_{\alpha\beta}^{(k)} \rangle = 0, \quad \overline{S}^{(k)} = C_t^{(k)-1} S^{(k)*}, \quad \langle \overline{S} \rangle = 0,$$

where  $E_{\alpha\beta}^{(k)*}$  and  $S^{(k)*}$  can be obtained from Eqs. (72), (73), (76) as well as the [interlaminar continuous](#) conditions in the last equation of Eq. (71).

Although  $y_3$  can help us obtain an energy expression asymptotically corrected up to the order of  $(h/l)^4 \eta^2$ , such an energy expression is too complex for practical use. We will still use the Reissner-Mindlin model to carry out the 2D plate analysis and use  $y_3$  for the second-order prediction of the 3D displacement/strain/stress field. As will be shown latter, this approach achieves excellent predictions even though only the Reissner-Mindlin plate model is used for the 2D plate analysis.

Finally, we can recover the 3D displacement field up to the second order as

$$U_i = u_i + x_3(C_{3i} - \delta_{3i}) + C_{ji}w_j + \delta_{3i}C_{3i}y_3 \quad (78)$$

and the strains up to the second order as

$$\Gamma_e = \epsilon + x_3\kappa + I_\alpha v_{\parallel,\alpha}, \quad 2\Gamma_s = v'_{\parallel} + e_\alpha C_\perp \mathcal{E}_{,\alpha}, \quad \Gamma_t = C'_\perp \mathcal{E} + y'_3. \quad (79)$$

Finally, we can recover the 3D stress field up to the second order as

$$\begin{aligned} [\sigma_{11} \ \sigma_{12} \ \sigma_{22}]^T &= C_{\parallel}(\epsilon + x_3\kappa) + C_{et}y'_3 + C_e I_\alpha v_{\parallel,\alpha}, \\ [\sigma_{13} \ \sigma_{23}]^T &= C_s(v'_{\parallel} + e_\alpha C_\perp \mathcal{E}_{,\alpha}), \\ \sigma_{33} &= C_{et}^T I_\alpha v_{\parallel,\alpha} + C_t y'_3. \end{aligned} \quad (80)$$

## Validation Examples

We have derived a general formulation to treat multilayer plates made of functionally graded materials with properties as functions of  $x_3$ . In the following, we will use several examples to demonstrate the

performance of the present theory.

The first example is a single-layer, simply supported, square, functionally graded plate. The width of the plate is denoted as  $a$ . The top surface of the FGM plate is ceramic rich and the bottom surface is metal rich. The region between the two surfaces is made of the mixture of ceramic-metal materials with continually varying of the volume fractions of the ceramic and metal. The volume fraction of the ceramics  $V_c$  is assumed to vary according to a power law as

$$V_c = V_c^- + (V_c^+ - V_c^-) \left( \frac{1}{2} + \frac{x_3}{h} \right)^p, \quad p \geq 0,$$

where  $V_c^+$  and  $V_c^-$  are the volume fractions of the ceramic on the top and the bottom surfaces, respectively;  $p$  is the volume fraction index, and  $h$  the thickness of the plate. The effective elastic moduli of the functionally graded metal-ceramic material are estimated by the Mori-Tanaka scheme as

$$\left\{ \begin{array}{l} \frac{K^* - K_m}{K_c - K_m} = \frac{V_c}{1 + (1 - V_c) \frac{K_c - K_m}{K_m + \frac{4}{3}\mu_m}}, \\ \frac{\mu^* - \mu_m}{\mu_c - \mu_m} = \frac{V_c}{1 + (1 - V_c) \frac{\mu_c - \mu_m}{\mu_m + s_1}} \end{array} \right., \quad (81)$$

where  $s_1 = \mu_m(9K_m + 8\mu_m)/(6(K_m + 2\mu_m))$ ,  $K_m$  and  $\mu_m$  represent the bulk and shear modulus of the metal and  $K_c$  and  $\mu_c$  represent the bulk and shear modulus of the ceramic material<sup>9,16</sup> The Young's modulus,  $E(x_3)$ , and Poisson's ratio,  $\nu(x_3)$ , are related to effective bulk and shear moduli by

$$K^*(x_3) = \frac{E(x_3)}{3[1 - 2\nu(x_3)]}, \quad \mu^*(x_3) = \frac{E(x_3)}{2[1 + \nu(x_3)]}. \quad (82)$$

For the purpose of illustration, we choose the properties of the constituent materials as  $E_m = 70$  GPa  $\nu_m = 0.3$  for Al and  $E_c = 427$  GPa,  $\nu_c = 0.17$  for SiC. Figure 2 plots through-the-thickness variation of effective Young's modulus and Poisson's ratio for various material index  $p$ .

The FGM plate is subjected to a sinusoidally distributed pressure on the top surface, described by:

$$\tau_3(x_1, x_2) = q_0 \sin(\pi x_1/a) \sin(\pi x_2/a).$$

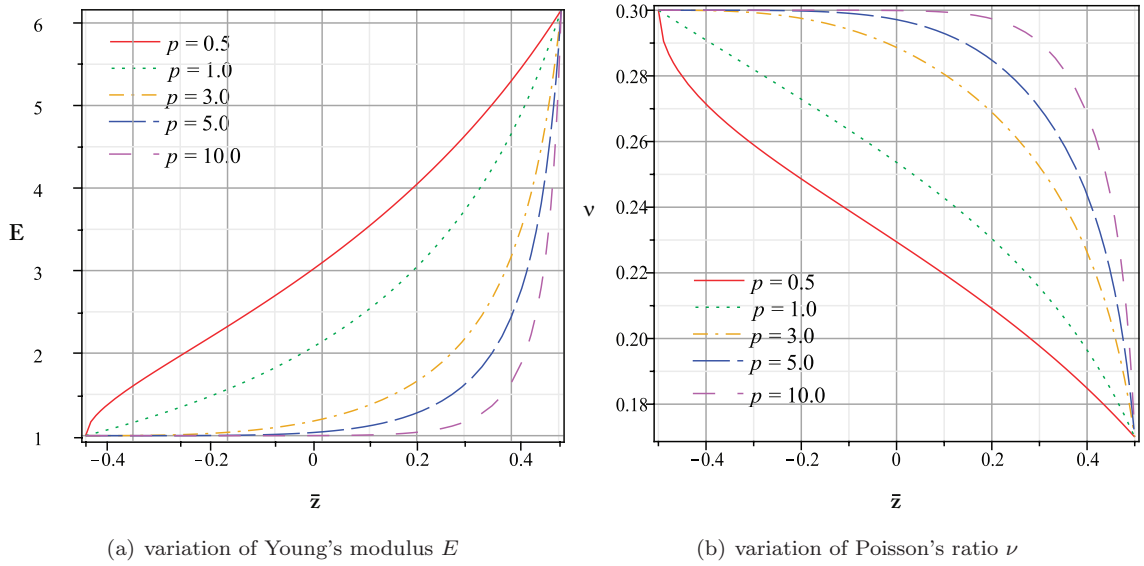


**Figure 2.** Through-the-thickness variation of effective Young's modulus  $E$  and Poisson's ratio  $\nu$  estimated by Mori-Tanaka scheme for different values of  $p$ .

There is no body force and the bottom surface is traction free. To facilitate our comparison, the physical quantities are nondimensionalized by the following relations:

$$\bar{U}_\alpha = \frac{100Eh^2U_\alpha}{q_0a^3}, \quad \bar{U}_3 = \frac{100Eh^3U_3}{q_0a^4},$$

$$\bar{\sigma}_{\alpha\beta} = \frac{10h^2\sigma_{\alpha\beta}}{q_0a^2}, \quad \bar{\sigma}_{\alpha 3} = \frac{10h\sigma_{\alpha 3}}{q_0a}, \quad \bar{\sigma}_{33} = \frac{\sigma_{33}}{q_0}.$$

Table 1 provides a detailed comparison of displacement and stress components with exact 3D solution<sup>9</sup> at various critical locations of the plate. Results in the top part of Table 1 ( $V_c^- = 0, V_c^+ = 0.5, p = 2$ ) indicate the effect of  $a/h$  on displacement and stress components. It shows an excellent match between the present plate theory and the 3D exact solution. The maximum percentage error occurs for  $\sigma_{13}$  (1.5%) when  $a/h = 5$ , with the percentage errors for other components being less than 0.21%. As expected, the relative errors for displacement and stress components decrease as  $a/h$  increases. For example, when  $a/h = 10$ , the maximum percentage error still occurs for  $\sigma_{13}$  with a value of 0.38% and the relative errors for other components being less than 0.04%. The effect of volume fraction of the ceramic constituent for a thick functionally graded plate ( $V_c^- = 0, p = 2, a/h = 5$ ) is provided in the bottom half of Table 1. Again, all stress and displacement results match very well with the exact solutions. The maximum percentage error takes the value of  $\sigma_{13} = 1.9\%$ ,  $\sigma_{13} = 1.4\%$ , and  $\sigma_{33} = 1.67\%$  for  $V_c^+ = 0.2, V_c^+ = 0.6$ , and  $V_c^+ = 1.0$ , respectively, while the relative errors

**Table 1. Comparison of displacements and stresses at specific locations with 3D elasticity solutions for Al/SiC functionally graded plates**

Variable	$V_c^- = 0, V_c^+ = 0.5, p = 2$					
	$a/h = 5$		$a/h = 10$		$a/h = 40$	
	exact	present	exact	present	exact	present
$\bar{U}_1(0, a/2, h/2)$	-2.9129	-2.9124	-2.8997	-2.8987	-2.8984	-2.8983
$\bar{U}_3(0, a/2, 0)$	2.5748	2.5716	2.2266	2.2256	2.1163	2.1163
$\bar{U}_3(0, a/2, h/2)$	2.5559	2.5524	2.2148	2.2139	2.1155	2.1154
$\bar{\sigma}_{11}(a/2, a/2, h/2)$	2.7562	2.7558	2.6424	2.6415	2.6093	2.6092
$\bar{\sigma}_{12}(0, 0, h/2)$	-1.5600	-1.5597	-1.5529	-1.5524	-1.5522	-1.5521
$\bar{\sigma}_{13}(0, a/2, 0)$	2.3100	2.2749	2.3239	2.3150	2.3281	2.3276
$\bar{\sigma}_{33}(a/2, a/2, h/4)$	0.8100	0.8117	0.8123	0.8127	0.8129	0.8129

Variable	$V_c^- = 0, p = 2, a/h = 5$					
	$V_c^+ = 0.2$		$V_c^+ = 0.6$		$V_c^+ = 1.0$	
	exact	present	exact	present	exact	present
$\bar{U}_1(0, a/2, h/2)$	-3.6982	-3.6966	-2.6708	-2.6697	-1.7421	-1.7359
$\bar{U}_3(0, a/2, 0)$	3.0254	3.0215	2.4326	2.4293	1.8699	1.8634
$\bar{U}_3(0, a/2, h/2)$	2.9852	2.9808	2.4196	2.4160	1.8767	1.8702
$\bar{\sigma}_{11}(a/2, a/2, h/2)$	2.3285	2.3273	2.9359	2.9347	4.1042	4.0899
$\bar{\sigma}_{12}(0, 0, h/2)$	-1.2163	-1.2158	-1.7106	-1.7099	-2.8534	-2.8433
$\bar{\sigma}_{13}(0, a/2, 0)$	2.3516	2.3065	2.2918	2.2604	2.1805	2.1683
$\bar{\sigma}_{33}(a/2, a/2, h/4)$	0.8300	0.8284	0.8024	0.8047	0.7623	0.7675

for other components are less than 0.14%, 0.29%, and 0.55% corresponding to these three cases. From this example, one can also observe that the present model, although based on asymptotic analysis of the small parameter  $h/l$  ( $l = a$  for this example), can provide fairly good prediction for not so small parameters such as for this case  $h/l = 0.2$ . However, because no further data of the 3D solutions is available from the reference, the accuracy of present plate model for thicker plates cannot be estimated. Nevertheless, the present 2D plate model can be shown to achieve a high accuracy even for fairly large ( $\frac{h}{l}$ ). For example, in Ref. [25], we analyzed the cylindrical bending of an isotropic homogeneous plate. For an extremely thick plate with  $\frac{h}{l} = 0.5$ , the maximum relative error among all the 3D fields less than 6%, in comparison to the 3D exact solution.

Further comparisons are also made for another FGM plate with  $V_c^- = 0, V_c^+ = 1, p = 1, a/h = 5$ . The results are plotted in Figure 3, where  $\bar{z} = x_3/h$ . Both magnitude and trend match very well with the exact solution, which again demonstrates that the present plate model can be used to accurately predict FGM plates.

The second example is two double-layer coating/substrate systems as discussed in Refs. [4, 5] including

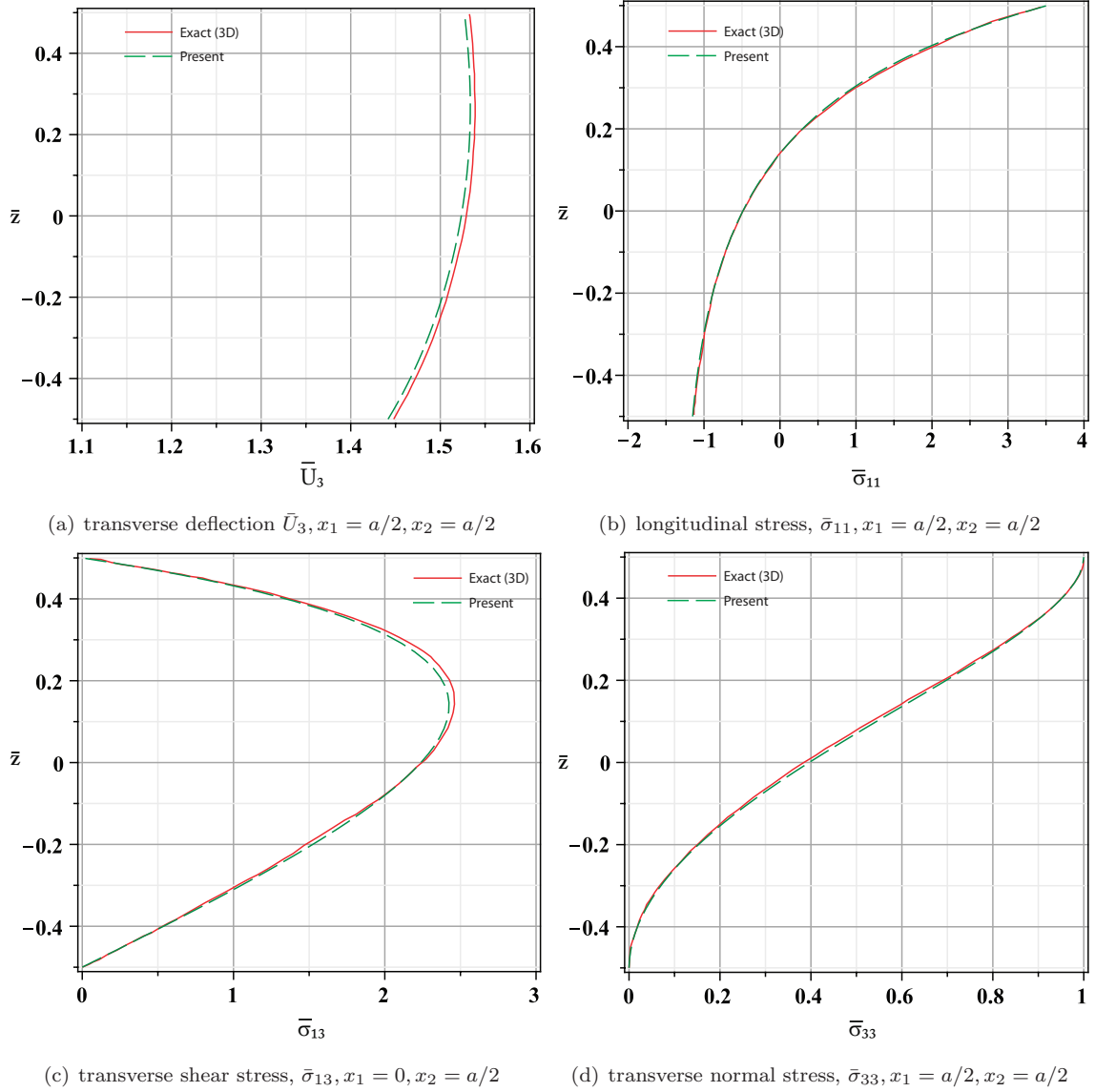


Figure 3. Nondimensional transverse deflection, longitudinal stress, transverse shear stress, transverse normal stress distributions along thickness direction for a Ai/Sic FGM square plate under sinusoidal pressure on the top surface,  $V_c^- = 0, V_c^+ = 1.0, p = 1, a/h = 5$ .

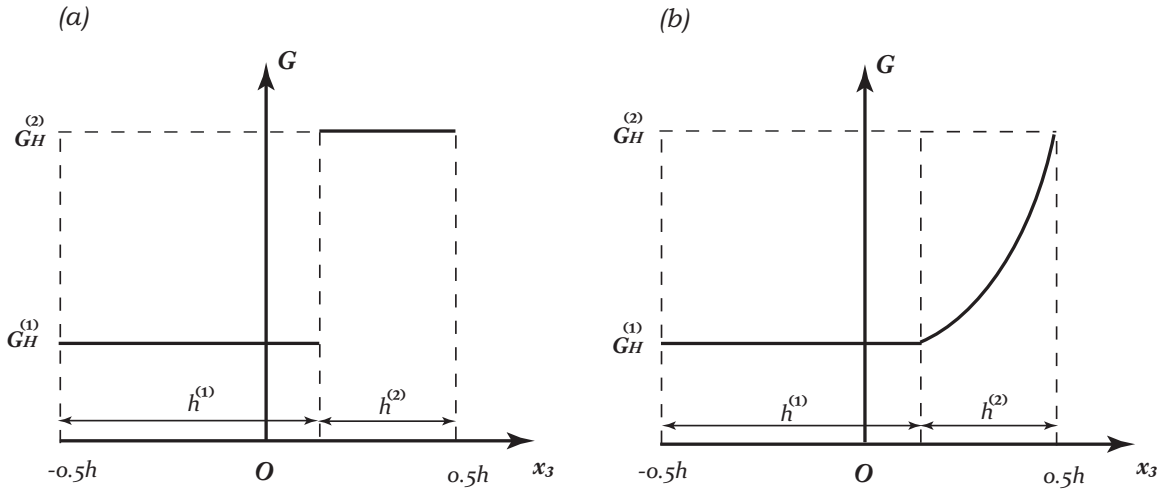


Figure 4. Through-the-thickness variation of shear moduli  $G$  in two coating/substrate systems: (a) system H; (b) system F.

a homogeneous substrate with a thin homogeneous coating (system H) and a homogeneous substrate with a thin functionally graded coating (system F). In both systems the Poisson's ratios for the substrate and the coating are assumed to be constants and equal, i.e.  $\nu_H^{(1)} = \nu_H^{(2)} = \nu_F^{(1)} = \nu_F^{(2)} = 0.3$ . The shear modulus of the substrate and the coating for system H takes the value of  $G_H^{(1)}$ ,  $G_H^{(2)}$ , respectively, while for system F the shear modulus of the substrate and the coating takes the form of:

$$G_F^{(1)} = G_H^{(1)},$$

$$G_F^{(2)}(x_3) = \xi G_H^{(2)} e^{\theta \left( \frac{x_3}{h} - 1 \right)},$$

where  $\xi = G_H^{(2)}/G_H^{(1)}$  is the ratio of the stiffness on the top of the functionally graded coating to that of the homogeneous substrate;  $\theta = h/h^{(2)} \ln \xi$  is the inhomogeneous parameter of the functionally graded coating;  $h^{(2)}$  is the coating thickness. The through-the-thickness variation of shear moduli  $G$  for two systems is shown in Figure 4. In the present analysis,  $\xi$  and  $h/h^{(2)}$  are chosen to be 10 and 5, respectively. The plate is assumed to be simply supported and subjected to the following boundary conditions:

$$x = 0, a : \quad \sigma_{11} = 0, \quad U_2 = U_3 = 0,$$

$$y = 0, b : \quad \sigma_{22} = 0, \quad U_1 = U_3 = 0.$$

The top surface of the coating at  $x_3 = h/2$  is subjected to a sinusoidally distributed pressure ( $\tau_3 = -q_0 \sin(\pi x_1/a) \sin(\pi x_2/b)$ ) while the bottom surface of the substrate is traction free. Again no body force is applied. The stress and displacement components are nondimensionalized as  $\bar{\sigma}_{ij} = \sigma_{ij}/q_0$  and  $\bar{U}_i = U_i G_H^{(2)}/(q_0 h)$ . A general solution procedure for inhomogeneous isotropic media free of body forces is developed by Plevako<sup>31</sup> and was applied to simplify supported multilayer functionally graded plates<sup>4,5</sup>. Because of some typos existing in the formulas in Ref. [4], the authors re-derived the 3D exact solutions for the multilayer functionally graded plate. Moreover, unlike in Refs. [4, 5] where solutions for homogeneous plate is approximated by using a small inhomogeneous parameter  $\gamma$ , exact solutions for homogeneous plate are derived and used in the results presented here.

Figure 5 depicts the through-thickness variation of nondimensional in-plane displacement  $\bar{U}_1$ , transverse displacement  $\bar{U}_3$ , longitudinal normal stress  $\bar{\sigma}_{11}$ , in-plane shear stress  $\bar{\sigma}_{12}$ , transverse shear stress  $\bar{\sigma}_{13}$ , and transverse normal stress  $\bar{\sigma}_{33}$  for a thick ( $a/h = b/h = 3$ ) homogeneous coating/substrate system (system H). It can be observed that all in-plane stress and displacement components, *i.e.*,  $\bar{U}_1$ ,  $\bar{\sigma}_{11}$ , and  $\bar{\sigma}_{12}$ , as well as transverse normal stress  $\bar{\sigma}_{33}$  match very well with the 3D exact solution. Because of the discontinuity of the shear modulus  $G$  for the homogeneous coating and homogeneous substrate, there exist some jumps for in-plane normal  $\bar{\sigma}_{11}$  stress and shear stress  $\bar{\sigma}_{12}$  at the interface. It seems that there exists a constant shift (about 5% of the maximum value) between the results of the present model and the 3D solution for the transverse displacement  $\bar{U}_3$ . [This may be attributed to that our plate model is reduced from the original 3D model and some information which cannot be captured by a 2D model are lost during the dimensional reduction process.](#) Further investigation shows that there are some discrepancies near the interface of the coating/substrate between the present theory and the 3D solution for the transverse shear stress  $\bar{\sigma}_{13}$ : the 3D solution presents a sharp change of  $\bar{\sigma}_{13}$  inside the coating layer while our model has a more smooth transition. Nevertheless, both results show similar maximum value for  $\bar{\sigma}_{13}$ .

The through-thickness variations of various displacement and stress components for a thick ( $a/h = b/h = 3$ ) double-layer functionally graded coating/substrate system (system F) are plotted in Figure 6. It can be observed from this figure that all displacement and stress components except for  $\bar{U}_3$  match well with the exact 3D solutions. Similar constant shift can be observed between the present model and the 3D exact solution. It is important to note that by adopting functionally graded coating the shear moduli  $G$  is now

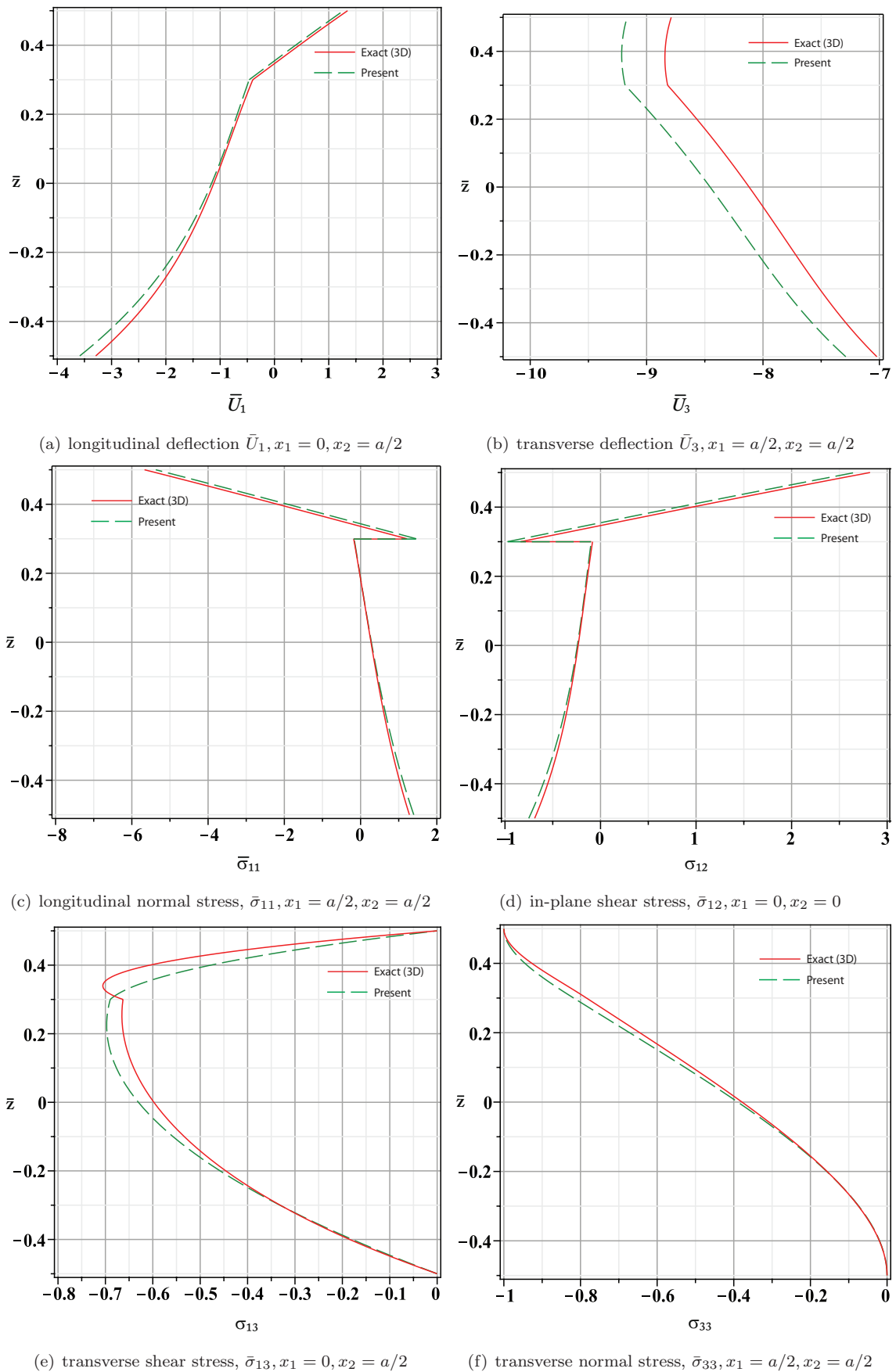
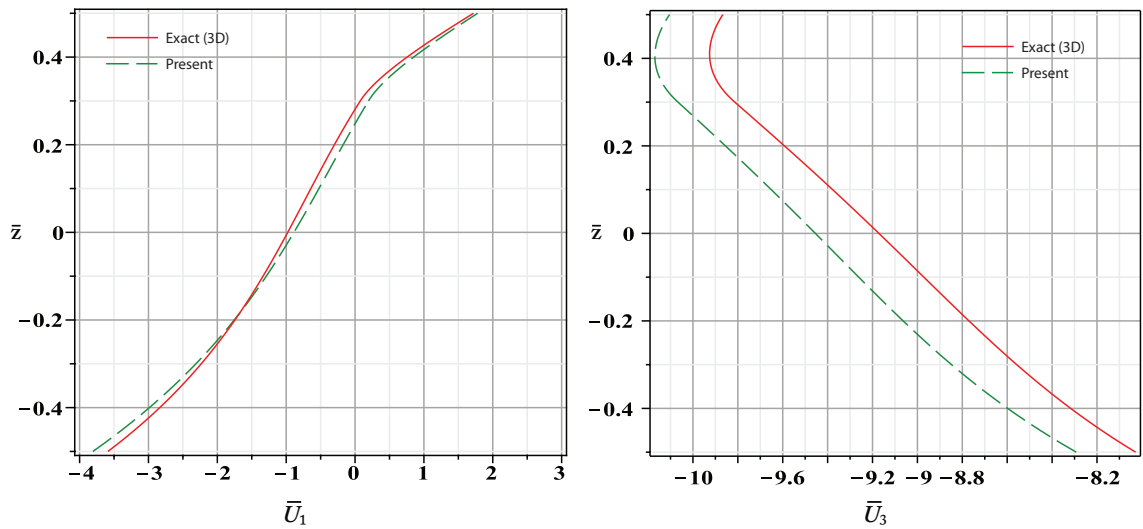
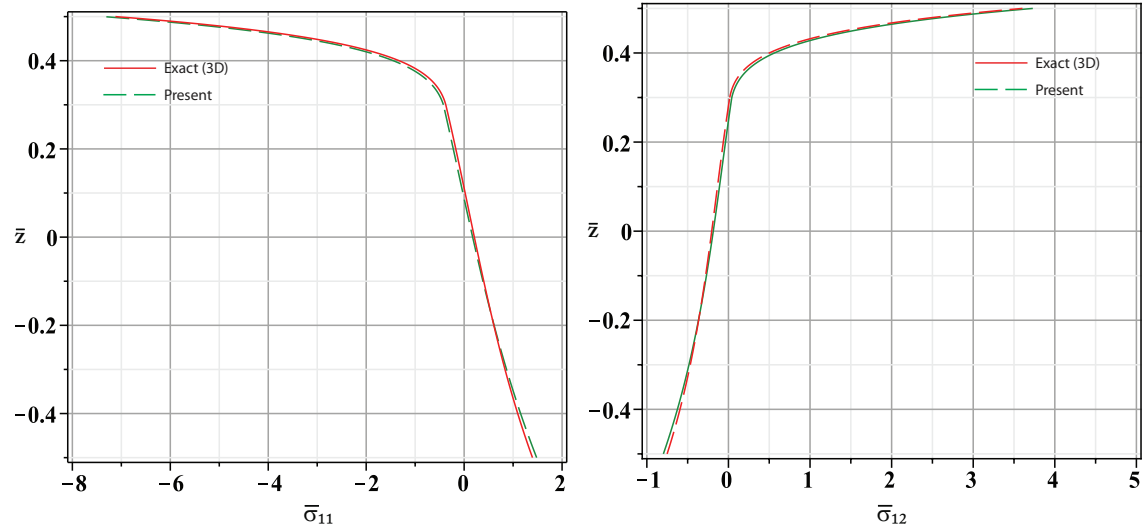


Figure 5. Through-the-thickness variation of nondimensional displacements and stresses for a thick two-layer homogeneous coating/substrate system (system H) under sinusoidal pressure on the top surface ( $a/h = b/h = 3$ ).



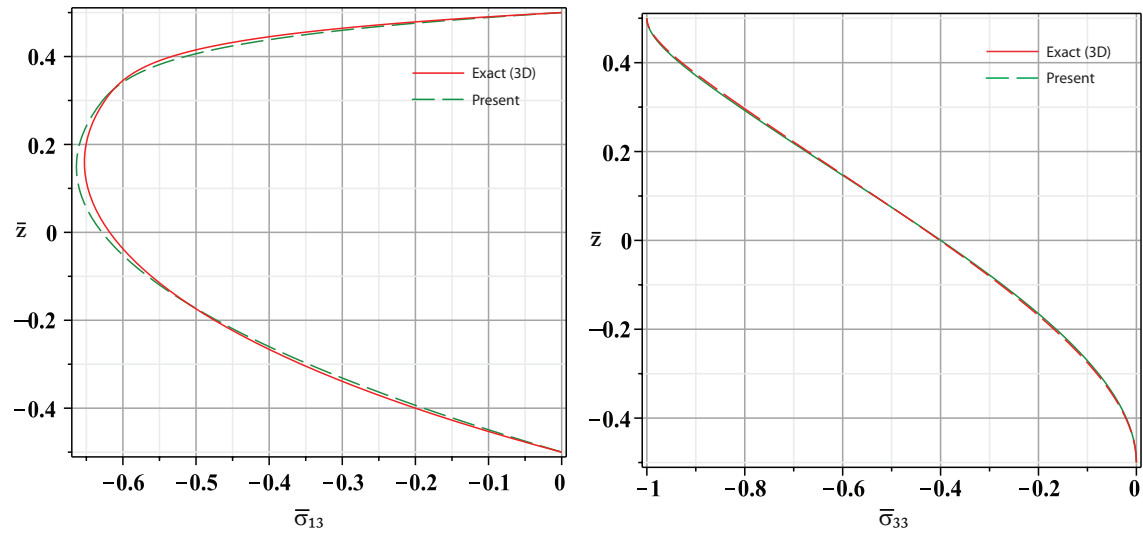
(a) longitudinal deflection  $\bar{U}_1, x_1 = 0, x_2 = a/2$

(b) transverse deflection  $\bar{U}_3, x_1 = a/2, x_2 = a/2$



(c) longitudinal normal stress,  $\bar{\sigma}_{11}, x_1 = a/2, x_2 = a/2$

(d) in-plane shear stress,  $\bar{\sigma}_{12}, x_1 = 0, x_2 = 0$



(e) transverse shear stress,  $\bar{\sigma}_{13}, x_1 = 0, x_2 = a/2$

(f) transverse normal stress,  $\bar{\sigma}_{33}, x_1 = a/2, x_2 = a/2$

Figure 6. Through-the-thickness variation of nondimensional displacements and stresses for a thick two-layer functionally graded coating/substrate system (system F) under sinusoidal pressure on the top surface ( $a/h = b/h = 3$ ).

continuous at the interface, the in-plane stress components such as  $\bar{\sigma}_{11}$  and  $\bar{\sigma}_{12}$ , therefore, become smooth throughout of the total thickness of the F system. In addition, no sharp peak appears for transverse shear stress  $\bar{\sigma}_{13}$ . Results presented in Figure 6 clearly show that using functionally graded coating instead of the homogeneous one will eliminate the mismatch of interface stress components to reduce the risk of cracking and rebounding of the coating.

## Conclusions

An efficient high-fidelity plate model for multilayer functionally graded plate has been developed using the variational asymptotic method (VAM). By taking advantage of the small parameter  $h/l$ , VAM is used to systematically reduce the original, nonlinear 3D model to a series of 2D models in terms of the small parameter. No *a priori* assumptions have been adopted during the derivation. The theory is applicable to functionally graded plates with material properties either being constant or changing continuously in each layer. Although the resulting plate theory is as simple as a single-layer FSDT, the recovered 3D displacement, strain, and stress results have excellent accuracy in comparison with the 3D elasticity. Moreover, [the present model is valid for large displacements and global rotations and can capture all the geometric nonlinearity of a plate when the strains are small](#). The present paper has built on the second author's previous work<sup>19,21</sup> with the following new contributions:

1. The present work has the capability of analyzing multilayer functionally graded plate with material properties as functions of transverse locations or constants while in previous work these properties are treated as constants for each layer;
2. Interface continuity conditions are explicitly derived and solved to obtain the multilayer solutions;
3. Simplifications have been made in deriving  $B$ ,  $C$ ,  $D$  matrices;
4. Explicit analytical solutions for the second-order approximation of warping functions have been provided;
5. A nondimensional scheme has been applied on solving the least square problem resulting in a more reliable estimation of the transverse shear stiffness matrix.

## Acknowledgements

The present work is supported, in part, by the Air Force Office of Scientific Research under Grant FA9550-08-1-0405. The program managers are Dr. Victor Giurgiutiu and Dr. David Stargel. The views and conclusions contained herein are those of the authors and should not be interpreted as necessarily representing the official policies or endorsement, either expressed or implied, of the funding agency.

## References

- <sup>1</sup>E. Müller, Č. Drašar, J. Schilz, and W. A. Kaysser. Functionally graded materials for sensor and energy applications. *Materials Science and Engineering*, A362:17– 39, 2003.
- <sup>2</sup>L. L. Mishnaevsky Jr. Functionally gradient metal matrix composites: Numerical analysis of the microstructure-strength relationships. *Composites Science and Technology*, 66:1873– 1887, 2006.
- <sup>3</sup>L.L. Shaw. Thermal residual stresses in plates and coatings composed of multi-layered and functionally graded materials. *Composites Part B*, 29:199– 210, 1998.
- <sup>4</sup>M. Kashtalyan and M. Menshykova. Three-dimensional elastic deformation of a functionally graded coating/substrate system. *International Journal of Solids and Structures*, 44:5272– 5288, 2007.
- <sup>5</sup>M. Kashtalyan and M. Menshykova. Three-dimensional analysis of a functionally graded coating/substrate system of finite thickness. *Philosophical Transactions of the Royal Society A: Mathematical, Physical and Engineering Sciences*, 366:1821– 1826, 2008.
- <sup>6</sup>M. Das, A. Barut, E. Madenci, and D. R. Ambur. A triangular plate element for thermo-elastic analysis of sandwich panels with a functionally graded core. *International Journal for Numerical Methods in Engineering*, 68:940– 966, 2006.
- <sup>7</sup>F. Shang, Z. Wang, and Z. Li. Analysis of thermally induced cylindrical flexure of laminated plates with piezoelectric layers. *Composite Part B*, 28B:185– 193, 1997.
- <sup>8</sup>E. Pan and P.R. Heyliger. Exact solution for magneto-electro-elastic laminates in cylindrical bending. *International Journal of Solids and Structures*, 40:6859– 6876, 2003.
- <sup>9</sup>S. S. Vel and R. C. Batra. Exact solution for thermoelastic deformations of functionally graded thick rectangular plates. *AIAA Journal*, 40:1421– 1433, 2002.
- <sup>10</sup>G. Altay and M.C. Dökmeci. Variational principles and vibrations of a functionally graded plate. *Computers and Structures*, 83:1340– 1354, 2005.
- <sup>11</sup>K.M. Liew, X. Q. He, T.Y. Ng, and S. Sivashanker. Active control of FGM plates subjected to a temperature gradient: Modelling via finite element method based on FSDT. *International Journal for Numerical Methods in Engineering*, 52:1253– 1271, 2001.

- <sup>12</sup>L.S. Ma and T.J. Wang. Relationships between axisymmetric bending and buckling solutions of FGM circular plates based on third-order plate theory and classical plate theory. *International Journal of Solids and Structures*, 41:85– 101, 2004.
- <sup>13</sup>Z. G. Bian, W. Q. Chen, C.W. Lim, and N. Zhang. Analytical solutions for single- and multi-span functionally graded plates in cylindrical bending. *International Journal of Solids and Structures*, 42:6433– 6456, 2005.
- <sup>14</sup>K. P. Soldatos and P. Watson. A method for improving the stress analysis performance of one-and two-dimensional theories for laminated composites. *Acta Mechanica*, 123:163– 186, 1997.
- <sup>15</sup>K. P. Soldatos and P. Watson. Accurate stress analysis of laminated plates combining a two-dimensional theory with the exact three-dimensional solution for simply supported edges. *Mathematics and Mechanics of Solids*, 2:459– 489, 1997.
- <sup>16</sup>D. F. Gilhooley, R. C. Batra, J.R. Xiao, M. A. McCarthy, and J. W. Gillespie Jr. Analysis of thick functionally graded plates by using higher-order shear and normal deformable plate theory and MLPG method with radial basis functions. *Composite Structures*, 80:539– 552, 2007.
- <sup>17</sup>W. Zhen and W. Chen. A higher-order theory and refine three-node triangular element for functionally graded plates. *European Journal of Mechanics, A/Solids*, 25:447– 463, 2006.
- <sup>18</sup>V. L. Berdichevsky. Variational-asymptotic method of constructing a theory of shells. *Journal of Applied Mathematics and Mechanics*, 52:711–736, 1979.
- <sup>19</sup>W. Yu, D.H. Hodges, and V.V. Volovoi. Asymptotic construction of Reissner-like composite plate theory with accurate strain recovery. *International Journal of Solids and Structures*, 39:5185– 5203, 2002.
- <sup>20</sup>W. Yu and D.H. Hodges. A simple thermopiezoelectric model for composite plates with accurate stress recovery. *Smart Materials and Structures*, 13:926– 938, 2004.
- <sup>21</sup>W. Yu. Mathematical construction of a Reissner-Mindlin plate theory for composite laminates. *International Journal of Solids and Structures*, 42:6680– 6699, 2005.
- <sup>22</sup>H. Chen and W. Yu. Postbuckling and mode jumping analysis of composite laminates using an asymptotically correct, geometrically non-linear theory. *International Journal of Non-linear Mechanics*, 41:1143– 1160, 2006.
- <sup>23</sup>L. Liao and W. Yu. Asymptotical construction of a fully coupled, Reissner-Mindlin model for piezoelectric composite plates. *Smart Materials and Structures*, 17(1), 2008. Article 015010.
- <sup>24</sup>L. Liao and W. Yu. An electromechanical reissner-mindlin model for laminated piezoelectric plates. *Composite Structures*, 88(3):394–402, 2009.
- <sup>25</sup>H. Chen and W. Yu. Asymptotical construction of an efficient high-fidelity model for functionally graded plates. In *Collection of Technical Papers–50th AIAA/ASME/ASCE/AHS/ASC Structures, Structural Dynamics, and Materials Conference*, pages AIAA2009–2135, Palm Spring, CA, May 4th–7th 2009. American Inst. Aeronautics and Astronautics Inc.
- <sup>26</sup>D. A. Danielson and D. H. Hodges. Nonlinear beam kinematics by decomposition of the rotation tensor. *Journal of Applied Mechanics, Transactions of the ASME*, 54:258– 262, 1987.
- <sup>27</sup>D. A. Danielson. Finite rotation with small strain in beams and plates. In *Proceedings of the 2nd Pan American Congress of Applied Mechanics*, Valparaiso, Chile, January 2 – 4 1991. Valparaiso Chile.

<sup>28</sup>Atilgan A. R. Hodges, D. H. and D. A. Danielson. [A Geometrically Nonlinear Theory of Elastic Plates](#). *Journal of Applied Mechanics, Transactions of the ASME*, 60:109–116, 1993.

<sup>29</sup>W. Yu. *Variational Asymptotic Modeling of Composite Dimensionally Reducible Structures*. PhD thesis, Aerospace Engineering, Georgia Institute of Technology, May 2002.

<sup>30</sup>A. R. Atilgan and D. H. Hodges. [On the strain energy of laminated composite plates](#). *International Journal of Solids and Structures*, 29(20):2527–2543, 1992.

<sup>31</sup>V. P.Plevako. On the theory of elasticity of inhomogeneous media. *Journal of Applied Mathematics and Mechanics*, 35:806– 813, 1971.

# Asymptotical Construction of an Efficient High-Fidelity Model for Functionally Graded Plates

Hui Chen\*

and

Wenbin Yu†

*Utah State University, Logan, Utah 84322-4130*

This paper constructs an efficient high-fidelity model for plates made of functionally graded material. By taking advantage of an inherent small parameter, the ratio of the thickness to the characteristic wavelength of the deformation of the reference surface, we apply the variational asymptotic method to rigorously decouple the original three-dimensional anisotropic elasticity problem into a one-dimensional through-the-thickness analysis and a two-dimensional plate analysis. The through-the-thickness analysis provides constitutive relations for the plate analysis as well as the recovery information for the three-dimensional fields, linking the original, complex three-dimensional anisotropic heterogeneous elasticity problem to a simple two-dimensional plate model which achieves the best compromise between efficiency and accuracy. Furthermore, the derived models are geometrically exact and valid for large deformations and global rotations with the restriction that strains are small. Excellent accuracy of present model has been validated by comparing the displacement and stress distributions with exact solutions both for the cylindrical bending of an isotropic plate and the behavior of a thick, simply-supported, two-constituent metal-ceramic functionally graded rectangular plate.

## Introduction

Functional graded materials (FGM) benefited from its coverage over a wide spectrum of functional operation principles have been under development world-widely in recent years. The various functional effects obtained by drawing advantages from FGM principles make it addressing a large variety of application fields, such as graded thermoelectrics and dielectrics, piezoelectrically graded materials applied for ultrasonic transducers, and tungsten-copper composites for high current connectors and diverter plates, to name but a few.<sup>1,2</sup> One widely analyzed FGM, typically used for constructing panels in aerospace systems, is made of a mixture of ceramics and metals and characterized by a continuously changing of its mechanical properties due to a smooth change in volume fraction of the constituent materials from one surface of the material to the other. The surface with high ceramic constituents can provide superior thermal-resistance for high temperature environments while the surface with high metal constituents offers strong mechanical performance, which reduces the risk of catastrophic fracture under extreme environments.

The promising application of FGM and piezoelectric materials in advanced aerospace structures has attracted great attentions from researchers who are seeking to develop efficient yet accurate models for the design and analysis of light-weight structures such as FGM plates and shells. It is interesting to note that such structures are all characterized by one of their dimensions (the thickness) being much smaller than the other two. Although all structures made of FGM and smart materials can be described using three-dimensional (3D) continuum formulation, exact solution exist only for a few specific problems with very idealized material types, geometry, and boundary conditions.<sup>3-5</sup> For more generalized cases, where exact solutions do not exist, one have to rely on 3D numerical simulation tools such as ANSYS and ABAQUS to

---

\*Research Engineer, Department of Mechanical and Aerospace Engineering. Member, AIAA and ASME.

†Associate Professor, Department of Mechanical and Aerospace Engineering. Senior Lifetime Member, AIAA; Member, ASME and AHS.

find numerical solutions. However, this approach is labor intensive and the prohibitive computational cost of 3D simulations makes that they are only justifiable for detailed analysis during the final design. By taking advantage of the fact that the thickness dimension is small, analysis of such structures can be simplified using two-dimensional (2D) models. Although many 2D models have been developed to analyze FGM plates and shells treating different topics, most of them rely on some *a priori* kinematic assumptions. Examples may be found in the application of classic Kirchhoff hypothesis in thermal residual stress and free vibration analyses;<sup>6,7</sup> the utilization of the first-order shear-deformation theory (FSDT) in active control analysis;<sup>8</sup> and the implementation of the third-order shear-deformation theory (TSDT) in bending and buckling analyses.<sup>9</sup> Classical lamination theory (CLT) ignores transverse shear effects and can provide reasonable results only for very thin plates. Moreover, in CLT, both the plain strain and plain stress assumptions are invoked which are conflicting with each other. A number of shear deformation theories have been developed to overcome some drawbacks of CLT, with the simplest of which being FSDT (equivalent to Reissner-Mindlin theory for plates made of isotropic homogeneous materials), where a constant distribution of shear strain through the thickness is assumed and a shear correction factor is required to account for the deviation of the real shear strain from the assumed constant one. The dependence of shear correction factor on the plate's geometric parameters as well as its material constituents make it hard to guarantee the accuracy of FSDT. By expanding the transverse displacement field of the plate using some assumed higher-order polynomials, higher order shear deformation plate theories are developed, which can account for both transverse normal and shear deformations, with no requirements on shear correction factors. However, as indicated by Bian et. al.,<sup>10</sup> for laminated plates and shells, even higher-order theories cannot give satisfactory stress estimation. By extending a generalized refined theory (referred as Soldatos plate theory<sup>11,12</sup>) which incorporates shape functions to guarantee the continuousness of transverse shear stress at interfaces, these authors provides analytical solutions for single and multiply spanned functionally graded plated under cylindrical bending. Higher-order shear deformation theories have also been coupled with finite element method (FEM) to analyze functionally graded plates. As a recent example, Gilhooley et. al., by combining a messless local Petrov-Galerkin and a higher-order shear deformation plate theory, provide a numerical investigation of a two-constituent metal-ceramic thick plate.<sup>13</sup> Despite of successfulness of the aforementioned methods in analyzing many functional and laminated plate problems, this type of approaches has two major disadvantages: (1) the *a priori* assumptions which are naturally extended from the analysis of isotropic homogeneous structures cannot not be easily justified for heterogeneous and anisotropic structures, such as FGM plates; (2) it is difficult for an analyst to determine the accuracy of the result and which assumption should be chosen for efficient yet accurate analysis of a particular problem.

Recently, the variational asymptotic method (VAM)<sup>14</sup> was used to develop a series of rigorous Reissner-Mindlin plate models for heterogeneous and anisotropic composite plates and smart plates.<sup>15-20</sup> These models have been proved to have excellent compromise between the efficiency and accuracy. In this paper, we expand this method to construct an efficient high-fidelity, geometrically exact model for FGM plates where the major challenge lies in that for current analysis the material properties become continuous functions of the transverse location while their values are piecewise constant in previous work. Some derivations have been further simplified to improve the efficiency of this plate model.

In present plate model, the 3D displacement field of an arbitrary material point of the plate are expressed in the most generalized form by introducing a deformed reference coordinate frame and three warping functions subject to certain constrains. The purposes of introducing these constrains on warping functions are two folds: (1) to eliminate redundancy in kinematic equations; and (2) to define the location and orientation of the reference coordinate frame. No *a priori* kinematic assumption has been invoked. The original 3D elasticity problem is then cast in an intrinsic form so that the theory can accommodate arbitrary large deformation and global rotation with the restriction that that the strain is small. By taking advantage of the small parameter  $h/l$ , with  $h$  denoting the thickness of the plate and  $l$  denoting the characteristic wavelength of the plate deformation, VAM is applied to systematically reduce the original 3D model to a series of 2D models in terms of  $h/l$ , resulting the rigorous splitting of the original nonlinear 3D problem into a linear one-dimensional (1D) through-the-thickness analysis and a 2D nonlinear plate analysis. To avoid the overwhelming complexity relates to the direct construction of plate model using asymptotic methods, the final form of the plate model has been transferred to a Reissner-Mindlin model with the transverse shear stiffness being calculated through a least square scheme.

In this work, two examples, i.e., the cylindrical bending of an isotropic plate and the deformation of a thick simply supported two-constituent metal-ceramic functionally graded rectangular plate, have been

analyzed and results are compared with 3D exact elasticity solutions.

### Three-dimension Formulation

The elastodynamic behavior of a solid is governed by the Hamilton principle:

$$\int_{t_1}^{t_2} [\delta(\mathcal{K} - \mathcal{U} + \overline{\delta\mathcal{W}})] dt = 0, \quad (1)$$

where  $t_1$  and  $t_2$  are arbitrary fixed times,  $\mathcal{K}$  is the kinetic energy,  $\mathcal{U}$  denotes the strain energy, and  $\overline{\delta\mathcal{W}}$  represents the virtual work of the applied loads. The overbar is used to indicate that the virtual work needs not be the variations of a functional.

A point in the plate can be described by its Cartesian coordinates  $x_i$ , see Figure 1, where  $x_\alpha$  are two orthogonal lines in the reference surface and  $x_3$  is the normal coordinate originating from the middle of the thickness (Here and throughout the paper, Greek indices assume values 1 and 2 while Latin indices assume 1, 2, and 3. Repeated indices are summed over their range except where explicitly indicated). Letting  $\mathbf{b}_i$  denote the unit vector along  $x_i$  for the undeformed plate, we can then describe the position of any material point in the undeformed configuration by its position vector  $\hat{\mathbf{r}}$  from a fixed point  $O$ , such that

$$\hat{\mathbf{r}} = \mathbf{r}(x_1, x_2) + x_3 \mathbf{b}_3, \quad (2)$$

where  $\mathbf{r}$  is the position vector from  $O$  to the point located by  $x_\alpha$  on the reference surface. When the reference surface of the undeformed plate coincides with its middle surface, we have

$$\langle \hat{\mathbf{r}}(x_1, x_2, x_3) \rangle = h \mathbf{r}(x_1, x_2), \quad (3)$$

where the angle brackets denote the definite integral through the thickness of the plate.

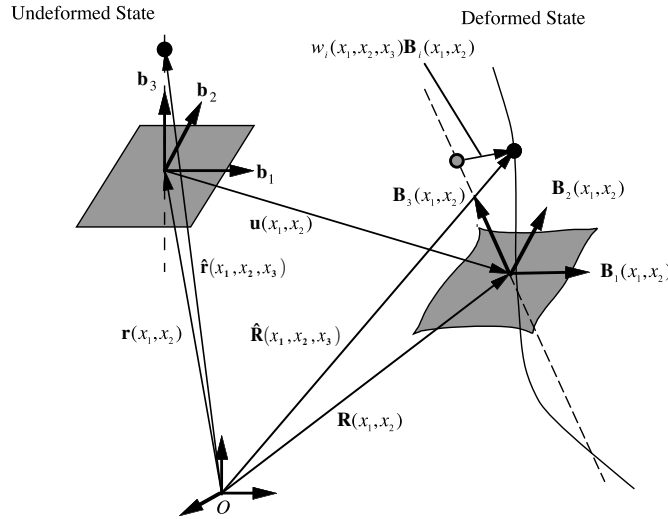


Figure 1. Schematic of plate deformation

When the plate deforms, the particle that had position vector  $\hat{\mathbf{r}}$  in the undeformed state now has position vector  $\hat{\mathbf{R}}$  in the deformed plate. The latter can be uniquely determined by the deformation of the 3D body. We introduce another orthonormal triad  $\mathbf{B}_i$  for the deformed configuration so that:

$$\mathbf{B}_i = \mathcal{C}_{ij} \mathbf{b}_j, \quad \mathcal{C}_{ij} = \mathbf{B}_i \cdot \mathbf{b}_j, \quad (4)$$

subjecting to the requirement that  $\mathbf{B}_i$  is coincident with  $\mathbf{b}_i$  when the structure is undeformed. The direction cosines matrix  $\mathcal{C}(x_1, x_2)$  represents the possible arbitrary rotation between  $\mathbf{B}_i$  and  $\mathbf{b}_i$ .

After deformation, the position vector  $\hat{\mathbf{R}}$  in the deformed state can be expressed as

$$\hat{\mathbf{R}}(x_1, x_2, x_3) = \mathbf{R}(x_1, x_2) + x_3 \mathbf{B}_3(x_1, x_2) + w_i(x_1, x_2, x_3) \mathbf{B}_i(x_1, x_2), \quad (5)$$

where  $\mathbf{R}$  is the position vector of the reference surface for the deformed plate and  $w_i(x_1, x_2, x_3)$  are the warping functions which are introduced to accommodate all possible deformations. Equation (5) can be considered as a change of variable for  $\hat{\mathbf{R}}$  in terms of  $\mathbf{R}$ ,  $\mathbf{B}_i$ , and  $w_i$  and it is six times redundant. The redundancy can be removed by choosing proper definitions for  $\mathbf{R}$  and  $\mathbf{B}_i$ . Similar to equation (3), the reference surface defined by  $\mathbf{R}$  can be chosen as being the average (along  $x_3$ ) surface of the plate. It follows that the warping functions must satisfy the three constrains

$$\langle w_i(x_1, x_2, x_3) \rangle = \left\{ \begin{array}{c} c_{\parallel} \\ 0 \end{array} \right\}, \text{ with } c_{\parallel} = \left\{ \begin{array}{c} c_1 \\ c_2 \end{array} \right\}, \quad (6)$$

where  $c_i$  are arbitrary functions of the in-plane coordinates  $x_{\alpha}$ , introduced for providing free variables for the construction of an optimal Reissner-Mindlin model which will be described later. Another two constraints can be specified by taking  $\mathbf{B}_3$  as the normal to the reference surface of the deformed plate. It should be noted that this choice has nothing to do with the well-known Kirchhoff hypothesis. In the Kirchhoff assumption, no local deformation of the transverse normal is allowed. However, in present derivation we allow all possible deformation using the warping functions. Because  $\mathbf{B}_{\alpha}$  can freely rotate around  $\mathbf{B}_3$ , we can introduce the last constraint as

$$\mathbf{B}_1 \cdot \mathbf{R}_{,2} = \mathbf{B}_2 \cdot \mathbf{R}_{,1}, \quad (7)$$

where  $(\cdot)_{,\alpha} = \partial(\cdot)/\partial x_{\alpha}$ .

Based on the concept of decomposition of rotation tensor<sup>21,22</sup> the Jauman-Biot-Cauchy strain components for small local rotation are given by

$$\Gamma_{ij} = \frac{1}{2}(F_{ij} + F_{ji}) - \delta_{ij}, \quad (8)$$

where  $F_{ij}$  is the mixed-basis component of the deformation gradient tensor such that

$$F_{ij} = \mathbf{B}_i \cdot \mathbf{G}_k \mathbf{g}^k \cdot \mathbf{b}_j. \quad (9)$$

Here  $\mathbf{G}_i = \partial \hat{\mathbf{R}} / \partial x_i$  is the covariant basis vector of the deformed configuration and  $\mathbf{g}^k$  the contravariant base vector of the undeformed configuration and  $\mathbf{g}^k = \mathbf{g}_k = \mathbf{b}_k$ . One can obtain  $\mathbf{G}_k$  with the help of the following definition of 2D generalized strains:

$$\mathbf{R}_{,\alpha} = \mathbf{B}_{\alpha} + \varepsilon_{\alpha\beta} \mathbf{B}_{\beta} \quad (10)$$

and

$$\mathbf{B}_{i,\alpha} = (-K_{\alpha\beta} \mathbf{B}_{\beta} \times \mathbf{B}_3 + K_{\alpha 3} \mathbf{B}_3) \times \mathbf{B}_i, \quad (11)$$

where  $\varepsilon_{\alpha\beta}$  and  $K_{\alpha\beta}$  are the 2D generalized strains. For geometrically nonlinear analysis, we can assume that both the 3D and 2D strains are small when compared to the unity and from which we can also conclude that warpings are of the order of the stain or smaller. Neglecting the products between warping and strain, one can express the 3D strain field as

$$\begin{aligned} \Gamma_e &= \epsilon + x_3 \kappa + I_1 w_{\parallel,1} + I_2 w_{\parallel,2} \\ 2\Gamma_s &= w'_{\parallel} + e_1 w_{3,1} + e_2 w_{3,2} \\ \Gamma_t &= w'_3 \end{aligned} \quad (12)$$

where  $(\cdot)' = \frac{\partial(\cdot)}{\partial x_3}$ ,  $(\cdot)_{\parallel} = [(\cdot)_1 \quad (\cdot)_2]^T$ , and

$$\begin{aligned} \Gamma_e &= [\Gamma_{11}, \quad 2\Gamma_{12} \quad \Gamma_{22}]^T, \quad 2\Gamma_s = [2\Gamma_{13} \quad 2\Gamma_{23}]^T, \quad \Gamma_t = \Gamma_{33}, \\ \epsilon &= [\varepsilon_{11} \quad 2\varepsilon_{12} \quad \varepsilon_{22}]^T, \quad \kappa = [K_{11} \quad K_{12} + K_{21} \quad K_{22}]^T, \end{aligned} \quad (13)$$

$$I_1 = \begin{bmatrix} 1 & 0 \\ 0 & 1 \\ 0 & 0 \end{bmatrix}, \quad I_2 = \begin{bmatrix} 0 & 0 \\ 1 & 0 \\ 0 & 1 \end{bmatrix}, \quad e_1 = \begin{Bmatrix} 1 \\ 0 \end{Bmatrix}, \quad e_2 = \begin{Bmatrix} 0 \\ 1 \end{Bmatrix}. \quad (14)$$

Up to this stage we have formulated the kinematics of the plate structure. With the knowledge of the elastic strain, the strain energy can be expressed as

$$\mathcal{U} = \int_{\Omega} \frac{1}{2} \left\langle \begin{Bmatrix} \Gamma_e \\ 2\Gamma_s \\ \Gamma_t \end{Bmatrix}^T \begin{bmatrix} C_e & C_{es} & C_{et} \\ C_{es}^T & C_s & C_{st} \\ C_{et}^T & C_{st}^T & C_t \end{bmatrix} \begin{Bmatrix} \Gamma_e \\ 2\Gamma_s \\ \Gamma_t \end{Bmatrix} \right\rangle d\Omega \equiv \int_{\Omega} \mathcal{U}_{\mathcal{A}} d\Omega \quad (15)$$

where  $C_e, C_{es}, C_{et}, C_s, C_{st}, C_t$  are the corresponding partition matrices of the 3D  $6 \times 6$  material matrix which are functions of positions for functionally graded materials. Here for simplicity, we restrict ourselves to FGM plates having material properties as functions of  $x_3$  only.

To calculate the kinetic energy, the absolute velocity (measured in the inertia frame) of a generic point in the structure is obtained by taking a time derivative of Eq. (5), resulting

$$v = V + \widetilde{\omega}(\xi + w) + \dot{w}, \quad (16)$$

where  $(\dot{\phantom{x}})$  is the partial derivative with respect to time;  $V$  is the absolute velocity of a point in the deformed reference surface;  $\omega$  is the inertial angular velocity of  $\mathbf{B}_i$  bases; and the notation  $\widetilde{(\phantom{x})}$  forms an antisymmetric matrix from a vector according to  $\widetilde{(\phantom{x})}_{ij} = -e_{ijk}(\phantom{x})_k$  using the permutation symbol  $e_{ijk}$ . In Eq. (16), the symbols  $v, V, \omega, w$  denote column matrices containing the components of corresponding vectors in  $\mathbf{B}_i$  bases, and  $\xi = [0 \ 0 \ x_3]^T$ . The kinetic energy of the plate structure can be obtained by

$$\mathcal{K} = \frac{1}{2} \int_{\mathcal{V}} \rho v^T v d\mathcal{V} = \mathcal{K}_{2D} + \mathcal{K}^* \quad (17)$$

with  $\rho$  denoting the mass density and

$$\mathcal{K}_{2D} = \frac{1}{2} \int_{\Omega} (\bar{\mu} V^T V + 2\omega^T \widetilde{\mu \xi} V + \omega^T j \omega) d\Omega \quad (18)$$

$$\mathcal{K}^* = \frac{1}{2} \int_{\mathcal{V}} \rho [(\widetilde{\omega} w + \dot{w})^T (\widetilde{\omega} w + \dot{w}) + 2(V + \widetilde{\omega} \xi)^T (\widetilde{\omega} w + \dot{w})] d\mathcal{V}, \quad (19)$$

where  $\bar{\mu}, \mu \bar{\xi}$ , and  $j$  are inertial constants commonly used in plate dynamics, which can be trivially obtained through simple integral operations taking over the thickness as:

$$\bar{\mu} = \langle \rho \rangle \quad \mu \bar{\xi} = [0 \ 0 \ \langle x_3 \rho \rangle]^T \quad j = \begin{bmatrix} \langle x_3^2 \rho \rangle & 0 & 0 \\ 0 & \langle x_3^2 \rho \rangle & 0 \\ 0 & 0 & 0 \end{bmatrix} \quad (20)$$

The virtual work of the structure can be calculated as

$$\overline{\delta \mathcal{W}} = \int_{\Omega} (\langle \phi \cdot \delta \hat{\mathbf{R}} \rangle + \boldsymbol{\tau} \cdot \delta \hat{\mathbf{R}}^+ + \boldsymbol{\beta} \cdot \delta \hat{\mathbf{R}}^-) d\Omega + \int_{\partial\Omega} \langle \mathbf{Q} \cdot \delta \hat{\mathbf{R}} \rangle ds \quad (21)$$

where  $\partial\Omega$  denotes the boundary of the reference surface;  $(\phantom{x})^\pm = (\phantom{x})|_{x_3=\pm h/2}$ ;  $\phi = \phi_i \mathbf{B}_i$  is the applied body force;  $\boldsymbol{\tau}, \boldsymbol{\beta}$  are tractions applied on the top and bottom surfaces, respectively;  $\mathbf{Q} = Q_i \mathbf{B}_i$  is the applied tractions along the lateral surfaces.  $\delta \hat{\mathbf{R}}$  is the Lagrangian variation of the displacement field which can be expressed as

$$\delta \hat{\mathbf{R}} = \overline{\delta q}_i \mathbf{B}_i + x_3 \delta \mathbf{B}_3 + \delta w_i \mathbf{B}_i + w_j \delta \mathbf{B}_j, \quad (22)$$

in which the virtual displacement and rotation are defined by

$$\overline{\delta q}_i = \delta \mathbf{R} \cdot \mathbf{B}_i, \quad \delta \mathbf{B}_i = (-\overline{\delta \psi}_2 \mathbf{B}_1 + \overline{\delta \psi}_1 \mathbf{B}_2 + \overline{\delta \psi}_3 \mathbf{B}_3) \times \mathbf{B}_i, \quad (23)$$

where  $\overline{\delta q}_i$  and  $\overline{\delta \psi}_i$  contain the components of the virtual displacement and rotation in the  $\mathbf{B}_i$  system, respectively. Since the warping functions are small, one may safely ignore products of the warping and virtual rotation in  $\delta \hat{\mathbf{R}}$  and obtain the virtual work due to applied loads as

$$\overline{\delta \mathcal{W}} = \overline{\delta \mathcal{W}}_{2D} + \overline{\delta \mathcal{W}}^*, \quad (24)$$

where

$$\overline{\delta \mathcal{W}}_{2D} = \int_{\Omega} (f_i \overline{\delta q}_i + m_\alpha \overline{\delta \psi}_\alpha) d\Omega + \int_{\partial\Omega} (\langle Q_i \rangle \overline{\delta q}_i + \langle x_3 Q_\alpha \rangle \overline{\delta \psi}_\alpha) ds, \quad (25)$$

$$\overline{\delta \mathcal{W}}^* = \int_{\Omega} (\langle \phi_i \delta w_i \rangle + \tau_i \delta w_i^+ + \beta_i \delta w_i^-) d\Omega + \int_{\partial\Omega} \langle Q_i \delta w_i \rangle ds, \quad (26)$$

with the generalized forces  $f_i$  and moments  $m_\alpha$  defined as

$$f_i = \langle \phi_i \rangle + \tau_i + \beta_i, \quad m_\alpha = \langle x_3 \phi_\alpha \rangle + \frac{h}{2}(\tau_\alpha - \beta_\alpha). \quad (27)$$

The second integration in Eq. (26) accounts for virtual work done through warping functions along the lateral boundaries of the plate. This term is necessary for the edge-zone problem, which is an important subject in its own right and beyond the scope of the present paper. For simplicity, we will drop this term hereafter. With the knowledge of Eqs. (17), (15), and (24), the Hamilton's principle in Eq. (1) becomes

$$\int_{t_1}^{t_2} \left[ \delta(\mathcal{K}_{2D} + \mathcal{K}^* - \mathcal{U}) + \overline{\delta\mathcal{W}}_{2D} + \overline{\delta\mathcal{W}^*} \right] dt = 0 \quad (28)$$

So far, we have presented a 3D formulation for the plate structure in terms of 2D displacements (represented by  $\mathbf{R} - \mathbf{r}$ ), rotations (represented by  $\mathbf{b}_i$  and  $\mathbf{B}_i$ ), and 3D warping functions ( $w_i$ ). If we attempt to solve this problem directly, we will meet the same difficulty as solving any full 3D problem with the additional difficulty coming from the anisotropy and heterogeneity of functional graded materials. The main complexity comes from the unknown 3D warping functions  $w_i$ . A common practice in the literature is to assume  $w_i$  to be, *a priori*, in terms of 2D displacements and rotations to straightforwardly reduce the original 3D continuum model into a 2D plate model. However, for plates made with general anisotropic and heterogeneous materials such as functionally graded materials, the imposition of such assumptions may introduce significant errors. Fortunately, VAM provides a useful technique to obtain  $w_i$  through an asymptotical analysis of the variational statement in Eq. (28) in terms of small parameters inherent in the problem which will be described in the next section.

## Dimensional Reduction

The dimensional reduction from the original 3D formulation to a 2D plate model can only be done approximately. One way to accomplish this is to take the advantage of the small parameters in the formulation to construct a 2D formulation so that the reduced model can achieve the minimum accuracy loss in comparison to the original 3D formulation.

In order to apply the methodology of VAM, we first need to assess the order of quantities in terms of small parameters. As mentioned previously, the ratio of the plate thickness to the characteristic wavelength of the deformation of the reference surface is much smaller than 1, which means  $h/l \ll 1$  with  $l$  representing the characteristic wavelength of the deformation of the reference surface. The strain is also small if we only interest on a geometrically nonlinear but physically linear 2D theory, *i.e.*,  $\epsilon_{\alpha\beta} \sim h\kappa_{\alpha\beta} \sim \eta \ll 1$ . From the plate equations of equilibrium, we can estimate the orders of the following quantities corresponding to the order of strains:

$$\begin{aligned} hP_3 \sim \tau_3 \sim \beta_3 \sim \mu(h/l)^2\eta, \quad hP_\alpha \sim \tau_\alpha \sim \beta_\alpha \sim \mu(h/l)\eta, \\ Q_\alpha \sim \mu\eta, \quad Q_3 \sim \mu(h/l)\eta, \end{aligned} \quad (29)$$

with  $\mu$  denoting the characteristic magnitude of the elastic constants. We can choose the characteristic scale of change of the displacements and warping functions in time in such a way that  $\mathcal{K}^*$  is much smaller than other terms in Eq. (28), which is valid for most realistic structural applications.

### Zeroth-order approximation

To clearly illustrate the application of VAM for FGM plates, we first construct a classical FGM plate model. By applying VAM, the zeroth-order approximation of the variational statement in Eq. (28) can be obtained as

$$\int_{t_1}^{t_2} \left[ \delta(\mathcal{K}_{2D} - \int_{\Omega} \mathcal{U}_{A0} d\Omega) + \overline{\delta\mathcal{W}}_{2D} \right] dt = 0 \quad (30)$$

where  $\mathcal{U}_{A0}$  can be obtained from Eq. (15) by dropping the derivatives with respect to  $x_\alpha$  in Equation (12), resulting

$$\begin{aligned} 2\mathcal{U}_{A0} = & 2 \langle (\epsilon + x_3\kappa)^T (C_{es} w_\parallel' + C_{et} w_3') + w_\parallel'^T C_{st} w_3' \rangle \\ & + \langle (\epsilon + x_3\kappa)^T C_e (\epsilon + x_3\kappa) + w_\parallel'^T C_s w_\parallel' + w_3' C_t w_3' \rangle \end{aligned} \quad (31)$$

It is obvious that the warping functions  $w_i$  can be obtained by solving the following variational statement

$$\delta\mathcal{U}_{A0} = 0, \quad (32)$$

along with the constraint equation expressed in Eq. (6). This results in the following Euler-Lagrange equations:

$$\begin{aligned} \left[ (\epsilon + x_3\kappa)^T C_{et} + w_{\parallel}^{0'T} C_{st} + w_3^{0'} C_t \right]' &= \lambda_3, \\ \left[ (\epsilon + x_3\kappa)^T C_{es} + w_{\parallel}^{0'T} C_s + w_3^{0'} C_{st}^T \right]' &= \lambda_{\parallel}, \end{aligned} \quad (33)$$

where  $\lambda_{\parallel}$  and  $\lambda_3$  are Lagrange multipliers corresponding to the constraint components of  $w_{\parallel}$  and  $w_3$ , respectively in Eq. (6). The expressions within the square brackets in Eq. (33) should vanish on the top and bottom surfaces of the FGM plate because the warping functions  $w_i$  are free to vary at those two surfaces. They should also be continuous on the interfaces if the FGM is formed by multiple layers as  $w_i$  must be continuous on this locations. From these conditions, we can solve  $w_i'$  as

$$\begin{aligned} w_{\parallel}'^T &= -(\epsilon + x_3\kappa)^T \hat{C}_{es} C_s^{-1}, \\ w_3' &= -(\epsilon + x_3\kappa)^T \hat{C}_{et} \hat{C}_t^{-1}, \end{aligned} \quad (34)$$

with the hatted quantities being expressed as:

$$\begin{aligned} \hat{C}_{es} &= C_{es} - \hat{C}_{et} C_{st}^T / C_t, & \hat{C}_{et} &= C_{et} - C_{es} C_s^{-1} C_{st}, \\ \hat{C}_t &= C_t - C_{st}^T C_s^{-1} C_{st}. \end{aligned} \quad (35)$$

Substituting Eq. (34) into Eq. (31), the first approximation of the strain energy can be expressed as

$$2\mathcal{U}_{A0} = \begin{Bmatrix} \epsilon \\ \kappa \end{Bmatrix}^T \begin{bmatrix} \hat{A} & \hat{B} \\ \hat{B}^T & \hat{D} \end{bmatrix} \begin{Bmatrix} \epsilon \\ \kappa \end{Bmatrix}, \quad (36)$$

with

$$\hat{A} = \langle \hat{C}_e \rangle, \quad \hat{B} = \langle x_3 \hat{C}_e \rangle, \quad \hat{D} = \langle x_3^2 \hat{C}_e \rangle, \quad \hat{C}_e = C_e - C_{es} C_s^{-1} \hat{C}_{es}^T - C_{et} \hat{C}_{et}^T / \hat{C}_t. \quad (37)$$

With the knowledge of  $\mathcal{U}_{A0}$  expressed in Eq. (36), the original 3D problem in Eq. (1) has been rigorously reduced to a 2D formulation in Eq. (30) which approximates the original problem asymptotically correct to the order of  $(\frac{h}{l})^0$ . If we define the force resultants  $\mathcal{N}$  and moment resultants  $\mathcal{M}$  in conjugate to  $\epsilon$  and  $\kappa$  by

$$\mathcal{N} = \frac{\partial \mathcal{U}_{A0}}{\partial \epsilon}, \quad \mathcal{M} = \frac{\partial \mathcal{U}_{A0}}{\partial \kappa} \quad (38)$$

we obtain a 2D constitutive model for the classical plate analysis of FGM plates, expressed as

$$\begin{Bmatrix} \mathcal{N} \\ \mathcal{M} \end{Bmatrix} = \begin{bmatrix} \hat{A} & \hat{B} \\ \hat{B}^T & \hat{D} \end{bmatrix} \begin{Bmatrix} \epsilon \\ \kappa \end{Bmatrix} \quad (39)$$

It is clear that although the plate is made of functionally gradient materials, the 2D plate model of the zeroth-order remains the same with the exception that the material properties are functions of  $x_3$ . Despite the similarity with the classical lamination theory (CLT), the present model is asymptotically correct and has the following features in contrast with CLT:

1. The normal line of undeformed plate does not remain straight and normal to the deformed plate; rather, it deforms in both the normal and in-plane directions in response to plate deformation ( $\epsilon$  and  $\kappa$ ).
2. This model can handle general functionally gradient materials with full anisotropy.

3. It can be easily observed that neither the normal strain nor the transverse shear strains vanish. The transverse normal and shear stresses can be shown to vanish, which are not assumed *a priori* but come out as a direct consequence from the model derivation.

It worth to emphasize that throughout the process of obtaining this solution no *a priori* assumptions, such as setting the transverse normal strain equal to zero, were used.

For the zeroth-order approximation, the 3D strain field can be recovered using Eqs. (12) by neglecting those terms whose order higher than  $(\frac{h}{l})^0$ , generating

$$\Gamma_e^0 = \epsilon + x_3\kappa \quad 2\Gamma_s^0 = w'_\parallel \quad \Gamma_t^0 = w'_3 \quad (40)$$

Up to this stage, the solution for  $w_i$  in Eq. (34) as well as the 2D strain energy in Eq. (36) are valid for FGM plates with fully populated  $6 \times 6$  material matrix  $C$ . As most engineering materials used in practical applications demonstrate a monoclinic symmetry about their own mid-plane, hereafter, monoclinic material matrix characterized by 13 independent material properties will be used, indicating  $C_{es} = 0$  and  $C_{st} = 0$  for the rest of derivation. This leads to much simpler expressions for the zeroth-order approximation of warping function:

$$w_\parallel = 0, \quad w_3 = C_\perp \mathcal{E}, \quad (41)$$

where,

$$C'_\perp = [-C_{et}^T/C_t \quad -x_3 C_{et}^T/C_t], \quad \mathcal{E} = [\epsilon \quad \kappa]^T, \quad \langle C_\perp \rangle = 0. \quad (42)$$

Note that inter-lamina continuity of  $C_\perp$  must be maintained due to the continuity of warping functions to produce a continuous displacement field. It should also be pointed out that we have constrained warpings to be zeros ( $\langle w_\parallel \rangle = 0$ ) in the zeroth-order approximation and, as a contrast, free constants in Eq. (6) are introduced for the construction of Reissner-Mindlin model to generate the first order approximation.

### First-order approximation

We notice that the zeroth-order warping is of order  $(h/l)^0\eta$ . According to the VAM, to accept this as the zeroth-order approximation, one needs to check whether or not the order of the next approximation is higher than this one. To obtain the first-order approximation, we simply perturb the zeroth-order result, resulting in warping functions of the form

$$w_\parallel = v_\parallel, \quad w_3 = v_3 + C_\perp \mathcal{E}. \quad (43)$$

Substituting Eq. (43) back into Eq. (12), and then Eqs. (15) (24) and (26), one can obtain the leading terms for the first-order approximation of variational statement in Eq. (28) as

$$\delta\Pi_1^* = \left\langle v_\parallel'^T C_s \delta v_\parallel' + v_3' C_t \delta v_3' + (\epsilon + x_3\kappa)^T C_\parallel I_\alpha \delta v_{\parallel,\alpha} + (e_\alpha C_\perp \mathcal{E}, \alpha)^T C_s \delta v_\parallel' - \phi_\parallel^T \delta v_\parallel \right\rangle - \tau_\parallel^T \delta v_\parallel^+ - \beta_\parallel^T \delta v_\parallel^-, \quad (44)$$

where,  $C_\parallel = C_e - C_{et} C_{et}^T / C_t$ . It is worth noting that the warping of the first-order approximation is of order  $(h/l)\eta$ , which is indeed one order higher than the zeroth-order approximation and the total energy  $\Pi_1^*$  is asymptotically correct to the order of  $O(h/l)^2\eta^2$ .

To carry out the variations of the functional, one should be aware that  $v_\parallel$  may be different functions for each layer. The continuity conditions on the interfaces can be derived following calculus of variations as:

$$[v_\parallel] = 0, \quad [D_s(v_\parallel' + e_\alpha C_\perp \mathcal{E}, \alpha)] = 0 \quad \text{on} \quad \Omega_i, \quad (45)$$

where  $\Omega_i$  denotes the interfaces between the  $i$ th layer and  $i + 1$ th layer and  $i = 1 \dots N - 1$  with  $N$  as the total number of layers and the bracket  $[\cdot]$  denotes the jump of the enclosed argument on the interface.

It can be easily observed that  $v_3$  is decoupled from  $v_\parallel$ . Considering the warping constrain in Eq. (6),  $v_3$  only has a trivial solution. The Euler-Lagrange equations for the functional given in Eq. (44) are

$$\begin{aligned} (C_s v_\parallel' + C_s e_\alpha C_\perp \mathcal{E}, \alpha)' &= D'_\alpha \mathcal{E}, \alpha + g' + \lambda_\parallel \\ (C_s v_\parallel' + C_s e_\alpha C_\perp \mathcal{E}, \alpha)^+ &= \tau_\parallel \\ (C_s v_\parallel' + C_s e_\alpha C_\perp \mathcal{E}, \alpha)^- &= -\beta_\parallel \end{aligned} \quad (46)$$

where  $D'_\alpha = -I_\alpha^T [C_\parallel \ x_3 C_\parallel]$ ,  $g' = -\phi_\parallel$ , and  $\lambda_\parallel$  are Lagrange multipliers to enforce the constraints applied on the warping field described in Eq. (6). The inter-lamina continuity on  $D_\alpha$  and  $g$  are maintained by taking advantage of the second condition in Eq. (45). It should be mentioned that since the goal is to obtain an interior solution for the plate without considering edge effects, integration by parts with respect to the in-plane coordinates is used hereafter and throughout the rest of the paper, whenever it is convenient for the derivation.

Solving Eq. (46) along with (6), one obtains the following warping functions

$$v_\parallel = (\bar{D}_\alpha + L_\alpha)\mathcal{E}_{,\alpha} + \bar{g}, \quad (47)$$

with

$$\begin{aligned} \bar{D}'_\alpha &= C_s^{-1} D_\alpha^*, \quad \langle \bar{D}_\alpha \rangle = 0, \quad \bar{g}' = C_s^{-1} g^*, \quad \langle \bar{g} \rangle = 0, \quad L_\alpha \mathcal{E}_{,\alpha} = c_\parallel / h, \\ D_\alpha^* &= D_\alpha + \frac{x_3}{h} D_\alpha^\mp - \frac{1}{2} D_\alpha^\pm - C_s e_\alpha C_\perp, \\ g^* &= g + \frac{x_3}{h} g^\mp - \frac{1}{2} g^\pm + \left( \frac{x_3}{h} + \frac{1}{2} \right) \tau_\parallel + \left( \frac{x_3}{h} - \frac{1}{2} \right) \beta_\parallel, \end{aligned} \quad (48)$$

where, the notation  $(\ )^\pm = (\ )^+ + (\ )^-$  and  $(\ )^\mp = (\ )^- - (\ )^+$ .

Now we are ready to obtain an expression for the total energy that is asymptotically correct through the order of  $\mu(h/l)^2 \varepsilon$ , viz.,

$$2\Pi_1 = \mathcal{E}^T A \mathcal{E} + \mathcal{E}_{,1}^T B \mathcal{E}_{,1} + 2\mathcal{E}_{,1}^T C \mathcal{E}_{,2} + \mathcal{E}_{,2}^T D \mathcal{E}_{,2} - 2\mathcal{E}^T F, \quad (49)$$

where,

$$\begin{aligned} A &= \begin{bmatrix} \langle C_\parallel \rangle & \langle x_3 C_\parallel \rangle \\ \langle x_3 C_\parallel \rangle & \langle x_3^2 C_\parallel \rangle \end{bmatrix}, \\ B &= \langle C_{s11} C_\perp^T C_\perp - D_1^{*T} C_s^{-1} D_1^* \rangle + L_1^T \langle D'_1 \rangle + \langle D'_1 \rangle^T L_1, \\ C &= \langle C_{s12} C_\perp^T C_\perp - D_1^{*T} C_s^{-1} D_2^* \rangle + L_1^T \langle D'_2 \rangle + \langle D'_1 \rangle^T L_2, \\ D &= \langle C_{s22} C_\perp^T C_\perp - D_2^{*T} C_s^{-1} D_2^* \rangle + L_2^T \langle D'_2 \rangle + \langle D'_2 \rangle^T L_2, \\ F &= C_\perp^{+T} \tau_3 + C_\perp^{-T} \beta_3 + \langle C_\perp^T \phi_3 \rangle - \langle D_\alpha^{*T} C_s^{-1} g_{,\alpha}^* \rangle - L_\alpha^T (\tau_\parallel + \beta_\parallel + \langle \phi_\parallel \rangle)_{,\alpha}. \end{aligned} \quad (50)$$

Eq. (49) is an energy functional expressed in terms of 2-D variables which can approximate the original 3D energy asymptotically. It is noted that quadratic terms in the applied loads, are neglected as they will not affect the 2D model.

## Transforming into a Reissner-Mindlin Model

Although Eq. (49) is asymptotically correct through the second order and straightforward use of this strain energy is possible, it involves more complicated boundary conditions than necessary since it contains derivatives of the generalized strain measures. To obtain an energy functional that is of practical use, one can transform Eq. (49) into a Reissner-Mindlin model. In a Reissner-Mindlin model, there are two additional degrees of freedom, which are the transverse shear strains incorporated into the rotation of transverse normal. We introduce another triad  $\mathbf{B}_i^*$  for the deformed plate, so that the definition of 2D strains becomes

$$\begin{aligned} \mathbf{R}_{,\alpha} &= \mathbf{B}_\alpha^* + \varepsilon_{\alpha\beta}^* \mathbf{B}_\beta^* + 2\gamma_{\alpha 3} \mathbf{B}_3^* \\ \mathbf{B}_{i,\alpha}^* &= (-K_{\alpha\beta}^* \mathbf{B}_\beta^* \times \mathbf{B}_3^* + K_{\alpha 3}^* \mathbf{B}_3^*) \times \mathbf{B}_i^* \end{aligned} \quad (51)$$

where the transverse shear strains are  $\gamma = [2\gamma_{13} \ 2\gamma_{23}]^T$ . Since  $\mathbf{B}_i^*$  is uniquely determined by  $\mathbf{B}_i$  and  $\gamma$ , one can derive the following kinematic identity between the strains measures  $\mathcal{R}$  of Reissner-Mindlin plate and  $\mathcal{E}$

$$\mathcal{E} = \mathcal{R} - \mathcal{D}_\alpha \gamma_{,\alpha} \quad (52)$$

where

$$\begin{aligned}\mathcal{D}_1 &= \begin{bmatrix} 0 & 0 & 0 & 1 & 0 & 0 \\ 0 & 0 & 0 & 0 & 1 & 0 \end{bmatrix}^T \\ \mathcal{D}_2 &= \begin{bmatrix} 0 & 0 & 0 & 0 & 1 & 0 \\ 0 & 0 & 0 & 0 & 0 & 1 \end{bmatrix}^T \\ \mathcal{R} &= [\varepsilon_{11}^* \quad 2\varepsilon_{12}^* \quad \varepsilon_{22}^* \quad K_{11}^* \quad K_{12}^* + K_{21}^* \quad K_{22}^*]^T\end{aligned}\quad (53)$$

Now one can express the strain energy asymptotically correct to the second order in terms of strains of the Reissner-Mindlin model as

$$\begin{aligned}2\Pi_1 &= \mathcal{R}^T A \mathcal{R} - 2\mathcal{R}^T A \mathcal{D}_1 \gamma_{,1} - 2\mathcal{R}^T A \mathcal{D}_2 \gamma_{,2} \\ &+ \mathcal{R}_{,1}^T B \mathcal{R}_{,1} + 2\mathcal{R}_{,1}^T C \mathcal{R}_{,2} + \mathcal{R}_{,2}^T D \mathcal{R}_{,2} - 2\mathcal{R}^T F\end{aligned}\quad (54)$$

The generalized Reissner-Mindlin model is of the form

$$2\Pi_{\mathcal{R}} = \mathcal{R}^T A \mathcal{R} + \gamma^T G \gamma - 2\mathcal{R}^T F_{\mathcal{R}} - 2\gamma^T F_{\gamma}\quad (55)$$

To find an equivalent Reissner-Mindlin model Eq. (55) for Eq. (54), one has to eliminate all partial derivatives of the strain. Here equilibrium equations are used to achieve this purpose. From the two equilibrium equations balancing bending moments, one can obtain the following formula

$$G\gamma - F_{\gamma} = D_{\alpha}^T A \mathcal{R}_{,\alpha} + \begin{Bmatrix} m_1 \\ m_2 \end{Bmatrix}\quad (56)$$

where  $F_{\mathcal{R},\alpha}$  is dropped because they are high order terms. Substituting Eq. (56) into Eq. (54), one can show that  $F_{\mathcal{R}} = F$  and  $F_{\gamma} = 0$ . Finally one can rewrite Eq. (54) as

$$2\Pi_1 = \mathcal{R}^T A \mathcal{R} + \gamma^T G \gamma - 2\mathcal{R}^T F + U^*\quad (57)$$

where

$$U^* = \mathcal{R}_{,1}^T \bar{B} \mathcal{R}_{,1} + 2\mathcal{R}_{,1}^T \bar{C} \mathcal{R}_{,2} + \mathcal{R}_{,2}^T \bar{D} \mathcal{R}_{,2}\quad (58)$$

and

$$\begin{aligned}\bar{B} &= B + A \mathcal{D}_1 G^{-1} \mathcal{D}_1^T A \\ \bar{C} &= C + A \mathcal{D}_1 G^{-1} \mathcal{D}_2^T A \\ \bar{D} &= D + A \mathcal{D}_2 G^{-1} \mathcal{D}_2^T A\end{aligned}\quad (59)$$

If we can drive  $U^*$  to be zero for any  $\mathcal{R}$ , then we have found an asymptotically correct Reissner-Mindlin plate model. For general anisotropic plates, this term will not be zero; but we can minimize the error to obtain a Reissner-Mindlin model that is as close to the asymptotically correct one as possible. The accuracy of the Reissner-Mindlin model depends on how close to zero one can drive this term. In other words, one needs to seek an optimal set of the 27 unknowns (3 unknowns for  $G$  and 24 unknowns  $L_{\alpha}$ ) so that the value of the quadratic form in Eq. (58) is as close to be zero as possible for arbitrary generalized strain measures. We let the distinct 78 terms in the symmetric  $12 \times 12$  coefficient matrix equal to zeros to formulate 78 equations. It is a linear system with 27 unknowns. Then we used the least square technique to solve the overdetermined system for the constants as done in Ref. [15]. Mathematically, the overdetermined system (78 equations with 27 unknowns, indicated by  $MX = b$ ) may demonstrate singularities for some material properties. For example, the rank of  $M^T M$  is only 26 for single layered isotropic and orthotropic plates. In this situation, singular value decomposing technique can be applied to solve this least square problem. Moreover, for an accurate estimation of the transverse shear matrix, a nondimensional scheme is used to guarantee that each of the 78 equations having the same physical unit.

After driving of  $U^*$  to be close to zero, we found the ‘‘best’’, from the asymptotic point of view, Reissner-Mindlin model to be used for 2D plate analysis in the following form

$$2\Pi_{\mathcal{R}} = \mathcal{R}^T A \mathcal{R} + \gamma^T G \gamma - 2\mathcal{R}^T F\quad (60)$$

with  $A$ ,  $G$ ,  $F$  capturing the material and geometric information eliminated in the reduced 2D plate analysis. It is worthy to emphasize that although the 2D constitutive model is constructed in a way dramatically different from traditional Reissner-Mindlin models, the plate analysis remains the same, with on changes in the governing equations and essential and natural boundary conditions except that the strain measures are now defined equivalently as in Eqs. (51).

## Recovery 3D Fields

From the above, we have obtained an optimized Reissner-Mindlin model for FGM plates being asymptotically correct in the sense of matching the total potential energy. This model can be carried out for various analyses on FGM plates, spanning from static, dynamic, buckling, to aeroelastic analyses. In many applications, however, the capability of predicting accurate 2D displacement fields of FGM plates is inadequate. Ultimately, the fidelity of a reduced-order model like this developed in current work should be evaluated based upon how well it can predict the 3D displacement/strain/stress fields for the original 3D problem. Therefore, it is necessary to provide recovery relations to complete the theory so that the results is comparable to those of the original 3D model. By referring to recovery relations, we mean expressions for 3D displacement, strain, and stress fields in terms of 2D quantities and  $x_3$ .

Using Eqs. (2), (4) and (5), one can recover the 3D displacement field through the first-order as

$$U_i = u_i + x_3(C_{3i} - \delta_{3i}) + C_{ji}w_j, \quad (61)$$

where  $w_\alpha = v_\alpha$ ,  $w_3 = C_\perp \mathcal{E}$ ,  $U_i$  and  $u_i$  are, respectively, 3D displacements and their 2D counterparts expressed in  $\mathbf{b}_i$  coordinate frame. From Eq. (12), the 3D strain field can be recovered up to the first-order as

$$\Gamma_e = \epsilon + x_3\kappa, \quad 2\Gamma_s = v'_\parallel + e_\alpha C_\perp \mathcal{E}_{,\alpha}, \quad \Gamma_t = C'_\perp \mathcal{E}. \quad (62)$$

Consequently, 3D stresses  $\sigma_{ij}$ , can be obtained by applying the 3D constitutive relations. Since we have obtained an optimum estimation of the shear stiffness matrix  $G$ , the recovered 3D results up to the first order are better than CLT and the conventional FSDT. However, the transverse normal stress ( $\sigma_{33}$ ) is a second-order small quantity with its magnitude being  $O((h/l)^2\eta)$  thus cannot be estimated during the first-order approximation. Despite that its magnitude is usually much smaller than those of other stress components,  $\sigma_{33}$  is critical for predicting some structural failure phenomenon such as layer delamination. In order to obtain a reasonable recovery for the transverse normal stress, VAM procedure is applied once more to find the warping functions with the second-order accuracy, i.e. warping are pursued to the order of  $(h/l)^2\eta$ . By using similar procedures described in previous sections, the warping functions can be expressed as

$$\hat{w}_\parallel = v_\parallel + y_\parallel, \quad \hat{w}_3 = C_\perp \mathcal{E} + y_3, \quad (63)$$

where,  $y_\parallel$  and  $y_3$  are second order warping functions. Consequently, it can be shown that the in-plane components  $y_\parallel$  vanishes and the Euler-Lagrangian equation on  $y_3$  is

$$\begin{aligned} (C_t y'_3 + C_{et}^T I_\alpha v_{\parallel,\alpha})' + e_\beta^T C_s (v'_\parallel + e_\alpha C_\perp \mathcal{E}_{,\alpha})_{,\beta} + \phi_3 &= \lambda_3, \\ (C_t y'_3 + C_{et}^T I_\alpha v_{\parallel,\alpha})^+ &= \tau_3, \\ (C_t y'_3 + C_{et}^T I_\alpha v_{\parallel,\alpha})^- &= -\beta_3, \\ [y_3] = 0 \quad [C_t y'_3 + C_{et}^T I_\alpha v_{\parallel,\alpha}] &= 0, \quad \text{on } \Omega_i \end{aligned} \quad (64)$$

where  $\lambda_3$  is the Lagrange multiplier to enforce the constraint  $\langle y_3 \rangle = 0$ . The solution of  $y_3$  is given by

$$y_3 = \bar{E}_{\alpha\beta} \mathcal{E}_{,\alpha\beta} + \bar{S}, \quad (65)$$

with

$$\begin{aligned} \bar{E}'_{\alpha\beta} &= C_t^{-1} E_{\alpha\beta}^*, \quad \langle \bar{E}_{\alpha\beta} \rangle = 0, \quad \bar{S}' = C_t^{-1} S^*, \quad \langle \bar{S} \rangle = 0, \\ E_{\alpha\beta}^* &= E_{\alpha\beta} + \frac{x_3}{h} E_{\alpha\beta}^\mp - \frac{1}{2} E_{\alpha\beta}^\pm - C_{et}^T I_\alpha (\bar{D}_\beta + L_\beta), \quad S' = - (e_\beta^T g_{\beta}^* + \phi_3), \\ S^* &= S + \frac{x_3}{h} S^\mp - \frac{1}{2} S^\pm + \left( \frac{x_3}{h} + \frac{1}{2} \right) \tau_3 + \left( \frac{x_3}{h} - \frac{1}{2} \right) \beta_3 - C_{et}^T I_\alpha \bar{g}_{,\alpha}. \end{aligned} \quad (66)$$

By finding  $y_3$ , we have obtained an energy expression asymptotically corrected up to the order of  $O((h/l)^4\eta^2)$ . Because such energy expression is too complicate to be used in practice, we will still rely on the previous derived Reissner-Mindlin model to carry out 2D plate analysis and use  $y_3$  for the second-order prediction of the 3D displacement/strain/stress field. As will be shown latter, this approach generates excellent accuracy on predicting 3D stresses even though only the Reissner-Mindlin plate model is used for 2D analysis.

Finally, we can write the recovery relations for the 3D displacement field as

$$U_i = u_i + x_3(C_{3i} - \delta_{3i}) + C_{ji}w_j + \delta_{3i}C_{3i}y_3 \quad (67)$$

and the strains as

$$\Gamma_e = \epsilon + x_3\kappa + I_\alpha v_{\parallel,\alpha}, \quad 2\Gamma_s = v'_{\parallel} + e_\alpha C_\perp \mathcal{E}_{,\alpha}, \quad \Gamma_t = C'_\perp \mathcal{E} + y'_3. \quad (68)$$

At last, the recovered 3D stress field take the form of

$$\begin{aligned} \sigma_e &\equiv [\sigma_{11} \ \sigma_{12} \ \sigma_{22}]^T = C_{\parallel}(\epsilon + x_3\kappa) + C_{et}y'_3 + C_e I_\alpha v_{\parallel,\alpha}, \\ \sigma_s &\equiv [\sigma_{13} \ \sigma_{23}]^T = C_s(v'_{\parallel} + e_\alpha C_\perp \mathcal{E}_{,\alpha}), \\ \sigma_t &\equiv \sigma_{33} = C_{et}^T I_\alpha v_{\parallel,\alpha} + C_t y'_3. \end{aligned} \quad (69)$$

## Validation Examples

Although the above formulation is general enough to treat multilayer plate made of arbitrary functionally graded materials with the properties as functions of  $x_3$ . We specify our formulation to deal with single-layer plates to valid our theory.

The first example is the cylindrical bending of an isotropic homogeneous plate which is infinitely long along  $x_2$  with a width  $a$  along  $x_1$ . The top surface at  $x_3 = h/2$  is subjected to a sinusoidally distributed pressure ( $q_3 = q_0 \sin(\pi x_1/L)$ ), the bottom surface is traction free, and no body force exist in the structure. To facility our comparison, the physical quantities are nondimensionlized by following relations:

$$\begin{aligned} \bar{U}_\alpha &= \frac{100Eh^2U_\alpha}{q_0a^3}, \quad \bar{U}_3 = \frac{100Eh^3U_3}{q_0a^4}, \\ \bar{\sigma}_{\alpha\beta} &= \frac{10h^2\sigma_{\alpha\beta}}{q_0a^2}, \quad \bar{\sigma}_{\alpha 3} = \frac{10h\sigma_{\alpha 3}}{q_0a}, \quad \bar{\sigma}_{33} = \frac{\sigma_{33}}{q_0}. \end{aligned}$$

where  $E$  is the Young's modulus of the material and the Poisson's ratio is assumed to be 0.3.

Figures 2 and 3 depict the through-the-thickness variation of nondimensional transverse deflection ( $U_3$ ), longitudinal stress ( $\sigma_{11}$ ), transverse shear stress ( $\sigma_{13}$ ), and transverse normal stress ( $\sigma_{33}$ ) for an isotropic plate under cylindrical bending with length to the thickness ratio being  $a/h = 5$  and  $a/h = 2$ , respectively. For a fairly think plate  $a/h = 5$ , all the recovered stress components matches pretty well with the exact 3D solutions. It is hard to distinguish the difference between these two sets of results for in-plane stress  $\sigma_{11}$  and the transverse normal stress  $\sigma_{33}$ . The maximum difference occurs for transverse shear stress  $\sigma_{13}$  but still less than 1.5%. The transverse displacement component demonstrates a slight offset form the 3D exact solution, with the maximum difference less than 1.5%. This may be attributed to that our plate model is reduced from the original 3D model and some information which cannot be captured by a 2D model are lost during the dimensional reduction process, which might cause the constant displacement shift of the present approach. Figure 3 demonstrates results for a extremely thick isotropic plate with  $a/h = 2$ . Again, the in-plane stress  $\sigma_{11}$  and the transverse normal stress  $\sigma_{33}$  matches well with the exaction solutions. Relatively large differences occur for transverse shear stress  $\sigma_{13}$  and transverse displacement  $U_3$ , with the maximum errors being 6% and 1%, respectively, for this extreme case.

The second example is a simply supported *Ai/SiC* functionally graded square plate. The top surface of the FGM plate is ceramic rich and the bottom surface is metal rich. The region between the two surfaces is made of the mixture of ceramic-metal materials with continually varying of the volume fraction of the ceramic and metal. Based upon the power law distribution, the variation of the volume fraction of the ceramics  $V_c$  versus the thickness coordinate ( $x_3$ ) with its origin placed at the middle of the thickness can be expressed as

$$V_c = V_c^- + (V_c^+ - V_c^-) \left( \frac{1}{2} + \frac{x_3}{h} \right)^p, \quad p \geq 0,$$

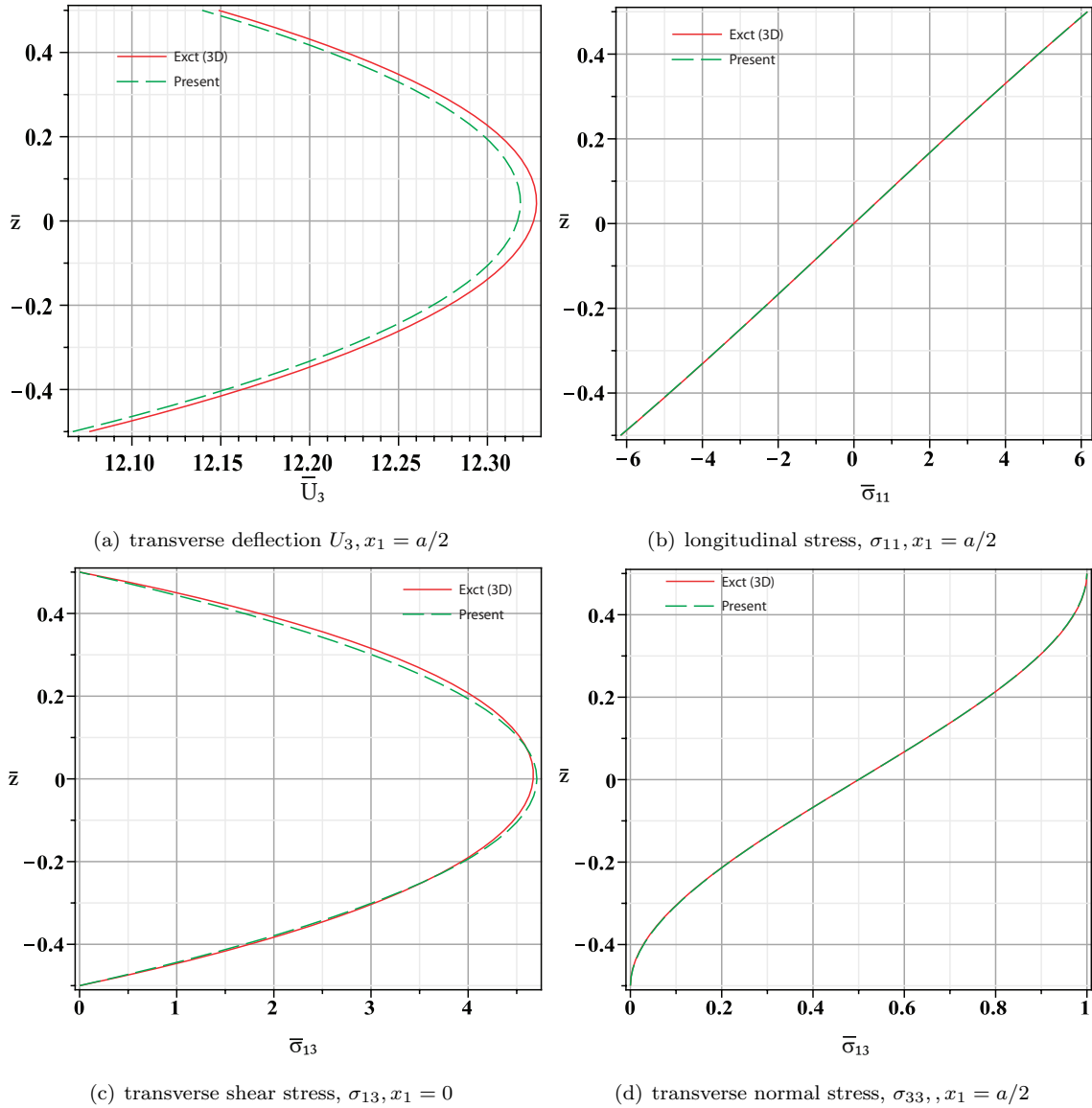


Figure 2. Nondimensional transverse deflection, longitudinal stress, transverse shear stress, transverse normal stress distributions along thickness direction for an isotropic plate under cylindrical bending,  $\nu = 0.3, a/h = 5$ .

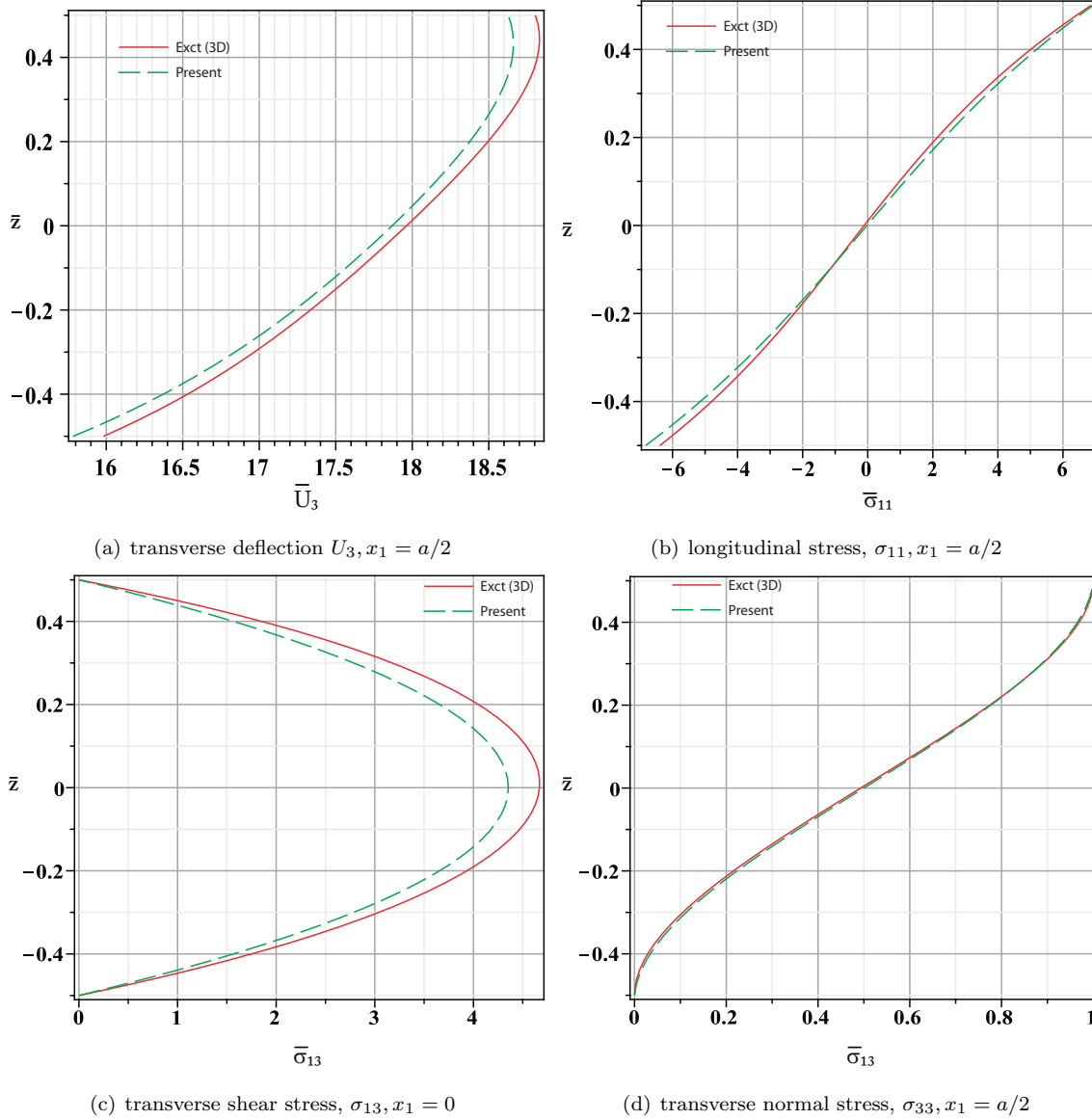


Figure 3. Nondimensional transverse deflection, longitudinal stress, transverse shear stress, transverse normal stress distributions along thickness direction for an isotropic plate under cylindrical bending,  $\nu = 0.3, a/h = 2$ .

where  $V_c^+$  and  $V_c^-$  are the volume fractions of the ceramic on the top and the bottom surfaces,  $p$  is the volume fraction index, and  $h$  the thickness of the plate. The effective elastic moduli of the functionally graded metal-ceramic material are estimated by the Mori-Tanaka scheme, a technique which is capable of taking account for the interaction among constituents thus well suitable for estimating the effective moduli for regions of the graded microstructure that have well-defined continuous matrix and a discontinuous particulate phase. According to the Mori-Tanaka scheme, the effective bulk modulus  $K$  and the effective shear modulus  $\mu$  can be determined by

$$\left\{ \begin{array}{l} \frac{K - K_m}{K_c - K_m} = \frac{V_c}{1 + (1 - V_c) \frac{K_c - K_m}{K_m + \frac{4}{3}\mu_m}} \\ \frac{\mu - \mu_m}{\mu_c - \mu_m} = \frac{V_c}{1 + (1 - V_c) \frac{\mu_c - \mu_m}{\mu_m + s_1}} \end{array} \right. , \quad (70)$$

where,  $s_1 = \mu_m(9K_m + 8\mu_m)/(6(K_m + 2\mu_m))$ ,  $K_m$ ;  $\mu_m$  represent the bulk and shear modulus of the metal material and  $K_c$ ,  $\mu_c$  represent the bulk and shear modulus of the ceramic material.<sup>5,13</sup> The through-thickness varying Young's modulus and Poisson's ratio at each material point are related to effective bulk and shear moduli by

$$K(x_3) = \frac{E(x_3)}{3[1 - 2\nu(x_3)]}, \quad \mu(x_3) = \frac{E(x_3)}{2[1 + \nu(x_3)]}. \quad (71)$$

For the purpose of illustration, we choose the constituent materials for functionally graded plate to be Al and SiC with following material properties. For Al:  $E_m = 70 \text{ GPa}$ ,  $\nu_m = 0.3$ . For SiC:  $E_c = 427 \text{ GPa}$ ,  $\nu_c = 0.17$ . Figure 4 reveals the through-thickness variation of effective Young's modulus and Poisson's ratio ( $E, \nu$ ) for various materials index  $p$ .

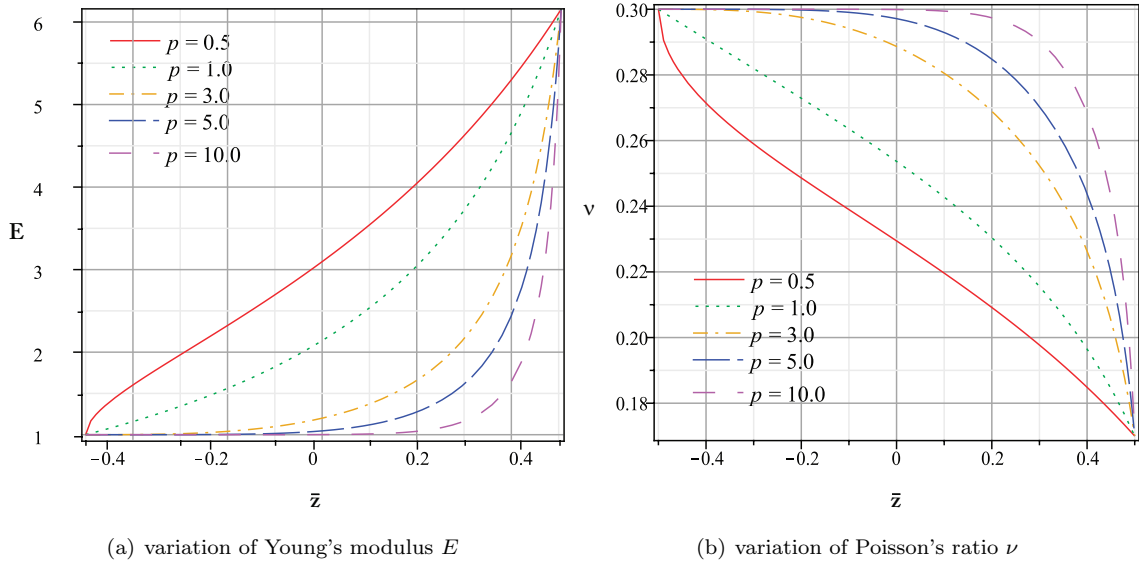


**Figure 4.** Through-the-thickness variation of effective Young's modulus  $E$  and Poisson's ratio  $\nu$  estimated by Mori-Tanaka scheme for different values of  $p$ .

The FGM plate is subjected to a sinusoidally distributed pressure on the top surface, described by:

$$\sigma_{i3}(x_1, x_2, h/2) = \delta_{i3}q_0 \sin(\pi x_1/a) \sin(\pi x_2/a)$$

Again there is no body force and the bottom surface is traction free.

Table 1 provides a detailed comparison of displacement and stress components with exact 3D solution<sup>5</sup> at various critical locations of the Al/SiC functionally graded plates. Results in the top part of Table 1 ( $V_c^- = 0, V_c^+ = 0.5, p = 2$ ) indicate the effect of  $a/h$  on displacement and stress components. It shows an excellent match between these two results. The maximum percentage error occurs for  $a/h = 5$  and  $\sigma_{13}$ , which

**Table 1. Comparison of displacements and stress at specific locations with 3D elasticity solutions for Al/SiC functionally graded square plates (sinusoidal pressure, Mori-Tanaka scheme).**

Variable	$V_c^- = 0, V_c^+ = 0.5, p = 2$					
	$a/h = 5$		$a/h = 10$		$a/h = 40$	
	ext	present	ext	present	ext	present
$\bar{U}_1(0, b/2, t/2)$	-2.9129	-2.9124	-2.8997	-2.8987	-2.8984	-2.8983
$\bar{U}_3(0, b/2, 0)$	2.5748	2.5716	2.2266	2.2256	2.1163	2.1163
$\bar{U}_3(0, b/2, t/2)$	2.5559	2.5524	2.2148	2.2139	2.1155	2.1154
$\bar{\sigma}_{11}(a/2, b/2, t/2)$	2.7562	2.7558	2.6424	2.6415	2.6093	2.6092
$\bar{\sigma}_{12}(0, 0, t/2)$	-1.5600	-1.5597	-1.5529	-1.5524	-1.5522	-1.5521
$\bar{\sigma}_{13}(0, b/2, 0)$	2.3100	2.2749	2.3239	2.3150	2.3281	2.3276
$\bar{\sigma}_{33}(a/2, b/2, t/4)$	0.8100	0.8117	0.8123	0.8127	0.8129	0.8129
Variable	$V_c^- = 0, p = 2, a/h = 5$					
	$V_c^+ = 0.2$		$V_c^+ = 0.6$		$V_c^+ = 1.0$	
	ext	present	ext	present	ext	present
$\bar{U}_1(0, b/2, t/2)$	-3.6982	-3.6966	-2.6708	-2.6697	-1.7421	-1.7359
$\bar{U}_3(0, b/2, 0)$	3.0254	3.0215	2.4326	2.4293	1.8699	1.8634
$\bar{U}_3(0, b/2, t/2)$	2.9852	2.9808	2.4196	2.4160	1.8767	1.8702
$\bar{\sigma}_{11}(a/2, b/2, t/2)$	2.3285	2.3273	2.9359	2.9347	4.1042	4.0899
$\bar{\sigma}_{12}(0, 0, t/2)$	-1.2163	-1.2158	-1.7106	-1.7099	-2.8534	-2.8433
$\bar{\sigma}_{13}(0, b/2, 0)$	2.3516	2.3065	2.2918	2.2604	2.1805	2.1683
$\bar{\sigma}_{33}(a/2, b/2, t/4)$	0.8300	0.8284	0.8024	0.8047	0.7623	0.7675

has an error of 1.5%, with the percentage errors for the rest components being less than 0.38%. The effect of volume fraction of the ceramic constituent for a thick functionally graded plate ( $V_c^- = 0, p = 2, a/h = 5$ ) is provided in the bottom half of table 1. Again, all stress and displacement results matches very well the the exact solutions.

Further comparisons are also made for a thick FGM plate with  $V_c^- = 0, V_c^+ = 1, p = 1, a/h = 5$ . The results are plotted in Figure 5. Both magnitude and trend match very well with exact solutions, which again demonstrates that our present model can be used to model FGM plates to get accurate prediction of the 3D fields.

## Conclusions

In present work a geometrically exact efficient high-fidelity plate model for functionally graded plate has been developed using the variational asymptomatic method (VAM). By taking advantage of the small parameter  $h/l$ , VAM is applied to systematically reduce the original nonlinear 3D model to a series of 2D models in terms of  $h/l$ , resulting the rigorous splitting of the original nonlinear 3D problem into a linear 1D through thickness analysis and a 2D nonlinear plate analysis. The theory is applicable to functionally graded plates whose material properties changes continuously through the plate thickness. Although the resulting plate theory is as simple as a single-layer FSDT, the recovered 3D displacement, strain, and stress results have excellent accuracy in comparison with the 3D elasticity solutions. The present paper has built on the second author's previous work in<sup>15,17</sup> with the following new contributions:

1. The present work treats material properties as functions of transverse locations while in previous work these properties are constants for each layer;
2. Simplifications have been made in deriving  $B, C, D$  matrices, making the present model computationally more efficient;
3. Explicit analytical solutions for the second-order approximation of warping functions have been provided;

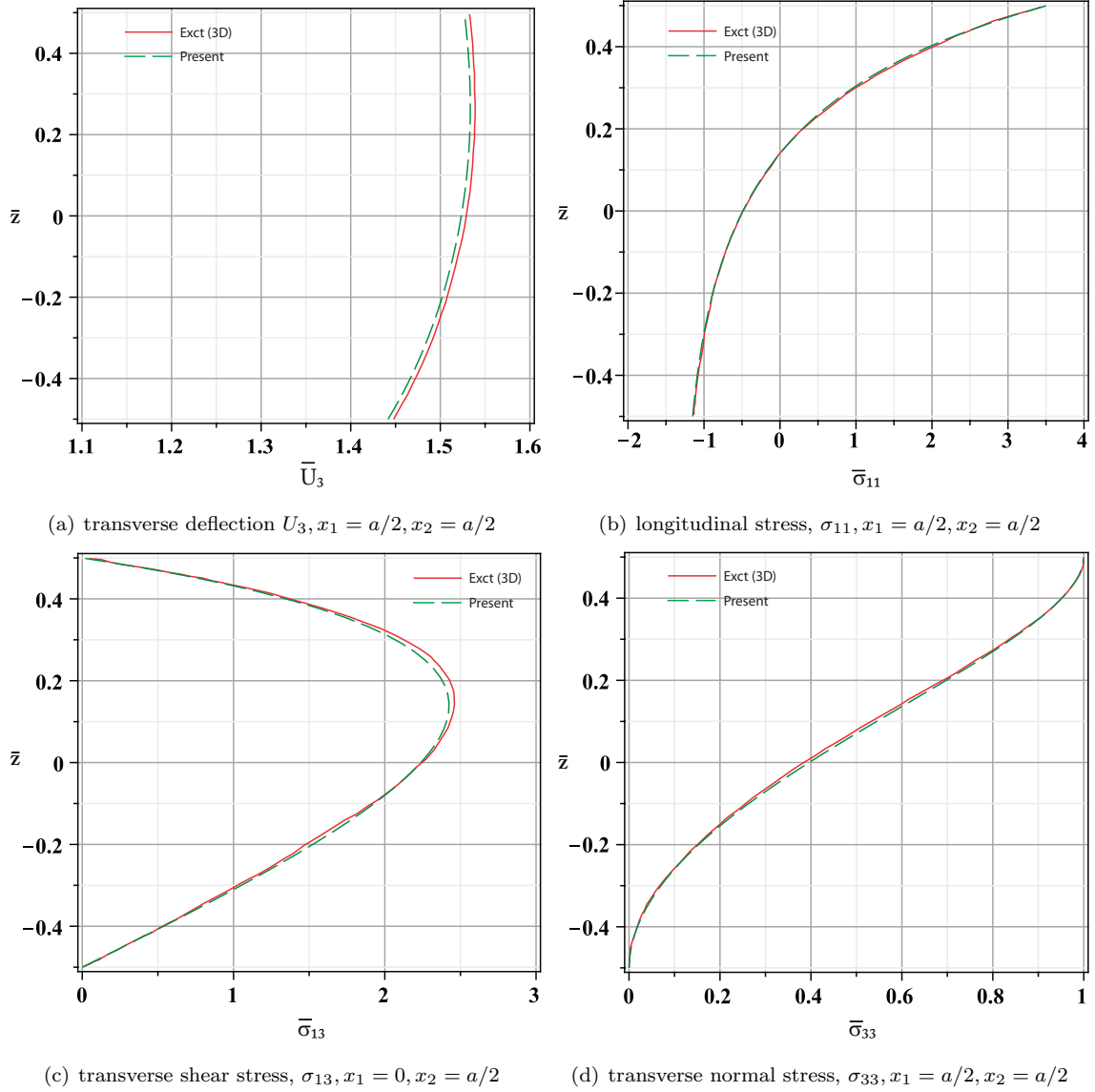


Figure 5. Nondimensional transverse deflection, longitudinal stress, transverse shear stress, transverse normal stress distributions along thickness direction for a Ai/Sic FGM square plate under sinusoidal pressure on the top surface,  $V_c^- = 0, V_c^+ = 1.0, p = 1, a/h = 5$ .

4. A nondimensional scheme has been applied on solving the least square problem resulting a more accurate estimation of the transverse shear stiffness matrix.

## Acknowledgements

The present work is supported, in part, by the Air Force Office of Scientific Research under Grant FA9550-08-1-0405. The program manager is Dr. Victor Giurgiutiu. The views and conclusions contained herein are those of the authors and should not be interpreted as necessarily representing the official policies or endorsement, either expressed or implied, of the funding agencies.

## References

- <sup>1</sup>E. Müller, Č. Drašar, J. Schilz, and W. A. Kaysser. Functionally graded materials for sensor and energy applications. *Materials Science and Engineering*, A362:17– 39, 2003.
- <sup>2</sup>L. L. Mishnaevsky Jr. Functionally gradient metal matrix composites: Numerical analysis of the microstructure-strength relationships. *Composites Science and Technology*, 66:1873– 1887, 2006.
- <sup>3</sup>D. A. Danielson and D. H. Hodges. Analysis of thermally induced cylindrical flexure of laminated plates with piezoelectric layers. *Composite Part B*, 28B:185– 193, 1997.
- <sup>4</sup>D. A. Danielson and D. H. Hodges. Exact solution for magneto-electro-elastic laminates in cylindrical bending. *International Journal of Solids and Structures*, 40:6859– 6876, 2003.
- <sup>5</sup>S. S. Vel and R. C. Batra. Exact solution for thermoelastic deformations of functionally graded thick rectangular plates. *AIAA Journal*, 40:1421– 1433, 2002.
- <sup>6</sup>L.L. Shaw. Thermal residual stresses in plates and coatings composed of multi-layered and functionally graded materials. *Composites Part B*, 29B:199– 210, 1998.
- <sup>7</sup>G. Altay and M.C. Dökmeci. Variational principles and vibrations of a functionally graded plate. *Computers and Structures*, 83:1340– 1354, 2005.
- <sup>8</sup>K.M. Liew, X. Q. He, T.Y. Ng, and S. Sivashanker. Active control of FGM plates subjected to a temperature gradient: Modelling via finite element method based on FSDT. *International Journal for Numerical Methods in Engineering*, 52:1253– 1271, 2001.
- <sup>9</sup>L.S. Ma and T.J. Wang. Relationships between axisymmetric bending and buckling solutions of FGM circular plates based on third-order plate theory and classical plate theory. *International Journal of Solids and Structures*, 41:85– 101, 2004.
- <sup>10</sup>Z. G. Bian, W. Q. Chen, C.W. Lim, and N. Zhang. Analytical solutions for single- and multi-span functionally graded plates in cylindrical bending. *International Journal of Solids and Structures*, 42:6433– 6456, 2005.
- <sup>11</sup>K. P. Soldatos and P. Watson. A method for improving the stress analysis performance of one-and two-dimensional theories for laminated composites. *Acta Mechanica*, 123:163– 186, 1997.
- <sup>12</sup>K. P. Soldatos and P. Watson. Accurate stress analysis of laminated plates combining a two-dimensional theory with the exact three-dimensional solution for simply supported edges. *Mathematics and Mechanics of Solids*, 2:459– 489, 1997.
- <sup>13</sup>D. F. Gilhooley, R. C. Batra, J.R. Xiao, M. A. McCarthy, and J. W. Gillespie Jr. Analysis of thick functionally graded plates by using higher-order shear and normal deformable plate theory and MLPG method with radial basis functions. *Composite Structures*, 80:539– 552, 2007.
- <sup>14</sup>V. L. Berdichevsky. Variational-asymptotic method of constructing a theory of shells. *Journal of Applied Mathematics and Mechanics*, 52:711–736, 1979.
- <sup>15</sup>W. Yu, D.H. Hodges, and V.V. Volovoi. Asymptotic construction of Reissner-like composite plate theory with accurate strain recovery. *International Journal of Solids and Structures*, 39:5185– 5203, 2002.
- <sup>16</sup>W. Yu and D.H. Hodges. A simple thermopiezoelectric model for composite plates with accurate stress recovery. *Smart Materials and Structures*, 13:926– 938, 2004.
- <sup>17</sup>W. Yu. Mathematical construction of a Reissner-Mindlin plate theory for composite laminates. *International Journal of Solids and Structures*, 42:6680– 6699, 2005.
- <sup>18</sup>H. Chen and W. Yu. Postbuckling and mode jumping analysis of composite laminates using an asymptotically correct, geometrically non-linear theory. *International Journal of Non-linear Mechanics*, 41:1143– 1160, 2006.
- <sup>19</sup>L. Liao and W. Yu. Asymptotical construction of a fully coupled, reissner-mindlin model for piezoelectric composite plates. *Smart Materials and Structures*, 17(1), 2008. Article 015010.
- <sup>20</sup>L. Liao and W. Yu. A variational asymptotic model for piezoelectric composite plates with electroded lateral boundaries. *Composite Structures*, 88(3):394–402, 2009.
- <sup>21</sup>D. A. Danielson and D. H. Hodges. Nonlinear beam kinematics by decomposition of the rotation tensor. *Journal of Applied Mechanics*, 54:258– 262, 1987.
- <sup>22</sup>D. A. Danielson. Finite rotation with small strain in beams and plates. In *Proceedings of the 2nd Pan American Congress of Applied Mechanics*, Valparaiso, Chile, January 2 – 4 1991. Valparaiso Chile.

# Assess the Accuracy of the Variational Asymptotic Plate and Shell Analysis (VAPAS) Using the Generalized Unified Formulation (GUF)

Luciano Demasi\*

*San Diego State University, San Diego, California 92182 USA*

Wenbin Yu†

*Utah state University, Logan, Utah 84322-4130 USA*

The accuracy of the Variational Asymptotic Plate and Shell Analysis (VAPAS) is assessed against several higher order, zig zag and layerwise theories generated by using the invariant axiomatic framework denoted as Generalized Unified Formulation (GUF). All the axiomatic and asymptotic theories are also compared against the elasticity solution developed for the case of a sandwich structure with high Face to Core Stiffness Ratio. GUF allows to use an infinite number of axiomatic theories (Equivalent Single Layer theories with or without zig zag effects and Layerwise theories as well) with any combination of orders of the displacements and it is an ideal tool to precisely assess the range of applicability of the Variational Asymptotic Plate and Shell Analysis or other theories in general. In fact, all the axiomatic theories generated by GUF are obtained from the kernels or fundamental nuclei of the Generalized Unified Formulation and changing the order of the variables is “naturally” and systematically done with GUF. It is demonstrated that VAPAS achieves accuracy comparable to a fourth (or higher) order zig-zag theory. The computational advantages of VAPAS are then demonstrated. The differences between the axiomatic Zig-zag models and VAPAS are also assessed. Range of applicability of VAPAS will be discussed in detail and guidelines for new developments based on GUF and VAPAS are provided.

## I. Introduction

### A. Background and Motivation

MOST of the aerospace structures can be analyzed using shell and plate models. Accurate theoretical formulations that minimize the CPU time without penalties on the quality of the results are then of fundamental importance.

The so-called axiomatic models present the advantage that the important physical behaviors of the structures can be modeled using the “intuition” of eminent scientists. The drawback of this approach is that some cases are not adequately modeled because the starting apriori assumptions might fail. Also, each existing approach presents a range of applicability and when the hypotheses used to formulate the theory are no longer valid the approach has to be replaced with another one usually named as “refined theory” or “improved theory”. In the framework of the mechanical case the Classical Plate Theory (CPT), also known as Kirchoff theory<sup>1</sup>, has the advantage of being simple and reliable for thin plates. However, if there is strong anisotropy of the mechanic properties, or if the composite plate is relatively thick, other advanced models such as First-order Shear Deformation Theory (FSDT) are required<sup>2-4</sup>. Higher-order Shear Deformation Theories (HSDT) have also been used<sup>5-7</sup> giving the possibility to increase the accuracy of

---

\*Assistant Professor, Department of Aerospace Engineering & Engineering Mechanics. Member AIAA.

Email: ldemasi@mail.sdsu.edu

†Associate Professor, Department of Mechanical and Aerospace Engineering. Senior Lifetime Member, AIAA; Member, ASME and AHS.

Email: wenbin.yu@usu.edu

numerical evaluations for moderately thick plates. But even these theories are not sufficient if local effects are important or accuracy in the calculation of transverse stresses is sought. Therefore, more advanced plate theories have been developed to include zig-zag effects.<sup>8–19</sup> In some challenging cases the previous type of theories are not sufficiently accurate. Therefore, the so-called Layerwise theories<sup>20–30</sup> have been introduced. In these theories the quantities are layer-dependent and the number of required Degrees of Freedom is much higher than the case of Equivalent Single Layer Models.

The first author introduced an invariant methodology named as Generalized Unified Formulation<sup>31</sup> in which an infinite number of axiomatic models can be included in just one formulation. All the combinations of orders (for example cubic order for the in-plane displacements and parabolic order for the out-of-plane displacement) are possible. Equivalent Single Layer Models (with or without zig-zag effects) and layerwise models can be analyzed. All these formulations derive from the expansion of six  $1 \times 1$  arrays which are invariant with respect to the type of theory (e.g. Equivalent Single Layer or Layerwise) and orders adopted for the displacement variables. This fact makes the Generalized Unified Formulation an ideal tool to test and compare other possible formulations. In particular, this paper assesses the Variational Asymptotic Plate and Shell Analysis (VAPAS) introduced by the second author and compares it with some of the infinite theories that can be generated from the six invariant arrays of the Generalized Unified Formulation. All the results are compared against the elasticity solution developed by the first author. A sandwich plate is analyzed. Different aspect ratios are considered. Different Face to Core Stiffness ratios (FCSRs) are adopted. It is demonstrated that VAPAS gives accurate results at least as a fourth-order axiomatic zig-zag theory but with a much smaller number of Degrees of Freedom. The range of applicability of the various theories generated with GUF and VAPAS is discussed.

## II. Variational Asymptotic Plate and Shell Analysis (VAPAS): Main Concepts

Mathematically, the approximation in the process of constructing a plate theory stems from elimination of the thickness coordinate as an independent variable of the governing equations, a dimensional reduction process. This sort of approximation is inevitable if one wants to take advantage of the relative smallness of the thickness to simplify the analysis. However, other approximations that are not absolutely necessary should be avoided, if at all possible. For example, for geometrically nonlinear analysis of plates, it is reasonable to assume that the thickness,  $h$ , is small compared to the wavelength of deformation of the reference plane,  $l$ . However, it is unnecessary to assume *a priori* some displacement field, although that is the way most plate theories are constructed. As pointed out by Ref. [32], the attraction of *a priori* hypotheses is caused by our inability to extract the necessary information from the 3D energy expression.

According to this line of logic, Yu and his co-workers adopted the variational asymptotic method (VAM),<sup>32</sup> to develop a new approach to modeling composite laminates.<sup>33–36</sup> These models are implemented in a computer program named VAPAS. In this approach, the original 3D anisotropic elasticity problem is first cast in an intrinsic form, so that the theory can accommodate arbitrarily large displacement and global rotation subject only to the strain being small. An energy functional can be constructed for this nonlinear 3D problem in terms of 2D generalized strain measures and warping functions describing the deformation of the transverse normal:

$$\Pi = \Pi(\epsilon_{11}, \epsilon_{12}, \epsilon_{22}, \kappa_{11}, \kappa_{12}, \kappa_{22}, w_1, w_2, w_3) \quad (1)$$

Here  $\epsilon_{11}, \epsilon_{12}, \epsilon_{22}, \kappa_{11}, \kappa_{12}, \kappa_{22}$  are the so-called 2D generalized strains<sup>37</sup> and  $w_1, w_2, w_3$  are unknown 3D warping functions, which characterize the difference between the deformation represented by the 2D variables and the actual 3D deformation for every material point within the plate. It is emphasized here that the warping functions are not assumed *a priori* but are unknown 3D functions to be solved using VAM. Then we can employ VAM to asymptotically expand the 3D energy functional into a series of 2D functionals in terms of the small parameter  $h/l$ , such that

$$\Pi = \Pi_0 + \Pi_1 \frac{h}{l} + \Pi_2 \frac{h^2}{l^2} + o\left(\frac{h^2}{l^2}\right) \quad (2)$$

where  $\Pi_0, \Pi_1, \Pi_2$  are governing functionals for different orders of approximation and are functions of 2D generalized strains and unknown warping functions. The unknown warping functions for each approximation can be obtained in terms of 2D generalized strains corresponding to the stationary points of the functionals, which are one-dimensional (1D) analyses through the thickness. Solutions for the warping functions can be

obtained analytically as shown in Ref. [33] and Ref. [36]. After solving for the unknown warping functions, one can substitute them back into the energy functionals in Eq. (1) to obtain 2D energy functionals for 2D plate analysis. For example, for the zeroth-order approximation, the 2D plate model of VAPAS is of the form

$$\Pi_0 = \Pi_0(\epsilon_{11}, \epsilon_{12}, \epsilon_{22}, \kappa_{11}, \kappa_{12}, \kappa_{22}) \quad (3)$$

It should be noted that the energy functional for the zeroth-order approximation,  $\Pi_0$ , coincides to that of CLT but without invoking the Kirchhoff hypothesis and the transverse normal is flexible during deformation.

Higher-order approximations can be used to construct refined models. For example, the approximation through second order ( $h^2/l^2$ ) should be used to handle transverse shear effects. However, there are two challenging issues associated with the second-order approximation:

- The energy functional asymptotically correct up through the second order is in terms of the CLT generalized strains *and their derivatives*. This form is not convenient for plate analysis because the boundary conditions cannot be readily associated with quantities normally specified on the boundary of plates.
- Only part of the second-order energy corresponds to transverse shear deformation, and no physical interpretation is known for the remaining terms.

VAPAS uses exact kinematical relations between derivatives of the generalized strains of CLT and the transverse shear strains along with equilibrium equations to meet these challenges. Minimization techniques are then applied to find the transverse shear energy that is closest to the asymptotically correct second-order energy. In other words, the loss of accuracy between the asymptotically correct model and a generalized Reissner-Mindlin model is minimized mathematically. For the purpose of establishing a direct connection between 2D Reissner-Mindlin plate finite element analysis, the through-thickness analysis is implemented using a 1D finite element discretization in the computer program VAPAS, which has direct connection with the plate/shell elements in commercial finite element packages and can be conveniently used by application-oriented engineers.

In comparison to most existing composite plate modeling approaches, VAPAS has several unique features:

- VAPAS adopts VAM to rigorously split the original geometrically-exact, nonlinear 3D problem into a linear, 1D, through-the-thickness analysis and a geometrically-exact, nonlinear, 2D, plate analysis. This novel feature allows the global plate analysis to be formulated exactly and intrinsically as a generalized 2D continuum over the reference plane and routes all the approximations into the through-the-thickness analysis, the accuracy of which is guaranteed to be the best by use of the VAM. The optimization procedure minimizes the loss of information in recasting the model to the generalized Reissner-Mindlin form.
- No kinematical assumptions are invoked in the derivation. All deformation of the normal line element is correctly described by the warping functions within the accuracy of the asymptotic approximation.
- VAPAS does not rely on integration of the 3D equilibrium equations through the thickness to obtain accurate distributions of transverse normal and shear strains and stresses.
- VAPAS exactly satisfies all continuity conditions, including those on both displacement and stress, at the interfaces as well as traction conditions on the top and bottom surfaces.

### III. Generalized Unified Formulation: Main Concepts

#### A. Classification of the Theories Obtained Using GUF

The main feature of the Generalized Unified Formulation is that the descriptions of Layerwise Theories, Higher-order Shear Deformation Theories and Zig-Zag Theories of any combination of orders *do not show any formal differences* and can all be obtained from six invariant kernels. So, with just one theoretical model an infinite number of different approaches can be considered. For example, in the case of moderately thick plates a higher order theory could be sufficient but for thick plates layerwise models may be required. With GUF the two approaches are formally identical because the kernels are invariant with respect to the type of

theory.

In the present work the concepts of *type of theory* and *class of theories* are introduced. The following types of displacement-based theories are discussed. The first type is named as Advanced Higher-order Shear Deformation Theories (AHSDT). These theories are Equivalent Single Layer models because the displacement field is unique and independent of the number of layers. The effects of the transverse normal strain  $\varepsilon_{zz}$  are retained.

The second type of theories is named as Advanced Higher-order Shear Deformation Theories with Zig-Zag effects included (AHSDTZ). These theories are Equivalent Single Layer models and the so called Zig-Zag form of the displacements is taken into account by using Murakami's Zig-Zag Function (MZZF). The effects of the transverse normal strain  $\varepsilon_{zz}$  are included. The third type of theories is named Advanced LayerWise Theories (ALWT). These theories are the most accurate ones because all the displacements have a layerwise description. The effects of the transverse normal strain  $\varepsilon_{zz}$  are included as well. These models are necessary when local effects need to be described. The price is of course (in FEM applications) in higher computational time. An infinite number of theories which have a particular logic in the selection of the used orders of expansion is defined as *class of theories*. For example, the infinite layerwise theories which have the displacements  $u_x$ ,  $u_y$  and  $u_z$  expanded along the thickness with a polynomial of order  $N$  are a class of theories. The infinite theories which have the in-plane displacements  $u_x$  and  $u_y$  expanded along the thickness with order  $N$ , the out of plane displacement expanded along the thickness with order  $N - 1$  are another class of theories.

## B. Basic Idea and Theoretical Formulation

Both layerwise and Equivalent Single Layer models are axiomatic approaches if the unknowns are expanded along the thickness by using *a chosen* series of functions.

When the Principal of Virtual Displacements is used, the unknowns are the displacements  $u_x$ ,  $u_y$  and  $u_z$ . When other variational statements are used the unknowns may also be all or some of the stresses and other quantities as well (multifield case).

The Generalized Unified Formulation is introduced here considering a generic layer  $k$  of a multilayered plate structure. This is the most general approach and the Equivalent Single Layer theories, which consider the displacement unknowns to be layer-independent, can be derived from this formulation with some simple formal techniques.<sup>31</sup> Consider a theory denoted as Theory I, in which the displacement in  $x$  direction  $u_x^k$  has

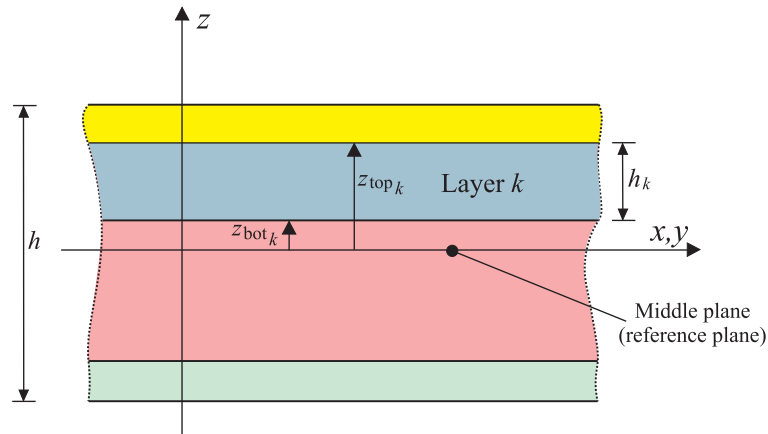


Figure 1. Multilayered plate: notations and definitions.

four Degrees of Freedom. Here by Degrees of Freedom it is intended the number of unknown quantities that are used to expand a variable. In the case under examination four Degrees of Freedom for the displacement  $u_x^k$  means that four unknowns are considered. Each unknown multiplies *a known function* of the thickness coordinate  $z$ . Where the origin of the coordinate  $z$  is measured is not important. However, from a practical point of view it is convenient to assume that the *middle plane* of the plate is also the plane with  $z = 0$ . This assumption does not imply that there is a symmetry with respect to the plane  $z = 0$ . The formulation is general.

For layer  $k$  the following relation holds:  $z_{\text{bot}_k} \leq z \leq z_{\text{top}_k}$ .  $z_{\text{bot}_k}$  is the global coordinate  $z$  of the bottom surface of layer  $k$  and  $z_{\text{top}_k}$  is the global coordinate  $z$  of the top surface of layer  $k$  (see Figure 1).  $h_k = z_{\text{top}_k} - z_{\text{bot}_k}$  is the thickness of layer  $k$  and  $h$  is the thickness of the plate. In the case of Theory I,  $u_x^k$  is expressed as follows:

$$u_x^k(x, y, z) = \underbrace{f_1^k(z)}_{\text{known}} \cdot \underbrace{u_{x_1}^k(x, y)}_{\text{unknown\#1}} + \underbrace{f_2^k(z)}_{\text{known}} \cdot \underbrace{u_{x_2}^k(x, y)}_{\text{unknown\#2}} + \underbrace{f_3^k(z)}_{\text{known}} \cdot \underbrace{u_{x_3}^k(x, y)}_{\text{unknown\#3}} + \underbrace{f_4^k(z)}_{\text{known}} \cdot \underbrace{u_{x_4}^k(x, y)}_{\text{unknown\#4}} \quad z_{\text{bot}_k} \leq z \leq z_{\text{top}_k} \quad (4)$$

The functions  $f_1^k(z)$ ,  $f_2^k(z)$ ,  $f_3^k(z)$  and  $f_4^k(z)$  are *known* functions (axiomatic approach). These functions could be, for example, a series of trigonometric functions of the thickness coordinate  $z$ . Polynomials (or even better orthogonal polynomials) could be selected. In the most general case each layer has different functions. For example,  $f_1^k(z) \neq f_1^{k+1}(z)$ . The next *formal step* is to modify the notation. The following functions are *defined*:

$$\begin{aligned} {}^x F_t^k(z) &= f_1^k(z) & {}^x F_2^k(z) &= f_2^k(z) \\ {}^x F_3^k(z) &= f_3^k(z) & {}^x F_b^k(z) &= f_4^k(z) \end{aligned} \quad (5)$$

The logic behind these definitions is the following. The *first* function  $f_1^k(z)$  is defined as  ${}^x F_t^k$ . Notice the superscript  $x$ . It was added to clarify that the displacement in  $x$  direction,  $u_x^k$ , is under investigation. The subscript  $t$  identifies the quantities at the “top” of the plate and, therefore, are useful in the assembling of the stiffness matrices in the thickness direction (see Ref. [31]).

The *last* function  $f_4^k(z)$  is defined as  ${}^x F_b^k$ . Notice again the superscript  $x$ . The subscript  $b$  means “bottom” and, again, its utility is discussed in Ref. [31].

The intermediate functions  $f_2^k(z)$  and  $f_3^k(z)$  are defined simply as  ${}^x F_2^k$  and  ${}^x F_3^k$ . To be consistent with the definitions of equation 5, the following unknown quantities are *defined*:

$$u_{x_t}^k(x, y) = u_{x_1}^k(x, y) \quad u_{x_b}^k(x, y) = u_{x_4}^k(x, y) \quad (6)$$

Using the definitions reported in equations 5 and 6, equation 4 can be rewritten as

$$u_x^k(x, y, z) = \underbrace{{}^x F_t^k(z)}_{\text{known}} \cdot \underbrace{u_{x_t}^k(x, y)}_{\text{unknown\#1}} + \underbrace{{}^x F_2^k(z)}_{\text{known}} \cdot \underbrace{u_{x_2}^k(x, y)}_{\text{unknown\#2}} + \underbrace{{}^x F_3^k(z)}_{\text{known}} \cdot \underbrace{u_{x_3}^k(x, y)}_{\text{unknown\#3}} + \underbrace{{}^x F_b^k(z)}_{\text{known}} \cdot \underbrace{u_{x_b}^k(x, y)}_{\text{unknown\#4}} \quad z_{\text{bot}_k} \leq z \leq z_{\text{top}_k} \quad (7)$$

It is supposed that each function of  $z$  is a polynomial. The order of the expansion is then 3 and indicated as  $N_{u_x}^k$ . Each layer has in general a different order. Thus, in general  $N_{u_x}^k \neq N_{u_x}^{k+1}$ . If the functions of  $z$  are not polynomials (for example, this is the case if trigonometric functions are used) then  $N_{u_x}^k$  is just a parameter related to the number of terms or Degrees of Freedom used to describe the displacement  $u_x^k$  in the thickness direction. The expression representing the displacement  $u_x^k$  (see equation 7) can be put in a compact form typical of the Generalized Unified Formulation presented here. In particular it is possible to write:

$$u_x^k(x, y, z) = {}^x F_{\alpha_{u_x}}^k(z) \cdot u_{x\alpha_{u_x}}^k(x, y) \quad \alpha_{u_x} = t, l, b; \quad l = 2, \dots, N_{u_x}^k \quad (8)$$

where, in the example,  $N_{u_x}^k = 3$ . The thickness primary master index  $\alpha$  has the subscript  $u_x$ . This subscript from now on will be called *slave index*. It is introduced to show that the displacement  $u_x$  is considered. Figure 2 explains these definitions. Consider another example. Suppose that the displacement  $u_x^k$  of a particular theory is expressed with 3 Degrees of Freedom. In that case it is possible to write:

$$u_x^k(x, y, z) = \underbrace{f_1^k(z)}_{\text{known}} \cdot \underbrace{u_{x_1}^k(x, y)}_{\text{unknown\#1}} + \underbrace{f_2^k(z)}_{\text{known}} \cdot \underbrace{u_{x_2}^k(x, y)}_{\text{unknown\#2}} + \underbrace{f_3^k(z)}_{\text{known}} \cdot \underbrace{u_{x_3}^k(x, y)}_{\text{unknown\#3}} \quad (9)$$

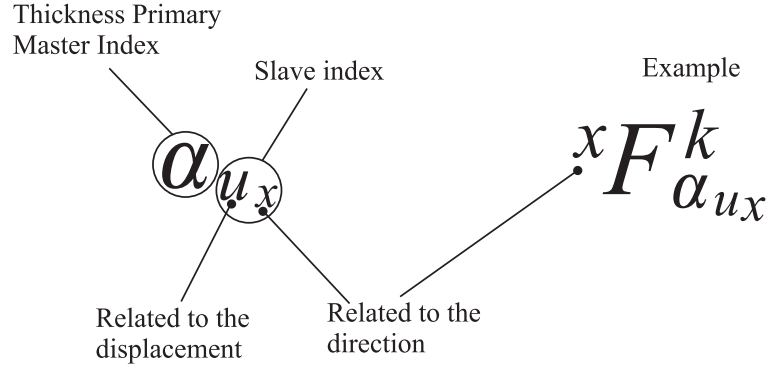


Figure 2. Generalized Unified Formulation. Master and slave indices.

By adopting the definitions earlier used for the case of 4 Degrees of Freedom it is possible to rewrite equation 9 in the following equivalent form:

$$u_x^k(x, y, z) = \underbrace{x F_t^k(z)}_{\text{known}} \cdot \underbrace{u_{x_t}^k(x, y)}_{\text{unknown\#1}} + \underbrace{F_2^k(z)}_{\text{known}} \cdot \underbrace{u_{x_2}^k(x, y)}_{\text{unknown\#2}} + \underbrace{x F_b^k(z)}_{\text{known}} \cdot \underbrace{u_{x_b}^k(x, y)}_{\text{unknown\#3}} \quad (10)$$

which can be put again in the form shown in equation 8 with  $N_{u_x}^k = 2$ . In general  $N_{u_x}^k$  is  $DOF_{u_x}^k - 1$ , where  $DOF_{u_x}^k$  is the number of Degrees of Freedom (at layer level) used for the displacement  $u_x^k$ . In the case of Zig-Zag theories it is possible to demonstrate that  $N_{u_x}^k = DOF_{u_x}^k - 2$  because one Degree of Freedom is used for the Zig-Zag function.

The minimum number of Degrees of Freedom is chosen to be 2. This is a choice used to facilitate the assembling in the thickness direction. In fact, the “top” and “bottom” terms will be always present. In the case in which  $DOF_{u_x}^k = 2$  the Generalized Unified Formulation is simply

$$u_x^k(x, y, z) = x F_{\alpha_{u_x}}^k(z) \cdot u_{x \alpha_{u_x}}^k(x, y) \quad \alpha_{u_x} = t, b \quad (11)$$

In this particular case the “ $l$ ” term of equation 8 is not present.

An *infinite* number of theories can be included in equation 8. It is in fact sufficient to change the value of  $N_{u_x}^k$ . It should be observed that *formally* there is no difference between two distinct theories (obtained by changing  $N_{u_x}^k$ ). It is deduced that  $\infty^1$  theories can be represented by equation 8.

The other displacements  $u_y^k$  and  $u_z^k$  can be treated in a similar fashion. The Generalized Unified Formulation for all the displacements is the following:

$$\begin{aligned} u_x^k &= x F_t u_{x_t}^k + x F_l u_{x_l}^k + x F_b u_{x_b}^k = x F_{\alpha_{u_x}} u_{x \alpha_{u_x}}^k & \alpha_{u_x} = t, l, b; \quad l = 2, \dots, N_{u_x} \\ u_y^k &= y F_t u_{y_t}^k + y F_m u_{y_m}^k + y F_b u_{y_b}^k = y F_{\alpha_{u_y}} u_{y \alpha_{u_y}}^k & \alpha_{u_y} = t, m, b; \quad m = 2, \dots, N_{u_y} \\ u_z^k &= z F_t u_{z_t}^k + z F_n u_{z_n}^k + z F_b u_{z_b}^k = z F_{\alpha_{u_z}} u_{z \alpha_{u_z}}^k & \alpha_{u_z} = t, n, b; \quad n = 2, \dots, N_{u_z} \end{aligned} \quad (12)$$

In equation 12, for simplicity it is assumed that the type of functions is the same for each layer and that the same number of terms is used for each layer. This assumption will make it possible to adopt the same Generalized Unified Formulation for all types of theories, and layerwise and equivalent single layer theories will *not* show formal differences. This concept means, for example, that if displacement  $u_y$  is approximated with five terms in a particular layer  $k$  then it will be approximated with five terms in *all* layers of the multilayered structure.

Each displacement variable can be expanded in  $\infty^1$  combinations. In fact, it is sufficient to change the number of terms used for each variable. Since there are three variables (the displacements  $u_x$ ,  $u_y$  and  $u_z$ ), it is concluded that equation 12 includes  $\infty^3$  different theories. In equation 12 the quantities are defined in a layerwise sense but it can be shown that the same concept is valid for the Equivalent Single Layer cases too (see Ref. [31]).

It can be shown that when a theory generated by using GUF has the orders of the expansions of all the displacements equal to each other, the results are numerically identical to the ones that can be obtained by

using Carrera's Unified Formulation (see Ref. [30]).

### C. Acronyms Used to Identify a Generic Theory Obtained by Using GUF

Three types of displacement-based theories can be obtained. As stated above, the first type is named Advanced Higher-order Shear Deformation Theories (AHSDT). A AHSDT theory with orders of expansion  $N_{u_x}$ ,  $N_{u_y}$  and  $N_{u_z}$  for the displacements  $u_x$ ,  $u_y$  and  $u_z$  respectively, is denoted as  $ED_{N_{u_x}N_{u_y}N_{u_z}}$ . "E" stands for "Equivalent Single Layer" and "D" stands for "Displacement-based" theory.

With similar logic, it is possible to define acronyms for the second type (Advanced Higher-order Shear Deformation Theories with Zig-Zag effects included (AHSDTZ)) and for the third type of theories (Advanced LayerWise Theories (ALWT)). The acronyms are  $EDZ_{N_{u_x}N_{u_y}N_{u_z}}$  and  $LD_{N_{u_x}N_{u_y}N_{u_z}}$  (more details can be found in Ref. [31]). For example, a AHSDTZ theory with cubic orders for all the displacements is indicated as  $EDZ_{333}$  whereas a ALWT theory with parabolic orders for all the displacements is indicated as  $LD_{222}$ .

## IV. Results

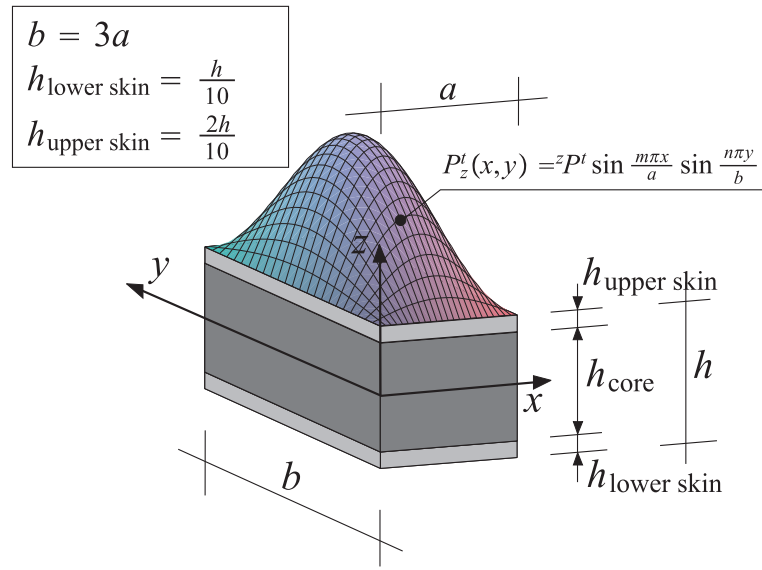


Figure 3. Test Case 2. Geometry of the plate sandwich structure.

The multilayered structure is a sandwich plate (see Figure 3) made of two skins and a core [ $h_{\text{lower skin}} = h/10$ ;  $h_{\text{upper skin}} = 2h/10$ ;  $h_{\text{core}} = (7/10)h$ ]. It is also  $\frac{E_{\text{lower skin}}}{E_{\text{upper skin}}} = 5/4$ . The plate is simply supported and the load is a sinusoidal pressure applied at the top surface of the plate ( $m = n = 1$ ). Different cases are proposed here:

- Face-to-Core Stiffness Ratio =  $FCSR = \frac{E_{\text{lower skin}}}{E_{\text{core}}} = 10^1$ ;  $a/h = 4, 10, 100$
- Face-to-Core Stiffness Ratio =  $FCSR = \frac{E_{\text{lower skin}}}{E_{\text{core}}} = 10^5$ ;  $a/h = 4, 100$

As far as Poisson's ratio is concerned, the following values are used:  $\nu_{\text{lower skin}} = \nu_{\text{upper skin}} = \nu_{\text{core}} = \nu = 0.34$ . In all cases  $b = 3a$ . In this test case there is no symmetry with respect the plane  $z = 0$ . The following

non-dimensional quantities are introduced:

$$\begin{aligned}
\hat{u}_x &= u_x \frac{E_{\text{core}}}{zP^t h \left(\frac{a}{h}\right)^3}; & \hat{u}_y &= u_y \frac{E_{\text{core}}}{zP^t h \left(\frac{a}{h}\right)^3}; & \hat{u}_z &= u_z \frac{100E_{\text{core}}}{zP^t h \left(\frac{a}{h}\right)^4}; \\
\hat{\sigma}_{zx} &= \frac{\sigma_{zx}}{zP^t \left(\frac{a}{h}\right)}; & \hat{\sigma}_{zy} &= \frac{\sigma_{zy}}{zP^t \left(\frac{a}{h}\right)}; & \hat{\sigma}_{zz} &= \frac{\sigma_{zz}}{zP^t}; \\
\hat{\sigma}_{xx} &= \frac{\sigma_{xx}}{zP^t \left(\frac{a}{h}\right)^2}; & \hat{\sigma}_{yy} &= \frac{\sigma_{yy}}{zP^t \left(\frac{a}{h}\right)^2}; & \hat{\sigma}_{xy} &= \frac{\sigma_{xy}}{zP^t \left(\frac{a}{h}\right)^2};
\end{aligned} \tag{13}$$

All the results have been compared with the solution obtained by solving the “exact” problem.<sup>38</sup> The exact value is indicated with the terminology “elasticity” and is the reference value corresponding to the solution of the differential equations that govern the problem. The details of this elasticity solution are here omitted for brevity.

Tables 1 and 2 compare a ALWT, AHSdT, AHSdTz and VAPAS with VAPAS0 denotes the zeroth-order approximation of VAPAS according to Eq. (3). As shown in Table 1, VAPAS0 has a similar prediction for transverse deflection as  $ED_{111}$  for a thick plate ( $a/h = 4$ ) for both  $FCSR = 10$  and  $FCSR = 10^5$ . It is noted that  $ED_{111}$  is very similar to CLT with a flexible transverse normal. For thin plates with mild modulus contrast, VAPAS0 has an accuracy similar to higher-order theories without zigzag effects ( $ED_{444}$ ,  $ED_{555}$ ,  $ED_{777}$ ). For thin plates with big modulus contrast ( $FCSR = 10^5$ ), VAPAS0 has an accuracy similar to  $ED_{444}$ . VAPAS results for the deflection prediction are generally better than VAPAS0 and has an accuracy comparable to higher-order theories with zig-zag effects such as  $EDZ_{444}$  and higher. The only anomaly case is that for thick plates with the big modulus contrast, VAPAS results are not meaningful. This could be explained that VAPAS is not constructed for such an extreme case. Note in Eq. (2), only the geometrical small parameter  $h/a$  is used for the asymptotical expansion, yet for this extreme case, the modulus contrast is a much smaller parameter than  $h/a$ . Hence, it is suggested that VAPAS is not suitable for thick sandwich plates with huge modulus contrast. Note for the sandwich plate with  $a/h = 100$  and  $FCSR = 10^5$ , VAPAS predicts reasonably well. Later we will use more examples to demonstrate that for moderate modulus contrast, VAPAS actually has a very good prediction. Similar observations can be made about the stress prediction as shown in Table 2. It is worthy to point out that VAPAS plate model only uses three DOFs for its zeroth-order approximation and five DOFs for its first-order approximation. The 2D plate element of VAPAS is the same as a FOSDT and is more efficient than all the theories listed in the tables. In other words, VAPAS presents a great compromise between the accuracy of the results and the number of DOFs. Tables 3-11 present a relatively thick sandwich plate with  $FCSR = 10$ . The out-of-plane stresses are not unknowns of the displaced-based theories based on GUF (this is not the case if a mixed variational theorem is used). Therefore, they can be calculated *a posteriori* by using Hooke’s law or by integrating the equilibrium equations. The first approach is usually not satisfactory for ESL theories. Therefore, all the axiomatic results presented in this work report the transverse stresses calculated by integrating the equilibrium equations. In all cases it is possible to see that VAPAS has an accuracy comparable or superior to AHSdTz. For this particular case we tested, VAPAS has a similar accuracy as, or for most cases better, than  $EDZ_{555}$  for displacement prediction and in-plane stress and transverse normal stress prediction and its accuracy is similar to  $LD_{222}$ . For transverse shear stresses, VAPAS predicts similar values as  $EDZ_{555}$ . However, if integration through the thickness is not used to obtain such values,  $ED_{555}$  will be expected to be worse than VAPAS results. For moderate  $FCSR$  values and thick plates ( $a/4 = 4$ , see Figures 4-7, VAPAS presents results that can be comparable of the results obtained by using the axiomatic zig-zag theory  $EDZ_{777}$ . This is particularly evident in figure 7. However, the VAPAS plate model only requires five DOFs, which is only less than 20% of the computational cost one would need for  $EDZ_{777}$  (27 DOFs). It is also noted, VAPAS plate model remains the same as the well-known Reissner-Mindlin elements universally available in all commercial finite element packages.

The Equivalent Single Layer and Layerwise axiomatic theories presented in this paper and a virtually infinite number of other theories can be implemented in a single FEM code based on the Generalized Unified Formulation. Accuracy and CPU time requirements can be easily met with an appropriate selection of the type of theory and the orders used in the expansions of the displacements.

$a/h$	4	100			
		$FCSR = 10^1$			
<i>Elasticity</i>	3.01123	<i>Err.%</i>	1.51021	<i>Err.%</i>	<i>DOF</i>
<i>LD</i> <sub>111</sub>	2.98058	(-1.02)	1.47242	(-2.50)	12
<i>LD</i> <sub>222</sub>	3.00982	(-0.05)	1.51021	(0.00)	21
<i>LD</i> <sub>555</sub>	3.01123	(0.00)	1.51021	(0.00)	48
<i>ED</i> <sub>111</sub>	1.58218	(-47.5)	1.10845	(-26.6)	6
<i>ED</i> <sub>444</sub>	2.79960	(-7.03)	1.50989	(-0.02)	15
<i>ED</i> <sub>555</sub>	2.84978	(-5.36)	1.50996	(-0.02)	18
<i>ED</i> <sub>777</sub>	2.86875	(-4.73)	1.50999	(-0.01)	24
<i>EDZ</i> <sub>111</sub>	2.34412	(-22.2)	1.15866	(-23.3)	9
<i>EDZ</i> <sub>444</sub>	2.97886	(-1.07)	1.51017	(0.00)	18
<i>EDZ</i> <sub>555</sub>	2.98737	(-0.79)	1.51018	(0.00)	21
<i>EDZ</i> <sub>777</sub>	2.99670	(-0.48)	1.51019	(0.00)	27
<i>VAPAS</i> <sub>0</sub>	1.5136	(-49.7)	1.50788	(-0.15)	3
<i>VAPAS</i>	3.0198	(0.28)	1.5102	(0.00)	5
		$FCSR = 10^5$			
<i>Elasticity</i>	$1.31593 \cdot 10^{-02}$	<i>Err.%</i>	$2.08948 \cdot 10^{-03}$	<i>Err.%</i>	
<i>LD</i> <sub>111</sub>	$9.79008 \cdot 10^{-03}$	(-25.6)	$1.96509 \cdot 10^{-03}$	(-5.95)	12
<i>LD</i> <sub>222</sub>	$1.31471 \cdot 10^{-02}$	(-0.09)	$2.08948 \cdot 10^{-03}$	(0.00)	21
<i>LD</i> <sub>555</sub>	$1.31593 \cdot 10^{-02}$	(0.00)	$2.08949 \cdot 10^{-03}$	(0.00)	48
<i>ED</i> <sub>111</sub>	$1.79831 \cdot 10^{-04}$	(-98.6)	$1.19941 \cdot 10^{-04}$	(-94.3)	6
<i>ED</i> <sub>444</sub>	$1.16851 \cdot 10^{-03}$	(-91.1)	$1.64835 \cdot 10^{-04}$	(-92.1)	15
<i>ED</i> <sub>555</sub>	$4.29224 \cdot 10^{-03}$	(-67.4)	$1.73120 \cdot 10^{-04}$	(-91.7)	18
<i>ED</i> <sub>777</sub>	$1.08119 \cdot 10^{-02}$	(-17.8)	$2.96304 \cdot 10^{-04}$	(-85.8)	24
<i>EDZ</i> <sub>111</sub>	$8.36735 \cdot 10^{-04}$	(-93.6)	$1.63329 \cdot 10^{-04}$	(-92.2)	9
<i>EDZ</i> <sub>444</sub>	$1.26288 \cdot 10^{-02}$	(-4.03)	$1.16305 \cdot 10^{-03}$	(-44.3)	18
<i>EDZ</i> <sub>555</sub>	$1.30409 \cdot 10^{-02}$	(-0.90)	$1.78411 \cdot 10^{-03}$	(-14.6)	21
<i>EDZ</i> <sub>777</sub>	$1.31363 \cdot 10^{-02}$	(-0.17)	$2.02060 \cdot 10^{-03}$	(-3.30)	27
<i>VAPAS</i> <sub>0</sub>	$1.6421 \cdot 10^{-04}$	(-98.7)	$1.6314 \cdot 10^{-04}$	(-92.2)	3
<i>VAPAS</i>	1.49076	(> 100)	$2.4667 \cdot 10^{-03}$	(18.0)	5

**Table 1.** Comparison of various theories to evaluate the transverse displacements amplitude (center plate deflection)  $\hat{u}_z = u_z \frac{100E_{\text{core}}}{zP^t h (\frac{a}{h})^4}$  in  $z = z_{\text{bottom}}^{\text{upper skin}} = \frac{3}{10}h$ ,  $x = a/2$ ,  $y = b/2$ .

$a/h$	4	<i>Err.</i>	100	<i>Err.</i>	
$FCSR = 10^1$					
<i>Elasticity</i>	0.32168	<i>Err.</i> %	0.33176	<i>Err.</i> %	<i>DOF</i>
<i>LD</i> <sub>111</sub>	0.31730	(-1.36)	0.32345	(-2.50)	12
<i>LD</i> <sub>222</sub>	0.32142	(-0.08)	0.33176	(0.00)	21
<i>LD</i> <sub>555</sub>	0.32168	(0.00)	0.33176	(0.00)	48
<i>ED</i> <sub>111</sub>	0.33178	(+3.14)	0.33178	(+0.01)	6
<i>ED</i> <sub>444</sub>	0.33240	(+3.33)	0.33178	(+0.01)	15
<i>ED</i> <sub>555</sub>	0.32884	(+2.23)	0.33178	(+0.01)	18
<i>ED</i> <sub>777</sub>	0.32707	(+1.68)	0.33177	(0.00)	24
<i>EDZ</i> <sub>111</sub>	0.34184	(+6.27)	0.34497	(+3.98)	9
<i>EDZ</i> <sub>444</sub>	0.32913	(+2.32)	0.33178	(+0.01)	18
<i>EDZ</i> <sub>555</sub>	0.32755	(+1.82)	0.33177	(0.00)	21
<i>EDZ</i> <sub>777</sub>	0.32530	(+1.12)	0.33177	(+0.00)	27
<i>VAPAS</i> <sub>0</sub>	0.33178	(+3.14)	0.33178	(+0.01)	3
<i>VAPAS</i>	0.31037	(-3.5)	0.33175	(+0.00)	5
$FCSR = 10^5$					
<i>Elasticity</i>	$5.40842 \cdot 10^{-04}$	<i>Err.</i> %	0.27797	<i>Err.</i> %	
<i>LD</i> <sub>111</sub>	$1.05700 \cdot 10^{-04}$	(-80.5)	0.26143	(-5.95)	12
<i>LD</i> <sub>222</sub>	$5.37740 \cdot 10^{-04}$	(-0.57)	0.27797	(0.00)	21
<i>LD</i> <sub>555</sub>	$5.40842 \cdot 10^{-04}$	(0.00)	0.27797	(0.00)	48
<i>ED</i> <sub>111</sub>	0.33242	(> 100)	0.33242	(+19.6)	6
<i>ED</i> <sub>444</sub>	0.30529	(> 100)	0.33238	(+16.6)	15
<i>ED</i> <sub>555</sub>	0.21639	(> 100)	0.33214	(+19.5)	18
<i>ED</i> <sub>777</sub>	$3.96907 \cdot 10^{-02}$	(> 100)	0.32865	(+18.2)	24
<i>EDZ</i> <sub>111</sub>	0.30971	(> 100)	0.33077	(+19.0)	9
<i>EDZ</i> <sub>444</sub>	$6.84336 \cdot 10^{-03}$	(> 100)	0.30392	(+9.34)	18
<i>EDZ</i> <sub>555</sub>	$1.87520 \cdot 10^{-03}$	(> 100)	0.28655	(+3.09)	21
<i>EDZ</i> <sub>777</sub>	$8.02443 \cdot 10^{-04}$	(+48.4)	0.27994	(+0.71)	27
<i>VAPAS</i> <sub>0</sub>	0.33242	(> 100)	0.33242	(+19.6)	3
<i>VAPAS</i>	0.30592	(> 100)	0.33238	(+16.6)	5

**Table 2.** Comparison of various theories to evaluate the transverse shear stress  $\hat{\sigma}_{zx} = \frac{\sigma_{zx}}{zPt(\frac{a}{h})}$  in  $z = z_{\text{bottom}}^{\text{upper skin}} = \frac{3}{10}h$ ,  $x = 0$ ,  $y = b/2$ . The indefinite equilibrium equations have been integrated along the thickness.

$a/h$	10		
	$FCSR = 10^1$		
<i>Elasticity</i>		<i>Err.%</i>	<i>DOF</i>
<i>LD</i> <sub>111</sub>	$-0.11087 \cdot 10^{-01}$	(-2.59)	12
<i>LD</i> <sub>222</sub>	$-0.11085 \cdot 10^{-01}$	(-0.01)	21
<i>LD</i> <sub>333</sub>	$-0.11087 \cdot 10^{-01}$	(-0.00)	30
<i>LD</i> <sub>444</sub>	$-0.11087 \cdot 10^{-01}$	(-0.00)	39
<i>ED</i> <sub>111</sub>	$-0.08627 \cdot 10^{-01}$	(-22.2)	6
<i>ED</i> <sub>222</sub>	$-0.11736 \cdot 10^{-01}$	(+5.85)	9
<i>ED</i> <sub>333</sub>	$-0.11358 \cdot 10^{-01}$	(+2.45)	12
<i>ED</i> <sub>444</sub>	$-0.11316 \cdot 10^{-01}$	(+2.07)	15
<i>ED</i> <sub>555</sub>	$-0.11242 \cdot 10^{-01}$	(+1.40)	18
<i>EDZ</i> <sub>111</sub>	$-0.08696 \cdot 10^{-01}$	(-21.6)	9
<i>EDZ</i> <sub>222</sub>	$-0.11161 \cdot 10^{-01}$	(+0.67)	12
<i>EDZ</i> <sub>333</sub>	$-0.11166 \cdot 10^{-01}$	(+0.71)	15
<i>EDZ</i> <sub>444</sub>	$-0.11164 \cdot 10^{-01}$	(+0.69)	18
<i>EDZ</i> <sub>555</sub>	$-0.11146 \cdot 10^{-01}$	(+0.53)	21
<i>VAPAS</i>	$-0.111009 \cdot 10^{-01}$	(+0.13)	5

**Table 3.** Comparison of various theories to evaluate the in-plane displacement  $\hat{u}_x = u_x \frac{E_{core}}{zP^t h (\frac{a}{h})^3}$  in  $z = z_{bottom}^{upper\ skin} = \frac{3}{10}h$ ,  $x = 0$ ,  $y = b/2$ .

$a/h$	10		
	$FCSR = 10^1$		
<i>Elasticity</i>		<i>Err.%</i>	<i>DOF</i>
<i>LD</i> <sub>111</sub>	$-0.36956 \cdot 10^{-02}$	(-2.59)	12
<i>LD</i> <sub>222</sub>	$-0.36952 \cdot 10^{-02}$	(-0.01)	21
<i>LD</i> <sub>333</sub>	$-0.36956 \cdot 10^{-02}$	(-0.00)	30
<i>LD</i> <sub>444</sub>	$-0.36956 \cdot 10^{-02}$	(-0.00)	39
<i>ED</i> <sub>111</sub>	$-0.28757 \cdot 10^{-02}$	(-22.2)	6
<i>ED</i> <sub>222</sub>	$-0.39120 \cdot 10^{-02}$	(+5.85)	9
<i>ED</i> <sub>333</sub>	$-0.37860 \cdot 10^{-02}$	(+2.45)	12
<i>ED</i> <sub>444</sub>	$-0.37721 \cdot 10^{-02}$	(+2.07)	15
<i>ED</i> <sub>555</sub>	$-0.37473 \cdot 10^{-02}$	(+1.40)	18
<i>EDZ</i> <sub>111</sub>	$-0.28986 \cdot 10^{-02}$	(-21.6)	9
<i>EDZ</i> <sub>222</sub>	$-0.37204 \cdot 10^{-02}$	(+0.67)	12
<i>EDZ</i> <sub>333</sub>	$-0.37220 \cdot 10^{-02}$	(+0.71)	15
<i>EDZ</i> <sub>444</sub>	$-0.37213 \cdot 10^{-02}$	(+0.69)	18
<i>EDZ</i> <sub>555</sub>	$-0.37153 \cdot 10^{-02}$	(+0.53)	21
<i>VAPAS</i>	$-0.37003 \cdot 10^{-02}$	(+0.13)	5

**Table 4.** Comparison of various theories to evaluate the in-plane displacement  $\hat{u}_y = u_y \frac{E_{core}}{zP^t h (\frac{a}{h})^3}$  in  $z = z_{bottom}^{upper\ skin} = \frac{3}{10}h$ ,  $x = a/2$ ,  $y = 0$ .

$a/h$	10		
	$FCSR = 10^1$		
<i>Elasticity</i>		<i>Err.%</i>	<i>DOF</i>
<i>LD</i> <sub>111</sub>	1.74265	(-1.93)	12
<i>LD</i> <sub>222</sub>	1.74247	(-0.01)	21
<i>LD</i> <sub>333</sub>	1.74265	(-0.00)	30
<i>LD</i> <sub>444</sub>	1.74265	(-0.00)	39
<i>ED</i> <sub>111</sub>	1.18207	(-32.2)	6
<i>ED</i> <sub>222</sub>	1.58561	(-9.01)	9
<i>ED</i> <sub>333</sub>	1.70006	(-2.44)	12
<i>ED</i> <sub>444</sub>	1.71032	(-1.85)	15
<i>ED</i> <sub>555</sub>	1.71796	(-1.42)	18
<i>EDZ</i> <sub>111</sub>	1.34741	(-22.7)	9
<i>EDZ</i> <sub>222</sub>	1.73669	(-0.34)	12
<i>EDZ</i> <sub>333</sub>	1.73805	(-0.26)	15
<i>EDZ</i> <sub>444</sub>	1.73836	(-0.25)	18
<i>EDZ</i> <sub>555</sub>	1.73938	(-0.19)	21
<i>VAPAS</i>	1.74265	(+0.00)	5

**Table 5.** Comparison of various theories to evaluate the transverse displacements amplitude (center plate deflection)  $\hat{u}_z = u_z \frac{100E_{core}}{zPt(\frac{a}{h})^4}$  in  $z = z_{bottom}^{upper\ skin} = \frac{3}{10}h$ ,  $x = a/2$ ,  $y = b/2$ .

$a/h$	10		
	$FCSR = 10^1$		
<i>Elasticity</i>		<i>Err.%</i>	<i>DOF</i>
<i>LD</i> <sub>111</sub>	0.33146	(-20.7)	12
<i>LD</i> <sub>222</sub>	0.33169	(+0.07)	21
<i>LD</i> <sub>333</sub>	0.33144	(-0.00)	30
<i>LD</i> <sub>444</sub>	0.33146	(+0.00)	39
<i>ED</i> <sub>111</sub>	0.36049	(+8.76)	6
<i>ED</i> <sub>222</sub>	0.35272	(+6.41)	9
<i>ED</i> <sub>333</sub>	0.34357	(+3.65)	12
<i>ED</i> <sub>444</sub>	0.34649	(+4.54)	15
<i>ED</i> <sub>555</sub>	0.34260	(+3.36)	18
<i>EDZ</i> <sub>111</sub>	0.35807	(+8.03)	9
<i>EDZ</i> <sub>222</sub>	0.32847	(-0.90)	12
<i>EDZ</i> <sub>333</sub>	0.33559	(+1.25)	15
<i>EDZ</i> <sub>444</sub>	0.33753	(+1.83)	18
<i>EDZ</i> <sub>555</sub>	0.33678	(+1.60)	21
<i>VAPAS</i>	0.33364	(+0.66)	5

**Table 6.** Comparison of various theories to evaluate the in-plane normal stress  $\hat{\sigma}_{xx} = \frac{\sigma_{xx}}{zPt(\frac{a}{h})^2}$  in  $z = z_{bottom}^{upper\ skin} = \frac{3}{10}h$ ,  $x = a/2$ ,  $y = b/2$ . Note that this stress is not a continuous function on the thickness direction. Hooke's law has been used.

$a/h$	10		
	$FCSR = 10^1$		
<i>Elasticity</i>		<i>Err.%</i>	<i>DOF</i>
<i>LD</i> <sub>111</sub>	0.08285	(-43.5)	12
<i>LD</i> <sub>222</sub>	0.14688	(+0.17)	21
<i>LD</i> <sub>333</sub>	0.14660	(-0.01)	30
<i>LD</i> <sub>444</sub>	0.14662	(+0.00)	39
<i>ED</i> <sub>111</sub>	0.21666	(+47.8)	6
<i>ED</i> <sub>222</sub>	0.15706	(+7.12)	9
<i>ED</i> <sub>333</sub>	0.15421	(+5.18)	12
<i>ED</i> <sub>444</sub>	0.15783	(+7.64)	15
<i>ED</i> <sub>555</sub>	0.15518	(+5.84)	18
<i>EDZ</i> <sub>111</sub>	0.21309	(+45.3)	9
<i>EDZ</i> <sub>222</sub>	0.14239	(-2.88)	12
<i>EDZ</i> <sub>333</sub>	0.14943	(+1.92)	15
<i>EDZ</i> <sub>444</sub>	0.15141	(+3.27)	18
<i>EDZ</i> <sub>555</sub>	0.15095	(+2.95)	21
<i>VAPAS</i>	0.14758	(+0.65)	5

**Table 7.** Comparison of various theories to evaluate the in-plane normal stress  $\hat{\sigma}_{yy} = \frac{\sigma_{yy}}{zPt(\frac{a}{h})^2}$  in  $z = z_{\text{bottom}}^{\text{upper skin}} = \frac{3}{10}h$ ,  $x = a/2$ ,  $y = b/2$ . Note that this stress is not a continuous function on the thickness direction. Hooke's law has been used.

$a/h$	10		
	$FCSR = 10^1$		
<i>Elasticity</i>		<i>Err.%</i>	<i>DOF</i>
<i>LD</i> <sub>111</sub>	$-0.69314 \cdot 10^{-01}$	(-2.59)	12
<i>LD</i> <sub>222</sub>	$-0.69305 \cdot 10^{-01}$	(-0.01)	21
<i>LD</i> <sub>333</sub>	$-0.69314 \cdot 10^{-01}$	(-0.00)	30
<i>LD</i> <sub>444</sub>	$-0.69314 \cdot 10^{-01}$	(-0.00)	39
<i>ED</i> <sub>111</sub>	$-0.53936 \cdot 10^{-01}$	(-22.2)	6
<i>ED</i> <sub>222</sub>	$-0.73372 \cdot 10^{-01}$	(+5.85)	9
<i>ED</i> <sub>333</sub>	$-0.71010 \cdot 10^{-01}$	(+2.45)	12
<i>ED</i> <sub>444</sub>	$-0.70749 \cdot 10^{-01}$	(+2.07)	15
<i>ED</i> <sub>555</sub>	$-0.70283 \cdot 10^{-01}$	(+1.40)	18
<i>EDZ</i> <sub>111</sub>	$-0.54366 \cdot 10^{-01}$	(-21.6)	9
<i>EDZ</i> <sub>222</sub>	$-0.69779 \cdot 10^{-01}$	(+0.67)	12
<i>EDZ</i> <sub>333</sub>	$-0.69808 \cdot 10^{-01}$	(+0.71)	15
<i>EDZ</i> <sub>444</sub>	$-0.69795 \cdot 10^{-01}$	(+0.69)	18
<i>EDZ</i> <sub>555</sub>	$-0.69684 \cdot 10^{-01}$	(+0.53)	21
<i>VAPAS</i>	$-0.69775 \cdot 10^{-01}$	(+0.67)	5

**Table 8.** Comparison of various theories to evaluate the in-plane shear stress  $\hat{\sigma}_{xy} = \frac{\sigma_{xy}}{zPt(\frac{a}{h})^2}$  in  $z = z_{\text{bottom}}^{\text{upper skin}} = \frac{3}{10}h$ ,  $x = 0$ ,  $y = 0$ . Note that this stress is not a continuous function on the thickness direction. Hooke's law has been used.

$a/h$	10		
	$FCSR = 10^1$		
<i>Elasticity</i>		<i>Err.%</i>	<i>DOF</i>
<i>LD</i> <sub>111</sub>	0.32998	(-2.29)	12
<i>LD</i> <sub>222</sub>	0.32994	(-0.01)	21
<i>LD</i> <sub>333</sub>	0.32998	(-0.00)	30
<i>LD</i> <sub>444</sub>	0.32998	(-0.00)	39
<i>ED</i> <sub>111</sub>	0.33178	(+0.55)	6
<i>ED</i> <sub>222</sub>	0.33210	(+0.64)	9
<i>ED</i> <sub>333</sub>	0.33081	(+0.25)	12
<i>ED</i> <sub>444</sub>	0.33178	(+0.54)	15
<i>ED</i> <sub>555</sub>	0.33117	(+0.36)	18
<i>EDZ</i> <sub>111</sub>	0.34444	(+4.38)	9
<i>EDZ</i> <sub>222</sub>	0.33154	(+0.47)	12
<i>EDZ</i> <sub>333</sub>	0.33140	(+0.43)	15
<i>EDZ</i> <sub>444</sub>	0.33124	(+0.38)	18
<i>EDZ</i> <sub>555</sub>	0.33096	(+0.30)	21
<i>VAPAS</i>	0.32836	(-0.50)	5

**Table 9.** Comparison of various theories to evaluate the transverse shear stress  $\hat{\sigma}_{zx} = \frac{\sigma_{zx}}{zP^t(\frac{a}{h})}$  in  $z = z_{\text{bottom}}^{\text{upper skin}} = \frac{3}{10}h$ ,  $x = 0$ ,  $y = b/2$ . The indefinite equilibrium equations have been integrated along the thickness for all the theories except VAPAS.

$a/h$	10		
	$FCSR = 10^1$		
<i>Elasticity</i>		<i>Err.%</i>	<i>DOF</i>
<i>LD</i> <sub>111</sub>	0.10999	(-2.29)	12
<i>LD</i> <sub>222</sub>	0.10998	(-0.01)	21
<i>LD</i> <sub>333</sub>	0.10999	(-0.00)	30
<i>LD</i> <sub>444</sub>	0.10999	(-0.00)	39
<i>ED</i> <sub>111</sub>	0.11059	(+0.55)	6
<i>ED</i> <sub>222</sub>	0.11070	(+0.64)	9
<i>ED</i> <sub>333</sub>	0.11027	(+0.25)	12
<i>ED</i> <sub>444</sub>	0.11059	(+0.54)	15
<i>ED</i> <sub>555</sub>	0.11039	(+0.36)	18
<i>EDZ</i> <sub>111</sub>	0.11481	(+4.38)	9
<i>EDZ</i> <sub>222</sub>	0.11051	(+0.47)	12
<i>EDZ</i> <sub>333</sub>	0.11047	(+0.43)	15
<i>EDZ</i> <sub>444</sub>	0.11041	(+0.38)	18
<i>EDZ</i> <sub>555</sub>	0.11032	(+0.30)	21
<i>VAPAS</i>	0.10945	(-0.49)	5

**Table 10.** Comparison of various theories to evaluate the transverse shear stress  $\hat{\sigma}_{zy} = \frac{\sigma_{zy}}{zP^t(\frac{a}{h})}$  in  $z = z_{\text{bottom}}^{\text{upper skin}} = \frac{3}{10}h$ ,  $x = a/2$ ,  $y = 0$ . The indefinite equilibrium equations have been integrated along the thickness for all the theories except VAPAS.

$a/h$	10		
	$FCSR = 10^1$		
<i>Elasticity</i>		<i>Err.%</i>	<i>DOF</i>
$LD_{111}$	0.87081	(-0.17)	12
$LD_{222}$	0.87233	(+0.00)	21
$LD_{333}$	0.87231	(+0.00)	30
$LD_{444}$	0.87231	(-0.00)	39
$ED_{111}$	0.51236	(-41.3)	6
$ED_{222}$	0.58831	(-32.6)	9
$ED_{333}$	0.77221	(-11.5)	12
$ED_{444}$	0.78478	(-10.0)	15
$ED_{555}$	0.81517	(-6.55)	18
$EDZ_{111}$	0.51803	(-40.6)	9
$EDZ_{222}$	0.83586	(-4.18)	12
$EDZ_{333}$	0.83769	(-3.97)	15
$EDZ_{444}$	0.83847	(-3.88)	18
$EDZ_{555}$	0.84631	(-2.98)	21
<i>VAPAS</i>	0.87354	(+0.14)	5

Table 11. Comparison of various theories to evaluate the transverse normal stress  $\hat{\sigma}_{zz} = \frac{\sigma_{zz}}{zPt}$  in  $z = z_{\text{bottom}}^{\text{upper skin}} = \frac{3}{10}h$ ,  $x = a/2$ ,  $y = b/2$ . The indefinite equilibrium equations have been integrated along the thickness for all the theories except VAPAS.

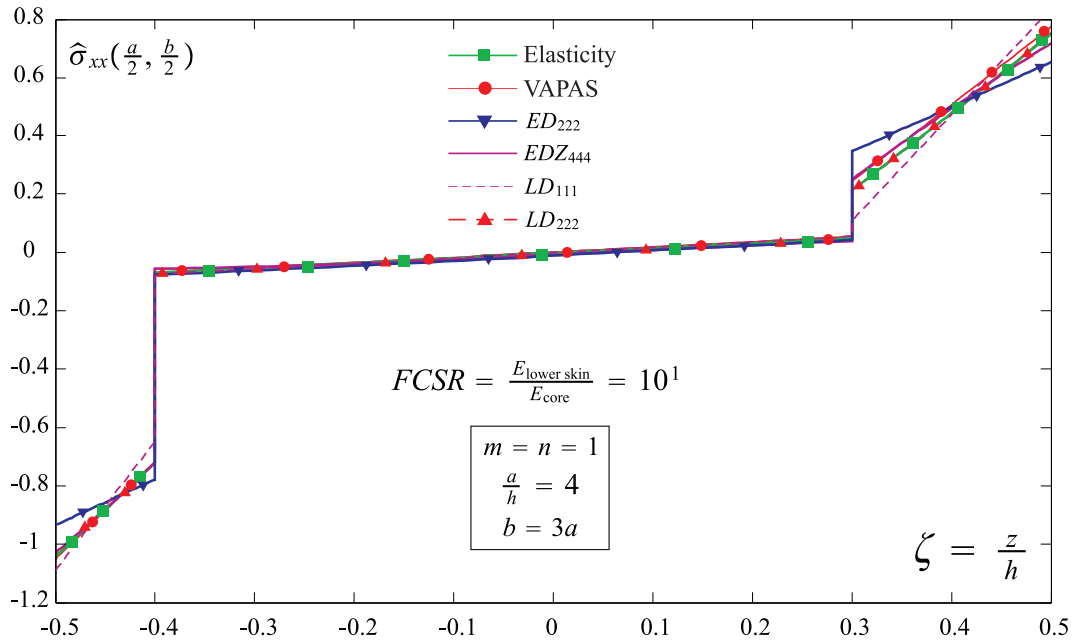


Figure 4. Comparison of various theories to evaluate the in-plane normal stress  $\hat{\sigma}_{xx} = \frac{\sigma_{xx}}{zPt(\frac{a}{h})^2}$  in  $x = a/2$ ,  $y = b/2$ . Note that this stress is not a continuous function on the thickness direction. Hooke's law has been used.

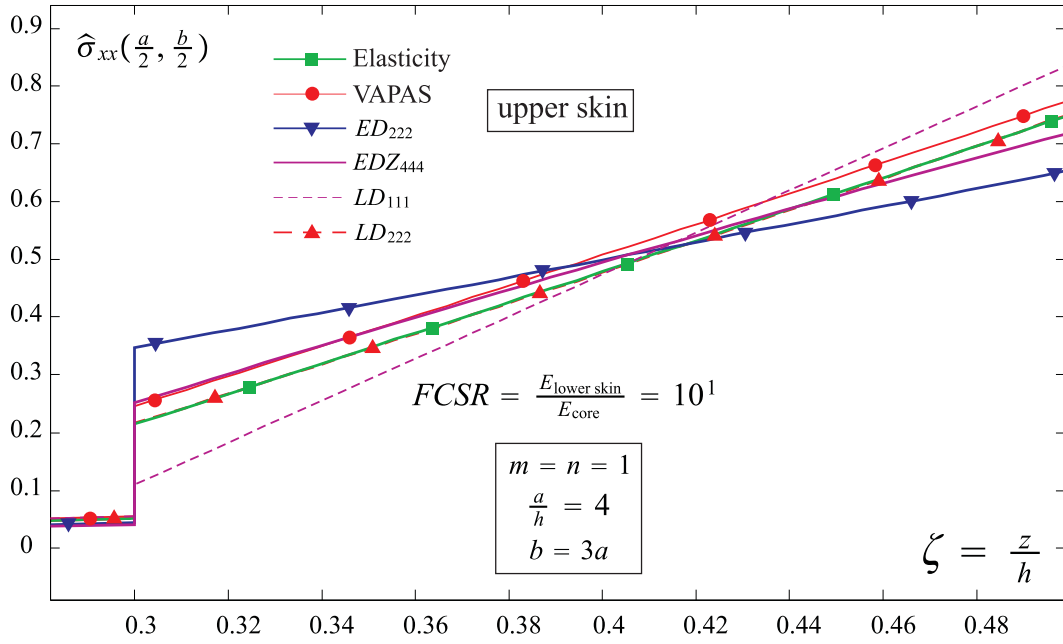


Figure 5. Comparison of various theories to evaluate the in-plane normal stress  $\hat{\sigma}_{xx} = \frac{\sigma_{xx}}{zPt(\frac{a}{h})^2}$  in  $x = a/2$ ,  $y = b/2$  (upper-skin). Hooke's law has been used.

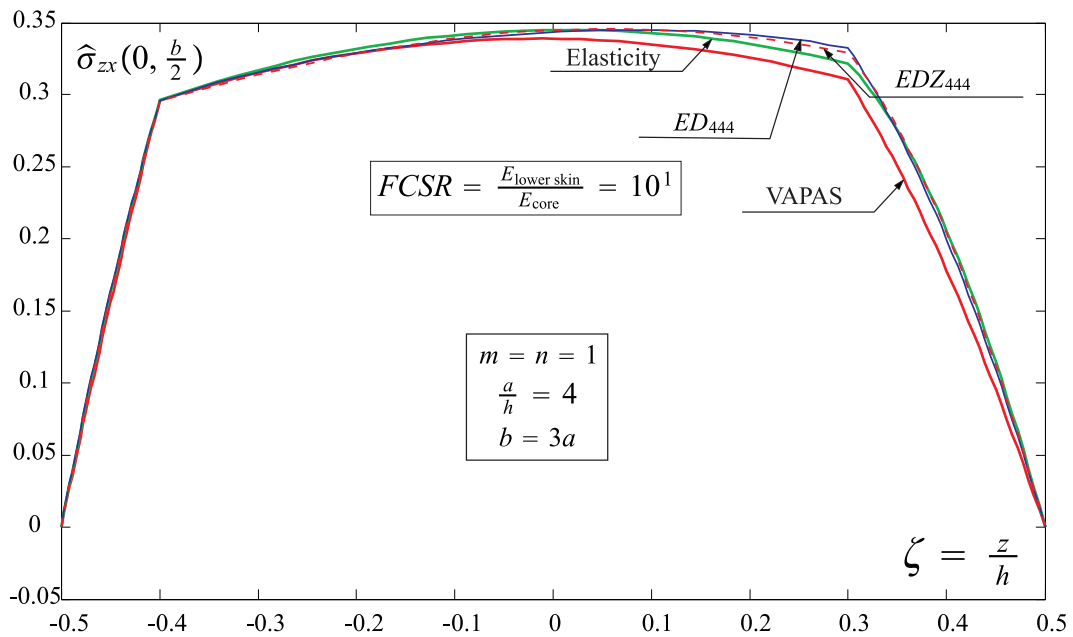


Figure 6. Comparison of various theories to evaluate the transverse shear stress  $\hat{\sigma}_{zx} = \frac{\sigma_{zx}}{zPt(\frac{a}{h})}$  in  $x = 0$ ,  $y = b/2$ . The indefinite equilibrium equations have been integrated along the thickness.

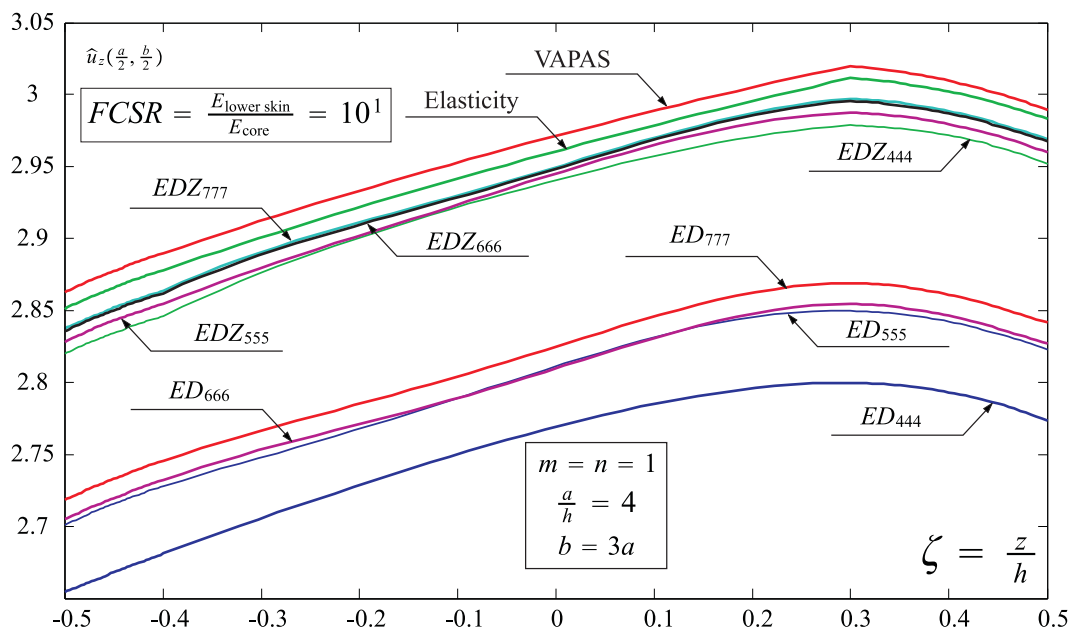


Figure 7. Comparison of various theories to evaluate the transverse displacements amplitude (center plate deflection)  $\hat{u}_z = u_z \frac{100 E_{\text{core}}}{z P t h (\frac{a}{h})^4}$  in  $x = a/2, y = b/2$ .

## V. Conclusion

The accuracy of the Variational Asymptotic Plate and Shell Analysis (VAPAS) is assessed against several higher order, zig zag and layerwise theories generated by using the invariant axiomatic framework denoted as Generalized Unified Formulation (GUF). Both the axiomatic models generated by GUF and VAPAS are also compared against the elasticity solution developed for the case of a sandwich structure with high Face to Core Stiffness Ratio. It has been shown that the fact that GUF allows to use an infinite number of axiomatic theories (Equivalent Single Layer theories with or without zig zag effects and Layerwise theories as well) with any combination of orders of the displacements provides an ideal tool to precisely assess the range of applicability of the Variational Asymptotic Plate and Shell Analysis or other theories in general. It is demonstrated that VAPAS achieves accuracy comparable to a fourth (or higher) order zig-zag theory or lower-order layerwise theories, while the plate model uses the least number degrees of freedom. Hence, in comparison to the axiomatic theories, VAPAS has achieved an excellent compromise between accuracy and efficiency. Except for extreme cases of thick sandwich with huge modulus contrast, VAPAS can be used as an effective alternative to avoid expensive 3D finite element analysis for design and analysis of composite laminated plates.

GUF can be implemented in a single FEM code and can generate a virtually infinite number of theories with accuracy that range from the low-order equivalent single-layer to the high-order layerwise theories and is the ideal tool for comparisons and assessments of different theories or for the creation of adaptive structural codes in optimization and probabilistic studies.

## Acknowledgements

The first author acknowledges the support by San Diego State University (University Grant Program).

The second author acknowledges the support by the Air Force Office of Scientific Research under Grant FA9550-08-1-0405. The program manager is Dr. Victor Giurgiutiu. The views and conclusions contained herein are those of the authors and should not be interpreted as necessarily representing the official policies or endorsement, either expressed or implied, of the funding agencies.

## References

- <sup>1</sup>Kirchhoff, G., "Über das Gleichgewicht und die Bewegung einer elastischen Scheibe," *J. Angew. Math.*, Vol. 40, 1850, pp. 51 – 88.
- <sup>2</sup>Reissner, E., "The effect of transverse shear deformation on the bending of elastic plates," *Journal of Applied Mechanics*, Vol. 12, 1945, pp. 69 – 76.
- <sup>3</sup>Mindlin, R., "Influence of rotatory inertia and shear in flexural motion of isotropic elastic plates," *Journal of Applied Mechanics*, Vol. 18, 1951, pp. 1031 – 1036.
- <sup>4</sup>Kärger, L., Wetzel, A., Rolfes, R., and Rohwer, K., "A three-layered sandwich element with improved transverse shear stiffness and stress based on FSDT," *Computers and Structures*, Vol. 84, No. 13-14, 2006, pp. 843 – 854.
- <sup>5</sup>Swaminathan, K. and Patil, S. S., "Analytical solutions using higher order refined computational model with 12 degrees of freedom for the free vibration analysis of antisymmetric angle-ply plates," *Composite Structures*, 2007, doi: 10.1016/j.compstruct.2007.01.001.
- <sup>6</sup>Kant, T. and Swaminathan, K., "Free vibration of isotropic, orthotropic, and multilayer plates based on higher order refined theories," *Journal of Sound and Vibration*, Vol. 241, No. 2, 2001, pp. 319–327.
- <sup>7</sup>Zhen, W., Cheung, Y. K., Lo, S. H., and Wanji, C., "Effects of higher-order global-local shear deformations on bending, vibration and buckling of multilayered plates," *Composite Structures*, 2007, DOI: 10.1016/j.compstruct.2007.01.017.
- <sup>8</sup>Murakami, H., "Laminated composite plate theory with improved in-plane response," *Journal of Applied Mechanics*, Vol. 53, 1986, pp. 661–666.
- <sup>9</sup>Lekhnitskii, S. G., "Strength calculation of composite beams," *Vestnik inzhener i tekhnikov*, Vol. 9, 1935.
- <sup>10</sup>Ambartsumian, S. A., "On a theory of bending of anisotropic plates," *Investiia Akad Nauk SSSR, Ot Tekh Nauk*, Vol. 4, 1958.
- <sup>11</sup>Ambartsumian, S. A., "On a general theory of anisotropic shells," *Prikl. Mat. Mekh.*, Vol. 22, No. 2, 1958, pp. 226–237.
- <sup>12</sup>Ambartsumian, S. A., "Analysis of two-layer orthotropic shells," *Investiia Akad Nauk SSSR, Ot Tekh Nauk*, Vol. 7, 1957.
- <sup>13</sup>Ambartsumian, S. A., "Two analysis method for two-layer orthotropic shells," *Izv An Arm SSR Seiya Fiz-Matem nauk*, Vol. X, No. 2, 1957.
- <sup>14</sup>Ren, J. G., "A new theory of laminated plates," *Compos. Sci. Technol.*, Vol. 26, 1986, pp. 225–239.
- <sup>15</sup>Ren, J., "Bending theory of laminated plates," *Compos. Sci. Technol.*, Vol. 27, 1986, pp. 225–248.
- <sup>16</sup>Demasi, L., "Refined multilayered plate elements based on Murakami zig-zag functions," *Composite Structures*, Vol. 70, 2005, pp. 308–16.
- <sup>17</sup>Carrera, E., "Historical review of Zig-Zag theories for multilayered plates and shells," *App Mech Rev*, Vol. 56, No. 3, 2003.
- <sup>18</sup>Librescu, L., "Improved linear theory of elastic anisotropic multilayered shells. Part I," *Polymer Mechanics (translated from Russian)*, Vol. 11, No. 6, 1975.
- <sup>19</sup>Fares, M. E. and Elmarghany, M. K., "A refined zigzag nonlinear first-order shear deformation theory of composite laminated plates," *Composite Structures*, 2007, doi: 10.1016/j.compstruct.2006.12.007.
- <sup>20</sup>Cho, K., Bert, C., and Striz, A., "Free vibrations of laminated rectangular plates analyzed by higher order individual-layer theory," *Journal of Sound and Vibration*, Vol. 145, 1991, pp. 429–442.
- <sup>21</sup>Nosier, A., Kapania, R., and Reddy, J. N., "Free vibration analysis of laminated plates using a layer-wise theory," *AIAA Journal*, 1993, pp. 2335–2346.
- <sup>22</sup>Robbins, D. and Reddy, J. N., "Modelling of thick composites using a layerwise laminate theory," *International Journal for Numerical Methods in Engineering*, Vol. 36, No. 4, 1993, pp. 655–677.
- <sup>23</sup>Reddy, J. N., "Mechanics of Laminated Composite Plates, Theory and Analysis," (2nd edn), CRC Press.: Boca Raton, London, New York, Washington, D. C., 2004.
- <sup>24</sup>Carrera, E., "Mixed Layer-Wise Models for Multilayered Plates Analysis," *Composite Structures*, Vol. 43, No. 1, 1998, pp. 57–70.
- <sup>25</sup>Carrera, E., "Evaluation of Layer-Wise Mixed Theories for Laminated Plates Analysis," *American Institute of Aeronautics and Astronautics Journal*, Vol. 26, No. 5, 1998, pp. 830–839.
- <sup>26</sup>Carrera, E., "Layer-Wise Mixed Theories for Accurate Vibration Analysis of Multilayered Plates," *Journal of Applied Mechanics*, Vol. 6, No. 4, 1998, pp. 820–828.
- <sup>27</sup>Tahani, M., "Analysis of laminated composite beams using layerwise displacement theories," *Composite Structures*, Vol. 79, 2007, pp. 535–547.
- <sup>28</sup>Gaudenzi, P., Barboni, R., and Mannini, A., "A finite element evaluation of single-layer and multi-layer theories for the analysis of laminated plates," *Composite Structures*, Vol. 30, 1995, pp. 427–440.
- <sup>29</sup>Reddy, J. N., "An evaluation of equivalent single layer and layerwise theories of composite laminates," *Composite Structures*, Vol. 25, 1993, pp. 21–35.
- <sup>30</sup>Carrera, E., "Theories and Finite Elements for Multilayered Plates and Shells: A Unified Compact Formulation with Numerical Assessment and Benchmarking," *Archives of Computational Methods in Engineering*, Vol. 10, No. 3, 2003, pp. 215–296.
- <sup>31</sup>Demasi, L., "An Invariant Model for any Composite Plate Theory and FEM applications: the Generalized Unified Formulation," *50th AIAA/ASME/ASCE/AHS/ASC structures, Structural Dynamics, and Materials Conference, Palm Springs, California, 4-7 May, 2009*.
- <sup>32</sup>Berdichevsky, V. L., "Variational-asymptotic method of constructing a theory of shells," *PMM*, Vol. 43, No. 4, 1979, pp. 664 – 687.
- <sup>33</sup>Yu, W., Hodges, D. H., and Volovoi, V. V., "Asymptotic construction of Reissner-like models for composite plates with accurate strain recovery," *International Journal of Solids and Structures*, Vol. 39, No. 20, 2002, pp. 5185 – 5203.

<sup>34</sup>Yu, W., Hodges, D. H., and Volovoi, V. V., “Asymptotically accurate 3-D recovery from Reissner-like composite plate finite elements,” *Computers and Structures*, Vol. 81, No. 7, 2003, pp. 439 – 454.

<sup>35</sup>Yu, W. and Hodges, D. H., “An asymptotic approach for thermoelastic analysis of laminated composite plates,” *Journal of Engineering Mechanics*, Vol. 130, No. 5, 2004, pp. 531 – 540.

<sup>36</sup>Yu, W., “Mathematical Construction of a Reissner-Mindlin Plate Theory for Composite Laminates,” *International Journal of Solids and Structures*, Vol. 42, 2005, pp. 6680–6699.

<sup>37</sup>Hodges, D. H., Atilgan, A. R., and Danielson, D. A., “A Geometrically Nonlinear Theory of Elastic Plates,” *Journal of Applied Mechanics*, Vol. 60, No. 1, March 1993, pp. 109 – 116.

<sup>38</sup>Demasi, L., “2D, Quasi 3D and 3D Exact Solutions for Bending of Thick and Thin Sandwich Plates,” *Journal of Sandwich Structures & Materials*, Vol. 10, No. 4, 2008, pp. 271–310.

# Asymptotical Construction of Geometrically Nonlinear Plate Model for Functionally Graded Magneto-Electro-Elastic Laminates

Hui Chen\*

and

Wenbin Yu†

*Utah State University, Logan, Utah 84322-4130*

This paper aims at constructing a geometrically nonlinear model using the variational asymptotic method for analyzing magneto-electro-elastic composite laminates. By taking advantage of the inherent small parameter characterized by the ratio of the thickness to the in-plane dimension of the plate, we systematically reduced the original multiphysically coupled three-dimensional model to a series of two-dimensional plate models. A companion one-dimensional through-the-thickness analysis provides the necessary constitutive models needed for the plate analysis. For practical uses, we also fit the asymptotically correct second-order electromagnetic enthalpy into a generalized Reissner-Mindlin model. The three-dimensional displacement/strain/stress fields as well as the electric/magnetic potentials and fluxes of the plate are obtained through recovery relations of the one-dimensional through-the-thickness analysis. Without introducing any *a priori* kinematic, electric, or magnetic assumptions in the derivation, the present plate model is rigorously derived to capture geometrical nonlinearity and is valid for large deformations and global rotations. The efficiency and the accuracy of the proposed method has been validated by comparing results with three-dimensional exact solutions for several problems featuring electromagnetic and elastic coupling.

## Introduction

As an analogy with the exhibition of electromechanical coupling by piezoelectric materials, magnetic materials respond to an externally applied magnetic field ( $H$ ) by exhibiting a shape change which is known as magnetostriction, demonstrating the Joule effect. On the other hand, these magnetic materials also demonstrate the Villari effect indicated by changing their magnetization and consequently the magnetic induction ( $B$ ) in response to the applied stress. Moreover, for composites containing piezoelectric phases and piezomagnetic phases there exists a magnetoelectric coupling effect. This capability of interactive transfer of magnetic, electric and mechanical energies from one type to another, has received considerable and increasing attentions for developing smart or active structures.<sup>1-4</sup> Application of this kind of smart composite materials spans from electronic package materials, magneto-electric-mechanical actuators and transducers, coil-less magnetic force control devices, to nuclear fusion reactor components. The new concept of multifunctional materials/structures featuring interactive elastic, electric, and magnetic fields is also likely to bring a new dimension to the development of advanced light-weighted multi-functional aerospace structures with many critical thin-walled components taking the form of beams, plates, shells, and stiffened panels.

The promising application of piezoelectric and piezomagnetic composites makes it imperative to develop new methods and analysis tools for better understanding the mechanisms and behavior of such structures which are under interactive actions among mechanical, electric and magnetic fields. Recently, increasing

---

\*Research Associate, Department of Mechanical and Aerospace Engineering. Member, AIAA and ASME.

†Associate Professor, Department of Mechanical and Aerospace Engineering. Senior Member, AIAA; Member, ASME and AHS.

researches have been started on studying static and dynamic behavior of smart plates. Various forms of constitutive equations for magneto-electro-elastic solids were derived in Ref. [5]. Pan et. al. developed a series of three-dimensional (3D) exact benchmark solutions to analyze the static behavior of multilayered anisotropic piezoelectric and piezomagnetic composite plates under cylindrical bending and simply supported boundary conditions.<sup>6-8</sup> These solutions are highly valuable for illustrating the complicated multiphysics nature of the interactive fields, however, they are restricted to a few specific problems with idealized material types, geometry and boundary conditions.

To overcome this limitation, a number of more generalized methods have been developed to explore the 3D behavior of the magnetoelectroelastic laminates. Most of these methods are constructed from the layerwise or discrete-layer laminate theory, utilizing various approximations to split the through-thickness behavior and the planar behavior of the laminate into separate functions. In Refs. [9,10], Heyliger et. al. use an approximate discrete-layer model to investigate the through-thickness variation of the elastic, electric, and magnetic fields of laminates composed of elastic, piezoelectric, and magnetostrictive layers. Semi-analytical approximation solutions to the weak form of the governing equations of equilibrium, charge, and magnetic flux are obtained for infinitely long laminates under cylindrical bending and rectangular laminates with arbitrary edge boundary conditions. By using a state space formulation, Chen and Lee constructed an alternative solution approach to investigate the nonhomogeneous magnetoelectric plates, where elastic displacements and electric/magnetic potentials as well as the transverse stresses, electric displacement, and magnetic flux are introduced as state variables.<sup>11</sup> Methods based upon the combination of layerwise plate theory with finite element method (FEM) have also been used to analyze the linear static and dynamic performance of multilayer smart plates. Examples include a layerwise FEM for analyzing piezoelectric composite plates<sup>12</sup> and a quasi-analytical through-thickness FEM for functionally graded magneto-electric-elastic plates.<sup>13</sup> In contrast to the classical FEM based on the principle of virtual displacements, layerwise mixed finite element formulation is built on Reissner mixed variational theorem (RMVT), where transverse stress assumptions are made in the framework of RMVT and the resulting finite elements describes *a priori* interlaminar continuous transverse shear and normal stresses. A detailed review on Reissner variational principle can be found in Ref. [14]. Recently, the layerwise mixed finite element formulation has been extended to analyze coupled magneto-electro-elastic problems. Related work has been reported for a partially mixed finite element formulation<sup>15</sup> and a layerwise modelling of magneto-electro-elastic plates.<sup>16</sup> To avoid the computational cost and complexity associated layerwise approaches, various simplified plate models have been developed to model smart plates. A simplified plate model based on the third-order shear-deformation theory (TOSDT) is developed to model the piezoelectric composite laminates.<sup>17</sup> Mitchell and Reddy presented a hybrid plate formulation for piezoelectric composite laminates, where an equivalent single-layer TOSDT is used for the mechanical displacement field and the electric potential is modeled using a layerwise discretization in the thickness direction.<sup>18</sup> Plane stress assumption is adopted during the modeling. Because results obtained by these two methods are only compared with those of the classical plate theory (CPT) and/or the first-order shear-deformation theory (FOSDT), their accuracy cannot be determined without extensive 3D validations. In Ref.[19], an analytic solution is developed for cylindrical bending of a piezoelectric laminate with elastic displacement terms being assumed taking the form of TOSDT and the electric potential being obtained by solving a second order differential equation. More complicated models have been developed for nonlinear dynamic analysis. By combining CPT with an energy-based statistical magnomechanical model, Datta et. al. studied the nonlinear dynamical response of a unimorph structure having a magnetostrictive iron-gallium patch to a non-magnetic aluminum substrate.<sup>20</sup> Several underlying assumptions were made on the total energy function as well as kinematic relations. Hasanyan et. al. have developed a geometrically nonlinear model for fully coupled magneto-thermo-elastic kinetics of laminated composite plates, with its kinematic relations constructed by the injection of the FOSDT with von-Kármán strain definition.<sup>21</sup> Despite of successfulness of the aforementioned simplified plate models in analyzing many multi-physically coupled plate problems, these approaches have two major disadvantages: (1) *a priori* assumptions on kinematics and the electromagnetic potentials introduced by these methods are naturally extended from the analysis of isotropic homogeneous elastic problems. They may not be justified for the multiphysically coupled, heterogeneous, and anisotropic structures; (2) it is difficult for an analyst to determine the accuracy of the result and which assumption should be chosen for efficient yet accurate analysis of a particular problem.

Recently, based on the variational asymptotic method (VAM), the authors and their co-workers have developed a series of rigorous Reissner-Mindlin plate models for heterogeneous and anisotropic functionally graded composite laminates and piezoelectric plates.<sup>22-26</sup> These models have been proven to have excellent

compromise between the efficiency and accuracy. In the present research, we extend our previous work to asymptotically construct a geometrical nonlinear plate model for smart composite laminates under the interactive actions of magneto-electric-elastic fields. Taking advantage of the small parameter  $h/l$  (with  $h$  denoting the thickness of the plate and  $l$  denoting the characteristic wavelength of the plate deformation), the 3D multiphysically coupled magneto-electric-elastic coupled problem is systematically reduced using VAM, resulting in a series of efficient high-fidelity 2D models asymptotically correct to different orders of  $h/l$ . The original 3D magneto-electric-elastic problem is then cast in an intrinsic form so that the theory can accommodate arbitrary large deformation and global rotation with the restriction that the strains are small. No *a priori* assumptions on the kinematics or electric or magnetic variables have been invoked. Continuity for primary variables such as elastic displacements, electric and magnetic potentials as well as for the secondary variables like transverse stresses, transverse electric displacement, and transverse magnetic induction are automatically satisfied in this model.

### Three-dimensional Formulation

The dynamic behavior of smart composite laminates is governed by the extended Hamilton principle:

$$\int_{t_1}^{t_2} [\delta(\mathcal{K} - \mathcal{U}) + \overline{\delta\mathcal{W}}] dt = 0, \quad (1)$$

where  $t_1$  and  $t_2$  are arbitrary fixed times,  $\mathcal{K}$  is the kinetic energy,  $\mathcal{U}$  is a term related with the total internal potential energy, and  $\overline{\delta\mathcal{W}}$  represents the virtual work of the applied loads, electric charge, and magnetic induction. The overbar is used to indicate that the virtual work  $\overline{\delta\mathcal{W}}$  does not necessarily represent the variation of a functional  $\mathcal{W}$ . For a smart composite plate made of piezoelectric and piezomagnetic materials,  $\mathcal{U}$  turns out to be the electromagnetic enthalpy which contains contributions from mechanical, electric, and magnetic fields and the coupling effect between them.

$$\mathcal{U} = \frac{1}{2} \int_{\mathcal{V}} \left( \boldsymbol{\Gamma} : \mathbf{C}^{E,H} : \boldsymbol{\Gamma} - \mathbf{E} \cdot \boldsymbol{\varepsilon}_d^{\Gamma,H} \cdot \mathbf{E} - \mathbf{H} \cdot \boldsymbol{\mu}^{\Gamma,E} \cdot \mathbf{H} - 2\mathbf{E} \cdot \mathbf{e}^H : \boldsymbol{\Gamma} - 2\mathbf{H} \cdot \mathbf{q}^E : \boldsymbol{\Gamma} - 2\mathbf{E} \cdot \boldsymbol{\alpha}^{\Gamma} \cdot \mathbf{H} \right) d\mathcal{V} \quad (2)$$

where  $\boldsymbol{\Gamma}$ ,  $\mathbf{E}$  and  $\mathbf{H}$  are the strain, electric field and magnetic field tensors, respectively;  $\mathbf{e}^H$ ,  $\mathbf{q}^E$ , and  $\boldsymbol{\alpha}^{\Gamma}$  are piezoelectric tensor (measured at constant magnetic field), piezomagnetic tensor (measured at constant electric field), and magnetoelectric tensor (measured at constant strain), respectively;  $\mathbf{C}^{E,H}$ ,  $\boldsymbol{\varepsilon}_d^{\Gamma,H}$ ,  $\boldsymbol{\mu}^{\Gamma,E}$  are elastic tensor (measured at constant electric and magnetic field), dielectric tensor (measured at constant strain and magnetic field), magnetic permeability tensor (measured at constant strain and electric field), respectively;  $\mathcal{V}$  is the space occupied by the structure.

It is worth noting that although the above equation refers directly to piezoelectric and piezomagnetic structures, the present formulation is equally applicable to smart structures made of other smart materials characterized by a constitutive model with the same mathematical structure as Eq. (2).

A point in the plate can be described by its Cartesian coordinates  $x_i$ , see Figure 1, where  $x_\alpha$  are two orthogonal lines in the reference surface and  $x_3$  is the normal coordinate originating from the middle of the thickness. Throughout the analysis, Greek indices assume values 1 and 2 while Latin indices assume 1, 2, and 3; repeated indices are summed over their range except where explicitly indicated. Letting  $\mathbf{b}_i$  denote the unit vector along  $x_i$  for the undeformed plate, we can then describe the position of any material point in the undeformed configuration by its position vector  $\hat{\mathbf{r}}$  from a fixed point  $O$ , such that

$$\hat{\mathbf{r}}(x_1, x_2, x_3, t) = \mathbf{r}(x_1, x_2, t) + x_3 \mathbf{b}_3, \quad (3)$$

where  $\mathbf{r}$  is the position vector from  $O$  to the point located by  $x_\alpha$  on the reference surface at a specific time  $t$ . When the reference surface of the undeformed plate coincides with its middle surface, we have

$$\langle \hat{\mathbf{r}}(x_1, x_2, x_3, t) \rangle = h \mathbf{r}(x_1, x_2, t), \quad (4)$$

where the angle brackets denote the definite integral through the thickness of the plate and  $h$  is the plate thickness.

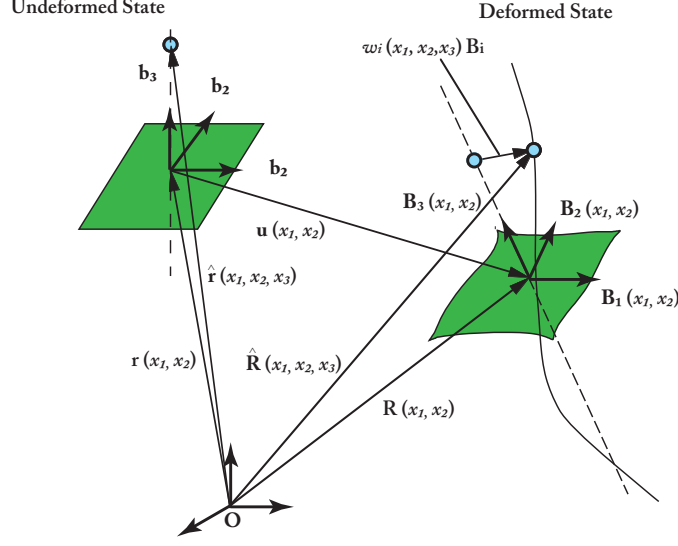


Figure 1. Schematic of plate deformation

When the plate deforms, the particle that had position vector  $\hat{\mathbf{r}}$  in the undeformed state now has position vector  $\hat{\mathbf{R}}$  in the deformed plate. The latter can be uniquely determined by the deformation of the 3D body. We introduce another orthonormal triad  $\mathbf{B}_i$  for the deformed configuration so that:

$$\mathbf{B}_i = C_{ij}\mathbf{b}_j, \quad C_{ij} = \mathbf{B}_i \cdot \mathbf{b}_j, \quad (5)$$

subjecting to the requirement that  $\mathbf{B}_i$  is coincident with  $\mathbf{b}_i$  when the structure is undeformed. The direction cosine matrix  $C(x_1, x_2)$  represents the possible arbitrary rotation between  $\mathbf{B}_i$  and  $\mathbf{b}_i$ .

After deformation, the position vector  $\hat{\mathbf{R}}$  in the deformed state can be expressed as

$$\hat{\mathbf{R}}(x_1, x_2, x_3, t) = \mathbf{R}(x_1, x_2, t) + x_3\mathbf{B}_3(x_1, x_2, t) + w_i(x_1, x_2, x_3, t)\mathbf{B}_i(x_1, x_2, t), \quad (6)$$

where  $\mathbf{R}$  is the position vector of the reference surface for the deformed plate and  $w_i(x_1, x_2, x_3, t)$  are the warping functions which are introduced to accommodate all possible deformations. Equation (6) can be considered as a change of variable for  $\hat{\mathbf{R}}$  in terms of  $\mathbf{R}$ ,  $\mathbf{B}_i$ , and  $w_i$ . Proper definitions of  $\mathbf{R}$  and  $\mathbf{B}_i$  are needed to introduce six constraints to ensure a one-to-one mapping of this change of variables. We can introduce the following three constraints for the warping functions:

$$\langle w_i(x_1, x_2, x_3, t) \rangle = \left\{ \begin{array}{c} c_{\parallel} \\ 0 \end{array} \right\}, \quad \text{with } c_{\parallel} = \left\{ \begin{array}{c} c_1 \\ c_2 \end{array} \right\}, \quad (7)$$

where  $c_i$  are functions of the in-plane coordinates  $x_\alpha$  and time  $t$ , introduced for providing free variables for the construction of an optimal Reissner-Mindlin model which will be described later. Two other constraints can be specified by taking  $\mathbf{B}_3$  as the normal to the reference surface of the deformed plate. It should be noted that this choice has nothing to do with the well-known Kirchhoff hypothesis. In the Kirchhoff assumption, no local deformation of the transverse normal is allowed. However, in present derivation we allow all possible deformation using the warping functions. Because  $\mathbf{B}_\alpha$  can freely rotate around  $\mathbf{B}_3$ , we can introduce the last constraint as

$$\mathbf{B}_1 \cdot \mathbf{R}_{,2} = \mathbf{B}_2 \cdot \mathbf{R}_{,1}, \quad (8)$$

where  $(\cdot)_{,\alpha} = \partial(\cdot)/\partial x_\alpha$ .

Based on the concept of decomposition of rotation tensor<sup>27, 28</sup> the Jauman-Biot-Cauchy strain components for small local rotation are given by

$$\Gamma_{ij} = \frac{1}{2}(F_{ij} + F_{ji}) - \delta_{ij}, \quad (9)$$

with

$$F_{ij} = \mathbf{B}_i \cdot \mathbf{G}_k \mathbf{b}_k \cdot \mathbf{b}_j. \quad (10)$$

Here  $\mathbf{G}_i = \partial \hat{\mathbf{R}} / \partial x_i$  is the covariant basis vector of the deformed configuration. The details for obtaining this concise expression for the Jauman-Biot-Cauchy strain tensor can be found in Ref. [27]. To express the 3D strain field in terms of 2D plate strains, we can define the 2D generalized strains following Ref. [29] as:

$$\mathbf{R}_{,\alpha} = \mathbf{B}_\alpha + \varepsilon_{\alpha\beta} \mathbf{B}_\beta \quad (11)$$

and

$$\mathbf{B}_{i,\alpha} = (-K_{\alpha\beta} \mathbf{B}_\beta \times \mathbf{B}_3 + K_{\alpha 3} \mathbf{B}_3) \times \mathbf{B}_i, \quad (12)$$

where  $\varepsilon_{\alpha\beta}$  and  $K_{\alpha\beta}$  are the 2D generalized strains. Using this definition, one can show that Eq. (8) implies  $\varepsilon_{12} = \varepsilon_{21}$ . The expressions for 2D generalized strained in terms of plate displacements and rotations can be found in Ref. [29].

For geometrically nonlinear analysis, we can assume that both the 3D and 2D strains are small when compared to the unity and from which we can also conclude that warpings are of the order of the strain or smaller. Neglecting the products between warping and strain (because of small strain), one can express the 3D strain field as

$$\begin{aligned} \Gamma_e &= \epsilon + x_3 \kappa + I_\alpha w_{\parallel,\alpha} \\ 2\Gamma_s &= w'_{\parallel} + e_\alpha w_{3,\alpha} \\ \Gamma_t &= w'_3 \end{aligned} \quad (13)$$

where  $()' = \frac{\partial(\cdot)}{\partial x_3}$ ,  $(\cdot)_{\parallel} = [(\cdot)_1 \ (\cdot)_2]^T$ , and

$$\begin{aligned} \Gamma_e &= [\Gamma_{11}, \ 2\Gamma_{12} \ \Gamma_{22}]^T, \quad 2\Gamma_s = [2\Gamma_{13} \ 2\Gamma_{23}]^T, \quad \Gamma_t = \Gamma_{33}, \\ \epsilon &= [\varepsilon_{11} \ 2\varepsilon_{12} \ \varepsilon_{22}]^T, \quad \kappa = [K_{11} \ K_{12} + K_{21} \ K_{22}]^T, \end{aligned} \quad (14)$$

$$I_1 = \begin{bmatrix} 1 & 0 \\ 0 & 1 \\ 0 & 0 \end{bmatrix}, \quad I_2 = \begin{bmatrix} 0 & 0 \\ 1 & 0 \\ 0 & 1 \end{bmatrix}, \quad e_1 = \begin{Bmatrix} 1 \\ 0 \end{Bmatrix}, \quad e_2 = \begin{Bmatrix} 0 \\ 1 \end{Bmatrix}. \quad (15)$$

Up to this stage we have formulated the kinematics of the plate structure. However, a complete description of the smart plate requires not only the elastic field but also the electric and magnetic fields defined by using the electric potential  $\phi(x_i)$  and magnetic potential  $\psi(x_i)$  as commonly used in literature:

$$\begin{cases} E_s = [E_1 \ E_2]^T = -[\phi_{,1} \ \phi_{,2}]^T, & E_t = E_3 = -\phi'; \\ H_s = [H_1 \ H_2]^T = -[\psi_{,1} \ \psi_{,2}]^T, & H_t = H_3 = -\psi'. \end{cases} \quad (16)$$

It worth noting that Eqs. (16) implicitly assume that electric and magnetic fields are irrotational which is equivalent to ignoring the effect of free current and the time variation of electric displacement  $D$  and magnetic induction  $B$ , i.e. the first two Maxwell equations corresponding to Faraday's law and Ampere's law become  $\nabla \times E = 0$  and  $\nabla \times H = 0$ .

In present study, we will focus on investigating common situations where at least one of the surfaces (or interfaces) of the composite plate is electroded and applied with prescribed electric and/or magnetic potentials. The prescribed electric potential and magnetic potential can be applied to different surfaces. It is also assumed that externally prescribed magnetic field is applied vertically to the plate. The most general situation for the applied electric and magnetic potentials is illustrated by Eq.(17).

$$\phi(x_1, x_2, z_i) = \phi_i, \quad \psi(x_1, x_2, z_j) = \phi_j, \quad (17)$$

where,  $\phi_i$  and  $\psi_j$  are prescribed electric and magnetic potentials at  $x_3 = z_i$  and  $x_3 = z_j$  surfaces, respectively. If there exist a boundary surface with no electric/magnetic potential specified, this surface is electric/magnetic free, i.e. electric displacement or magnetic induction is zero ( $D_z = 0$  or  $B_z = 0$ ). Without losing generality, we will focus our investigation on piezoelectric and piezomagnetic laminated composites in which each lamina exhibits a monoclinic symmetry about its mid-plane. This allows the orthotropic piezoelectric and piezomagnetic materials in each layer being arranged at arbitrary lay-up angles as it is the case in most practical applications.

With the knowledge of the elastic strain and electric and magnetic fields, the electromagnetic enthalpy from equation (2) can be expressed as

$$\mathcal{U} = \int_{\Omega} \mathcal{H} d\Omega, \quad (18)$$

with  $\Omega$  denoting the domain of the reference surface and

$$\begin{aligned} 2\mathcal{H} = & \left\langle \left\langle \begin{Bmatrix} \Gamma_e \\ 2\Gamma_s \\ \Gamma_t \end{Bmatrix} \right\rangle^T \begin{bmatrix} C_e & 0 & C_{et} \\ 0 & C_s & 0 \\ C_{et}^T & 0 & C_t \end{bmatrix} \begin{Bmatrix} \Gamma_e \\ 2\Gamma_s \\ \Gamma_t \end{Bmatrix} \right\rangle - \left\langle \left\langle \begin{Bmatrix} E_s \\ E_t \end{Bmatrix} \right\rangle^T \begin{bmatrix} \varepsilon_{ds} & 0 \\ 0 & \varepsilon_{dt} \end{bmatrix} \begin{Bmatrix} E_s \\ E_t \end{Bmatrix} \right\rangle \\ & - \left\langle \left\langle \begin{Bmatrix} H_s \\ H_t \end{Bmatrix} \right\rangle^T \begin{bmatrix} \mu_s & 0 \\ 0 & \mu_t \end{bmatrix} \begin{Bmatrix} H_s \\ H_t \end{Bmatrix} \right\rangle - 2 \left\langle \left\langle \begin{Bmatrix} \Gamma_e \\ 2\Gamma_s \\ \Gamma_t \end{Bmatrix} \right\rangle^T \begin{bmatrix} 0 & e_{et} \\ e_s & 0 \\ 0 & e_t \end{bmatrix} \begin{Bmatrix} E_s \\ E_t \end{Bmatrix} \right\rangle \\ & - 2 \left\langle \left\langle \begin{Bmatrix} \Gamma_e \\ 2\Gamma_s \\ \Gamma_t \end{Bmatrix} \right\rangle^T \begin{bmatrix} 0 & q_{et} \\ q_s & 0 \\ 0 & q_t \end{bmatrix} \begin{Bmatrix} H_s \\ H_t \end{Bmatrix} \right\rangle - 2 \left\langle \left\langle \begin{Bmatrix} E_s \\ E_t \end{Bmatrix} \right\rangle^T \begin{bmatrix} \alpha_s & 0 \\ 0 & \alpha_t \end{bmatrix} \begin{Bmatrix} H_s \\ H_t \end{Bmatrix} \right\rangle, \end{aligned} \quad (19)$$

where  $C_e$ ,  $C_{et}$ ,  $C_s$ , and  $C_t$  are the corresponding partition matrices of the  $6 \times 6$  elastic material matrix;  $\varepsilon_{ds}$  and  $\varepsilon_t$  are the corresponding partition matrices of the  $3 \times 3$  dielectric coefficient matrix;  $\mu_s$  and  $\mu_t$  are the corresponding partition matrices of the  $3 \times 3$  magnetic permeability coefficient matrix;  $e_{et}$ ,  $e_s$ , and  $e_t$  are the corresponding partition matrices of the  $6 \times 3$  piezoelectric coefficient matrix;  $q_{et}$ ,  $q_s$ , and  $q_t$  are the corresponding partition matrices of the  $6 \times 3$  piezomagnetic coefficient matrix;  $\alpha_s$  and  $\alpha_t$  are the corresponding partition matrices of the  $3 \times 3$  magnetoelectric coupling coefficient matrix.

To calculate the kinetic energy, the absolute velocity (measured in the inertia frame) of a generic point in the structure is obtained by taking a time derivative of Eq. (6), resulting

$$v = V + \tilde{\omega}(\xi + w) + \dot{w}, \quad (20)$$

where  $\dot{(\ )}$  is the partial derivative with respect to time;  $V$  is the absolute velocity of a point in the deformed reference surface;  $\omega$  is the inertial angular velocity of  $\mathbf{B}_i$  bases; and the notation  $\tilde{(\ )}$  forms an antisymmetric matrix from a vector according to  $\tilde{(\ )}_{ij} = -e_{ijk}(\ )_k$  using the permutation symbol  $e_{ijk}$ . In Eq. (20), the symbols  $v, V, \omega, w$  denote column matrices containing the components of corresponding vectors in  $\mathbf{B}_i$  bases, and  $\xi = [0 \ 0 \ x_3]^T$ . The kinetic energy of the plate structure can be obtained by

$$\mathcal{K} = \frac{1}{2} \int_{\mathcal{V}} \rho v^T v d\mathcal{V} = \mathcal{K}_{2D} + \mathcal{K}^* \quad (21)$$

with  $\rho$  denoting the mass density and

$$\mathcal{K}_{2D} = \frac{1}{2} \int_{\Omega} (\bar{\mu} V^T V + 2\omega^T \tilde{\mu} \xi V + \omega^T j \omega) d\Omega \quad (22)$$

$$\mathcal{K}^* = \frac{1}{2} \int_{\mathcal{V}} \rho [(\tilde{\omega} w + \dot{w})^T (\tilde{\omega} w + \dot{w}) + 2(V + \tilde{\omega} \xi)^T (\tilde{\omega} w + \dot{w})] d\mathcal{V}, \quad (23)$$

where  $\bar{\mu}$ ,  $\tilde{\mu}$ , and  $j$  are inertial constants commonly used in plate dynamics, which can be trivially obtained by taking integral operations through the thickness direction:

$$\bar{\mu} = \langle \rho \rangle \quad \tilde{\mu} = [0 \ 0 \ \langle x_3 \rho \rangle]^T \quad j = \begin{bmatrix} \langle x_3^2 \rho \rangle & 0 & 0 \\ 0 & \langle x_3^2 \rho \rangle & 0 \\ 0 & 0 & 0 \end{bmatrix} \quad (24)$$

If no electric charges and magnetic induction applied on the surfaces or inside the body, the virtual work of the structure can be calculated as

$$\delta \bar{\mathcal{W}} = \int_{\Omega} (\langle \mathbf{P} \cdot \delta \hat{\mathbf{R}} \rangle + \boldsymbol{\tau} \cdot \delta \hat{\mathbf{R}}^+ + \boldsymbol{\beta} \cdot \delta \hat{\mathbf{R}}^-) d\Omega + \int_{\partial\Omega} \langle \mathbf{Q} \cdot \delta \hat{\mathbf{R}} \rangle ds \quad (25)$$

where  $\partial\Omega$  denotes the boundary of the reference surface;  $(\ )^\pm = (\ )|_{x_3=\pm h/2}$ ;  $\mathbf{P} = P_i\mathbf{B}_i$  is the applied body force;  $\boldsymbol{\tau}, \boldsymbol{\beta}$  are tractions applied on the top and bottom surfaces, respectively;  $\mathbf{Q} = Q_i\mathbf{B}_i$  is the applied tractions along the lateral surfaces.  $\delta\hat{\mathbf{R}}$  is the Lagrangian variation of the displacement field which can be expressed as

$$\delta\hat{\mathbf{R}} = \bar{\delta}q_i\mathbf{B}_i + x_3\delta\mathbf{B}_3 + \delta w_i\mathbf{B}_i + w_j\delta\mathbf{B}_j, \quad (26)$$

in which the virtual displacement and rotation are defined by

$$\bar{\delta}q_i = \delta\mathbf{R} \cdot \mathbf{B}_i, \quad \delta\mathbf{B}_i = (-\bar{\delta}\psi_2\mathbf{B}_1 + \bar{\delta}\psi_1\mathbf{B}_2 + \bar{\delta}\psi_3\mathbf{B}_3) \times \mathbf{B}_i, \quad (27)$$

where  $\bar{\delta}q_i$  and  $\bar{\delta}\psi_i$  contain the components of the virtual displacement and rotation in the  $\mathbf{B}_i$  system, respectively. Since the warping functions are small, one may safely ignore products of the warping and virtual rotation in  $\delta\hat{\mathbf{R}}$  and obtain the virtual work due to applied loads as

$$\bar{\delta}\mathcal{W} = \bar{\delta}\mathcal{W}_{2D} + \bar{\delta}\mathcal{W}^*, \quad (28)$$

where

$$\bar{\delta}\mathcal{W}_{2D} = \int_{\Omega} (f_i\bar{\delta}q_i + m_\alpha\bar{\delta}\psi_\alpha) d\Omega + \int_{\partial\Omega} (\langle Q_i \rangle \bar{\delta}q_i + \langle x_3 Q_\alpha \rangle \bar{\delta}\psi_\alpha) ds, \quad (29)$$

$$\bar{\delta}\mathcal{W}^* = \int_{\Omega} (\langle P_i \delta w_i \rangle + \tau_i \delta w_i^+ + \beta_i \delta w_i^-) d\Omega + \int_{\partial\Omega} \langle Q_i \delta w_i \rangle ds, \quad (30)$$

with the generalized forces  $f_i$  and moments  $m_\alpha$  defined as

$$f_i = \langle P_i \rangle + \tau_i + \beta_i, \quad m_\alpha = \langle x_3 P_\alpha \rangle + \frac{h}{2}(\tau_\alpha - \beta_\alpha). \quad (31)$$

The second integration in Eq. (30) accounts for virtual work done through warping functions along the lateral boundaries of the plate. This term is necessary for the edge-zone problem, which is an important subject in its own right and beyond the scope of the present paper. For simplicity, we will drop this term hereafter. With the knowledge of Eqs. (21), (19), and (28), the extended Hamilton's principle in Eq. (1) becomes

$$\int_{t_1}^{t_2} \left[ \delta(\mathcal{K}_{2D} + \mathcal{K}^* - \mathcal{U}) + \bar{\delta}\mathcal{W}_{2D} + \bar{\delta}\mathcal{W}^* \right] dt = 0 \quad (32)$$

So far, we have presented a 3D formulation for the electro-magneto-elastic problem of smart plates in terms of 2D displacements (represented by  $\mathbf{R} - \mathbf{r}$ ), rotations (represented by  $\mathbf{b}_i$  and  $\mathbf{B}_i$ ), electric and magnetic potentials ( $\phi, \psi$ ), and 3D warping functions ( $w_i$ ). If we attempt to solve this problem directly, we will meet the same difficulty as solving any full 3D problem. The main complexity comes from the unknown 3D warping functions  $w_i$  as well as the coupled 3D potentials  $\phi$  and  $\psi$ . A common practice in the literature is the direct expression of  $w_i, \phi$  and  $\psi$  in terms of 2D displacements, rotations, and electric and magnetic potentials based on some a priori assumptions to straightforwardly reduce the original 3D continuum model into a 2D plate model. However, for composite laminates made with general anisotropic and heterogeneous materials, the imposition of such assumptions may introduce significant errors. This is especially true for problems involving multi-field coupling. Fortunately, VAM provides a useful technique to obtain  $w_i, \phi, \psi$  through an asymptotical analysis of the variational statement in Eq. (32) in terms of small parameters inherent in the problem which will be described in the next section.

## Dimensional Reduction

The dimensional reduction from the original 3D formulation to a 2D plate model can only be done approximately. One way to accomplish this is to take the advantage of the small parameters in the formulation to construct a 2D formulation so that the reduced model can achieve the minimum accuracy loss in comparison to the original 3D formulation.

In order to apply VAM, we first need to assess the order of quantities in terms of small parameters. As mentioned previously, the ratio of the plate thickness to the characteristic wavelength of the deformation of the reference surface is much smaller than 1, which means  $h/l \ll 1$ . The strains are also small for a

geometrically nonlinear but physically linear 2D theory, *i.e.*,  $\epsilon_{\alpha\beta} \sim h\kappa_{\alpha\beta} \sim \eta \ll 1$ . From the plate equations of equilibrium, we can estimate the orders of the following quantities corresponding to the order of strains:

$$\begin{aligned} hP_3 &\sim \tau_3 \sim \beta_3 \sim \xi(h/l)^2\eta, & hP_\alpha &\sim \tau_\alpha \sim \beta_\alpha \sim \xi(h/l)\eta, \\ Q_\alpha &\sim \xi\eta, & Q_3 &\sim \xi(h/l)\eta, \end{aligned} \quad (33)$$

with  $\xi$  denoting the characteristic magnitude of the elastic constants. We can choose the characteristic scale of change of the displacements and warping functions with respect to time in such a way that  $\mathcal{K}^*$  is much smaller than other terms in Eq. (32). In other words, here we are only interested the accurate description of low frequency dynamic problems.

### Zeroth-order reduction

To clearly illustrate the application of VAM for the multi-physically coupled magneto-electro-elastic problem, we first construct a classical smart plate model. By applying VAM and in view of the order assessments in Eqs. (33), we can obtain the leading terms of the variational statement in Eq. (32) by neglecting smaller terms to get

$$\int_{t_1}^{t_2} \left[ \delta(\mathcal{K}_{2D} - \int_{\Omega} \mathcal{H}_0 d\Omega) + \overline{\delta\mathcal{W}}_{2D} \right] dt = 0, \quad (34)$$

where the zeroth-order approximation of the magnetoelectric enthalpy density  $\mathcal{H}_0$  can be calculated from Eq. (19) by dropping derivatives with respect to  $x_\alpha$  in Eqs. (13) and (16), resulting in

$$\begin{aligned} 2\mathcal{H}_0 &= \left\langle (\epsilon + x_3\kappa)^T C_e (\epsilon + x_3\kappa) + w_{\parallel}^T C_s w_{\parallel} + w'_3 C_t w'_3 - \phi' \varepsilon_{dt} \phi' - \psi' \mu_t \psi' \right\rangle \\ &\quad + 2 \left\langle (\epsilon + x_3\kappa)^T (C_{et} w'_3 + e_{et} \phi' + q_{et} \psi') \right\rangle + 2 \left\langle w'_3 e_t \phi' + w'_3 q_t \psi' - \phi' \alpha_t \psi' \right\rangle \end{aligned} \quad (35)$$

The warping functions  $w_i$ , electric potential  $\phi$ , and magnetic potential  $\psi$  in  $\mathcal{H}_0$  can be obtained by solving the following simple variational statement:

$$\delta\mathcal{H}_0 = 0 \quad (36)$$

along with the constraint equation in Eq. (7), with  $c_{\parallel} = [0, 0]^T$  for the zeroth-order approximation. To carry out the variations of the functional, one should be aware that functions  $w_{\parallel}$ ,  $w_3$ ,  $\phi$ , and  $\psi$  may differ from layer to layer. The continuity conditions on the interfaces can be derived from the calculus of variations to give:

$$\begin{aligned} [w_{\parallel}^T C_s] &= 0, & [(\epsilon + x_3\kappa)^T C_{et} + C_t w'_3 + e_t \phi' + q_t \psi'] &= 0, \\ [(\epsilon + x_3\kappa)^T e_{et} + e_t w'_3 - \varepsilon_{dt} \phi' - \alpha_t \psi'] &= [(\epsilon + x_3\kappa)^T q_{et} + q_t w'_3 - \alpha_t \phi' - \mu_t \psi'] = 0, & \text{on } \Omega_i, \end{aligned} \quad (37)$$

where  $\Omega_i$  denotes the interface between the  $i$ th layer and  $i+1$ th layer and  $i = 1 \dots N-1$  with  $N$  as the total number of layers; the bracket  $[\cdot]$  denotes the jump of the enclosed argument on the interface. The boundary conditions and Euler-Lagrange equations derived from Eqs. (36) take the form of:

$$\begin{aligned} (w_{\parallel}^T C_s)^+ &= 0, & [(\epsilon + x_3\kappa)^T C_{et} + C_t w'_3 + e_t \phi' + q_t \psi']^+ &= 0, \\ (w_{\parallel}^T C_s)^- &= 0, & [(\epsilon + x_3\kappa)^T C_{et} + C_t w'_3 + e_t \phi' + q_t \psi']^- &= 0, \\ \delta\phi^{+/-} &= 0, & \text{or } [(\epsilon + x_3\kappa)^T e_{et} + e_t w'_3 - \varepsilon_{dt} \phi' - \alpha_t \psi']^{+/-} &= 0, \\ \delta\psi^{+/-} &= 0, & \text{or } [(\epsilon + x_3\kappa)^T q_{et} + q_t w'_3 - \alpha_t \phi' - \mu_t \psi']^{+/-} &= 0, \end{aligned} \quad (38)$$

and

$$\begin{aligned} (w_{\parallel}^T C_s)' &= \lambda_{\parallel}^T, \\ [(\epsilon + x_3\kappa)^T C_{et} + C_t w'_3 + e_t \phi' + q_t \psi']' &= \lambda_3, \\ [(\epsilon + x_3\kappa)^T e_{et} + e_t w'_3 - \varepsilon_{dt} \phi' - \alpha_t \psi']' &= 0, \\ [(\epsilon + x_3\kappa)^T q_{et} + q_t w'_3 - \alpha_t \phi' - \mu_t \psi']' &= 0, \end{aligned} \quad (39)$$

respectively.  $\lambda_{\parallel}$  and  $\lambda_3$  are Lagrange multipliers introduced to enforce the constraints applied on the warping field described in Eq. (7) with  $c_{\parallel} = [0, 0]^T$ . The interlamina continuity conditions for transverse stresses and transverse electric displacement and magnetic flux have been automatically derived, Eq. (37). The last two equations in Eq. (38) indicate that electric and magnetic potentials can either be prescribed at the top or bottom boundary surfaces or be free to vary at these surfaces. In the latter case the boundary conditions are determined by free electric displacement ( $D_3 = 0$ ) and/or free magnetic induction ( $B_3 = 0$ ).

Solving the Euler-Lagrange equations along with the boundary conditions in Eq. (38), the continuity conditions in (37), and the constraints in (7), one can show that  $\lambda_{\parallel} = \lambda_3 = w_{\parallel} = 0$ . The solution for the rest of unknowns ( $w_3, \phi, \psi$ ) can be expressed as

$$\begin{aligned} C_t w'_3 + e_t \phi' + q_t \psi' &= -(\epsilon + x_3 \kappa)^T C_{et} \\ e_t w'_3 - \varepsilon_{dt} \phi' - \alpha_t \psi' &= -(\epsilon + x_3 \kappa)^T e_{et} + \mathcal{P}_e \\ q_t w'_3 - \alpha_t \phi' - \mu_t \psi' &= -(\epsilon + x_3 \kappa)^T q_{et} + \mathcal{P}_m, \end{aligned} \quad (40)$$

where  $\mathcal{P}_e$  and  $\mathcal{P}_m$  are integration constants for electric potential  $\phi$  and magnetic potential  $\psi$ , respectively. Because material properties may vary from layer to layer, one may intuitively expect  $\mathcal{P}_e$  and  $\mathcal{P}_m$  to be different for different layers. However, as we will prove later, they are constants.  $w'_3, \phi'$ , and  $\psi'$  for each layer can be solved from Eq. (40) as

$$\begin{aligned} w'_3 &= C_{et}^{*T} C_t^{*-1} (\epsilon + x_3 \kappa) + (\mathcal{P}_e M_{12}^* + \mathcal{P}_m M_{13}^*) C_t^{*-1}, \\ \phi' &= e_{et}^{*T} C_t^{*-1} (\epsilon + x_3 \kappa) + (\mathcal{P}_e M_{22}^* + \mathcal{P}_m M_{23}^*) C_t^{*-1}, \\ \psi' &= q_{et}^{*T} C_t^{*-1} (\epsilon + x_3 \kappa) + (\mathcal{P}_e M_{23}^* + \mathcal{P}_m M_{33}^*) / C_t^{*-1}, \end{aligned} \quad (41)$$

with

$$\begin{aligned} C_{et}^* &= -(C_{et} M_{11}^* + e_{et} M_{12}^* + q_{et} M_{13}^*), & e_{et}^* &= -(C_{et} M_{12}^* + e_{et} M_{22}^* + q_{et} M_{23}^*), \\ q_{et}^* &= -(C_{et} M_{13}^* + e_{et} M_{23}^* + q_{et} M_{33}^*), & C_t^* &= \det(M), \\ M &= \begin{bmatrix} C_t & e_t & q_t \\ e_t & -\varepsilon_{dt} & -\alpha_t \\ q_t & -\alpha_t & -\mu_t \end{bmatrix}, \end{aligned} \quad (42)$$

where  $M_{ij}^*$  is the cofactor of matrix  $M$  defined as the subdeterminant of the element  $m_{ij}$  multiplied by the sign factor  $(-1)^{i+j}$ , e.g.,  $M_{12} = (e_t \mu_t - q_t \alpha_t)$ .

Although the explicit expressions of  $\mathcal{P}_e$  and  $\mathcal{P}_m$  can only be determined with the knowledge of the actual construction of the smart plate, their most general expressions must take the form as:

$$\begin{aligned} \mathcal{P}_e &= \epsilon^T \mathcal{P}_{e\epsilon} + \kappa^T \mathcal{P}_{e\kappa} + \mathcal{P}_{e0}, \\ \mathcal{P}_m &= \epsilon^T \mathcal{P}_{m\epsilon} + \kappa^T \mathcal{P}_{m\kappa} + \mathcal{P}_{m0}. \end{aligned} \quad (43)$$

Substituting Eq. (41) into Eq. (35), we can obtain the first approximation of the electric enthalpy as

$$2\mathcal{H}_0 = \begin{Bmatrix} \epsilon \\ \kappa \end{Bmatrix}^T \begin{bmatrix} A^* & B^* \\ B^{*T} & D^* \end{bmatrix} \begin{Bmatrix} \epsilon \\ \kappa \end{Bmatrix} + 2 \begin{Bmatrix} \epsilon \\ \kappa \end{Bmatrix}^T \begin{Bmatrix} S_{\epsilon} \\ S_{\kappa} \end{Bmatrix} \quad (44)$$

with

$$\begin{aligned} A^* &= \left\langle C_e^* + [\mathcal{P}_{e\epsilon} \ \mathcal{P}_{m\epsilon}] M^{**} \begin{Bmatrix} \mathcal{P}_{e\epsilon}^T \\ \mathcal{P}_{m\epsilon}^T \end{Bmatrix} \right\rangle, & B^* &= \left\langle x_3 C_e^* + [\mathcal{P}_{e\epsilon} \ \mathcal{P}_{m\epsilon}] M^{**} \begin{Bmatrix} \mathcal{P}_{e\kappa}^T \\ \mathcal{P}_{m\kappa}^T \end{Bmatrix} \right\rangle \\ D^* &= \left\langle x_3^2 C_e^* + [\mathcal{P}_{e\kappa} \ \mathcal{P}_{m\kappa}] M^{**} \begin{Bmatrix} \mathcal{P}_{e\kappa}^T \\ \mathcal{P}_{m\kappa}^T \end{Bmatrix} \right\rangle, & M^{**} &= \frac{1}{C_t^*} \begin{bmatrix} M_{22} & M_{23} \\ M_{23} & M_{33} \end{bmatrix} \\ S_{\epsilon} &= \left\langle [\mathcal{P}_{e\epsilon} \ \mathcal{P}_{m\epsilon}] M^{**} \begin{Bmatrix} \mathcal{P}_{e0} \\ \mathcal{P}_{m0} \end{Bmatrix} \right\rangle, & S_{\kappa} &= \left\langle [\mathcal{P}_{e\kappa} \ \mathcal{P}_{m\kappa}] M^{**} \begin{Bmatrix} \mathcal{P}_{e0} \\ \mathcal{P}_{m0} \end{Bmatrix} \right\rangle \\ C_e^* &= C_e + (C_{et} C_{et}^{*T} + e_{et} e_{et}^{*T} + q_{et} q_{et}^{*T}) / C_t^* \end{aligned} \quad (45)$$

In Eq. (44), a quadratic term relating only to the prescribed electric and magnetic potentials is dropped because it will not affect the derivation of the 2D model. It is obvious that the stiffness matrices ( $A^*$ ,  $B^*$ , and  $D^*$ ) depend not only on elastic, piezoelectric, and piezomagnetic materials properties but also on the externally applied electric and magnetic potentials. Additional contributions to the electromagnetic enthalpy from the generalized electric and magnetic forces  $S_\epsilon$  and  $S_\kappa$  will, in general, exist except for some specific boundary conditions.

With the knowledge of  $\mathcal{H}_0$  expressed in Eq. (44), the original 3D problem in Eq. (1) has been rigorously reduced to a 2D formulation in Eq. (34) which approximates the original problem asymptotically correct to the order of  $(\frac{h}{l})^0$ . If the force resultants  $\mathcal{N}$  and moment resultants  $\mathcal{M}$  are defined as follows

$$\mathcal{N} = \frac{\partial \mathcal{H}_0}{\partial \epsilon}, \quad \mathcal{M} = \frac{\partial \mathcal{H}_0}{\partial \kappa}, \quad (46)$$

the 2D constitutive model for the zero-th order analysis of smart plates takes the form as

$$\begin{Bmatrix} \mathcal{N} \\ \mathcal{M} \end{Bmatrix} = \begin{bmatrix} A^* & B^* \\ B^{*T} & D^* \end{bmatrix} \begin{Bmatrix} \epsilon \\ \kappa \end{Bmatrix} + \begin{Bmatrix} S_\epsilon \\ S_\kappa \end{Bmatrix}. \quad (47)$$

It is clear that the zeroth-order 2D analysis of the smart magnetolectric plate is similar to the thermal analysis of the plate using the classic plate theory except for the necessity of updating matrices  $A^*$ ,  $B^*$ ,  $C^*$  to account for magnetolectric effects and replacing the thermal resultants with the generalized electric and magnetic forces. Despite its similarity to the classical lamination theory (CLT), the present model is asymptotically correct and preserves the following features:

1. The normal line of undeformed plate does not remain straight or normal to the deformed plate; rather, it is free to deform in the normal in response to plates deformations ( $\epsilon$  and  $\kappa$ ) as well as the prescribed electric and magnetic actuations.
2. It can be easily observed that the normal strain does not vanish. Although it can be prove that the transverse normal and shear stresses do vanish, this result is a direct outcome from the the mathematical derivation and not taken as *a priori* assumptions.

For the zeroth-order approximation, the 3D strain field and electric field can be recovered using Eqs. (13) and (16) with higher-order terms neglected as

$$\begin{aligned} \Gamma_e^0 &= \epsilon + x_3 \kappa, & 2\Gamma_s^0 &= w_{||}^{0'} = 0, & \Gamma_t^0 &= w_3^{0'}, \\ E_s^0 &= H_s^0 = 0, & E_t^0 &= -\phi^{0'}, & H_t^0 &= -\psi^{0'}. \end{aligned} \quad (48)$$

The 3D multiphysical fields for stress, electric displacement, and magnetic induction can be calculated by using the 3D constitutive relations based on Eq. (19) as:

$$\begin{aligned} \begin{Bmatrix} \sigma_e \\ \sigma_s \\ \sigma_{33} \end{Bmatrix} &= \begin{bmatrix} C_e & 0 & C_{et} \\ 0 & C_s & 0 \\ C_{et}^T & 0 & C_t \end{bmatrix} \begin{Bmatrix} \Gamma_e^0 \\ 2\Gamma_s^0 \\ \Gamma_t^0 \end{Bmatrix} - \begin{Bmatrix} e_{et} E_t^0 \\ 0 \\ e_t E_t^0 \end{Bmatrix} - \begin{Bmatrix} q_{et} H_t^0 \\ 0 \\ q_t H_t^0 \end{Bmatrix} \\ \begin{Bmatrix} D_s \\ D_3 \end{Bmatrix} &= \begin{bmatrix} 0 & e_s^T & 0 \\ e_{et}^T & 0 & e_t \end{bmatrix} \begin{Bmatrix} \Gamma_e^0 \\ 2\Gamma_s^0 \\ \Gamma_t^0 \end{Bmatrix} + \begin{Bmatrix} 0 \\ \epsilon_{dt} E_t^0 \end{Bmatrix} + \begin{Bmatrix} 0 \\ \alpha_t H_t^0 \end{Bmatrix} \\ \begin{Bmatrix} B_s \\ B_3 \end{Bmatrix} &= \begin{bmatrix} 0 & q_s^T & 0 \\ q_{et}^T & 0 & q_t \end{bmatrix} \begin{Bmatrix} \Gamma_e^0 \\ 2\Gamma_s^0 \\ \Gamma_t^0 \end{Bmatrix} + \begin{Bmatrix} 0 \\ \mu_t H_t^0 \end{Bmatrix} + \begin{Bmatrix} 0 \\ \alpha_t E_t^0 \end{Bmatrix} \end{aligned} \quad (49)$$

with

$$\sigma_e = [\sigma_{11} \ \sigma_{12} \ \sigma_{22}]^T, \quad \sigma_s = [\sigma_{13} \ \sigma_{23}]^T, \quad D_s = [D_1 \ D_2]^T, \quad B_s = [B_1 \ B_2]^T.$$

where  $\sigma_{ij}$ ,  $D_i$ , and  $B_i$  are 3D stresses, electric displacements, and magnetic inductions, respectively. In view of Eq. (40), it can be concluded that  $\sigma_s$  and  $\sigma_{33}$  are identically zero regardless the material properties,

indicating that the zeroth-order approximation (similar to the classical plate model) can not predict out-of-plane stresses. Eq. (40) also reveals that the transverse electric displacement  $D_3$  and magnetic induction  $B_3$  are identically equal to  $\mathcal{P}_e$  and  $\mathcal{P}_m$ , respectively. By considering the continuity conditions on interfaces Eq. (37), it can be easily deduced that  $\mathcal{P}_e$  and  $\mathcal{P}_m$  are indeed constants throughout the thickness, independent of layer-up configurations. In order to predict the out-of-plane stresses, one more step is necessary to carry out the asymptotic expansion of the 3D variational statement in Eq. (1) into a higher order. This will be presented in the next section.

The zeroth-order approximation of warping functions  $w_3$ , electric  $\phi$ , and magnetic potentials  $\psi$  can be solved from equation (41) along with the continuity conditions on the interfaces in Eq. (37) as well as the constraints expressed in Eq. (7), given:

$$w_3^0 = C_\perp \mathcal{E} + w_{3em}^0, \quad \phi^0 = C_\phi \mathcal{E} + \phi_{em}^0, \quad \psi^0 = C_\psi \mathcal{E} + \psi_{em}^0, \quad (50)$$

with

$$\begin{aligned} \mathcal{E} &= [\epsilon, \kappa]^T, \\ C'_\perp &= \left[ \frac{C_{et}^{*T} + M_{12}^* \mathcal{P}_{e\epsilon}^T + M_{13}^* \mathcal{P}_{m\epsilon}^T}{C_t^*}, \frac{x_3 C_{et}^{*T} + M_{12}^* \mathcal{P}_{e\kappa}^T + M_{13}^* \mathcal{P}_{m\kappa}^T}{C_t^*} \right], & w_{3em}^{0'} &= \frac{M_{12}^* \mathcal{P}_{e0} + M_{13}^* \mathcal{P}_{m0}}{C_t^*}, \\ C'_\phi &= \left[ \frac{e_{et}^{*T} + M_{22}^* \mathcal{P}_{e\epsilon}^T + M_{23}^* \mathcal{P}_{m\epsilon}^T}{C_t^*}, \frac{x_3 e_{et}^{*T} + M_{22}^* \mathcal{P}_{e\kappa}^T + M_{23}^* \mathcal{P}_{m\kappa}^T}{C_t^*} \right], & \phi_{em}^{0'} &= \frac{M_{22}^* \mathcal{P}_{e0} + M_{23}^* \mathcal{P}_{m0}}{C_t^*}, \\ C'_\psi &= \left[ \frac{q_{et}^{*T} + M_{23}^* \mathcal{P}_{e\epsilon}^T + M_{33}^* \mathcal{P}_{m\epsilon}^T}{C_t^*}, \frac{x_3 q_{et}^{*T} + M_{23}^* \mathcal{P}_{e\kappa}^T + M_{33}^* \mathcal{P}_{m\kappa}^T}{C_t^*} \right], & \psi_{em}^{0'} &= \frac{M_{23}^* \mathcal{P}_{e0} + M_{33}^* \mathcal{P}_{m0}}{C_t^*}. \end{aligned}$$

### First-order approximation

To obtain the first-order approximation, we simply perturb the warping functions and electric and magnetic potentials as:

$$\begin{aligned} w_\parallel &= v_\parallel + o\left(\frac{h}{l}\eta\right), & w_3 &= v_3^0 + v_3 + o\left(\frac{h}{l}\eta\right), \\ \phi &= \phi^0 + \tilde{\phi} + o\left(\frac{h}{l}\eta\right), & \psi &= \psi^0 + \tilde{\psi} + o\left(\frac{h}{l}\eta\right). \end{aligned} \quad (51)$$

Substituting Eq. (51) back into Eq. (13), then using Eqs. (19), (28), and (30), one can obtain the leading terms for the first-order approximation of the variational statement in Eq. (32) as

$$\begin{aligned} \delta\Pi_1 &= \left\langle \left[ (\epsilon + x_3 \kappa)^T C_e^* - (\mathcal{P}_e e_{et}^{*T} + \mathcal{P}_m q_{et}^{*T}) C_t^{*-1} \right] I_\alpha \delta v_{\parallel, \alpha} + \left[ (v'_\parallel + e_\alpha w_{3, \alpha}^0)^T C_s + \phi_{, \parallel}^0 e_s^T \right. \right. \\ &\quad \left. \left. + \psi_{, \parallel}^0 q_s^T \right] \delta v'_\parallel + (v'_3 C_t + \tilde{\phi}' e_t + \tilde{\psi}' q_t) \delta v'_3 + (\mathcal{P}_e + v'_3 e_t - \tilde{\phi}' \epsilon_{dt} - \tilde{\psi}' \alpha_t) \delta \tilde{\phi}' \right. \\ &\quad \left. + (\mathcal{P}_m + v'_3 q_t - \tilde{\phi}' \alpha_t - \tilde{\psi}' \mu_t) \delta \tilde{\psi}' \right\rangle - \left\langle P_\parallel^T \delta v_\parallel \right\rangle - \tau_\parallel^T \delta v_\parallel^+ - \beta_\parallel^T \delta v_\parallel^-, \end{aligned} \quad (52)$$

where  $\phi_{, \parallel}^0 = [\phi_{, 1}^0, \phi_{, 2}^0]^T$  and  $\psi_{, \parallel}^0 = [\psi_{, 1}^0, \psi_{, 2}^0]^T$ . With warping functions as well as electric and magnetic potentials being expressed in the order of  $O(h/l)\eta$ , the first-order approximation of the total electromagnetic enthalpy is asymptotically correct to the order of  $O(h/l)^2\eta^2$ . It can be observed from the above functional that  $v_\parallel$  is decoupled from  $v_3, \tilde{\phi}$ , and  $\tilde{\psi}$  and can be solved separately. It is also worth noting that terms  $\langle \mathcal{P}_e \delta \tilde{\phi}' + \mathcal{P}_m \delta \tilde{\psi}' \rangle$  will vanish for all possible boundary conditions (with top and bottom surfaces either being prescribed with electric/magnetic potential(s) or being subjected to free electric displacement/magnetic flux). To carry out the variations of the functional, one needs to be aware that  $v_\parallel$  as well as  $v_3, \tilde{\phi}$ , and  $\tilde{\psi}$  may be different for each layer. The continuity conditions on the interface can be derived by following variational calculus, resulting:

$$\begin{aligned} \left[ C_s (v'_\parallel + e_\alpha w_{3, \alpha}^0) + e_s \phi_{, \parallel}^0 + q_s \psi_{, \parallel}^0 \right] &= \tau_\parallel, & \left[ C_t v'_3 + e_t \tilde{\phi}' + q_t \tilde{\psi}' \right] &= 0, & \text{on } \Omega_i, \\ \left[ e_t v'_3 - \epsilon_{dt} \tilde{\phi}' - \alpha_t \tilde{\psi}' \right] &= 0, & \left[ q_t v'_3 - \alpha_t \tilde{\phi}' - \mu_t \tilde{\psi}' \right] &= 0, & \text{on } \Omega_i. \end{aligned} \quad (53)$$

Boundary conditions take the form of

$$\begin{aligned}
\left[ C_s(v'_\parallel + e_\alpha w_{3,\alpha}^0) + e_s \phi_{,\parallel}^0 + q_s \psi_{,\parallel}^0 \right]^+ &= \tau_\parallel; & \left[ C_s(v'_\parallel + e_\alpha w_{3,\alpha}^0) + e_s \phi_{,\parallel}^0 + q_s \psi_{,\parallel}^0 \right]^- &= \beta_\parallel; \\
\left( C_t v'_3 + e_t \tilde{\phi}' + q_t \tilde{\psi}' \right)^+ &= 0; & \left( C_t v'_3 + e_t \tilde{\phi}' + q_t \tilde{\psi}' \right)^- &= 0; \\
\delta\phi^+ = 0, \text{ or } \left( e_t v'_3 - \varepsilon_{dt} \tilde{\phi}' - \alpha_t \tilde{\psi}' \right)^+ &= 0; & \delta\phi^- = 0, \text{ or } \left( e_t v'_3 - \varepsilon_{dt} \tilde{\phi}' - \alpha_t \tilde{\psi}' \right)^- &= 0; \\
\delta\psi^+ = 0, \text{ or } \left( q_t v'_3 - \alpha_t \tilde{\phi}' - \mu_t \tilde{\psi}' \right)^+ &= 0; & \delta\psi^- = 0, \text{ or } \left( q_t v'_3 - \alpha_t \tilde{\phi}' - \mu_t \tilde{\psi}' \right)^- &= 0.
\end{aligned} \tag{54}$$

And the Euler-Lagrange equations are given by:

$$\begin{aligned}
\left[ C_s(v'_\parallel + e_\alpha w_{3,\alpha}^0) + e_s \phi_{,\parallel}^0 + q_s \psi_{,\parallel}^0 \right]' &= D'_\alpha \mathcal{E}_{,\alpha} + g' + \bar{\lambda}_\parallel, \\
\left( C_t v'_3 + e_t \tilde{\phi}' + q_t \tilde{\psi}' \right)' &= \bar{\lambda}_3, \\
\left( e_t v'_3 - \varepsilon_{dt} \tilde{\phi}' - \alpha_t \tilde{\psi}' \right)' &= 0, \\
\left( q_t v'_3 - \alpha_t \tilde{\phi}' - \mu_t \tilde{\psi}' \right)' &= 0,
\end{aligned} \tag{55}$$

where,  $\bar{\lambda}_\parallel$  and  $\bar{\lambda}_3$  are Lagrange multipliers for the first-order approximation to enforce the constraints applied on the warping fields described in Eq. (7);  $D'_\alpha$  and  $g'$  are given by

$$\begin{aligned}
D'_\alpha &= -I_\alpha^T \left[ C_e^* - \frac{e_{et}^* \mathcal{P}_{e\varepsilon}^T + q_{et}^* \mathcal{P}_{m\varepsilon}^T}{C_t^*}, x_3 \left( C_e^* - \frac{e_{et}^* \mathcal{P}_{e\kappa}^T + q_{et}^* \mathcal{P}_{m\kappa}^T}{C_t^*} \right) \right] \\
g' &= I_\alpha^T (\mathcal{P}_{e0} e_{et}^* + \mathcal{P}_{m0} q_{et}^*),_\alpha C_t^{*-1} - P_\parallel.
\end{aligned}$$

The boundary and inter-lamina continuity conditions on transverse components of stresses, electric displacement and magnetic induction are specified explicitly in Eqs. (53) and (54). It should be mentioned that since the goal is to obtain an interior solution for the plate without considering the edge effect, integration by parts with respect to the in-plane coordinates is used hereinafter and throughout the rest of the paper, whenever it is convenient for the derivation.

By taking through-thickness integration and considering the warping constrain in Eq. (7), it can be shown that  $\bar{\lambda}_3 = 0$  and the last three equations in Eq. (55) can be further simplified as:

$$\begin{aligned}
C_t v'_3 + e_t \tilde{\phi}' + q_t \tilde{\psi}' &= 0, \\
e_t v'_3 - \varepsilon_{dt} \tilde{\phi}' - \alpha_t \tilde{\psi}' &= \tilde{\mathcal{P}}_e, \\
q_t v'_3 - \alpha_t \tilde{\phi}' - \mu_t \tilde{\psi}' &= \tilde{\mathcal{P}}_m,
\end{aligned} \tag{56}$$

where,  $\tilde{\mathcal{P}}_e$  and  $\tilde{\mathcal{P}}_m$  are integration coefficients for the last two equations in Eq. (55), respectively.  $v_3$ ,  $\tilde{\phi}$ , and  $\tilde{\psi}$  can be solved by integrating Eq. (56) while in the mean time taking account of the warping constraints in Eq (7). After a careful analysis, it can be proved that  $\tilde{\mathcal{P}}_e$  and  $\tilde{\mathcal{P}}_m$  vanish for all possible combinations of boundary conditions. Therefore, for the first-order approximation,  $v_3$ ,  $\tilde{\phi}$ , and  $\tilde{\psi}$  are all zeros, indicating that first-order approximation provides no further information for  $w_3$ ,  $\phi$ , and  $\psi$ .

As  $v_\parallel$  is decoupled with  $v_3$ ,  $\tilde{\phi}$ , and  $\tilde{\psi}$ , it can be solved separately. Solving the first equation in Eq. (55), one obtained the following in-plane warping functions:

$$v_\parallel = (\bar{D}_\alpha + L_\alpha) \mathcal{E}_{,\alpha} + \bar{g}, \tag{57}$$

with,

$$\begin{aligned}
\bar{D}'_\alpha &= C_s^{-1} D_\alpha^*, & \langle \bar{D}_\alpha \rangle &= 0, & \bar{g}' &= C_s^{-1} g^*, & \langle \bar{g}_\alpha \rangle &= 0, & L_\alpha \mathcal{E}_{,\alpha} &= c_\parallel / h, \\
D_\alpha^* &= D_\alpha + \frac{x_3}{h} D_\alpha^\mp - \frac{1}{2} D_\alpha^\pm - (C_s e_\alpha C_\perp + e_s e_\alpha C_\phi + q_s e_\alpha C_\psi), \\
g^* &= g + \frac{x_3}{h} g^\mp - \frac{1}{2} g^\pm - (w_{3em}^0 C_s + \phi_{em}^0 e_s + \psi_{em}^0 q_s),_\alpha e_\alpha + \left( \frac{x_3}{h} + \frac{1}{2} \right) \tau_\parallel + \left( \frac{x_3}{h} - \frac{1}{2} \right) \beta_\parallel,
\end{aligned}$$

where,  $( )^\pm = ( )^+ + ( )^-$ ,  $( )^\mp = ( )^- - ( )^+$ ;  $L_\alpha$  are integration coefficients that will be determined in the next section through a least square approach by transferring the first-order approximation of magnetoelectric enthalpy into a Reissner-Mindlin Model.

With the first approximation of  $v_{\parallel}$  given in Eq. (57) and  $v_3 = \tilde{\phi} = \tilde{\psi} = 0$ , now we are ready to obtain an expression for the total energy that is asymptotically correct to order of  $O\left(\left(\frac{h}{l}\right)^2 \eta^2\right)$ , viz.,

$$2\Pi_1 = \mathcal{E}^T A \mathcal{E} + \mathcal{E}_{,1}^T B \mathcal{E}_{,1} + 2\mathcal{E}_{,1}^T C \mathcal{E}_{,2} + \mathcal{E}_{,2}^T D \mathcal{E}_{,2} - 2\mathcal{E}^T F, \quad (58)$$

where,

$$\begin{aligned} A &= \begin{bmatrix} A^* & B^* \\ B^{*T} & D^* \end{bmatrix}, \quad S_{\epsilon\kappa} = \begin{Bmatrix} S_{\epsilon} \\ S_{\kappa} \end{Bmatrix}, \\ B &= \left\langle C_{s(11)} C_{\perp}^T C_{\perp} - D_1^{*T} C_s^{-1} D_1^* - \sum_{I=1,2} \sum_{J=1,2} \mathcal{J}_{IJ(11)} C_{\theta I}^T C_{\theta J} \right. \\ &\quad \left. + \sum_{I=1,2} \mathcal{G}_{I(11)} (C_{\theta I}^T C_{\perp} + C_{\perp}^T C_{\theta I}) \right\rangle + L_1^T \langle D'_1 \rangle + \langle D'_1 \rangle^T L_1, \\ C &= \left\langle C_{s(12)} C_{\perp}^T C_{\perp} - D_1^{*T} C_s^{-1} D_2^* - \frac{1}{2} \sum_{I=1,2} \sum_{J=1,2} (\mathcal{J}_{IJ(12)} C_{\theta I}^T C_{\theta J} + \mathcal{J}_{IJ(21)} C_{\theta J}^T C_{\theta I}) \right. \\ &\quad \left. + \sum_{I=1,2} (\mathcal{G}_{I(21)} C_{\theta I}^T C_{\perp} + \mathcal{G}_{I(12)} C_{\perp}^T C_{\theta I}) \right\rangle + L_1^T \langle D'_2 \rangle + \langle D'_1 \rangle^T L_2, \\ D &= \left\langle C_{s(22)} C_{\perp}^T C_{\perp} - D_2^{*T} C_s^{-1} D_2^* - \sum_{I=1,2} \sum_{J=1,2} \mathcal{J}_{IJ(22)} C_{\theta I}^T C_{\theta J} \right. \\ &\quad \left. + \sum_{I=1,2} \mathcal{G}_{I(22)} (C_{\theta I}^T C_{\perp} + C_{\perp}^T C_{\theta I}) \right\rangle + L_2^T \langle D'_2 \rangle + \langle D'_2 \rangle^T L_2, \\ F &= -S_{\epsilon\kappa} + \langle C_{\perp}^T P_3 \rangle + C_{\perp}^{+T} \tau_3 + C_{\perp}^{-T} \beta_3 - \langle D_{\alpha}^{*T} C_s^{-1} g_{,\alpha}^* \rangle - L_{\alpha}^T (\tau_{\parallel} + \beta_{\parallel} - \langle g' \rangle)_{,\alpha}, \\ &\quad + \left\langle \left[ C_{s(\alpha\beta)} C_{\perp}^T w_{3em}^0 - \frac{1}{2} \sum_{I=1,2} \sum_{J=1,2} \mathcal{J}_{IJ(\alpha\beta)} (C_{\theta I}^T \theta_{Jem}^0 + C_{\theta J}^T \theta_{Iem}^0) \right. \right. \\ &\quad \left. \left. + \sum_{I=1,2} \mathcal{G}_{I(\beta\alpha)} (C_{\theta I}^T w_{3em}^0 + C_{\perp}^T \theta_{Iem}^0) \right]_{,\alpha\beta} \right\rangle, \end{aligned} \quad (59)$$

with

$$\begin{aligned} \theta_1^0 &= \phi^0, & \theta_2^0 &= \psi^0, & \mathcal{G}_1 &= e_s, & \mathcal{G}_2 &= q_s, \\ \mathcal{J}_{11} &= \varepsilon_{ds}, & \mathcal{J}_{12} &= \alpha_s, & \mathcal{J}_{21} &= \alpha_s^T, & \mathcal{J}_{22} &= \mu_s, \\ C_{\theta 1} &= C_{\phi}, & C_{\theta 2} &= C_{\psi}, & \theta_{1em}^0 &= \phi_{em}^0, & \theta_{2em}^0 &= \psi_{em}^0, \end{aligned}$$

and notation  $(\ )_{(\alpha\beta)}$  indicating the  $\alpha, \beta$ th element of matrix  $(\ )$ . Eq. (58) is an energy (enthalpy) functional expressed in terms of 2D variables which can asymptotically approximate the original 3D energy. It is noted that quadratic terms which are not functions of the 2D general strain  $\mathcal{E}$  are dropped because they do not affect the 2D model.

## Transforming into the Reissner-Mindlin Model

Although Eq. (58) is asymptotically correct through the second order and the straightforward use of this magnetoelectric enthalpy is possible, it involves more complex boundary conditions than necessary since it contains derivatives of the generalized strain measures. To obtain a magnetoelectric enthalpy functional that is convenient for practical use, an alternative choice is to transform Eq. (58) into the Reissner-Mindlin model. In the Reissner-Mindlin model, there are two additional degree of freedoms, i.e. the transverse shear strains incorporated into the rotation of transverse normal. By introducing another triad  $\mathbf{B}_i^*$  for the deformed plate,

the definition of 2D strains becomes

$$\begin{aligned}\mathbf{R}_{,\alpha} &= \mathbf{B}_\alpha^* + \varepsilon_{\alpha\beta}^* \mathbf{B}_\beta^* + 2\gamma_{\alpha 3} \mathbf{B}_3^*, \\ \mathbf{B}_{i,\alpha}^* &= (-K_{\alpha\beta}^* \mathbf{B}_\beta^* \times \mathbf{B}_3^* + K_{\alpha 3}^* \mathbf{B}_3^*) \times \mathbf{B}_i^*,\end{aligned}\quad (60)$$

where the transverse shear strains are  $\gamma = [2\gamma_{13} \ 2\gamma_{23}]^T$ . Since  $\mathbf{B}_i^*$  is uniquely determined by  $\mathbf{B}_i$  and  $\gamma$ , one can derive the following kinematic identity between the strains measures  $\mathcal{R}$  of Reissner-Mindlin plate and  $\mathcal{E}$ .

$$\mathcal{E} = \mathcal{R} - \mathcal{D}_\alpha \gamma_{,\alpha}, \quad (61)$$

where

$$\begin{aligned}\mathcal{D}_1 &= \begin{bmatrix} 0 & 0 & 0 & 1 & 0 & 0 \\ 0 & 0 & 0 & 0 & 1 & 0 \end{bmatrix}^T \\ \mathcal{D}_2 &= \begin{bmatrix} 0 & 0 & 0 & 0 & 1 & 0 \\ 0 & 0 & 0 & 0 & 0 & 1 \end{bmatrix}^T \\ \mathcal{R} &= [\varepsilon_{11}^* \ 2\varepsilon_{12}^* \ \varepsilon_{22}^* \ K_{11}^* \ K_{12}^* + K_{21}^* \ K_{22}^*]^T\end{aligned}\quad (62)$$

Now it is possible to express the magnetolectric enthalpy asymptotically correct to the second order in terms of strains of the Reissner-Mindlin model as

$$\begin{aligned}2\Pi_1 &= \mathcal{R}^T A \mathcal{R} - 2\mathcal{R}^T A \mathcal{D}_1 \gamma_{,1} - 2\mathcal{R}^T A \mathcal{D}_2 \gamma_{,2} \\ &\quad + \mathcal{R}_{,1}^T B \mathcal{R}_{,1} + 2\mathcal{R}_{,1}^T C \mathcal{R}_{,2} + \mathcal{R}_{,2}^T D \mathcal{R}_{,2} - 2\mathcal{R}^T F.\end{aligned}\quad (63)$$

The generalized Reissner-Mindlin model takes the form of

$$2\Pi_{\mathcal{R}} = \mathcal{R}^T A \mathcal{R} + \gamma^T G \gamma - 2\mathcal{R}^T F_{\mathcal{R}} - 2\gamma^T F_\gamma. \quad (64)$$

To find an equivalent expression of Eq. (63) for the Reissner-Mindlin model Eq. (64), it is necessary to eliminate all partial derivatives of the 2D strain. This is achieved by applying equilibrium equations. From the two equilibrium equations relating with the equilibrium of bending moments,<sup>30</sup> the following formula can be obtained

$$G\gamma - F_\gamma = \mathcal{D}_\alpha^T A \mathcal{R}_{,\alpha} - \mathcal{D}_\alpha^T F_{\mathcal{R},\alpha} + \begin{Bmatrix} m_1 \\ m_2 \end{Bmatrix}. \quad (65)$$

where  $F_{\mathcal{R},\alpha}$  is dropped because they are high order terms. By substituting Eq. (65) into Eq. (63), it can be shown that  $F_{\mathcal{R}} = F$  and  $F_\gamma = -\mathcal{D}_\alpha^T S_{\varepsilon\kappa,\alpha}$ . Finally Eq. (63) can be rewritten as

$$2\Pi_1 = \mathcal{R}^T A \mathcal{R} + \gamma^T G \gamma - 2\mathcal{R}^T F + U^*, \quad (66)$$

with

$$U^* = \mathcal{R}_{,1}^T \bar{B} \mathcal{R}_{,1} + 2\mathcal{R}_{,1}^T \bar{C} \mathcal{R}_{,2} + \mathcal{R}_{,2}^T \bar{D} \mathcal{R}_{,2}, \quad (67)$$

and

$$\begin{aligned}\bar{B} &= B + A \mathcal{D}_1 G^{-1} \mathcal{D}_1^T A, \\ \bar{C} &= C + A \mathcal{D}_1 G^{-1} \mathcal{D}_2^T A, \\ \bar{D} &= D + A \mathcal{D}_2 G^{-1} \mathcal{D}_2^T A.\end{aligned}\quad (68)$$

If we can drive  $U^*$  to be zero for any  $\mathcal{R}$ , then we have found an asymptotically correct Reissner-Mindlin plate model. For smart plates with anisotropic material properties, this term in general will not be zero. However, we can minimize the nonzero  $U^*$  term to obtain a Reissner-Mindlin model for multiphysically coupled smart plates to be as asymptotically correct as possible. The accuracy of the Reissner-Mindlin model depends on how close  $U^*$  can be driven to zero. In other words, our task is to seek an optimal set of the 27 unknowns (3 unknowns for  $G$  and 24 unknowns for  $L_\alpha$ ) so that the value of the quadratic form in Eq. (67) is as close to zero as possible for arbitrary multiphysically coupled generalized strain measures.

This is achieved by letting 78 distinct coefficients in  $B$ ,  $C$ , and  $D$  matrices equal to zero to obtain 78 equations. The obtained equations construct a linear system with 27 unknowns. A least square technique is implemented to solve the overdetermined system to obtain 27 unknowns. From a Mathematical point of view, the overdetermined system (78 equations with 27 unknowns, indicated by  $MX = b$ ) may be singular for some material properties. For example, the rank of  $M^T M$  is only 26 for single-layer isotropic and orthotropic piezoelectric and piezomagnetic plates. Under this situation, Singular Value Decomposing technique can be applied to solve this least square problem. Moreover, for an accurate estimation of the transverse shear matrix, a nondimensional scheme is used to guarantee that each of the 78 equations has the same physical unit.

By driving  $U^*$  to zero, we obtain the “best” Reissner-Mindlin model which will be used for the 2D magneto-electro-elastic plate analysis:

$$2\Pi_{\mathcal{R}} = \mathcal{R}^T A \mathcal{R} + \gamma^T G \gamma - 2\mathcal{R}^T F, \quad (69)$$

where  $A$ ,  $G$ ,  $F$  capture the necessary material and geometric information obtained from the dimensional reduction process. It is worthy to emphasize that although the 2D constitutive model is constructed in a way dramatically different from the traditional Reissner-Mindlin model, the plate analysis remains the same, with no changes in the governing equations except that the effect of electric and magnetic couplings have already been taken into account in matrices  $\bar{A}$ ,  $\bar{B}$ ,  $\bar{C}$ ,  $\bar{D}$  and strain measures are now defined using Eqs. (60).

## The Recovery of 3D Multiphysics Fields

Thus far, we have obtained a generalized Reissner-Mindlin model based on the asymptotically correct second-order magnetoelectric enthalpy for magneto-electric-elastic plates. This model can be used for various analyses of smart plates, spanning from static, dynamic, buckling, to aeroelastic analyses. In many applications, however, the capability of predicting accurate 2D displacement fields of the magnetic, electric, and elastic coupling plates is not sufficient. Ultimately, the fidelity of a reduced-order model should be evaluated based on how well it can predict the 3D mechanical fields (displacements and stresses) and electric and magnetic fields (magnetic and electric potentials, electric displacements, magnetic inductions) for the original 3D problem. Therefore, it is necessary to provide recovery relations to express the aforementioned 3D multiphysics fields in terms of 2D quantities and  $x_3$ .

By using Eqs. (3), (5) and (6), the 3D displacement field can be recovered to the first order of accuracy:

$$U_i = u_i + x_3(\mathcal{C}_{3i} - \delta_{3i}) + \mathcal{C}_{ji} w_j, \quad (70)$$

where  $w_\alpha = v_\alpha$ ,  $w_3 = w_3^0$ . The electric and magnetic potentials are given by  $\phi = \phi^0$  and  $\psi = \psi^0$ .

Consequently, the 3D stresses  $\sigma_{ij}$ , electric displacements  $D_i$ , and magnetic induction  $B_i$  can be obtained by applying the 3D constitutive relations. Since we have obtained an optimal estimation of the shear stiffness matrix  $G$ , the recovered 3D results up to the first order are better than CLT and FSDT. However, because the first-order approximation can only provide a linear prediction of the multiphysics fields and some stress, electric displacement, and magnetic induction components may require higher order functions for a better description their 3D behaviors, it is necessary to derive a more refined recovery procedure with reasonable accuracy. The transverse normal stress ( $\sigma_{33}$ ) serves well as a suitable illustrative example and this have been described in Refs. [25, 26] for analyzing multilayered composite plates:  $\sigma_{33}$  is a second-order quantity and it cannot be predicted by the first-order approximation; a better prediction of this quantity requires the perturbation of the warping functions to the second-order of accuracy.

A similar 3D recovery procedure is developed here for the investigation of the multiphysics problem. To obtain a reasonable accurate estimation of elastic stresses, electric displacements, and magnetic fluxes, VAM is applied one step further to find the warping functions and electric/magnetic potentials with the second-order of accuracy. The second-order perturbation of the warping functions as well as the electric and magnetic potentials is

$$\begin{aligned} w_{\parallel} &= v_{\parallel} + y_{\parallel} + o\left(\left(\frac{h}{l}\right)^2 \eta\right), & w_3 &= w_3^0 + y_3 + o\left(\left(\frac{h}{l}\right)^2 \eta\right), \\ \phi &= \phi^0 + \tilde{\phi} + o\left(\left(\frac{h}{l}\right)^2 \eta\right), & \psi &= \psi^0 + \tilde{\psi} + o\left(\left(\frac{h}{l}\right)^2 \eta\right), \end{aligned} \quad (71)$$

where,  $y_{\parallel}$  and  $y_3$  are the second-order warping functions;  $\tilde{\phi}$  and  $\tilde{\psi}$  are the second-order electric and magnetic potentials.

By substituting these expressions into the 3D strain as well as the electric and magnetic fields then into magnetoelectric enthalpy and applying the similar procedure introduced in the first-order approximation, it can be shown that the second-order in-plane components  $y_{\parallel}$  vanish. The continuity and boundary conditions for the second-order transverse normal stress  $\sigma_t$ , electric displacement  $D_t$ , and magnetic inductions  $B_t$  are given by:

$$\begin{aligned} [C_t y'_3 + C_{et}^T I_{\alpha} v_{\parallel, \alpha} + e_t \tilde{\phi} + q_t \tilde{\psi}] &= 0, \quad \text{on } \Omega_i, \\ [e_t y'_3 + e_{et}^T I_{\alpha} v_{\parallel, \alpha} - \varepsilon_{dt} \tilde{\phi} - \alpha_t \tilde{\psi}] &= 0, \quad \text{on } \Omega_i, \\ [q_t y'_3 + q_{et}^T I_{\alpha} v_{\parallel, \alpha} - \alpha_t \tilde{\phi} - \mu_t \tilde{\psi}] &= 0, \quad \text{on } \Omega_i, \end{aligned} \quad (72)$$

and

$$\begin{aligned} [C_t y'_3 + C_{et}^T I_{\alpha} v_{\parallel, \alpha} + e_t \tilde{\phi} + q_t \tilde{\psi}]^+ &= \tau_3, \\ [C_t y'_3 + C_{et}^T I_{\alpha} v_{\parallel, \alpha} + e_t \tilde{\phi} + q_t \tilde{\psi}]^- &= \beta_3, \\ [e_t y'_3 + e_{et}^T I_{\alpha} v_{\parallel, \alpha} - \varepsilon_{dt} \tilde{\phi} - \alpha_t \tilde{\psi}]^{+/-} &= 0, \quad \text{or } \tilde{\phi}^{+/-} = 0, \\ [q_t y'_3 + q_{et}^T I_{\alpha} v_{\parallel, \alpha} - \alpha_t \tilde{\phi} - \mu_t \tilde{\psi}]^{+/-} &= 0, \quad \text{or } \tilde{\psi}^{+/-} = 0, \end{aligned} \quad (73)$$

The Euler-Lagrange equations governing  $y_3$ ,  $\tilde{\phi}$  and  $\tilde{\psi}$  take the form of

$$\begin{aligned} (C_t y'_3 + C_{et}^T I_{\alpha} v_{\parallel, \alpha} + e_t \tilde{\phi} + q_t \tilde{\psi})' &= E'_{\alpha\beta} \mathcal{E}_{,\alpha\beta} + S' + \Lambda_3, \\ (e_t y'_3 + e_{et}^T I_{\alpha} v_{\parallel, \alpha} - \varepsilon_{dt} \tilde{\phi} - \alpha_t \tilde{\psi})' &= E'_{\phi\alpha\beta} \mathcal{E}_{,\alpha\beta} + S'_{\phi}, \\ (q_t y'_3 + q_{et}^T I_{\alpha} v_{\parallel, \alpha} - \alpha_t \tilde{\phi} - \mu_t \tilde{\psi})' &= E'_{\psi\alpha\beta} \mathcal{E}_{,\alpha\beta} + S'_{\psi}, \end{aligned} \quad (74)$$

with  $\Lambda_3$  representing the Lagrange multiplier for the second-order approximation and

$$\begin{aligned} E'_{\alpha\beta} &= -(e_{\beta}^T D_{\alpha}^* + C_{s(\beta\alpha)} C_{\perp} + e_{s(\beta\alpha)} + q_{s(\beta\alpha)} C_{\psi}), \\ E'_{\phi\alpha\beta} &= -e_{\beta}^T e_s^T C_s^{-1} D_{\alpha}^* - e_{s(\alpha\beta)} C_{\perp} + \frac{1}{2} (\varepsilon_{ds(\alpha\beta)} + \varepsilon_{ds(\beta\alpha)}) C_{\phi} + \alpha_{s(\beta\alpha)} C_{\psi}, \\ E'_{\psi\alpha\beta} &= -e_{\beta}^T q_s^T C_s^{-1} D_{\alpha}^* - q_{s(\alpha\beta)} C_{\perp} + \frac{1}{2} (\mu_{s(\alpha\beta)} + \mu_{s(\beta\alpha)}) C_{\psi} + \alpha_{s(\alpha\beta)} C_{\phi}, \\ S' &= -[e_{\beta}^T g_{,\beta}^* + (C_{s(\beta\alpha)} w_{3em}^0 + e_{s(\beta\alpha)} \phi_{em}^0 + q_{s(\beta\alpha)} \psi_{em}^0)_{,\alpha\beta} + P_3], \\ S'_{\phi} &= -e_{\beta}^T e_s^T C_s^{-1} g_{,\beta}^* + \left[ -e_{s(\alpha\beta)} w_{3em}^0 + \frac{1}{2} (\varepsilon_{ds(\alpha\beta)} + \varepsilon_{ds(\beta\alpha)}) \phi_{em}^0 + \alpha_{s(\beta\alpha)} \psi_{em}^0 \right]_{,\alpha\beta}, \\ S'_{\psi} &= -e_{\beta}^T q_s^T C_s^{-1} g_{,\beta}^* + \left[ -q_{s(\alpha\beta)} w_{3em}^0 + \frac{1}{2} (\mu_{s(\alpha\beta)} + \mu_{s(\beta\alpha)}) \psi_{em}^0 + \alpha_{s(\alpha\beta)} \phi_{em}^0 \right]_{,\alpha\beta}. \end{aligned}$$

$y_3$ ,  $\tilde{\phi}$ , and  $\tilde{\psi}$  can be solved from Eq. (74) in conjunction with Eqs. (72) and (73).

Although the successful prediction of  $y_3$ ,  $\tilde{\phi}$ , and  $\tilde{\psi}$  enables us to obtain an magnetoelectric enthalpy expression asymptotically corrected up to the order of  $O((h/l)^4 \eta^2)$ , such an enthalpy expression is too complex for practical uses. We will still use the Reissner-Mindlin model to carry out the 2D plate analysis while use  $y_3$  for the second-order prediction of the 3D displacement/strain/stress fields and use  $\tilde{\phi}$  and  $\tilde{\psi}$  for the second-order predictions of electric fields/displacements and magnetic fields/inductions. As will be shown latter, this approach can achieve a good accuracy for moderate thick plates even though only the equivalent single-layer Reissner-Mindlin plate model is used for the 2D plate analysis.

To this stage, we can recover the 3D displacements, electric and magnetic potentials up to the second order as

$$\begin{aligned}\hat{U}_i &= u_i + x_3(\mathcal{C}_{3i} - \delta_{3i}) + \mathcal{C}_{ji}w_j + \delta_{3i}\mathcal{C}_{3i}y_3, \\ \hat{\phi} &= \phi^0 + \tilde{\phi}, \\ \hat{\psi} &= \psi^0 + \tilde{\psi}.\end{aligned}\tag{75}$$

The second-order estimation of elastic strains as well as electric and magnetic fields then becomes

$$\begin{aligned}\hat{\Gamma}_e &= \epsilon + x_3\kappa + I_\alpha v_{\parallel,\alpha}, & 2\hat{\Gamma}_s &= v'_{\parallel} + e_\alpha w_{3,\alpha}^0, & \hat{\Gamma}_t &= w_3^{0'} + y_3', \\ \hat{E}_s &= -\phi'_{\parallel}, & \hat{E}_t &= -(\phi^{0'} + \tilde{\phi}'), \\ \hat{H}_s &= -\psi'_{\parallel}, & \hat{H}_t &= -(\psi^{0'} + \tilde{\psi}'),\end{aligned}\tag{76}$$

Finally, we can recover the 3D multiphysstress field up to the second order as

$$\begin{aligned}\begin{Bmatrix} \sigma_e \\ \sigma_s \\ \sigma_t \end{Bmatrix} &= \begin{bmatrix} C_e & 0 & C_{et} \\ 0 & C_s & 0 \\ C_{et}^T & 0 & C_t \end{bmatrix} \begin{Bmatrix} \hat{\Gamma}_e \\ 2\hat{\Gamma}_s \\ \hat{\Gamma}_t \end{Bmatrix} - \begin{bmatrix} 0 & e_{et} \\ e_s & 0 \\ 0 & e_t \end{bmatrix} \begin{Bmatrix} \hat{E}_s \\ \hat{E}_t \end{Bmatrix} - \begin{bmatrix} 0 & q_{et} \\ q_s & 0 \\ 0 & q_t \end{bmatrix} \begin{Bmatrix} \hat{H}_s \\ \hat{H}_t \end{Bmatrix}, \\ \begin{Bmatrix} D_s \\ D_t \end{Bmatrix} &= \begin{bmatrix} 0 & e_s & 0 \\ e_{et} & 0 & e_t^T \end{bmatrix} \begin{Bmatrix} \hat{\Gamma}_e \\ 2\hat{\Gamma}_s \\ \hat{\Gamma}_t \end{Bmatrix} + \begin{bmatrix} \varepsilon_{ds} & 0 \\ 0 & \varepsilon_{dt} \end{bmatrix} \begin{Bmatrix} \hat{E}_s \\ \hat{E}_t \end{Bmatrix} + \begin{bmatrix} \alpha_s & 0 \\ 0 & \alpha_t \end{bmatrix} \begin{Bmatrix} \hat{H}_s \\ \hat{H}_t \end{Bmatrix}, \\ \begin{Bmatrix} B_s \\ B_t \end{Bmatrix} &= \begin{bmatrix} 0 & q_s & 0 \\ q_{et} & 0 & q_t^T \end{bmatrix} \begin{Bmatrix} \hat{\Gamma}_e \\ 2\hat{\Gamma}_s \\ \hat{\Gamma}_t \end{Bmatrix} + \begin{bmatrix} \alpha_s^T & 0 \\ 0 & \alpha_t \end{bmatrix} \begin{Bmatrix} \hat{E}_s \\ \hat{E}_t \end{Bmatrix} + \begin{bmatrix} \mu_s & 0 \\ 0 & \mu_t \end{bmatrix} \begin{Bmatrix} \hat{H}_s \\ \hat{H}_t \end{Bmatrix}.\end{aligned}\tag{77}$$

## Validation Examples

We have derived a general formulation to treat smart plates made of piezoelectric and magnetostrictive materials with properties as functions of  $x_3$ . In the following, we will use several examples to demonstrate the performance of the present theory. The primary focus of this study is to evaluate the capability of the present asymptotic plate model on predicting multi-physics components for different smart plates subjected to various boundary and load (mechanical, electric, and magnetic) combinations.

To validate of the present model initially, results are compared with 3D exact solutions. 3D exact solution approaches are developed by following the methodology described by Pan et. al. in Refs. [7,8]. However, some modifications have been made to enable the solution procedure suitable for more general eigenvalue problems (complex, real, and imaginary) so that it can be used for more general material types. Two different materials are used in the validation examples. The first is the magnetostrictive material  $CoFe_2O_4$  and the second is the much studied piezoelectric material PZT-4. Material properties of these two materials are listed in Table 1. For all validation examples, the plate is infinitely long along the  $x_1$  direction and two edges parallel to  $x_2$  are subjected to simply supported boundary conditions (i.e.  $u_3 = \phi = \psi = \sigma_{33} = D_3 = B_3 = 0$  along the edge length).

### Magnetostrictive Plate Under Mechanical Loading

The first example considered is a magnetostrictive ( $CoFe_2O_4$ ) plate with width  $b$  and thickness  $h$  subjected to a sinusoidally distributed normal traction on the top surface of the plate:  $\tau_3(x_2) = q_0 \sin(\pi x_2/b)$ . All other tractions are zero on top and bottom surfaces. Zero electric and magnetic potentials are specified on the bottom surface while the top surface is maintained to be electrically and magnetically free (zero electric displacement and magnetic flux).

To facilitate our comparison, the physical quantities for this example are nondimensionlized by the

**Table 1. Material properties for two materials used in validation examples ( $\varepsilon_0 = 8.8541 \times 10^{-12} C^2/(Nm^2)$  is the dielectric constant of vacuum)**

Material properties for <i>PZT</i> - 4				Material properties for <i>CoFe<sub>2</sub>O<sub>4</sub></i>			
$E_1 = E_2$ [Gpa]	81.3	$E_3$ [Gpa]	64.5	$C_{11} = C_{22}$ [Gpa]	286.0	$C_{33}$ [Gpa]	269.5
$G_{13} = G_{23}$ [Gpa]	25.6	$G_{12}$ [Gpa]	30.6	$C_{13} = C_{23}$ [Gpa]	170.5	$C_{12}$ [Gpa]	173
$\nu_{13} = \nu_{23}$	0.432	$\nu_{12}$	0.329	$C_{44} = C_{55}$ [Gpa]	45.3	$C_{66}$ [Gpa]	56.5
$e_{31} = e_{32}$ [C/m <sup>2</sup> ]	-5.2	$e_{33}$ [C/m <sup>2</sup> ]	15.08	$q_{31} = q_{32}$ [N/(Am)]	580.3	$q_{33}$ [N/(Am)]	699.7
$e_{24} = e_{15}$ [C/m <sup>2</sup> ]	12.72	$\varepsilon_{11}/\varepsilon_0 = \varepsilon_{22}/\varepsilon_0$ (/)	1475	$q_{24} = q_{15}$ [N/(Am)]	550	$\varepsilon_{11} = \varepsilon_{22}$ [C <sup>2</sup> /(Nm <sup>2</sup> )]	$8.0 \times 10^{-11}$
$\varepsilon_{33}/\varepsilon_0$ (/)	1300	$\mu_{11} = \mu_{22}$ [Ns <sup>2</sup> /C <sup>2</sup> ]	$5.0 \times 10^{-6}$	$\varepsilon_{33}$ [C <sup>2</sup> /(Nm <sup>2</sup> )]	$9.3 \times 10^{-11}$	$\mu_{11} = \mu_{22}$ [Ns <sup>2</sup> /C <sup>2</sup> ]	$-5.9 \times 10^{-4}$
$\varepsilon_{33}$ [Ns <sup>2</sup> /C <sup>2</sup> ]	$10.0 \times 10^{-6}$			$\varepsilon_{33}$ [Ns <sup>2</sup> /C <sup>2</sup> ]	$1.57 \times 10^{-4}$		

following relations:

$$\begin{aligned} \bar{U}_i &= \frac{C_{11}h^3U_i}{q_0b^4}, & \bar{\sigma}_{ij} &= \frac{\sigma_{ij}}{q_0}, & \bar{\phi} &= \frac{e_{31}\phi}{q_0b}, \\ \bar{\psi} &= \frac{q_{31}\psi}{q_0b}, & \bar{D}_i &= \frac{C_{11}D_i}{e_{31}q_0}, & \bar{B}_i &= \frac{C_{11}B_i}{q_{31}q_0}. \end{aligned} \quad (78)$$

Figures 2, 3, and 4 depict the through-the-thickness variation of the maximum values of nondimensional displacements ( $U_i$ ), stresses ( $\sigma_{ij}$ ), magnetic potential ( $\psi$ ), and magnetic fluxes  $B_i$  for two moderate thick magnetostrictive plates with length to thickness ratios  $b/h$  being 10 and 15. Throughout this paper,  $\bar{z} = x_3/h$  indicates the nondimensional  $x_3$  coordinate. As there is no magnetoelectric coupling ( $\alpha_{ij} = 0$ ), electric components are all zeros. All elastic variables (displacements and stresses) matches excellently well with the 3D solutions as evidenced by the override of the two solution curves for all these components except for  $\sigma_{23}$ , of which the maximum relative errors are still within 0.18% and 0.41% for  $b/h = 15$  and 10 respectively. In fact, the tendency of this excellent match of elastic variables are maintained for a wide range of the width to thickness ratio, up to  $b/h = 2.5$  (see Table 2). For this example, the accuracy of present model is majorly determined by the passively induced magnetic components, i.e. the magnetic potential  $\phi$  and fluxes  $B_2, B_3$ . Out of all 9 components compared, the maximum relative error occurs for the transverse magnetic flux  $B_3$ . The maximum errors of  $\phi$  and fluxes  $B_2, B_3$  take values of 1.31%, 4.99%, and 6.62%, respectively for the moderate aspect ratio of 15, while for  $b/h = 10$  these errors become relatively large, taking values of 10.16%, 11.45%, and 14.87%, respectively.

It is well known that in nearly all plate theories the behavior of field variables changes dramatically as the aspect ratio varies. This aspect ratio influence is illustrated in Table 2 where the maximum value of various field variables evaluated at appropriate  $(x_2, x_3)$  locations are compared with their 3D counterparts for plates with different  $b/h$ s. Because for this example in-plane displacement and stress fields can always be calculated more accurately than the transverse elastic components, they are not listed in Table 2.

It can be observed from Table 2 that the present plate model can provide an excellent prediction of elastic components for plates varying from thin to extremely thick (up to  $b/h = 2.5$ ), however, the accurate prediction of magnetic components ( $\psi, B_2$ , and  $B_3$ ) can only be achieved for thin and moderate thick plates (up to  $b/h = 15$ ). These passively induced magnetic fields demonstrate stronger 3D behavior than those elastic components which exhibit more plate like behavior. 3D exact simulations show that as the plate becomes thicker the curves of these passively induced variables take more complicated forms, indicating the accurate 3D behavior of these magnetic fields can only be captured by higher order functions. This phenomena will be further explained in example 3.

### Piezoelectric Plate Under Mechanical Loading

The second example is related to a piezoelectric plate subjected to the same sinusoidally distributed normal traction on the top surface of the plate:  $\tau_3(x_2) = q_0 \sin(\pi x_2/b)$ . The major difference between this example

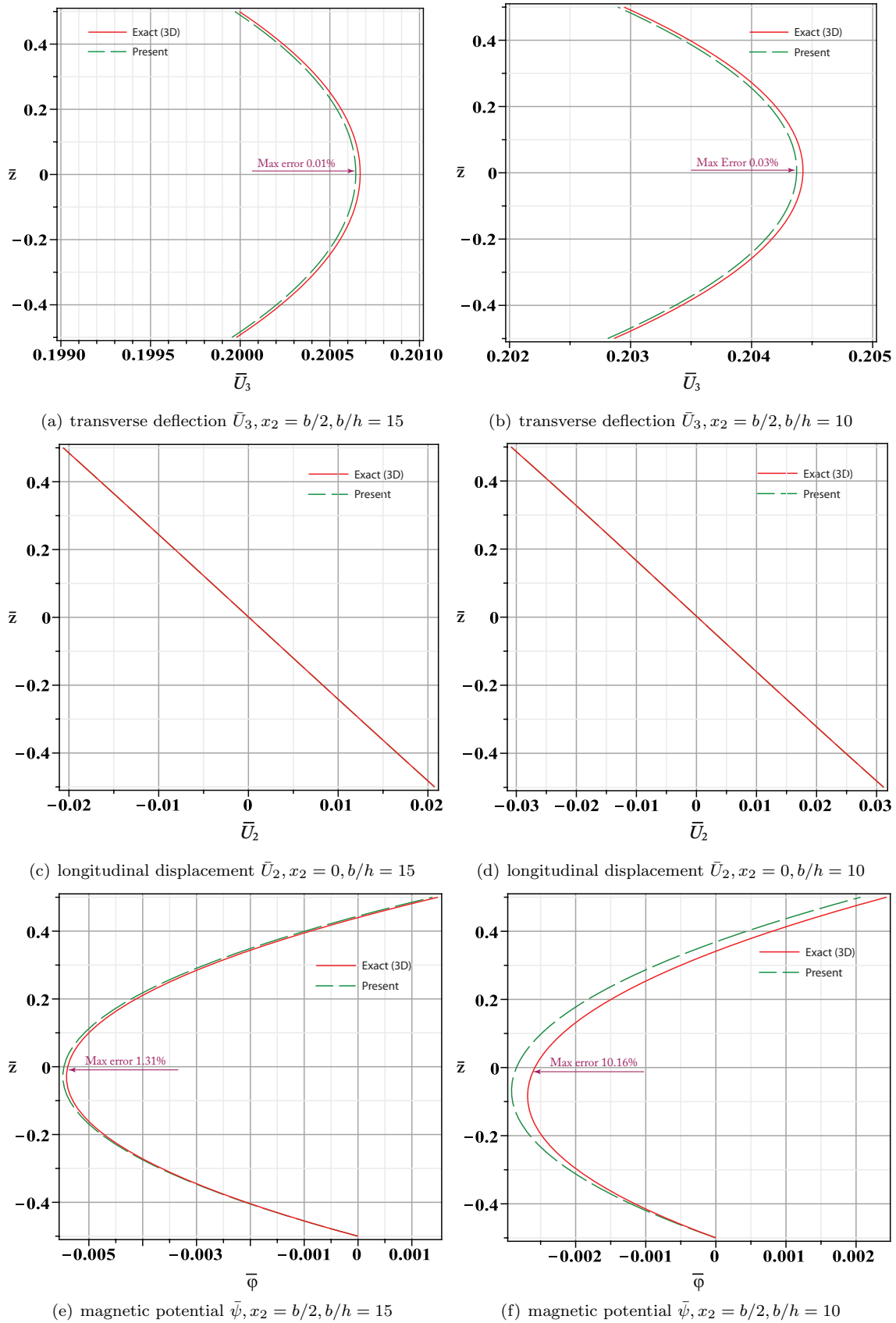
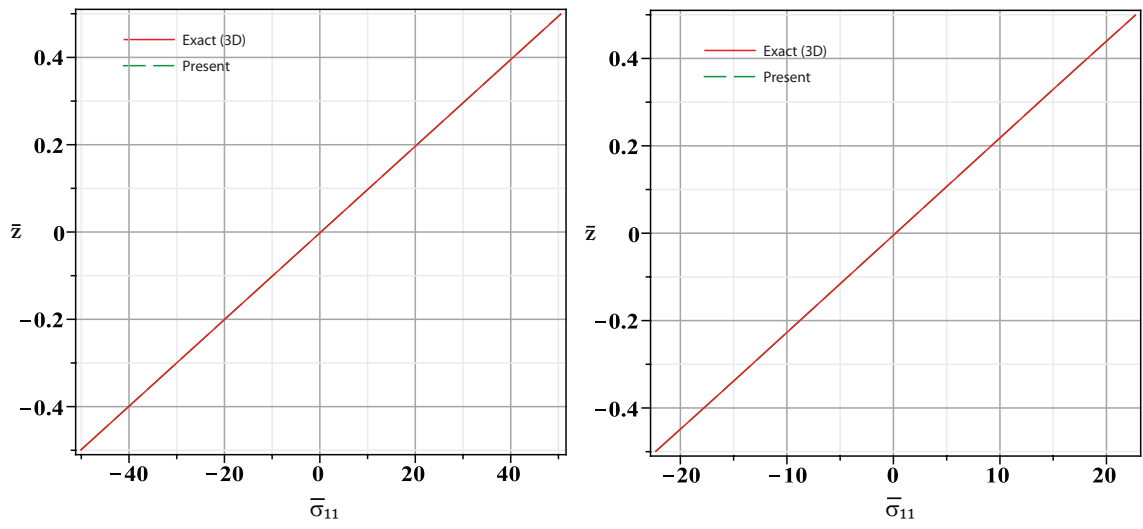
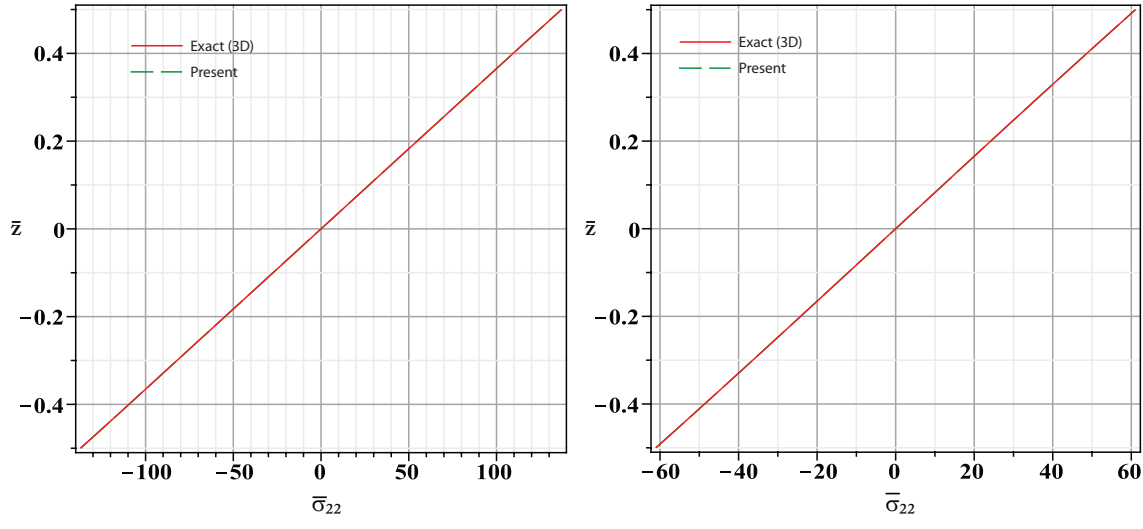


Figure 2. Variation of maximum nondimensional transverse deflection, longitudinal displacement, and magnetic potential along the thickness direction for a cylindrically bent magnetostrictive ( $CoFe_2O_4$ ) plate subjected to a sinusoidal pressure on the top surface (moderate thick plates with  $b/h = 10$  and  $15$ ).



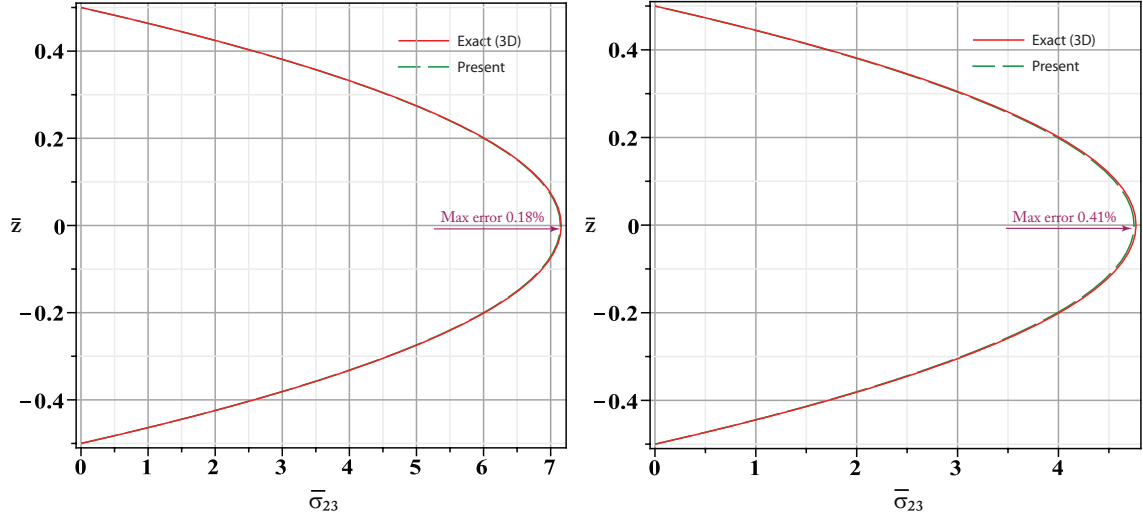
(a) in-plane normal stress  $\bar{\sigma}_{11}, x_2 = b/2, b/h = 15$

(b) in-plane normal stress  $\bar{\sigma}_{11}, x_2 = b/2, b/h = 10$



(c) in-plane normal stress  $\bar{\sigma}_{22}, x_2 = b/2, b/h = 15$

(d) in-plane normal stress  $\bar{\sigma}_{22}, x_2 = b/2, b/h = 10$



(e) transverse shear stress  $\bar{\sigma}_{23}, x_2 = 0, b/h = 15$

(f) transverse shear stress  $\bar{\sigma}_{23}, x_2 = 0, b/h = 10$

Figure 3. Variation of maximum nondimensional in-plane normal and transverse shear stresses along the thickness direction for a cylindrically bent magnetostrictive ( $CoFe_2O_4$ ) plate subjected to a sinusoidal pressure on the top surface (moderate thick plates with  $b/h = 10$  and  $15$ ).

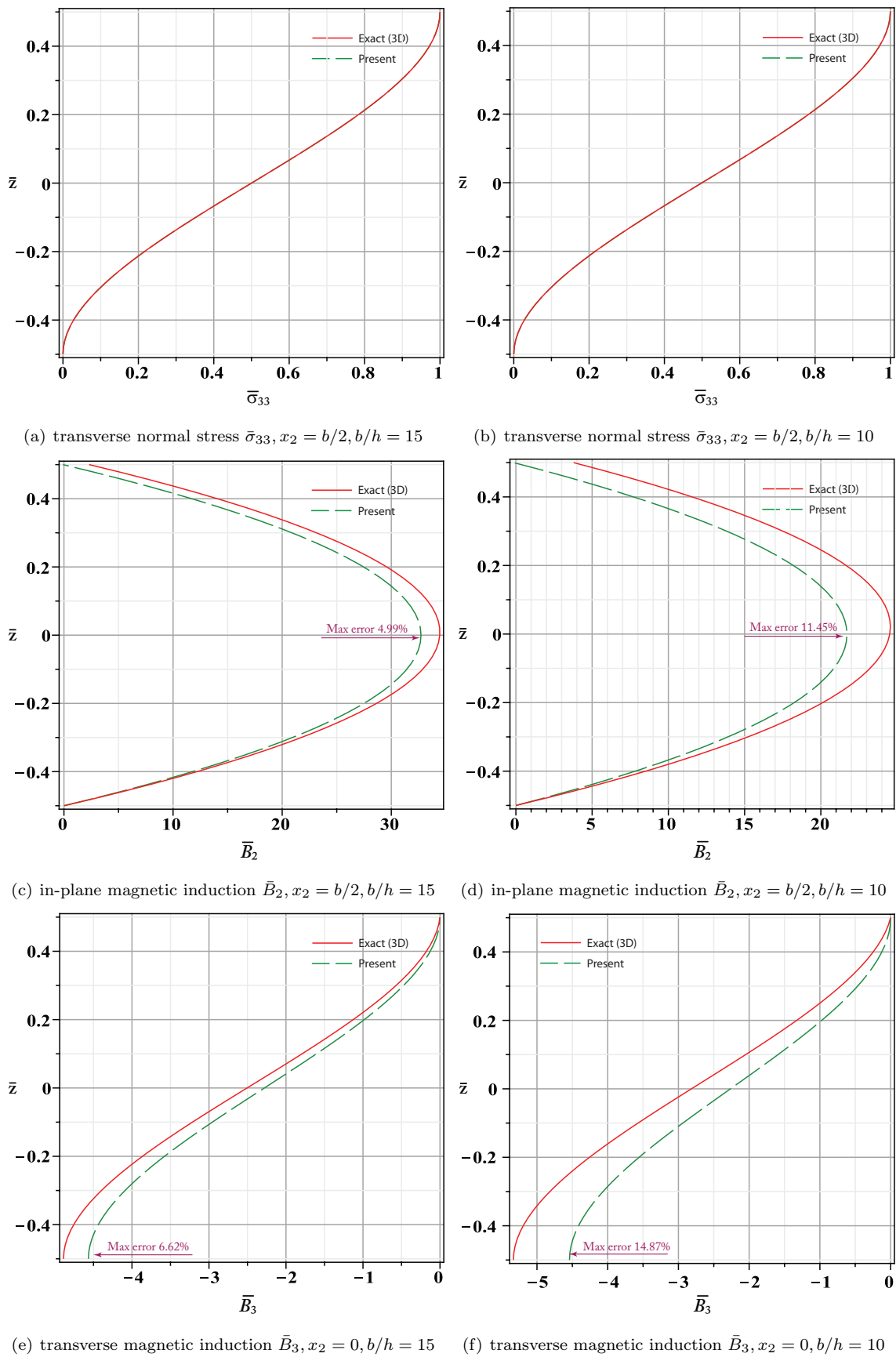


Figure 4. Variation of maximum nondimensional transverse normal stress and magnetic inductions along the thickness direction for a cylindrically bent magnetostrictive ( $CoFe_2O_4$ ) plate subjected to a sinusoidal pressure on the top surface (moderate thick plates with  $b/h = 10$  and  $15$ ).

**Table 2. Influence of aspect ratio for mechanically loaded magnetostrictive plates with one surface subjected to zero electric and magnetic potentials and the other being electric and magnetic free.**

$b/h$	$U_3(b/2, 0)$		$\psi(b/2, 0)$		$\sigma_{23}(0, 0)$		$\sigma_{33}(b/2, 0)$		$B_2(0, 0)$		$B_3(b/2, -h/2)$	
	present	3D	present	3D	present	3D	present	3D	present	3D	present	3D
20	0.199	0.199	-7.848E-03	-7.820E-03	9.537	9.547	0.500	0.500	43.702	44.955	-4.575	-4.752
18	0.200	0.200	-6.910E-03	-6.870E-03	8.581	8.591	0.500	0.500	39.313	40.716	-4.572	-4.792
15	0.201	0.201	-5.464E-03	-5.393E-03	7.145	7.158	0.500	0.500	32.723	34.441	-4.566	-4.889
12	0.202	0.202	-3.939E-03	-3.795E-03	5.709	5.725	0.500	0.500	26.123	28.353	-4.554	-5.079
10	0.204	0.204	-2.845E-03	-2.582E-03	4.750	4.769	0.500	0.500	21.713	24.520	-4.540	-5.333
8	0.208	0.208	-1.637E-03	-1.072E-03	3.789	3.813	0.500	0.500	17.288	21.148	-4.514	-5.878
5	0.224	0.224	6.500E-04	4.875E-03	2.337	2.377	0.500	0.500	10.580	21.809	-4.403	-10.751
2.5	0.303	0.305	3.778E-03	-5.282E-03	1.094	1.172	0.500	0.497	4.738	-1.207	-3.853	2.888
$b/h$	Error %		Error %		Error %		Error %		Error %		Error %	
20	0.01		0.37		0.10		0.00		2.79		3.72	
18	0.01		0.58		0.13		0.00		3.45		4.60	
15	0.01		1.31		0.18		0.00		4.99		6.62	
12	0.02		3.80		0.29		0.00		7.86		10.33	
10	0.03		10.16		0.41		0.00		11.45		14.87	
8	0.04		52.72		0.64		0.01		18.26		23.20	
5	0.01		86.67		1.65		0.05		51.49		59.05	
2.5	0.72		171.53		6.68		0.58		492.62		233.41	

and the previous one is that in the current situation all electric and magnetic potentials are specified to be zero on both top and bottom surfaces of the plate. All other boundary conditions are the same as example 1 except that the material of the plate is now changed to be PZT-4. Similar to example 1, physical quantities for this example are nondimensionlized according to Eq. (78).

Figures 5 and 6 provide a complete comparison of all 9 nonzero multiphysics fields obtained by using present plate model with their corresponding 3D solutions for a extremely thick plate with  $b/h = 2.5$ . Through-thickness variation of the maximum values of all these variables are plotted. Because no magneto-electric coupling exists for the PZT-4 material ( $\alpha_{ij} = 0$ ), all magnetic components in this example are all identically zeros. Unlike the previous example, the present plate model provides an excellent prediction of all 9 multiphysics field variables for an extremely thick piezoelectric plate with ( $b/h = 2.5$ ). The maximum relative error among elastic components occurs for  $\sigma_{23}$  which takes the value of 5.04%, while the maximum relative error among electric variables is 1.89%, corresponding to  $D_3$ . As usual, this model provides a better prediction of in-plane multiphysics components than the transverse components, consisting with the fact that high order perturbation and recovery procedures are required for obtaining transverse components during the theoretical derivation.

To illustrate the influence of the aspect ratio on multiphysics fields, a detailed comparison with the 3D exact solutions is given in Table 3. As expected, the accuracy of the present model increases as  $b/h$  increases. For this particular example, an excellent accuracy of 5.04% can be achieved even for an extremely thick plate ( $b/h = 2.5$ ). This example also pointed out an important fact, i.e., a systematical comparison with 3D solutions for carefully selected load and boundary combinations is required for a true validation and estimation of a specific plate theory, especially for problems with coupled multiphysics fields. Comparisons made only on some specific cases may not be enough to guarantee the accuracy of the developed theory.

### Piezoelectric Plate Subjected to Electric Potentials

To complete the systematical evaluation of the present plate theory, the third example under investigation is a PZT-4 piezoelectric plate subjected to sinusoidally distributed electric potential on both the top and bottom surface of the plate, with  $\phi(x_2, h/2) = \frac{\phi_0}{2} \sin(\frac{\pi x_2}{b})$ ,  $\phi(x_2, -h/2) = -\frac{\phi_0}{2} \sin(\frac{\pi x_2}{b})$ , and zero magnetic potentials  $\psi(x_2, h/2) = \psi(x_2, -h/2) = 0$ . In addition, on both of these boundary surfaces the plate is traction

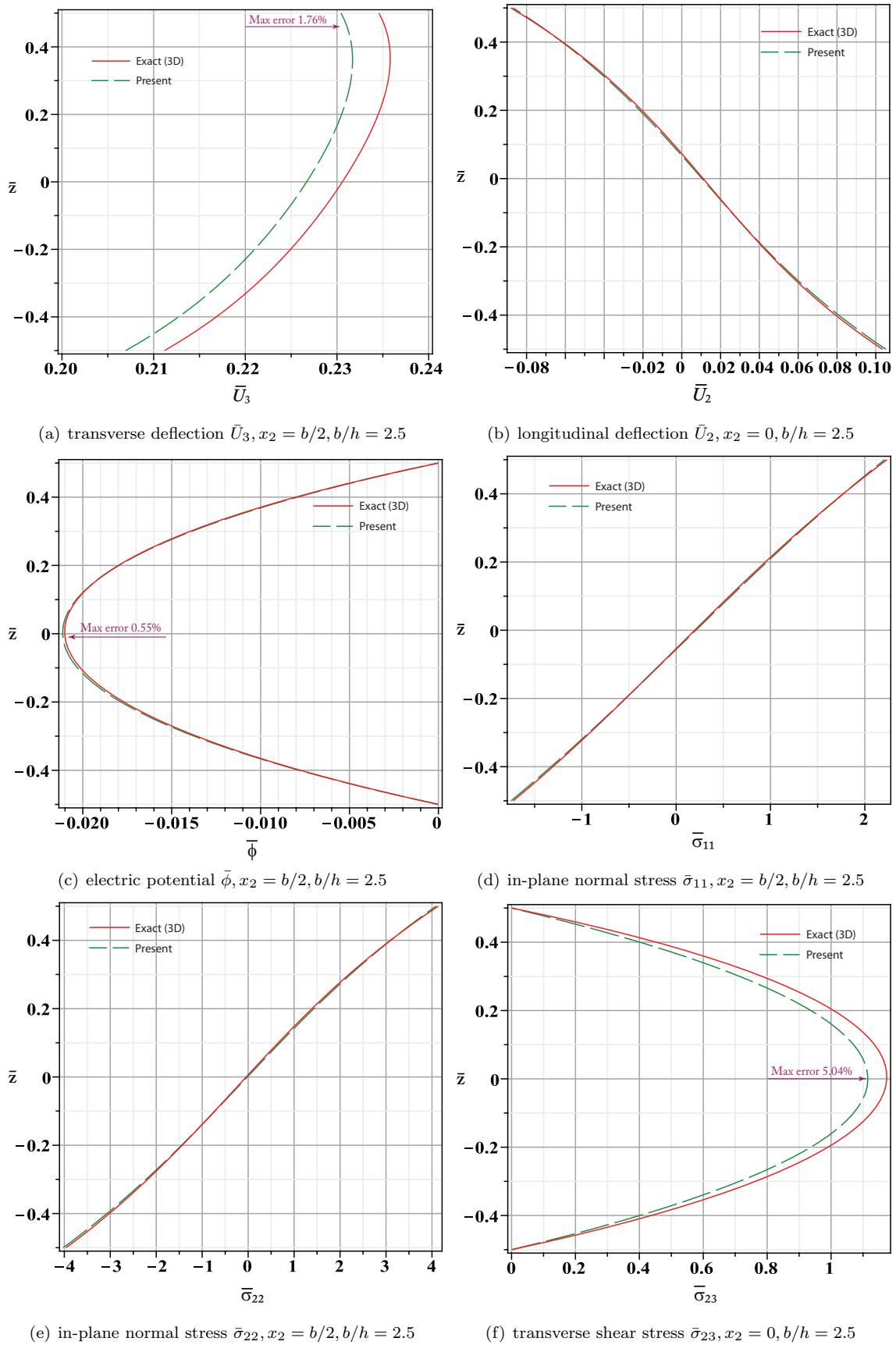
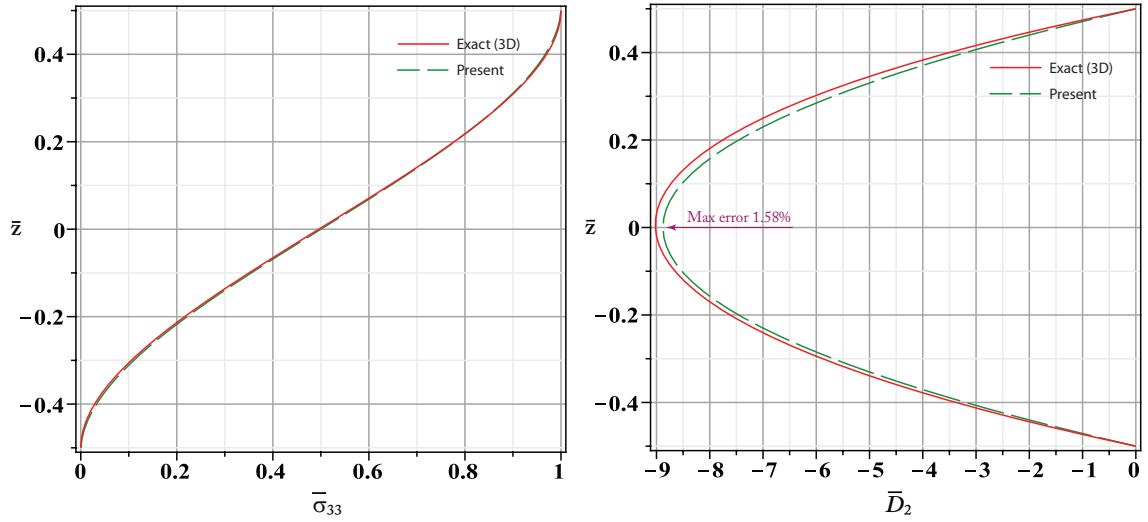
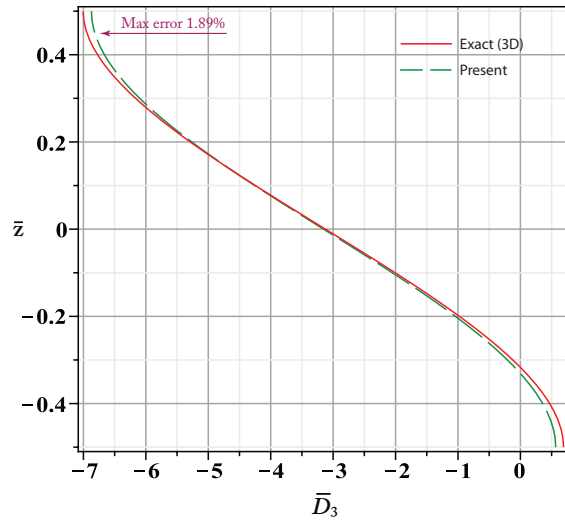


Figure 5. Variation of maximum nondimensional elastic displacements, electric potential, in-plane normal stresses, and transverse shear stress along the thickness direction for a cylindrically bent piezoelectric (PZT-4) plate subjected to a sinusoidal pressure on the top surface,  $\phi = \psi = 0$  at top and bottom surfaces (an extremely thick plate with  $b/h = 2.5$ ).



(a) transverse normal stress  $\bar{\sigma}_{33}, x_2 = b/2, b/h = 2.5$  (b) in-plane electric displacement  $\bar{D}_2, x_2 = b/2, b/h = 2.5$



(c) transverse electric displacement  $\bar{D}_3, x_2 = 0, b/h = 2.5$

Figure 6. Variation of maximum nondimensional transverse normal stress and electric displacements along the thickness direction for a cylindrically bent piezoelectric (PZT-4) plate subjected to a sinusoidal pressure on the top surface,  $\phi = \psi = 0$  at top and bottom surfaces (an extremely thick plate with  $b/h = 2.5$ ).

**Table 3. Influence of aspect ratio for mechanically loaded piezoelectric plates with both top and bottom surface subjected to zero electric and magnetic potentials.**

$b/h$	$U_3(b/2, h/2)$		$\psi(b/2, 0)$		$\sigma_{23}(0, 0)$		$D_2(0, 0)$		$D_3(b/2, h/2)$	
	present	3D	present	3D	present	3D	present	3D	present	3D
20	0.160	0.160	-0.162	-0.162	9.539	9.547	-75.945	-75.955	-7.130	-7.132
18	0.160	0.160	-0.146	-0.146	8.583	8.592	-68.334	-68.346	-7.129	-7.131
15	0.161	0.161	-0.122	-0.122	7.149	7.159	-56.913	-56.927	-7.127	-7.130
12	0.161	0.162	-0.098	-0.098	5.713	5.726	-45.484	-45.502	-7.123	-7.127
10	0.163	0.163	-0.081	-0.081	4.755	4.770	-37.855	-37.877	-7.118	-7.124
8	0.165	0.165	-0.065	-0.065	3.795	3.814	-30.214	-30.242	-7.108	-7.119
5	0.174	0.175	-0.041	-0.041	2.348	2.378	-18.694	-18.744	-7.069	-7.096
2.5	0.230	0.235	-0.021	-0.021	1.115	1.174	-8.878	-9.021	-6.872	-7.005
$b/h$	Error %		Error %		Error %		Error %		Error %	
20	0.04		0.03		0.08		0.01		0.02	
18	0.04		0.04		0.10		0.02		0.03	
15	0.06		0.06		0.14		0.03		0.04	
12	0.10		0.09		0.22		0.04		0.06	
10	0.14		0.13		0.31		0.06		0.09	
8	0.22		0.19		0.49		0.09		0.15	
5	0.53		0.38		1.26		0.27		0.39	
2.5	1.76		0.55		5.04		1.58		1.89	

free. Physical quantities in this example are normalized as follows:

$$\begin{aligned}
 \bar{U}_i &= \frac{C_{11}h^3U_i}{e_{31}b^3\phi_0}, & \bar{\sigma}_{ij} &= \frac{\sigma_{ij}b}{e_{31}\phi_0}, & \bar{\phi} &= \frac{\phi}{\phi_0}, \\
 \bar{\psi} &= \frac{q_{31}\psi}{e_{31}\phi_0}, & \bar{D}_i &= \frac{C_{11}D_ib}{e_{31}^2\phi_0}, & \bar{B}_i &= \frac{C_{11}B_ib}{q_{31}e_{31}\phi_0}.
 \end{aligned} \tag{79}$$

Similar to previous examples, a detailed comparison of all 9 nonzero electric and mechanical components with their 3D counterparts for an extremely thick PZT-4 piezoelectric plate ( $b/h = 2.5$ ) subjected to the action of a sinusoidal electric potential difference prescribed on the top and bottom surfaces is shown Figures 7 and 8. Again, all plots reveal the through-thickness variation of the maximum values of these multiphysics variables. On the contrary to example 1 where mechanically loaded magnetostrictive plates with the fixed-free magnetic and electric boundary conditions on top and bottom surfaces are analyzed, in this example (with fixed-fixed electric and magnetic boundaries), all electric fields ( $\phi$ ,  $D_2$ , and  $D_3$ ) predicted by the current plate model demonstrate excellent accuracies, however, some mechanical components ( $\sigma_{23}$  and  $\sigma_{33}$ ) exhibit a strong 3D behavior. Among 3 electric field variables,  $D_2$  has the maximum relative error of 5.56% which occurs at  $\bar{z} \approx 0.3$ . Among the remaining 4 elastic components (excluding of  $\sigma_{23}$  and  $\sigma_{33}$ ), the maximum relative error is 17.97% and occurs for  $\sigma_{22}$ . In Figure 7(a), the passively induced transverse displacement  $U_3$  clearly demonstrates a 3D movement rather than the regular bending movement as studied in many elastic examples, indicating that the passively induced mechanical components demonstrate strong 3D behaviors. This is further evidenced by the curves of  $\sigma_{23}$  and  $\sigma_{33}$  plotted in 7(f) and 8(a)), where the shapes of the transverse normal and shear stresses become more complicated than those can be obtained in pure elastic studies. Figures 7(f) and 8(a) show that the  $\sigma_{23}$  and  $\sigma_{33}$  predicted by the current plate model are identically zero. And these results are also identically zeros for all other aspect ratios. A Taylor expansion of the 3D exact solution of  $\sigma_{23}$  and  $\sigma_{33}$  with respect to  $x_3$  reveals that the dominated part in the series of  $\sigma_{23}$  is the  $x_3^3$  term while dominated part for  $\sigma_{33}$  is the term related to  $x_3^4$ . As previously indicated in the theoretical derivation, the recovered transverse shear stress ( $\sigma_{23}$ ) is of the first-order accuracy (to the order of  $x_3^2$ ) while the transverse normal stress ( $\sigma_{33}$ ) is asymptotically correct to the second order (to order of  $x_3^3$ ). For this reason, it is not surprising to explain why the present plate model and in general all other currently available plate theories based on the equivalent single-layer model cannot capture  $\sigma_{23}$  and  $\sigma_{33}$ . From above analysis it is clear that it is necessary to push the recovery procedure one step further to obtain a better prediction of  $\sigma_{23}$  and  $\sigma_{33}$ . However, this is beyond the scope of the this paper and will be studied in our future work.

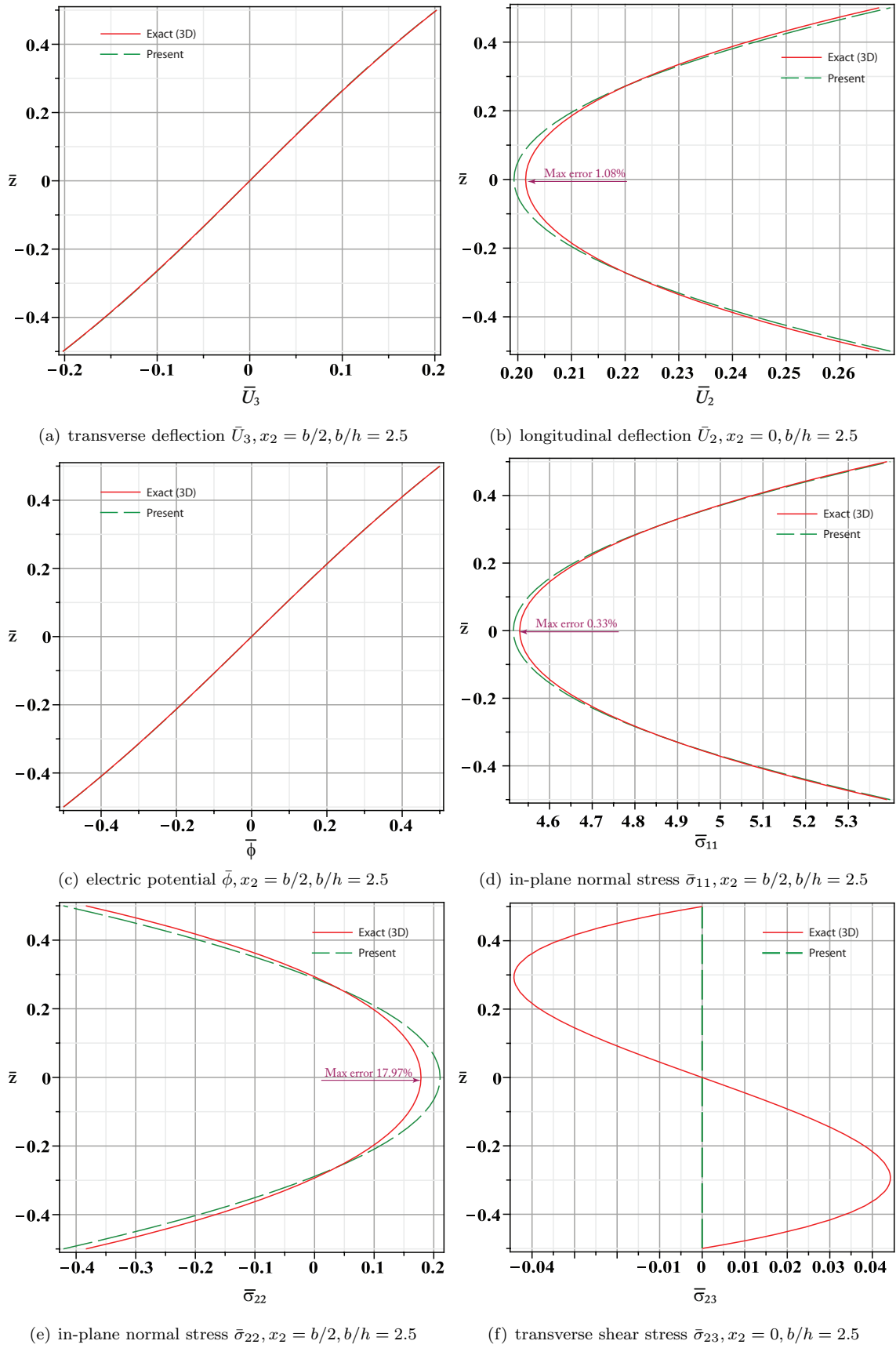
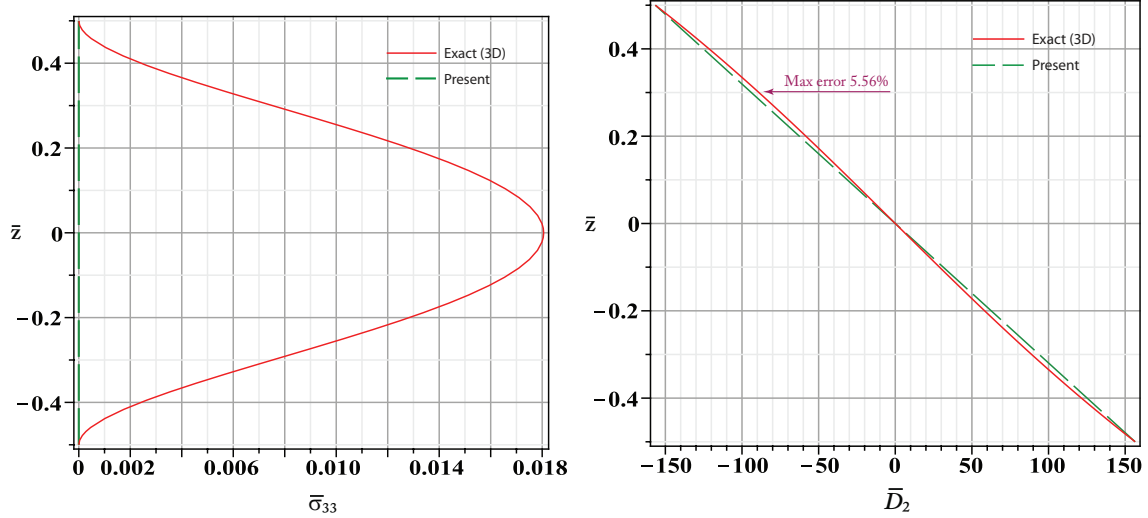
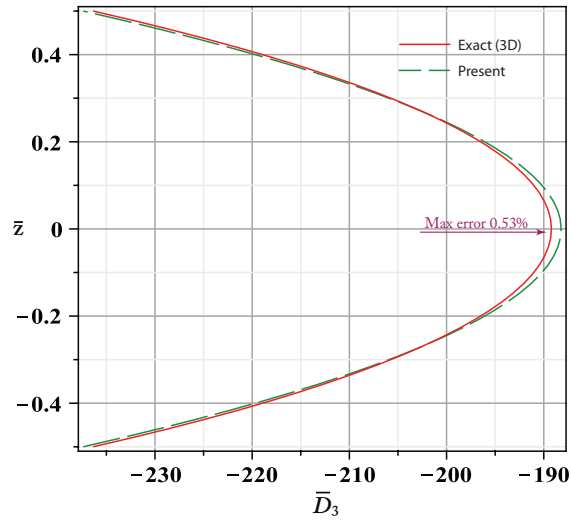


Figure 7. Variation of maximum nondimensional elastic deflections, electric potential, in-plane normal stresses, and transverse shear stress along the thickness direction for a cylindrically bent piezoelectric (PZT-4) plate subjected to sinusoidal electric potentials on top and bottom surfaces,  $\phi = \frac{1}{2}\phi_0 \sin(\frac{\pi x_2}{b})$ ,  $\phi = -\frac{1}{2}\phi_0 \sin(\frac{\pi x_2}{b})$  (an extremely thick plate with  $b/h = 2.5$ ).



(a) transverse normal stress  $\bar{\sigma}_{33}, x_2 = b/2, b/h = 2.5$  (b) in-plane electric displacement  $\bar{D}_2, x_2 = b/2, b/h = 2.5$



(c) transverse electric displacement  $\bar{D}_3, x_2 = 0, b/h = 2.5$

Figure 8. Variation of maximum nondimensional transverse normal stress and electric displacements along the thickness direction for a cylindrically bent piezoelectric (PZT-4) plate subjected to sinusoidal electric potentials on top and bottom surfaces,  $\phi = \frac{1}{2}\phi_0 \sin(\frac{\pi x_2}{b})$ ,  $\phi = -\frac{1}{2}\phi_0 \sin(\frac{\pi x_2}{b})$  (an extremely plate with  $b/h = 2.5$ ).

## Concluding Remarks

This paper provides a novel asymptotically correct and geometrically nonlinear plate model for piezoelectric and magnetostrictive smart plates. Unlike most prevailing plate theories which rely on *a priori* assumptions on describing the 3D elastic, electric, and magnetic fields, the present model is derived based on a variational asymptotical approach with no assumptions invoked for any multiphysics fields. The simplified 2D plate model is obtained by a systematic dimensional reduction approach so that the resulting variational statement is asymptotically correct to different orders of  $h/l$ . The original 3D magneto-electric-elastic problem is then cast in an intrinsic form so that the theory can accommodate arbitrary large deformation and global rotation with the restriction that the strains are small.

The accuracy of the present model has been validated by comparing results with 3D exact solutions. Its capability and limitation have also been systematically investigated by analyzing three carefully selected examples, namely, a mechanically loaded magnetostrictive plate with fix-free electric and magnetic boundary conditions, a mechanically loaded piezoelectric plate with zero electric and magnetic potentials specified on top and bottom surfaces, and a piezoelectric plate subjected to the prescribed electric potential difference. As the development of this asymptotical plate model follows a mathematically rigorous derivation, most conclusions drawn upon here are applicable for other plate theories developed based upon the equivalent single-layer model.

For mechanical loading cases, the present plate model can, in general, provide excellent accuracy for smart plates with moderate thickness. Although under some particular situations (e.g. with both boundary surfaces specified with zero electric and magnetic potentials) this plate model can achieve excellent accuracy for an extremely thick plate ( $b/h = 2.5$ ), the prediction capability is limited by the plate subjected to the electric/magnetic fix-free boundary condition, for which good accuracy can only be achieved for thin and moderate thick plates.

For smart plates subjected to pure electric or magnetic potential differences, excellent accuracy can be achieved for all electric/magnetic components (electric potential and displacements, magnetic potential and fluxed) as well all elastic displacements and in-plane stresses even though the plate becomes extremely thick. However, because the transverse shear and normal stresses demonstrate strong 3D behaviors and their behaviors are dominated by high order terms, the current plate model with the second-order stress recovery cannot capture these two fields. In the future, we plan to push our recovery procedure one step further to improve the prediction capability of the current plate model.

## Acknowledgements

The present work is supported, in part, by the Air Force Office of Scientific Research under Grant FA9550-08-1-0405. The program managers are Dr. Victor Giurgiutiu and Dr. David Stargel. The views and conclusions contained herein are those of the authors and should not be interpreted as necessarily representing the official policies or endorsement, either expressed or implied, of the funding agency.

## References

- <sup>1</sup>C. W. Nan. Magnetolectric effect in composites of piezoelectric and piezomagnetic phases. *Physical Review B*, 50:6082–6088, 1994.
- <sup>2</sup>J. H. Huang. Analytical predictions for the magnetoelastic coupling in piezomagnetic materials reinforced by piezoelectric ellipsoidal inclusions. *Physical Review B*, 58:12– 15, 1998.
- <sup>3</sup>T. Ueno and T. Higuchi. Design of magnetostrictive/piezoelectric laminate composite for coil-less magnetic force control. *IEEE Transactions on Magnetics*, 41:1233– 1237, 2005.
- <sup>4</sup>Y. Tanaka, K. Okamoto, and Fujimoto Y. Coupled vibration analysis of magnetizable plate in steady magnetic field with considering geometric nonlinearity. *IEEE Transactions on Magnetics*, 45:1254– 1257, 2009.
- <sup>5</sup>A.K. Soh. and J.X. Liu. On the constitutive equations of magneto-electro-elastic solids. *Journal of Intelligent Material Systems and Structures*, 16:597– 602, 2005.
- <sup>6</sup>E. Pan. Exact solution for simply supported and multilayered magneto-electro-elastic plates. *Journal of Applied Mechanics*, 68:608– 618, 2001.
- <sup>7</sup>E. Pan and P. R. Heyliger. Exact solutions for magneto-electro-elastic laminates in cylindrical bending. *International Journal of Solids and Structures*, 40:6859– 6876, 2003.
- <sup>8</sup>E. Pan and F. Han. Exact solution for functionally graded and layered magneto-electro-elastic plates. *International Journal of Engineering Science*, 43:321– 339, 2005.

- <sup>9</sup>P. R. Heyliger, F. Ramirez, and E. Pan. Two-dimensional static fields in magneto-electroelastic laminates. *Journal of Intelligent Material Systems and Structures*, 15:689–709, 2004.
- <sup>10</sup>P. R. Heyliger and E. Pan. Static fields in magneto-electroelastic laminates. *AIAA Journal*, 42:1435–1443, 2004.
- <sup>11</sup>W. Q. Chen and K. Y. Lee. Alternative state space formulations for piezoelectric thermoelasticity with transverse isotropy and the application to bending analysis of nonhomogeneous plates. *International Journal of Solids and Structures*, 40:5689–5705, 2003.
- <sup>12</sup>D.A. Saravanos, P. R. Heyliger, and D. A. Hopkins. Layerwise mechanics and finite element for the dynamic analysis of piezoelectric composite plates. *International Journal of Solids and Structures*, 34:359–378, 1997.
- <sup>13</sup>R. K. Bhangale and N. Ganesan. Static analysis of simply supported functionally graded and layered magneto-electric-elastic plates. *International Journal of Solids and Structures*, 43:3230–3253, 2006.
- <sup>14</sup>E. Carrera. Developements, ideas, and elalutations based upon Reissner’s Mixed Variational Theorem in the modeling of multilayered paltres and shells. *Applied Mechanics Reviews*, 54:301–329, 2001.
- <sup>15</sup>R. G. Lage, C. M. M. Soares, C.A. M. Soares, and J. N. Reddy. Layerwise partial mixed finite element analysis of magneto-electro-elastic plates. *Computers and Structures*, 82:1293–1301, 2004.
- <sup>16</sup>S. S. Phoenix, S. K. Satsangi, and B.N. Singh. Layer-wise modelling of magneto-electro-elastic plates. *Journal of Sound and Vibration*, 324:798–815, 2009.
- <sup>17</sup>Y. L. Zhou. Modeling of piezoelectric composite laminates using a third-order plate theory. In *Proceesings of the Eve-lenth (2001) International Offshear and Polar Engineering Conference*, pages 131–139, Stavanger, Norway, June 2001. The International Society of Offshore and Polar Engineers.
- <sup>18</sup>J. A. Mitchell and J. N. Reddy. A refined hybrid plate theory for composite laminates with piezoelectric laminae. *International Journal of Solids and Structures*, 32:2345–2367, 1995.
- <sup>19</sup>T. Kant and S. M. Shiyekar. Cylindrical bending of piezoelectric laminates with a higher order shear and normal deformation theory. *Computers & Structures*, 86:1594–1603, 2008.
- <sup>20</sup>S. Datta, J. Atulasimha, and A. B. Flatau. The modelling of magnetomechanical sensors in laminated structures. *Smart Materials and Structures*, 17:1–9, 2008.
- <sup>21</sup>D. Hasanyan, L. Librescu, Z. Qin, and D. R. Ambur. Magneto-thermo-elastokinetics of geometrically nonlinear laminated composite plates. part 1: fundation of the theory. *Journal of Sound and Vibrations*, 287:153–175, 2005.
- <sup>22</sup>L. Liao and W. Yu. Asymptotical construction of a fully coupled, reissner-mindlin model for piezoelectric composite plates. *Smart Materials and Structures*, 17(1), 2008. Article 015010.
- <sup>23</sup>L. Liao and W. Yu. A variational asymptotic model for piezoelectric composite plates with electroded lateral boundaries. *Composite Structures*, 88(3):394–402, 2009.
- <sup>24</sup>L. Liao and W. Yu. An electromechanical reissner-midlin model for laminated piezoelectric plates. *Composite Structures*, 88:394–402, 2009.
- <sup>25</sup>H. Chen and W. Yu. Asymptotical construction of an efficient high-fidelity model for functionally graded plates. In *Proceedings of 50th AIAA/ASME/ASCE/AHS/ASC Structures, Structural Dynamics, and Materials Conference*, pages AIAA 2009–2135, Palm Springs, California, 2009.
- <sup>26</sup>H. Chen and W. Yu. Asymptotical construction of an efficient high-fidelity model for multilayer functionally graded plates. *AIAA Journal*, 2009. in press.
- <sup>27</sup>D. A. Danielson and D. H. Hodges. Nonlinear beam kinematics by decomposition of the rotation tensor. *Journal of Applied Mechanics*, 54:258–262, 1987.
- <sup>28</sup>D. A. Danielson. Finite rotation with small strain in beams and plates. In *Proceedings of the 2nd Pan American Congress of Applied Mechanics*, Valparaiso, Chile, January 2 – 4 1991. Valparaiso Chile.
- <sup>29</sup>Atilgan A. R. Hodges, D. H. and D. A. Danielson. A geometrically nonlinear theory of elastic plates. *Journal of Applied Mechanics, Transactions of the ASME*, 60:109–116, 1993.
- <sup>30</sup>A. R. Atilgan and D. H. Hodges. On the strain energy of laminated coposite plates. *International Journal of Solids and Structures*, 29(20):2527–2543, 1992.

# Variational Asymptotic Homogenization and Dimensional Reduction of Composite Plates with In-Plane Heterogeneity

Chang-Yong Lee,\*Wenbin Yu†

*Utah State University, Logan, Utah 84322-4130*

and

Maxwell Blair‡, William G. Baron§, Michael A. Falugi¶

*Air Force Research Laboratory, Wright-Patterson AFB, Ohio 45433-7542*

The variational asymptotic method is used to construct a new model for composite plates which could have in-plane heterogeneity due to both geometry and material. We first formulate the original three-dimensional problem in an intrinsic form which is suitable for geometrically nonlinear analysis. Taking advantage of smallness of the plate thickness and heterogeneity, we use the variational asymptotic method to systematically obtain an effective plate model unifying a homogenization process and a dimensional reduction process. This approach is implemented in the computer code VAPAS using the finite element method for the purpose of dealing with real heterogeneous plates in application. A few examples are used to demonstrate the capability of this new model.

## I. Introduction

Along with the rapidly increasing popularity of composite materials and structures, research on accurate and general modeling of structures made of them has remained as a very active field in the last several decades. Moreover the increased knowledge and fabrication techniques of them are possible to manufacture new materials and structures with optimized microstructures to achieve the ever-increasing performance requirements. Although it is logically sound to use the well-established finite element method (FEM) to analyze such materials and structures by meshing all the details of constituent microstructures, it is not a practical and efficient way, which requires an inordinate number of degree of freedom (*i.e.*, computing cost) to capture the micro-scale behavior.

Fortunately, most composite materials exhibit statistical homogeneity<sup>1</sup> so that we can define a representative volume element (RVE), which is entirely typical of the whole mixture on average and contains a sufficient number of inclusions for the apparent overall properties to be effectively independent of the boundary conditions<sup>2</sup> Although different definitions are given for an RVE in the literature,<sup>3</sup> we give a practice-oriented definition for an RVE as any block of material the analyst wants to use for the micromechanical analysis to find the effective properties and replace it with an equivalent homogeneous material. The term unit cell (UC) is also used extensively in the literature and defined as the building block of the heterogeneous material. In our work, we define UC as the smallest RVE. In other words, one RVE could contain several UCs. These definitions essentially imply that it is the analyst's judgement to determine what should be contained in an RVE or UC. To be consistent with statistical homogeneity, a well-formulated micromechanics model should not depend on the size of an RVE, which means the effective properties obtained from an RVE containing

\*Postdoctoral research fellow, Department of Mechanical and Aerospace Engineering. Member, AIAA.

†Associate Professor, Department of Mechanical and Aerospace Engineering. Senior Member, AIAA.

‡Aerospace Engineer, Air Vehicles Directorate. Associate Fellow, AIAA.

§Aerospace Engineer, Air Vehicles Directorate. Associate Fellow, AIAA.

¶Aerospace Engineer, Air Vehicles Directorate. Associate Fellow, AIAA.

multiple UCs should be the same as those obtained from a UC. In this sense, we consider the heterogeneous structure as a periodic assembly of many UCs.

If the size of UC ( $d$ ) is much smaller than the size of the structure ( $L$ ) (i.e.  $\eta = d/L \ll 1$ ), it is possible to homogenize the heterogeneous UC with a set of effective material properties through a micromechanical analysis of the UC. With these effective properties, the analyst can replace the original heterogeneous structure with a homogeneous one and carry out structural analysis for global behavior. In the past several decades, numerous micromechanical approaches have been suggested in the literature, such as the self-consistent model,<sup>4-6</sup> the variational approach,<sup>7,8</sup> the method of cells,<sup>9-12</sup> recursive cell method,<sup>13</sup> mathematical homogenization theories,<sup>14-16</sup> finite element approaches using conventional stress analysis of a representative volume element,<sup>17</sup> variational asymptotic method for unit cell homogenization (VAMUCH),<sup>18,19</sup> and many others (see Ref. [20-22] for reviews of the field).

In real applications, many composite structures are dimensionally reducible structures<sup>23</sup> with one or two dimensions much smaller than others. For example, many load bearing components are flat panels with the thickness  $h$  much smaller than the in-plane dimensions (i.e.  $e = h/L \ll 1$ ) and they can be effectively modeled using plate models. If there are still many unit cells along the thickness direction (i.e.  $\eta \ll e$ ), we can use the traditional two-step approach that performs homogenization using micromechanics first to obtain effective properties of the heterogeneous material, then performs a dimensional reduction to construct a plate model for structural analysis. Usually, composite plates do not have many unit cells along the thickness direction. For example, for plates made of textiles, the textile microstructure might be as large as the plate thickness. That is, the periodicity is exhibited only in-plane and we have either  $e \ll \eta$  or  $e \sim \eta$ . As pointed out by Kohn and Vogelius,<sup>24</sup> if  $e \ll \eta$ , the order of the aforementioned two-step approach should be reversed. That is, we need to carry out the dimensional reduction to construct plate models first, then homogenize the heterogeneous surface with periodically varying plate properties. If  $e \sim \eta$ , the two steps in the two-step approach should be performed at the same time, that is, both small parameters ( $e$  and  $\eta$ ) should be considered during modeling of such structures. And several studies have shown that models considering  $e$  and  $\eta$  simultaneously also give accurate results for the case  $e \ll \eta$ .<sup>25,26</sup>

In recent years, the formal asymptotic method has been used to study this problem.<sup>24,25,27-29</sup> It is a modification to the asymptotic homogenization method which is a direct application of the formalism of two scales to the original three-dimensional (3D) equations governing the plate structure. However, although these models are mathematically elegant and rigorous without introducing *ad hoc* assumptions, it is not easy to relate the equations derived using this method with simple engineering models and extend this approach to geometrical nonlinear problems. Sometimes, the displacement field predicted using this approach is not compatible with the stress field. For example, the displacement field in Eqs. (1.3.5) of Ref. [29] implies zero transverse normal strain which further implies nonzero normal stress due to Poisson's effect, which is not compatible with the stress field given in Eq. (1.3.6) of Ref. [29]. Last but not least, it is difficult to implement these theories numerically.

As a remedy to the shortcomings of formal asymptotic method, we propose to use the variational asymptotic method (VAM)<sup>30</sup> to carry out simultaneous homogenization and dimensional reduction to construct a model suitable for plates made of heterogeneous materials. First, the 3D anisotropic elasticity problem is formulated in an intrinsic form suitable for geometrically nonlinear analysis. Then, considering both  $e$  and  $\eta$ , we use VAM to rigorously decouple the original 3D anisotropic, heterogeneous problem into a nonlinear two-dimensional (2D) surface analysis (i.e. plate analysis) on the macroscopic level and a linear micromechanical analysis. The micromechanical analysis can be easily implemented using the finite element method for numerically obtaining the effective plate constants for the 2D plate analysis and recovering the local displacement, strain, and stress fields based on the macroscopic behavior. Several examples are used to demonstrate the application and accuracy of this new model and the companion code VAPAS.

## II. Three-Dimensional Formulation

A plate may be considered geometrically as a smooth 2D reference plane  $\omega$  surrounded by a layer of matter with thickness  $h$  to form a 3D body with one dimension much smaller than the other two. In general, a point in the plate can be represented mathematically by its Cartesian coordinates  $x_i$ , where  $x_\alpha$  are two orthogonal lines in the reference plane and  $x_3$  is the normal coordinates (Here and throughout the paper, Greek indices assume values 1 and 2 while Latin indices assume 1, 2, and 3. Repeated indices are summed over their range except where explicitly indicated). Without loss of generality, we choose the middle of the

plate as the origin of  $x_3$ . Let us now consider a heterogeneous plate formed by many UCs ( $\Omega$ ) in the reference plane (see Fig. 1). To describe the rapid change in the material characteristics in the in-plane directions, we need to introduce two so-called ‘fast’ coordinates  $y_\alpha$  parallel to  $x_\alpha$ . These two sets of coordinates are related as  $y_\alpha = x_\alpha/\eta$ .

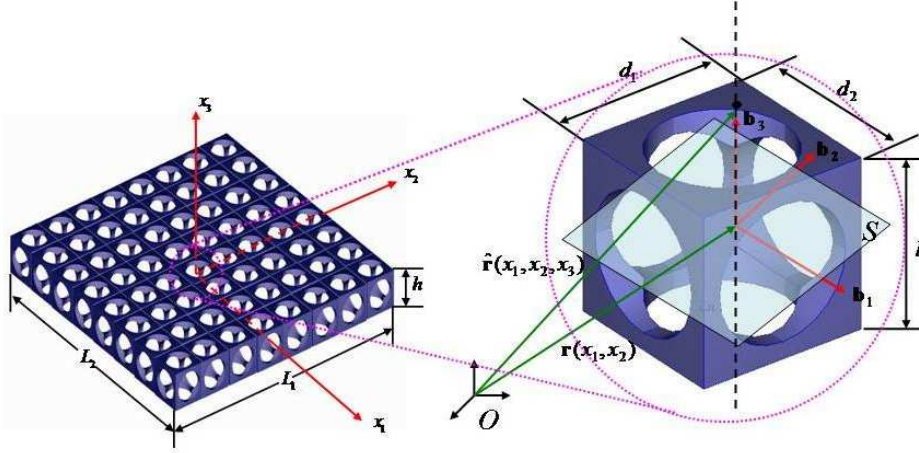


**Figure 1. A heterogeneous plate with representative periodicity cell**

If the UC is a cuboid as depicted in Fig. 1, we can describe the domain ( $\Omega$ ) occupied by the UC using  $y_\alpha$  and  $x_3$  as

$$\Omega = \left\{ (y_1, y_2, x_3) \mid -\frac{d_1}{2} < y_1 < \frac{d_1}{2}, -\frac{d_2}{2} < y_2 < \frac{d_2}{2}, -\frac{h}{2} < x_3 < \frac{h}{2} \right\} \quad (1)$$

As our goal is to homogenize the heterogenous material, we need to assume that the exact solution of the field variables have volume averages over  $\Omega$ . For example, if  $u_i(x_1, x_2, x_3; y_1, y_2)$  are the exact displacements within the UC, there exists  $v_i(x_1, x_2)$  such that

$$v_i = \frac{1}{\Omega} \int_{y_1} \int_{y_2} \int_{x_3} u_i dy_1 dy_2 dx_3 = \frac{1}{\Omega} \int_{\Omega} u_i d\Omega \equiv \langle u_i \rangle \quad (2)$$

Due to the existence of a distinct scale separation between two types of spatial variations described by  $y_\alpha$  and  $x_\alpha$ , the derivative of a function,  $u_i$ , defined in  $\Omega$  can be evaluated as

$$\frac{\partial u_i(x_1, x_2, x_3; y_1, y_2)}{\partial x_\alpha} = \frac{\partial u_i}{\partial x_\alpha} \Big|_{y_\alpha = \text{const}} + \frac{1}{\eta} \frac{\partial u_i}{\partial y_\alpha} \Big|_{x_i = \text{const}} \equiv u_{i,\alpha} + \frac{1}{\eta} u_{i|\alpha} \quad (3)$$

Note that in real derivation,  $\eta$  is not a number but denoting the order of the term it is associated with.

Letting  $\mathbf{b}_i$  denote a unit vector along  $x_i$  for the undeformed plate, one can then describe the position of any material point in the undeformed configuration by its position vector  $\hat{\mathbf{r}}$  relative to a point  $O$  fixed in an inertial frame, such that

$$\hat{\mathbf{r}}(x_1, x_2, x_3) = \mathbf{r}(x_1, x_2) + x_3 \mathbf{b}_3 \quad (4)$$

where  $\mathbf{r}$  is the position vector from  $O$  to the point located by  $x_\alpha$  on the reference plane.

When the plate deforms, the particle that had position vector  $\hat{\mathbf{r}}$  in the undeformed state now has position vector  $\hat{\mathbf{R}}$  in the deformed configuration. The latter can be uniquely determined by the deformation of the 3D body. To this end, we need to introduce a new triad  $\mathbf{B}_i$  for the deformed plate as unit vectors to express vectors and tensors in their component form during the derivation. The relation between  $\mathbf{B}_i$  and  $\mathbf{b}_i$  can be specified by an arbitrary large rotation in terms of the matrix of direction cosines  $C(x_1, x_2)$  so that

$$\mathbf{B}_i = C_{ij} \mathbf{b}_j \quad \text{with} \quad C_{ij} = \mathbf{B}_i \cdot \mathbf{b}_j \quad (5)$$

subject to the requirement that  $\mathbf{B}_i$  is coincident with  $\mathbf{b}_i$  when the structure is undeformed. Following Hodges *at el.*<sup>31</sup> and Yu *at el.*,<sup>32</sup> the position vector  $\hat{\mathbf{R}}$  can be represented as

$$\hat{\mathbf{R}}(x_i; y_\alpha) = \mathbf{R}(x_1, x_2) + x_3 \mathbf{B}_3(x_1, x_2) + w_i(x_1, x_2, x_3; y_1, y_2) \mathbf{B}_i(x_1, x_2) \quad (6)$$

where  $\mathbf{R}$  denotes the position vector describing the deformed reference surface and  $w_i$  denotes the warping functions describing the deformation not captured by  $\mathbf{R}$  and  $\mathbf{B}_i$ . Because of the way we introduce ‘fast’ coordinates,  $w_i$  are periodic functions in  $y_\alpha$ , that is

$$\begin{aligned} w_i(x_1, x_2, x_3; d_1/2, y_2) &= w_i(x_1, x_2, x_3; -d_1/2, y_2) \\ w_i(x_1, x_2, x_3; y_1, d_2/2) &= w_i(x_1, x_2, x_3; y_1, -d_2/2) \end{aligned} \quad (7)$$

Eq. (6) can be considered as a change of variable and six constraints are needed to ensure a one-to-one mapping between  $\hat{\mathbf{R}}$  and  $(\mathbf{R}, \mathbf{B}_i, w_i)$ . If we define  $\mathbf{R} = \langle \hat{\mathbf{R}} \rangle$ , then we have the following three constraints

$$\langle w_i \rangle = 0 \quad (8)$$

The other three constraints can be obtained by a proper definition of  $\mathbf{B}_i$ . Two constraints can be specified by defining  $\mathbf{B}_3$  as the normal to the reference surface of the deformed plate. The last constraint can be specified by the rotation of  $\mathbf{B}_\alpha$  around  $\mathbf{B}_3$  such that

$$\mathbf{B}_1 \cdot \frac{\partial \mathbf{R}}{\partial x_2} = \mathbf{B}_2 \cdot \frac{\partial \mathbf{R}}{\partial x_1} \quad (9)$$

Following Ref. [33], the plate strains can be defined using  $\mathbf{R}$  and  $\mathbf{B}_i$  as

$$\frac{\partial \mathbf{R}}{\partial x_\alpha} = \mathbf{B}_\alpha + \varepsilon_{\alpha\beta} \mathbf{B}_\beta \quad (10)$$

and

$$\frac{\partial \mathbf{B}_i}{\partial x_\alpha} = (-\kappa_{\alpha\beta} \mathbf{B}_\beta \times \mathbf{B}_3 + \kappa_{\alpha 3} \mathbf{B}_3) \times \mathbf{B}_i \quad (11)$$

It can be shown that the last constraint in Eq. (9) actually implies that symmetry of in-plane strains ( $\varepsilon_{\alpha\beta} = \varepsilon_{\beta\alpha}$ ).

Based on the concept of decomposition of rotation tensor,<sup>34</sup> the Jauman-Biot-Cauchy strain components for small local rotation are given by

$$\Gamma_{ij} = \frac{1}{2} (F_{ij} + F_{ji}) - \delta_{ij} \quad (12)$$

where  $\delta_{ij}$  is the Kronecker symbol, and  $F_{ij}$  is the mixed-basis component of the deformation gradient tensor such that

$$F_{ij} = \mathbf{B}_i \cdot \mathbf{G}_k \mathbf{g}^k \cdot \mathbf{b}_j \quad (13)$$

Here  $\mathbf{g}^i$  is the contravariant base vector of the undeformed configuration and in a plate case,  $\mathbf{g}^i = \mathbf{g}_i = \mathbf{b}_i$ , while  $\mathbf{G}_i$  is the 3D covariant basis vectors of the deformed configuration, which can be obtained in the following way:

$$\begin{aligned} \mathbf{G}_\alpha &= \frac{\partial \hat{\mathbf{R}}}{\partial x_\alpha} = \hat{\mathbf{R}}_{,\alpha} + \frac{1}{\eta} \hat{\mathbf{R}}_{|\alpha} \\ \mathbf{G}_3 &= \frac{\partial \hat{\mathbf{R}}}{\partial x_3} \equiv \hat{\mathbf{R}}_{|3} \end{aligned} \quad (14)$$

With the assumption that the plate strains are small compared to unity which is sufficient for geometrical nonlinear analysis, we can neglect all the terms that are products of the warping and the generalized strains

and obtain the 3D strain field as

$$\begin{aligned}
\Gamma_{11} &= \varepsilon_{11} + x_3 \kappa_{11} + w_{1,1} + \frac{1}{\eta} w_{1|1} \\
2\Gamma_{12} &= 2\varepsilon_{12} + x_3 (\kappa_{12} + \kappa_{21}) + w_{1,2} + w_{2,1} + \frac{1}{\eta} (w_{1|2} + w_{2|1}) \\
\Gamma_{22} &= \varepsilon_{22} + x_3 \kappa_{22} + w_{2,2} + \frac{1}{\eta} w_{2|2} \\
2\Gamma_{13} &= w_{1|3} + w_{3,1} + \frac{1}{\eta} w_{3|1} \\
2\Gamma_{23} &= w_{2|3} + w_{3,2} + \frac{1}{\eta} w_{3|2} \\
\Gamma_{33} &= w_{3|3}
\end{aligned} \tag{15}$$

Especially, for use in our computational procedure later, one can express the 3D strain field in matrix form from Eq. (15) as:

$$\Gamma = \Gamma_h w + \Gamma_\varepsilon \varepsilon + \Gamma_{L_\alpha} w_{,\alpha} \tag{16}$$

where  $\Gamma = [\Gamma_{11} \ 2\Gamma_{12} \ \Gamma_{22} \ 2\Gamma_{13} \ 2\Gamma_{23} \ \Gamma_{33}]^T$ ,  $w = [w_1 \ w_2 \ w_3]^T$ ,  $\varepsilon = [\varepsilon_{11} \ 2\varepsilon_{12} \ \varepsilon_{22} \ \kappa_{11} \ \kappa_{12} + \kappa_{21} \ \kappa_{22}]^T$ , and

$$\Gamma_h = \begin{bmatrix} \frac{\partial}{\partial y_1} & 0 & 0 \\ \frac{\partial}{\partial y_2} & \frac{\partial}{\partial y_1} & 0 \\ 0 & \frac{\partial}{\partial y_2} & 0 \\ \frac{\partial}{\partial x_3} & 0 & \frac{\partial}{\partial y_1} \\ 0 & \frac{\partial}{\partial x_3} & \frac{\partial}{\partial y_2} \\ 0 & 0 & \frac{\partial}{\partial x_3} \end{bmatrix} \quad \Gamma_\varepsilon = \begin{bmatrix} 1 & 0 & 0 & x_3 & 0 & 0 \\ 0 & 1 & 0 & 0 & x_3 & 0 \\ 0 & 0 & 1 & 0 & 0 & x_3 \\ 0 & 0 & 0 & 0 & 0 & 0 \\ 0 & 0 & 0 & 0 & 0 & 0 \\ 0 & 0 & 0 & 0 & 0 & 0 \end{bmatrix} \quad \Gamma_{L_1} = \begin{bmatrix} 1 & 0 & 0 \\ 0 & 1 & 0 \\ 0 & 0 & 0 \\ 0 & 0 & 1 \\ 0 & 0 & 0 \\ 0 & 0 & 0 \end{bmatrix} \quad \Gamma_{L_2} = \begin{bmatrix} 0 & 0 & 0 \\ 1 & 0 & 0 \\ 0 & 1 & 0 \\ 0 & 0 & 0 \\ 0 & 0 & 1 \\ 0 & 0 & 0 \end{bmatrix} \tag{17}$$

The strain energy stored in the heterogeneous plate can be obtained as:

$$U = \frac{1}{2} \int_{x_1} \int_{x_2} \langle \Gamma^T D \Gamma \rangle dx_1 dx_2 = \frac{1}{2} \int_{\omega} \langle \Gamma^T D \Gamma \rangle d\omega \tag{18}$$

where  $D(x_3; y_1, y_2)$  is the 3D  $6 \times 6$  material matrix, which consists of elements of the fourth-order elasticity tensor expressed in the local in-plane coordinate system  $y_\alpha$  and the thickness coordinate system  $x_3$ .

To deal with the applied loads, we follow Yu *et al.*<sup>32</sup> At first, we will leave open the existence of a potential energy and alternatively develop the virtual work of the applied loads. The virtual displacement is taken as the Lagrangean variation of the displacement field, such that

$$\delta \hat{\mathbf{R}} = \overline{\delta q}_{B_i} \mathbf{B}_i + x_3 \overline{\delta \psi}_{B_i} \mathbf{B}_i \times \mathbf{B}_3 + \delta w_i \mathbf{B}_i + \overline{\delta \psi}_{B_i} \mathbf{B}_i \times w_j \mathbf{B}_j \tag{19}$$

where the virtual displacement of the reference surface is given by

$$\overline{\delta q}_{B_i} = \delta \mathbf{u} \cdot \mathbf{B}_i \tag{20}$$

and the virtual rotation of the reference surface is defined such that

$$\delta \mathbf{B}_i = \overline{\delta \psi}_{B_j} \mathbf{B}_j \times \mathbf{B}_i \tag{21}$$

Because of small strain assumption, we may safely ignore products of the warping and the loading in the virtual rotation term. Then, the work done through a virtual displacement due to the applied loads  $\tau_i \mathbf{B}_i$  at the top surface ( $S^+$ ) and  $\beta_i \mathbf{B}_i$  at the bottom surface ( $S^-$ ) and body force  $\phi_i \mathbf{B}_i$  is

$$\begin{aligned}
\overline{\delta W} &= (\overline{\tau}_i + \overline{\beta}_i + \langle \phi_i \rangle) \overline{\delta q}_{B_i} + \overline{\delta \psi}_{B_\alpha} \left[ \frac{h}{2} (\overline{\tau}_\alpha - \overline{\beta}_\alpha) + \langle x_3 \phi_\alpha \rangle \right] \\
&+ \delta (\overline{\tau}_i w_i^+ + \overline{\beta}_i w_i^- + \langle \phi_i w_i \rangle)
\end{aligned} \tag{22}$$

with

$$\bar{\tau}_i = \frac{1}{S^+} \int_{S^+} \tau_i dS^+ \quad \text{and} \quad \bar{\beta}_i = \frac{1}{S^-} \int_{S^-} \beta_i dS^- \quad (23)$$

or in the matrix form

$$\overline{\delta W} = \overline{\delta q}^T f + \overline{\delta \psi}^T m + \delta \left( \bar{\tau}^T w^+ + \bar{\beta}^T w^- + \langle \phi^T w \rangle \right) \quad (24)$$

with

$$f = \bar{\tau} + \bar{\beta} + \langle \phi \rangle$$

$$m = \begin{Bmatrix} \frac{h}{2} (\bar{\tau}_1 - \bar{\beta}_1) + \langle x_3 \phi_1 \rangle \\ \frac{h}{2} (\bar{\tau}_2 - \bar{\beta}_2) + \langle x_3 \phi_2 \rangle \\ 0 \end{Bmatrix} \quad (25)$$

where  $\tau_i$ ,  $\beta_i$ , and  $\phi_i$  are taken to be independent of the deformation and  $()^+ = ()|_{x_3=h/2}$  and  $()^- = ()|_{x_3=-h/2}$ .

Now, the complete statement of the problem can be presented in terms of the principle of virtual work, such that

$$\delta U - \overline{\delta W} = 0 \quad (26)$$

In spite of the possibility of accounting for nonconservative forces in Eq. (26), the problem that governs the 3D unknown warping functions is conservative. Thus, one can pose the problem that governs the warping as the minimization of a total potential functional

$$\Pi = U + W \quad (27)$$

so that

$$\delta \Pi = 0 \quad (28)$$

in which only the warping displacement is varied, subject to the constraints in Eqs. (7) and (8). This implies that the potential of the applied loads for this portion of the problem is given by

$$W = -\tau^T w^+ - \beta^T w^- - \langle \phi^T w \rangle \quad (29)$$

Below, for simplicity of terminology, we will refer to  $\Pi$  as the total potential energy, or the total energy.

By principle of minimum total potential energy, one can solve the unknown warping functions by minimizing the functional in Eq. (27) subject to the constraints of Eq. (8) and periodic boundary conditions Eq. (7). Up to this point, this is simply an alternative formulation of the original 3D elasticity problem. If we attempt to solve this problem directly, we will meet the same or even more difficulty as solving any full 3D nonlinear elasticity problem. Fortunately, as shown in Refs. [18, 19, 32], VAM can be used to calculate the 3D unknown functions asymptotically. Although, the minimization problem can be solved analytically as shown in Refs. [18, 32], the procedure becomes very tedious, even with the help of the power of present day computers and very sophisticated software packages such Mathematica™ and Matlab™. For general cases we need to turn to numerical techniques such as FEM for approximate solutions. To this end, we need to express  $w$  using shape functions defined over  $\Omega$  as

$$w(x_1, x_2, x_3; y_1, y_2) = \bar{S}(y_1, y_2, x_3) V(x_1, x_2) \quad (30)$$

where  $\bar{S}$  represents the shape functions and  $V$  a column matrix of the nodal values of the warping functions. Substituting Eq. (30) into Eq. (16), one can express the total energy in discretized form as

$$2\Pi_\Omega = V^T E V + 2V^T (D_{h\varepsilon} \varepsilon + D_{hL_\alpha} V_{,\alpha}) + \varepsilon^T D_{\varepsilon\varepsilon} \varepsilon$$

$$+ V_{,\alpha}^T D_{L_\alpha L_\beta} V_{,\beta} + 2V_{,\alpha}^T D_{L_\alpha \varepsilon} \varepsilon + 2V^T L \quad (31)$$

where  $L$  contains the load related terms such that

$$L = -\bar{S}^{+T} \bar{\tau} - \bar{S}^{-T} \bar{\beta} - \langle \bar{S}^T \phi \rangle \quad (32)$$

The new matrix variables carry the properties of both geometry and material:

$$\begin{aligned}
E &= \left\langle [\Gamma_h \bar{S}]^T D [\Gamma_h \bar{S}] \right\rangle & D_{h\varepsilon} &= \left\langle [\Gamma_h \bar{S}]^T D [\Gamma_\varepsilon] \right\rangle \\
D_{hL_\alpha} &= \left\langle [\Gamma_h \bar{S}]^T D [\Gamma_{L_\alpha} \bar{S}] \right\rangle & D_{\varepsilon\varepsilon} &= \left\langle \Gamma_\varepsilon^T D \Gamma_\varepsilon \right\rangle \\
D_{L_\alpha L_\beta} &= \left\langle [\Gamma_{L_\alpha} \bar{S}]^T D [\Gamma_{L_\beta} \bar{S}] \right\rangle & D_{L_\alpha \varepsilon} &= \left\langle [\Gamma_{L_\alpha} \bar{S}]^T D \Gamma_\varepsilon \right\rangle
\end{aligned} \tag{33}$$

The discretized forms of Eq. (8) is

$$V^T H \psi = 0 \tag{34}$$

where  $H = \left\langle \bar{S}^T \bar{S} \right\rangle$  and  $\psi$  is the normalized kernel matrix of  $E$  such that  $\psi^T H \psi = I$ . Now our problem is transformed to minimize Eq. (31) numerically, subject to the periodic boundary conditions in Eq. (7) and the constraints in Eq. (34).

### III. Dimensional Reduction

To rigorously reduce the original 3D problem to a 2D plate model, one must attempt to reproduce the energy stored in the 3D structure in a 2D formulation. The best one can do is to accomplish it asymptotically taking advantage of the small parameters inherent in the structure. As pointed out previously we have two small parameters in our problem:  $e$  denoting the smallness of the thickness and  $\eta$  denoting the smallness of heterogeneity. Following Ref. [25, 26], we also assume that these two small parameters are of the same order as models constructed this way also give accurate results when  $e \ll \eta$ .

In this paper, VAM will be used to mathematically reduce the 3D problem to a 2D plate model. To proceed by this method, first one has to assess and keep track of the orders of all the quantities in the formulation. Following Sutyrin,<sup>35</sup> the quantities of interest have the following orders:

$$\varepsilon_{\alpha\beta} \sim h\kappa_{\alpha\beta} \sim \hat{\varepsilon} \quad f_3 \sim \mu (h/L)^2 \hat{\varepsilon} \quad f_\alpha \sim \mu (h/L) \hat{\varepsilon} \quad m_\alpha \sim \mu h (h/L) \hat{\varepsilon} \tag{35}$$

where  $\hat{\varepsilon}$  is the order of the plate strains and  $\mu$  is the order of the material constants (all of which are assumed to be of the same order). It is noted that  $m_3 = 0$ .

The VAM requires one to find the leading terms of the functional according to the different orders. For the zeroth-order approximation, these leading terms of Eq. (31) are

$$2\Pi_\Omega^0 = V^T E V + 2V^T D_{h\varepsilon} \varepsilon + \varepsilon^T D_{\varepsilon\varepsilon} \varepsilon \tag{36}$$

The periodic constraints in Eq. (7) and the average constraints in Eq. (34) can be easily handled as normally done in FEM through assembly for obtaining the functional in Eq. (36). Minimizing  $\Pi_\Omega^0$  in Eq. (36), gives us the following linear system

$$E V = -D_{h\varepsilon} \varepsilon \tag{37}$$

It is clear that  $V$  will linearly depend on the 2D plate strains  $\varepsilon$ , which means it is unnecessary to assign values to  $\varepsilon$  (even 1's and 0's as in common practice), and they can be treated as symbols without entering the computation. The solution can be symbolically written as

$$V = \bar{V}_0 \varepsilon \equiv V_0 \tag{38}$$

Substituting Eq. (38) back into Eq. (36), we can calculate the energy functional storing in the UC, asymptotically correct through the order of  $\mu \hat{\varepsilon}^2$  as

$$2\Pi_\Omega^0 = \varepsilon^T \left( \bar{V}_0^T D_{h\varepsilon} + D_{\varepsilon\varepsilon} \right) \varepsilon \equiv \varepsilon^T \bar{A} \varepsilon \tag{39}$$

where  $\bar{A}$  is the effective plate stiffness to be used for the classical plate theory (CPT). However, unlike the standard procedure of CPT, the effective plate stiffness are calculated from knowledge of complex geometric and material characteristics in a representative UC at the microscopic level considering the smallness of both thickness and heterogeneity.

Here we notice that the zeroth-order warping is of order  $h\hat{\varepsilon}$ . According to the VAM, to accept this as the zeroth-order approximation, one needs to check whether or not the order of the next approximation is

higher than this one. To obtain the first-order approximation, we simply perturb the zeroth-order result, resulting in warping functions of the form

$$V = V_0 + V_1 \quad (40)$$

Substituting Eq. (40) back into Eq. (16) and then into Eq. (31), one can obtain the leading terms for the first-order approximation as

$$2\Pi_{\Omega}^{1*} = V_1^T E V_1 + 2V_1^T D_{\alpha} \varepsilon_{,\alpha} + 2V_1^T L \quad (41)$$

where

$$D_{\alpha} = (D_{hL_{\alpha}} - D_{hL_{\alpha}}^T) \bar{V}_0 - D_{L_{\alpha}\varepsilon} \quad (42)$$

Similarly as in the zeroth-order approximation, one can solve the first-order warping field as

$$V_1 = V_{11}\varepsilon_{,1} + V_{12}\varepsilon_{,2} + V_{1L} \quad (43)$$

and obtain a total energy that is asymptotically correct up to the order of  $\mu (h/L)^2 \hat{\varepsilon}^2$

$$\begin{aligned} 2\Pi_{\Omega}^1 = & \varepsilon^T \bar{A} \varepsilon + \varepsilon_{,1}^T \bar{B} \varepsilon_{,1} + 2\varepsilon_{,1}^T \bar{C} \varepsilon_{,2} + \varepsilon_{,2}^T \bar{D} \varepsilon_{,2} \\ & + 2\varepsilon^T \bar{F} \varepsilon_{,1} + 2\varepsilon^T \bar{J} \varepsilon_{,2} + 2\varepsilon^T \bar{M} + \bar{N} \end{aligned} \quad (44)$$

where

$$\begin{aligned} \bar{A} &= \bar{V}_0^T D_{h\varepsilon} + D_{\varepsilon\varepsilon} \\ \bar{B} &= \bar{V}_0^T D_{L_1 L_1} \bar{V}_0 + V_{11}^T D_1 \\ \bar{C} &= \bar{V}_0^T D_{L_1 L_2} \bar{V}_0 + 0.5 (V_{11}^T D_2 + D_1^T V_{12}) \\ \bar{D} &= \bar{V}_0^T D_{L_2 L_2} \bar{V}_0 + V_{12}^T D_2 \\ \bar{F} &= \bar{V}_0^T D_{hL_1} \bar{V}_0 + D_{L_1 \varepsilon}^T \bar{V}_0 \\ \bar{J} &= \bar{V}_0^T D_{hL_2} \bar{V}_0 + D_{L_2 \varepsilon}^T \bar{V}_0 \\ \bar{M} &= \bar{V}_0^T L - 0.5 (D_1^T V_{1L,1} + V_{11}^T L_{,1} + D_2^T V_{1L,2} + V_{12}^T L_{,2}) \\ \bar{N} &= V_{1L}^T L \end{aligned} \quad (45)$$

It is noted that  $\bar{N}$  is a quadratic term involving applied loads that cannot be varied in the 2D model. When there is no load, this term vanishes. It comes from the applied load and the warping of refined approximations introduced by the applied load. The applied loads should not vary rapidly over the plate surface; otherwise,  $\bar{N}$  will not be of sufficiently high order to meet the requirement of asymptotical correctness.

#### IV. Transforming into Reissner-Mindlin Model

Although Eq. (44) is asymptotically correct through the second-order and straightforward use of this strain energy is possible, it involves more complicated boundary conditions than necessary since it contains derivatives of the generalized strain measures. To obtain an energy functional that is of practical use, one can transform the present approximation into a Reissner-Mindlin model.

In a Reissner-Mindlin model, there are two additional degrees of freedom, which are the transverse shear strains incorporated into the rotation of transverse normal. We introduce another triad  $\mathbf{B}_i^*$  for the deformed plate, so that the definition of 2D strains becomes

$$\mathbf{R}_{,\alpha} = \mathbf{B}_{\alpha}^* + \varepsilon_{\alpha\beta}^* \mathbf{B}_{\beta}^* + 2\gamma_{\alpha 3} \mathbf{B}_3^* \quad (46)$$

and

$$\mathbf{B}_{i,\alpha}^* = (-\kappa_{\alpha\beta}^* \mathbf{B}_{\beta}^* \times \mathbf{B}_3^* + \kappa_{\alpha 3}^* \mathbf{B}_3^*) \times \mathbf{B}_i^* \quad (47)$$

where the transverse shear strains are  $\gamma = [2\gamma_{13} \ 2\gamma_{23}]^T$ . Using the procedures listed in Ref. [32], one can express the classical strain measures  $\varepsilon$  in terms of the strain measures  $\mathcal{R}$  and the transverse shear strains  $\gamma$  of the Reissner-Mindlin plate model:

$$\varepsilon = \mathcal{R} - \mathcal{D}_{\alpha} \gamma_{,\alpha} \quad (48)$$

where

$$\begin{aligned}
\mathcal{D}_1 &= \begin{bmatrix} 0 & 0 & 0 & 1 & 0 & 0 \\ 0 & 0 & 0 & 0 & 1 & 0 \end{bmatrix}^T \\
\mathcal{D}_2 &= \begin{bmatrix} 0 & 0 & 0 & 0 & 1 & 0 \\ 0 & 0 & 0 & 0 & 0 & 1 \end{bmatrix}^T \\
\mathcal{R} &= [\varepsilon_{11}^* \quad 2\varepsilon_{12}^* \quad \varepsilon_{22}^* \quad \kappa_{11}^* \quad \kappa_{12}^* + \kappa_{21}^* \quad \kappa_{22}^*]^T
\end{aligned} \tag{49}$$

Now one can express the strain energy, Eq. (44), asymptotically correct to the second order, in terms of strains of the Reissner-Mindlin model as

$$\begin{aligned}
2\Pi_{\Omega}^1 &= \mathcal{R}^T \bar{A} \mathcal{R} - 2\mathcal{R}^T \bar{A} \mathcal{D}_{\alpha} \gamma_{,\alpha} + \mathcal{R}_{,1}^T \bar{B} \mathcal{R}_{,1} + 2\mathcal{R}_{,1}^T \bar{C} \mathcal{R}_{,2} + \mathcal{R}_{,2}^T \bar{D} \mathcal{R}_{,2} \\
&\quad + 2\mathcal{R}^T \bar{F} \mathcal{R}_{,1} + 2\mathcal{R}^T \bar{J} \mathcal{R}_{,2} + 2\mathcal{R}^T \bar{M} + \bar{N}
\end{aligned} \tag{50}$$

The generalized Reissner-Mindlin model used in many practical 2D analysis is of the form

$$2\Pi_{\mathcal{R}} = \mathcal{R}^T X \mathcal{R} + \gamma^T G \gamma + 2\mathcal{R}^T F_{\mathcal{R}} + 2\gamma^T F_{\gamma} \tag{51}$$

To find an equivalent Reissner-Mindlin model Eq. (51) for Eq. (50), one has to eliminate all partial derivatives of the strain measure. Here equilibrium equations are used to achieve this purpose. From the two equilibrium equations balancing bending moments with applied moments  $m_{\alpha}$  which is calculated from Eq. (25), one can obtain the following formula

$$G\gamma + F_{\gamma} = \mathcal{D}_{\alpha}^T \bar{A} \mathcal{R}_{,\alpha} + \begin{Bmatrix} m_1 \\ m_2 \end{Bmatrix} \tag{52}$$

Using Eq. (52), one can rewrite Eq. (50) as

$$2\Pi_1 = \mathcal{R}^T X \mathcal{R} + \gamma^T G \gamma + 2\mathcal{R}^T \bar{M} + \hat{N} + U^* \tag{53}$$

where

$$U^* = \mathcal{R}_{,1}^T \hat{B} \mathcal{R}_{,1} + 2\mathcal{R}_{,1}^T \hat{C} \mathcal{R}_{,2} + \mathcal{R}_{,2}^T \hat{D} \mathcal{R}_{,2} + 2\mathcal{R}^T \bar{F} \mathcal{R}_{,1} + 2\mathcal{R}^T \bar{J} \mathcal{R}_{,2} \tag{54}$$

and

$$\begin{aligned}
X &= \bar{A} \\
\hat{B} &= \bar{B} + X \mathcal{D}_1 G^{-1} \mathcal{D}_1^T (2\bar{A} - X) \\
\hat{C} &= \bar{C} + 0.5 [(2\bar{A} - X) \mathcal{D}_1 G^{-1} \mathcal{D}_2^T X + X \mathcal{D}_1 G^{-1} \mathcal{D}_2^T (2\bar{A} - X)] \\
\hat{D} &= \bar{D} + \bar{A} \mathcal{D}_2 G^{-1} \mathcal{D}_2^T (2\bar{A} - X) \\
\hat{N} &= \bar{N} - \begin{Bmatrix} m_1 \\ m_2 \end{Bmatrix}^T G^{-1} \begin{Bmatrix} m_1 \\ m_2 \end{Bmatrix}
\end{aligned} \tag{55}$$

If we can drive  $U^*$  to be zero for any  $\mathcal{R}$ , then we have found an asymptotically correct Reissner-Mindlin plate model. For general anisotropic plates, this term will not be zero; but we can minimize the error to obtain a Reissner-Mindlin model that is as close to asymptotical correctness as possible. The accuracy of the Reissner-Mindlin model depends on how close to zero one can drive this term of the energy.<sup>32</sup>

One could proceed with the optimization at this point, but the problem will require a least squares solution for 3 unknowns (the shear stiffness matrix  $G$ ) from a linear system of 78 equations (12×12 and symmetric). This optimization problem is too rigid. The solution will be better if we can bring more unknowns into the problem. As stated in Ref. [35], there is no unique plate theory of a given order. One can relax the constraints in Eq. (8) to be  $\langle w_i \rangle = \text{const}$  and still obtain an asymptotically correct strain energy. Since the zeroth-order approximation gives us an asymptotic model corresponding to classical plate theory, we only relax the constraints for the first-order approximation. This relaxation will modify the warping field to be

$$\bar{V}_1 = V_{11}\varepsilon_{,1} + V_{12}\varepsilon_{,2} + V_{1L} + L_1\varepsilon_{,1} + L_2\varepsilon_{,2} \tag{56}$$

where  $L_1, L_2$  consist of 24 constants. The remaining energy  $U^*$  will also be modified to be

$$U^* = \mathcal{R}_{,1}^T \hat{B}^* \mathcal{R}_{,1} + 2\mathcal{R}_{,1}^T \hat{C}^* \mathcal{R}_{,2} + \mathcal{R}_{,2}^T \hat{D}^* \mathcal{R}_{,2} + 2\mathcal{R}^T \bar{F} \mathcal{R}_{,1} + 2\mathcal{R}^T \bar{J} \mathcal{R}_{,2} \quad (57)$$

and

$$\begin{aligned} \hat{B}^* &= \hat{B} + 2L_1^T D_1 \\ \hat{C}^* &= \hat{C} + (L_1^T D_2 + D_1^T L_2) \\ \hat{D}^* &= \hat{D} + 2L_2^T D_2 \end{aligned} \quad (58)$$

Since now we have 27 unknowns, the optimization is much more flexible. It can give us a more optimal solution for the shear stiffness matrix  $G$  to fit the second-order, asymptotically-correct energy into a Reissner-Mindlin model. In other words, here we have found the Reissner-Mindlin model that describes as closely as possible the 2D energy that is asymptotically correct through the second order in  $h/L$ . Let us recall, that the Reissner-Mindlin theory that has been constructed only ensures a good fit with the asymptotically correct 3D strain field (thus stress field) of the first order (while energy is approximated to the second order). Thus, in order to obtain recovering relations that are valid to the same order as the energy, the VAM iteration needs to be applied one more time. Using the same procedure, the second-order warping can be obtained and expressed symbolically as

$$V_2 = V_{21}\varepsilon_{,11} + V_{22}\varepsilon_{,12} + V_{23}\varepsilon_{,22} \quad (59)$$

Here Eq. (59) is obtained by taking the original first-order warping  $V_1$  to be the result of the first-order approximation. It is clear that  $V_2$  is one order higher than  $V_1$  which confirms that  $V_1$  is the first-order approximation.

Finally after minimizing  $U^*$ , the total energy to be used for the 2D plate solver can be expressed as:

$$2\Pi_{\mathcal{R}} = \mathcal{R}^T \bar{A} \mathcal{R} + \gamma^T G \gamma + 2\mathcal{R}^T \bar{M} \quad (60)$$

The quadratic term of loads  $\hat{N}$  is dropped from Eq. (53) because it will not affect the 2D governing equations. It should be noted that the load-related terms in  $\bar{M}$  are a new feature in the present development. One must slightly modify traditional Reissner-Mindlin plate solvers to accommodate these terms.

## V. Recovering Relations

If the local fields within the UC are of interest, we can recover those fields based on the 2D global displacements  $u_{2d}$ , 2D global strains  $\varepsilon$ , and the 3D local warping functions  $w_i$ . From Eqs. (4) and (6), we can obtain the 3D displacement field through the second-order as:

$$\mathbf{U}_{3d} = \hat{\mathbf{R}} - \hat{\mathbf{r}} = \mathbf{R} - \mathbf{r} + x_3(\mathbf{B}_3 - \mathbf{b}_3) + w_i \mathbf{B}_i \quad (61)$$

which can also be expressed in the following matrix form as

$$U_{3d} = u_{2d} + x_3 \begin{bmatrix} C_{31} \\ C_{32} \\ C_{33} - 1 \end{bmatrix} + C^T S (V_0 + \bar{V}_1 + V_2) \quad (62)$$

where  $U_{3d}$  is the column matrix containing 3D displacement components in the  $\mathbf{b}_i$  basis and  $u_{2d}$  is the column matrix containing the 2D plate displacements in the  $\mathbf{b}_i$  basis.  $C$  is the direction-cosine matrix relating  $\mathbf{B}_i$  and  $\mathbf{b}_i$ , given in Eq. (5).

From Eqs. (16), one can recover the 3D local strain field  $\Gamma$  through the second-order as

$$\begin{aligned} \Gamma &= \Gamma_h S (V_0 + \bar{V}_1 + V_2) + \Gamma_\varepsilon \varepsilon \\ &+ \Gamma_{L_1} S (V_{0,1} + \bar{V}_{1,1}) + \Gamma_{L_2} S (V_{0,2} + \bar{V}_{1,2}) \end{aligned} \quad (63)$$

Finally, the local 3D stress field  $\sigma$  can be recovered straightforwardly using the original 3D constitutive relations as

$$\sigma = D\Gamma \quad (64)$$

We just derived the model for heterogeneous plates with the UC periodically varying along both  $x_1$  and  $x_2$ . It is easy to deduce that it is also applicable to degenerated cases such as the UC is only periodically varying along one direction. For example if it is periodic along  $x_1$ , then the partial derivative with respect to  $y_1$  vanishes in  $\Gamma_h$  operator of Eq. (16). That is, we only need to solve a 2D problem in  $y_2$  and  $x_3$ . If the plate is uniform in plane, then the partial derivatives with respect to  $y_1$  and  $y_2$  both vanish and the theory reduces to a 1D through-the-thickness as that of the classical plate theory derived using VAM as in Ref. [32]. The present theory is implemented in the computer code VAPAS (Variational Asymptotic Plate and Shell Analysis). In the following section, we are going to use a few examples to assess the validity of the present theory and the companion code VAPAS.

## VI. Validation Examples

First, we investigate plates made of binary composites. The effective plate stiffness obtained by the present theory and VAPAS is compared to those obtained from conventional two-step approach. Second, heterogeneous plates having more complex UCs with different geometric and material characteristics at the microscopic level are used to demonstrate the accuracies and capabilities of the new theory and the differences between the conventional two-step approach and the present approach.

### A. Plates made of binary composites

First, let us consider plates made of  $N$  binary composites each of which is formed by two different orthotropic layers with the material axes the same as the global coordinates  $x_i$ . Overall, there are  $2N$  layers in the plate. The material is uniform in the  $x_\alpha$  plane and varies along  $x_3$  direction. Let  $\varphi_1$  and  $\varphi_2$  denote the volume fractions of the bottom layer and top layer, respectively, and we have  $\varphi_1 + \varphi_2 = 1$ . The plate structure can be considered periodic along  $x_1$  and/or  $x_2$  directions. Using the present theory, we can either model it using three approaches: (1) as a one-dimensional (1D) UC with no periodicity; (2) as a 2D UC with periodicity either in  $x_1$  or  $x_2$ ; (3) as a 3D unit cell with periodicity in both  $x_1$  and  $x_2$ . Each UC will have  $N$  same binary composites along the thickness. We have verified that all these three modeling approaches yield the same effective plate stiffness which can be written in the following matrix form:

$$\bar{D} = \begin{bmatrix} \bar{d}_{11} & 0 & \bar{d}_{13} & \bar{d}_{14} & 0 & \bar{d}_{16} \\ 0 & \bar{d}_{22} & 0 & 0 & \bar{d}_{25} & 0 \\ \bar{d}_{13} & 0 & \bar{d}_{33} & \bar{d}_{16} & 0 & \bar{d}_{36} \\ \bar{d}_{14} & 0 & \bar{d}_{16} & \bar{d}_{44} & 0 & \bar{d}_{46} \\ 0 & \bar{d}_{25} & 0 & 0 & \bar{d}_{55} & 0 \\ \bar{d}_{16} & 0 & \bar{d}_{36} & \bar{d}_{46} & 0 & \bar{d}_{66} \end{bmatrix} \quad (65)$$

Particularly, modeling it as a 1D UC with no periodicity can be carried out analytically and the result is the same as classical plate model derived using VAM considering the plate is made of  $2N$  layers.<sup>32</sup>

To analyze this structure using the two-step approach (TSA), the analyst needs to first homogenize the binary composites to obtain effective 3D material properties which can be expressed in the following matrix

$$\bar{D}^{3D} = \begin{bmatrix} \bar{c}_{11} & 0 & \bar{c}_{13} & 0 & 0 & \bar{c}_{16} \\ 0 & \bar{c}_{22} & 0 & 0 & 0 & 0 \\ \bar{c}_{13} & 0 & \bar{c}_{33} & 0 & 0 & \bar{c}_{36} \\ 0 & 0 & 0 & \bar{c}_{44} & 0 & 0 \\ 0 & 0 & 0 & 0 & \bar{c}_{55} & 0 \\ \bar{c}_{16} & 0 & \bar{c}_{36} & 0 & 0 & \bar{c}_{66} \end{bmatrix} \quad (66)$$

Here for the sake of saving space, the expressions for  $\bar{c}_{ij}$  are not listed here. Interested users can refer to Yu<sup>18</sup> for analytical expressions of all the terms in Eq. (66) with a rearrangement to be consistent with the ordering of 3D strains used in this paper. Then, the analyst needs to carry out a dimensional reduction to

obtain the classical plate model, of which the corresponding stiffness terms based on Eq. (66) are

$$\begin{aligned}\bar{d}_{11} &= \langle c_{11}^* \rangle_{x_3} & \bar{d}_{13} &= \langle c_{13}^* \rangle_{x_3} & \bar{d}_{22} &= \langle \bar{c}_{22} \rangle_{x_3} & \bar{d}_{33} &= \langle c_{33}^* \rangle_{x_3} \\ \bar{d}_{14} &= \langle x_3 c_{11}^* \rangle_{x_3} & \bar{d}_{16} &= \langle x_3 c_{13}^* \rangle_{x_3} & \bar{d}_{25} &= \langle x_3 \bar{c}_{22} \rangle_{x_3} & \bar{d}_{36} &= \langle x_3 c_{33}^* \rangle_{x_3} \\ \bar{d}_{44} &= \langle x_3^2 c_{11}^* \rangle_{x_3} & \bar{d}_{46} &= \langle x_3^2 c_{13}^* \rangle_{x_3} & \bar{d}_{55} &= \langle x_3^2 \bar{c}_{22} \rangle_{x_3} & \bar{d}_{66} &= \langle x_3^2 c_{33}^* \rangle_{x_3}\end{aligned}\quad (67)$$

with  $\langle a \rangle_{x_3} = \int_{-h/2}^{h/2} a dx_3$  and

$$c_{11}^* = \bar{c}_{11} - \frac{\bar{c}_{16}^2}{\bar{c}_{66}} \quad c_{13}^* = \bar{c}_{13} - \frac{\bar{c}_{16}\bar{c}_{36}}{\bar{c}_{66}} \quad c_{33}^* = \bar{c}_{33} - \frac{\bar{c}_{36}^2}{\bar{c}_{66}}$$

We can prove that the present theory and TSA predict the same extensional stiffness,  $\bar{D}_{ij}$  ( $i = 1, 2, 3, j = 1, 2, 3$ ) ( $A$  matrix in CPT). The present theory will predict different coupling stiffness  $\bar{D}_{ij}$  ( $i = 1, 2, 3, j = 4, 5, 6$ ) ( $B$  matrix in CPT) as the coupling stiffness according to TSA always remains zero. The coupling stiffness  $B$  predicted by the present theory is:

$$B = \frac{h^2}{2N} \varphi_1 \varphi_2 D^* \quad (68)$$

with

$$D^* = \begin{bmatrix} \hat{c}_{11}^{(2)} - \hat{c}_{11}^{(1)} & 0 & \hat{c}_{13}^{(2)} - \hat{c}_{13}^{(1)} \\ 0 & \hat{c}_{22}^{(2)} - \hat{c}_{22}^{(1)} & 0 \\ \hat{c}_{13}^{(2)} - \hat{c}_{13}^{(1)} & 0 & \hat{c}_{33}^{(2)} - \hat{c}_{33}^{(1)} \end{bmatrix}$$

where the subscripts denote which layer the value evaluated for. For example  $\hat{c}_{11}^{(2)}$  denotes  $\hat{c}_{11}$  evaluated for the top layer of the binary composite. The hatted quantities are calculated as

$$\hat{c}_{11} = c_{11} - \frac{c_{16}^2}{c_{66}} \quad \hat{c}_{13} = c_{13} - \frac{c_{16}c_{36}}{c_{66}} \quad \hat{c}_{33} = c_{33} - \frac{c_{36}^2}{c_{66}} \quad (69)$$

where  $c_{ij}$  are the stiffness components of the stiffness matrix arranged from the fourth-order elasticity for each constituent material of the binary composite. Only if these hatted quantities are the same for both layers, the coupling stiffness  $B$  in Eq. (68) predicted by the present theory will vanish as that predicted by TSA.

The present theory will also predict different bending stiffness  $\bar{D}_{ij}$  ( $i = 4, 5, 6, j = 4, 5, 6$ ) ( $D$  matrix in CPT). If we use  $D$  and  $D_{TSA}$  to denote the bending stiffness predicted by the present theory and TSA, respectively, we have

$$D - D_{TSA} = \frac{h^3}{6N^2} \varphi_1 \varphi_2 (\varphi_1 - \varphi_2) D^* \quad (70)$$

If the hatted quantities in Eq. (69) are the same for both layers, the present theory will predict the same bending stiffness as TSA. Even if the hatted quantities in Eq. (69) are different for each layer, the present theory will predict the same bending stiffness as TSA if  $\varphi_1 = \varphi_2$  (i.e. the two layers of the binary composites are of equal thickness).

From Eqs. (68) and (70), we observe for a large  $N$ , the differences between the present approach and TSA become negligible which is expected as TSA is only valid when there are many UCs along the thickness. In real situations, this plate can only be made of a finite number of binary composites. For a finite number  $N$ , the error caused by TSA for bending stiffness decreases proportionally to  $1/N^2$  which is much faster than the coupling stiffness which decreases proportionally to  $1/N$ .

## B. Plates made of unidirectional composites

The second example is a plate made of a single layer of unidirectional composites as sketched in Figure 2 with  $d_1 = h = 10\mu\text{m}$  studied in Ref. [36]. The unidirectional composite has a E-glass fiber ( $E_f = 70$  GPa,  $\nu_f = 0.2$ ), and an epoxy matrix ( $E_m = 3.5$  GPa,  $\nu_m = 0.35$ ). The volume fraction of matrix is  $\phi_m = 0.4$ . The fiber direction is along  $x_2$  and the plate is periodically varying along  $x_1$ . The effective plate stiffness predicted by different approaches are listed in Table 1, where SAM, FEM, and TSA results are directly taken from Table 6 of Ref. [36] with SAM denoting the results obtained by a selective averaging method,

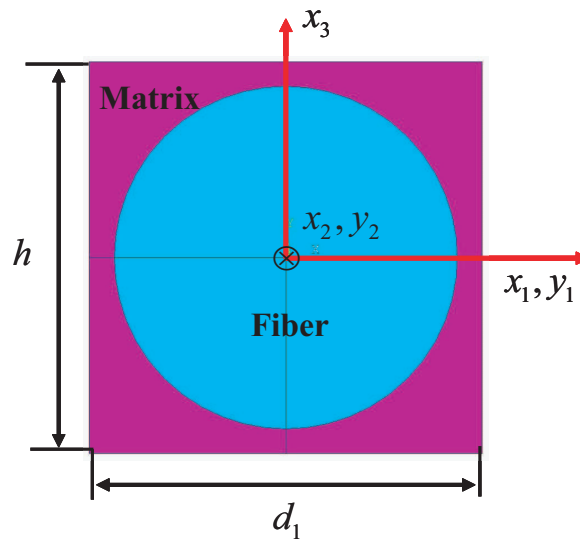


Figure 2. A unit cell for a unidirectional fiber reinforced composite

Table 1. Effective plate constants of unidirectional composite plates predicted by different methods

	SAM	FEM	TSA	VAPAS
$\bar{d}_{11}$ ( $10^6$ N/m)	0.443	0.452	0.444	0.443
$\bar{d}_{13}$ ( $10^6$ N/m)	0.074	0.062	0.039	0.035
$\bar{d}_{22}$ ( $10^6$ N/m)	0.040	0.114	0.045	0.047
$\bar{d}_{33}$ ( $10^6$ N/m)	0.261	0.285	0.151	0.145
$\bar{d}_{44}$ ( $10^{-6}$ Nm)	2.308	2.256	3.702	2.246
$\bar{d}_{46}$ ( $10^{-6}$ Nm)	0.446	0.224	0.328	0.176
$\bar{d}_{55}$ ( $10^{-6}$ Nm)	0.195	0.568	0.371	0.547
$\bar{d}_{66}$ ( $10^{-6}$ Nm)	1.799	0.873	1.262	0.653

FEM denoting the results obtained by 3D FEA with periodic displacement and traction boundary conditions imposed on opposite surfaces of the unit cell, and TSA denoting the results obtained a the two-step approach with elastic constants obtained using Halpin-Tsai equations.

Significant differences are observed among the results predicted by different approaches. The best way to tell which set of plate constants is accurate is to use these constants to carry out the corresponding plate analysis and compare the global plate behavior with those predict by a different 3D finite element analysis of the original plate structure. Suppose a square plate composed of 20 UCs is under a uniform pressure and is simply supported at the four edges. Because of symmetry, only 1/4 of the structures needs to be analyzed; see Figure 3 for sketches for the geometry and finite element model of this structure. We found out that the max deflection using VAPAS constants is only 0.5% off from the direct 3D FEA analysis, while that using SAM constants is 5% off, and by FEM is 7.0% off, and TSA is 23%. Clearly the plate analysis based on VAPAS can accurately reproduce the original 3D FEA direct analysis.

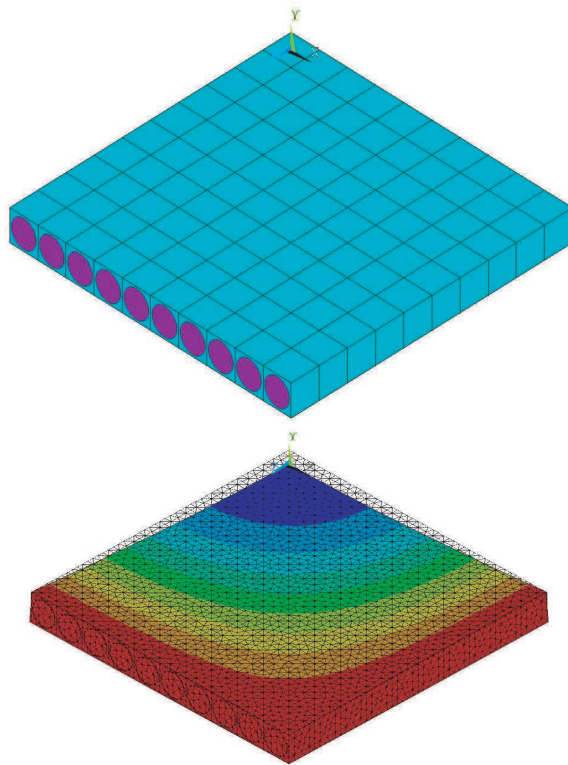


Figure 3. Direct 3D FEA model of plate made of unidirectional composites

### C. Model integrated thermal protection system as a heterogeneous plate

The third example is to model a corrugated-core sandwich panel, a concept used for Integrated Thermal Protection System (ITPS) studied in Ref. [37]. The ITPS panel along with the details of the unit cell is sketched in Figure 4. The geometry parameters are  $t_T = 1.2$  mm,  $t_B = 7.49$  mm,  $t_W = 1.63$  mm,  $p = 25$  mm,  $d = 70$  mm, and  $\theta = 85^\circ$ . Both materials are isotropic with  $E_1 = 109.36$  GPa,  $\nu_1 = 0.3$ ,  $E_2 = 209.482$  GPa,  $\nu_2 = 0.063$ . Although a 3D UC is needed for the study in Ref. [37], only a 2D UC is necessary for VAPAS as it is uniform along one of the in-plane directions. The results obtained in Ref. [37] are compared with VAPAS in Tables 2, 3 and 4. VAPAS predictions agree very well with those in Ref. [37] with the biggest difference (around 1%) appearing for the extension-bending coupling stiffness ( $\bar{d}_{14}$ ). However, the present approach is much more efficient than that in Ref. [37] because one needs to carry out six analyses of a 3D unit cells under six different sets of boundary conditions and load conditions and postprocess the 3D stresses to compute the plate stress resultants, while using the present approach, one only needs to carry out one analysis of a 2D UC and postprocessing computing is not needed.

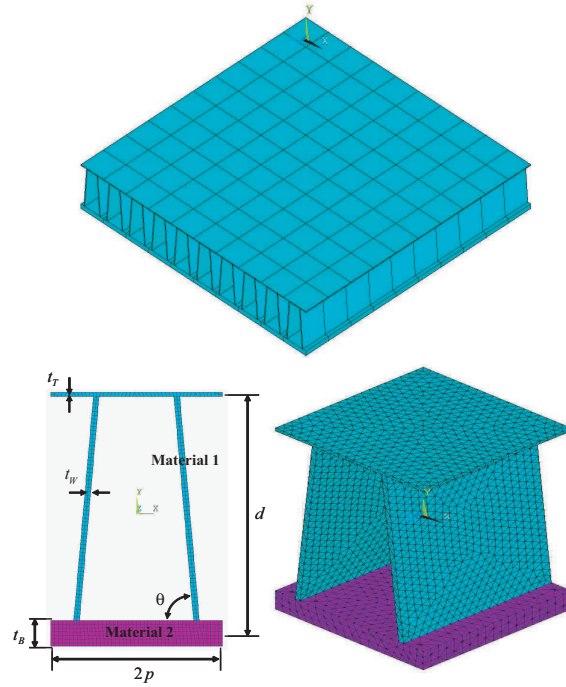


Figure 4. Sketch of the ITPS panel and its unit cell

Table 2. Effective extension stiffness ( $10^9\text{N/m}$ ) of ITPS

	$\bar{d}_{11}$	$\bar{d}_{13}$	$\bar{d}_{22}$	$\bar{d}_{33}$
Ref. [37]	2.83	0.18	1.07	2.33
VAPAS	2.80	0.18	1.08	2.33

Table 3. Effective bending stiffness ( $10^6\text{Nm}$ ) of ITPS

	$\bar{d}_{44}$	$\bar{d}_{46}$	$\bar{d}_{55}$	$\bar{d}_{66}$
Ref. [37]	3.06	0.22	1.32	2.85
VAPAS	3.03	0.22	1.32	2.87

Table 4. Effective coupling stiffness ( $10^6\text{N}$ ) of ITPS

	$\bar{d}_{14}$	$\bar{d}_{16}$	$\bar{d}_{25}$	$\bar{d}_{36}$
Ref. [37]	-71.45	-3.36	-34.05	-71.45
VAPAS	-70.67	-3.31	-34.06	-71.42

We also analyzed a simply supported square panel under uniform pressure with the ITPS microstructure. We find out that with 20 UCs along the width, the max deflection predicted by the plate analysis using the effective plate constants is about 55% off the direct 3D FEA analysis. The difference will decrease with increased number of UCs; for example if the plate is composed of 30 UCs, the difference is 48% and if the plate is composed of 40 UCs, the difference is 42%. The fact that big differences exist even if the plate is very thin (the aspect ratio of the 40 UC plate is around 7:200) is because transverse shear deformation of this type of structure, which is neglected in CPT, is significant. A refined plate theory, such as the Reissner-Mindlin model, which is capable of capturing the shear deformation should be used. The present theory and the VAPAS code is also used to compute the Reissner-Mindlin plate model with the effective transverse shear stiffness listed in Table 5. Using a shear-deformation plate theory plus the plate constants given in Table ?? and Table 5, we found out that the max deflection using the refined plate theory is only 4.76% off the direct 3D FEA analysis.

**Table 5. Effective transverse shear stiffness N/m of ITPS**

	$\bar{g}_{11}(10^8\text{N/m})$	$\bar{g}_{22}(10^5\text{N/m})$
VAPAS	1.97	4.05

## VII. Conclusions

The variational asymptotic method is used to construct a new model for composite plates with in-plane heterogeneity. This model serves as a rigorous link between the original 3D problem of plate structures made of materials with complex microstructures and the simple engineering plate models such as the Kirchhoff plate model and the Reissner-Mindlin plate model. This model not only computes the effective plate stiffness needed for the engineering plate models but also can recover the local displacement, strain, and stress fields based on the global behavior obtained from the plate analysis. The resulting plate model is also suitable for geometrical nonlinear analysis as only small strain assumption is used for obtaining the kinematics. This new model is implemented in the computer code VAPAS using the finite element method. VAPAS can be used as an alternative of the 3D FEA for efficient yet accurate analysis of composite plates with or without in-plane heterogeneity. The validity and capability of this new model are demonstrated using a few examples.

## Acknowledgements

The present work is supported, in part, by the Air Force Office of Scientific Research under Grant FA9550-08-1-0405 (the program manager is Dr. David Stargel) and AFRL/RB Summer Faculty Research Program. The views and conclusions contained herein are those of the authors and should not be interpreted as necessarily representing the official policies or endorsement, either expressed or implied, of the funding agency.

## References

- <sup>1</sup>Hashin, Z., "Analysis of Composite Materials-A Survey," *Applied Mechanics Review*, Vol. 50, 1983, pp. 481–505.
- <sup>2</sup>Hill, R., "Elastic Properties of Reinforced Solids: Some Theoretical Principles," *Journal of Mechanics and Physics of Solids*, Vol. 11, 1963, pp. 357–372.
- <sup>3</sup>Nemat-Nasser, S. and Hori, M., *Micromechanics: Overall Properties of Heterogeneous Materials*, North-Holland, Amsterdam, 1993.
- <sup>4</sup>Hill, R., "Theory of Mechanical Properties of Fibre-Strengthened Materials-III. Self-consistent Model," *Journal of Mechanics and Physics of Solids*, Vol. 13, 1965, pp. 189–198.
- <sup>5</sup>Dvorak, G. and Bahei-El-Din, Y., "Elastic-Plastic Behavior of Fibrous Composites," *Journal of Mechanics and Physics of Solids*, Vol. 27, 1979, pp. 51–72.
- <sup>6</sup>Accorsi, M. L. and Nemat-Nasser, S., "Bounds on the Overall Elastic and Instantaneous Elastoplastic Moduli of Periodic Composites," *Mechanics of Materials*, Vol. 5, No. 3, 1986, pp. 209–220.
- <sup>7</sup>Hashin, Z. and Shtrikman, S., "A Variational Approach to the Theory of the Elastic Behaviour of Polycrystals," *Journal of Mechanics and Physics of Solids*, Vol. 10, 1962, pp. 343–352.
- <sup>8</sup>Milton, G., *Theory of Composites*, Cambridge University Press, 2001.

- <sup>9</sup>Aboudi, J., "A Continuum Theory for Fiber-Reinforced Elastic-Visoplastic Composites," *International Journal of Engineering Science*, Vol. 20, No. 5, 1982, pp. 605–621.
- <sup>10</sup>Aboudi, J., "Micromechanical Analysis of Composites by the Method of Cells," *Applied Mechanics Reviews*, Vol. 42, No. 7, 1989, pp. 193–221.
- <sup>11</sup>Paley, M. and Aboudi, J., "Micromechanical analysis of composites by the generalized cells model," *Mechanics of Materials*, Vol. 14, 1992, pp. 127–139.
- <sup>12</sup>Williams, T., "A Two-dimensional, Higher-order, Elasticity-based Micromechanics Model," *International Journal of Solids and Structures*, Vol. 42, 2005, pp. 1009–1038.
- <sup>13</sup>Banerjee, B. and Adams, D., "On Predicting the Effective Elastic Properties of Polymer Bonded Explosive using the Recursive Cell Method," *International Journal of Solids and Structures*, Vol. 41, No. 2, 2004, pp. 481–509.
- <sup>14</sup>Bensoussan, A., Lions, J., and Papanicolaou, G., *Asymptotic Analysis for Periodic Structures*, North-Holland, Amsterdam, 1978.
- <sup>15</sup>Sanchez-Palencia, E., *Non-homogeneous Media and Vibration Theory*, Springer Berlin, 1980.
- <sup>16</sup>Murakami, H. and Toledano, A., "A Higher-order Mixture Homogenization of Bi-laminated Composites," *Journal of Applied Mechanics*, Vol. 57, 1990, pp. 388–396.
- <sup>17</sup>Sun, C. and Vaidya, R., "Prediction of composite properties from a representative volume element," *Composites Science and Technology*, Vol. 56, 1996, pp. 171–179.
- <sup>18</sup>Yu, W., "A Variational-Asymptotic Cell Method for Periodically Heterogeneous Materials," *Proceedings of the 2005 ASME International Mechanical Engineering Congress and Exposition*, ASME, Orlando, Florida, Nov. 5–11 2005.
- <sup>19</sup>Yu, W. and Tang, T., "Variational Asymptotic Method for Unit Cell Homogenization of Periodically Heterogeneous Materials," *International Journal of Solids and Structures*, Vol. 44, 2007, pp. 3738–3755.
- <sup>20</sup>Hollister, S. J. and Kikuchi, N., "A Comparison of Homogenization and Standard Mechanics Analyses for Periodic Porous Composites," *Computational Mechanics*, 1992.
- <sup>21</sup>Kalamkarov, A. L., Andrianov, I. V., and Danishevskiy, V. V., "Asymptotic Homogenization of Composite Materials and Structures," *Applied Mechanics Reviews*, Vol. 62, 2009, pp. 030802.
- <sup>22</sup>Kanouté, P., Boso, D., Chaboche, J. L., and Schrefler, B., "Multiscale methods for composites: A review," *Archives of Computational Methods in Engineering*, Vol. 16, 2009, pp. 31–75.
- <sup>23</sup>Yu, W., *Variational Asymptotic Modeling of Composite Dimensionally Reducible Structures*, Ph.D. thesis, Aerospace Engineering, Georgia Institute of Technology, May 2002.
- <sup>24</sup>Kohn, R. and Vogelius, M., "A new model for thin plates with rapidly varying thickness," *International Journal of Solids and Structures*, Vol. 20, No. 4, 1984, pp. 333–350.
- <sup>25</sup>Lewiński, T., "Effective models of composite periodic plates – part I. asymptotic solution," *International Journal of Solids and Structures*, Vol. 27, No. 8, 1991, pp. 1155–1172.
- <sup>26</sup>Buannic, N. and Cartraud, P., "Higher-order effective modeling of periodic heterogeneous beams. I. Asymptotic expansion method," *International Journal of Solids and Structures*, Vol. 38, 2001, pp. 7139–7161.
- <sup>27</sup>Caillerie, D., "Thin elastic and periodic plates," *Mathematical Methods in the Applied Sciences*, Vol. 6, 1984, pp. 159–191.
- <sup>28</sup>Kalamkarov, A., *Composite and Reinforced Elements of Construction*, Wiley Chichester, 1992.
- <sup>29</sup>Kalamkarov, A. and Kolpakov, A., *Analysis, Design and Optimization of Composite Structures*, Wiley Chichester, 1997.
- <sup>30</sup>Berdichevsky, V., "Variational-asymptotic method of constructing a theory of shells," *PMM*, Vol. 43, No. 4, 1979, pp. 664–687.
- <sup>31</sup>Hodges, D., Atilgan, A., and Danielson, D., "A geometrically nonlinear theory of elastic plates," *Journal of Applied Mechanics*, Vol. 60, No. 1, 1993, pp. 109–116.
- <sup>32</sup>Yu, W., Hodges, D., and Volovoi, V., "Asymptotic construction of Reissner-like models for composite plates with accurate strain recovery," *International Journal of Solids and Structures*, Vol. 39, No. 17, 2002, pp. 5185–5203.
- <sup>33</sup>Atilgan, A. and Hodges, D., "On the strain energy of laminated composite plates," *International Journal of Solids and Structures*, Vol. 29, 1992, pp. 2527–2543.
- <sup>34</sup>Danielson, D. and Hodges, D., "Nonlinear beam kinematics by decomposition of the rotation tensor," *Journal of Applied Mechanics*, Vol. 54, 1987, pp. 258–262.
- <sup>35</sup>Sutyrin, V., "Derivation of plate theory accounting asymptotically correct shear deformation," *Journal of Applied Mechanics*, Vol. 64, 1997, pp. 905–915.
- <sup>36</sup>Sankar, B. V. and Marrey, R. V., "Analytical Method for Micromechanics of Textile Composites," *Composites Science and Technology*, Vol. 57, 1997, pp. 703–713.
- <sup>37</sup>Sharma, A., Sankar, B. V., and Haftka, R. T., "Homogenization of Plates with Microstructure and Application to Corrugated Core Sandwich Panels," *Proceedings of the 51st AIAA/ASME/ASCE/AHS/ASC Structures, Structural Dynamics, and Materials Conference*, AIAA, Orlando, Florida, Apr. 12–15 2010.

# Assess the Accuracy of the Variational Asymptotic Plate and Shell Analysis Using the Generalized Unified Formulation

Luciano Demasi<sup>1</sup>

*Department of Aerospace Engineering & Engineering Mechanics  
San Diego State University, San diego, CA 92182-1308 USA*

Wenbin Yu

*Department of Mechanical and Aerospace Engineering  
Utah state University, Logan, Utah 84322-4130 USA*

---

## Abstract

The accuracy of the Variational Asymptotic Plate and Shell Analysis (VAPAS) is assessed against several higher order, zig zag and layerwise theories generated by using the invariant axiomatic framework denoted as Generalized Unified Formulation (GUF). All the axiomatic and asymptotic theories are also compared against the elasticity solution developed for the case of a sandwich structure with high Face to Core Stiffness Ratio. GUF allows to use an infinite number of axiomatic theories (Equivalent Single Layer theories with or without zig zag effects and Layerwise theories as well) with any combination of orders of the displacements and it is an ideal tool to precisely assess the range of applicability of the Variational Asymptotic Plate and Shell Analysis or other theories in general. In fact, all the axiomatic theories generated by GUF are obtained from the kernels or fundamental nuclei of the Generalized Unified Formulation and changing the order of the variables is “naturally” and systematically done with GUF. It is demonstrated that VAPAS achieves accuracy comparable to a fourth (or higher) order zig-zag theory or lower-order layerwise theories with the least number degrees of freedom. The differences between the axiomatic Zig-zag models and VAPAS are also assessed. Range of applicability of VAPAS will be discussed in detail and guidelines for new developments based on GUF and VAPAS are provided.

---

*Email addresses:* [ldemasi@mail.sdsu.edu](mailto:ldemasi@mail.sdsu.edu) (Luciano Demasi),  
[wenbin.yu@usu.edu](mailto:wenbin.yu@usu.edu) (Wenbin Yu).

*URLs:* [www.lucianodemasi.com](http://www.lucianodemasi.com) (Luciano Demasi),  
<http://www.mae.usu.edu/faculty/wenbin> (Wenbin Yu).

<sup>1</sup> Corresponding author. Department of Aerospace Engineering and Engineering Mechanics, College of Engineering San Diego State University, 5500 Campanile Drive, San diego, CA 92182-1308

# 1 Introduction

## 1.1 Background and Motivation

Most of the aerospace structures can be analyzed using shell and plate models. Accurate theoretical formulations that minimize the CPU time without penalties on the quality of the results are then of fundamental importance.

The so-called axiomatic models present the advantage that the important physical behaviors of the structures can be modeled using the “intuition” of eminent scientists. The drawback of this approach is that some cases are not adequately modeled because the starting apriori assumptions might fail. Also, each existing approach presents a range of applicability and when the hypotheses used to formulate the theory are no longer valid the approach has to be replaced with another one usually named as “refined theory” or “improved theory”. In the framework of the mechanical case the Classical Plate Theory (CPT), also known as Kirchoff theory[21], has the advantage of being simple and reliable for thin plates. However, if there is strong anisotropy of the mechanic properties, or if the composite plate is relatively thick, other advanced models such as First-order Shear Deformation Theory (FSDT) are required[30, 25, 24]. Higher-order Shear Deformation Theories (HSDT) have also been used[34, 20, 40], giving the possibility to increase the accuracy of numerical evaluations for moderately thick plates. But even these theories are not sufficient if local effects are important or accuracy in the calculation of transverse stresses is sought. Therefore, more advanced plate theories have been developed to include zig-zag effects [26, 22, 4, 3, 1, 2, 31, 32, 13, 9, 23, 17]. In some challenging cases the previous type of theories are not sufficiently accurate. Therefore, the so-called Layerwise theories[12, 27, 33, 29, 8, 6, 7, 35, 18, 28, 10] have been introduced. In these theories the quantities are layer-dependent and the number of required Degrees of Freedom is much higher than the case of Equivalent Single Layer Models.

The first author introduced an invariant methodology named as Generalized Unified Formulation[15] in which an infinite number of axiomatic models can be included in just one formulation. All the combinations of orders (for example cubic order for the in-plane displacements and parabolic order for the out-of-plane displacement) are possible. Equivalent Single Layer Models (with or without zig-zag effects) and layerwise models can be analyzed. All these formulations derive from the expansion of six  $1 \times 1$  arrays which are invariant with respect to the type of theory (e.g. Equivalent Single Layer or Layerwise) and orders adopted for the displacement variables. This fact makes the Generalized Unified Formulation an ideal tool to test and compare other possible formulations. In particular, this paper assesses the Variational Asymptotic Plate and Shell Analysis (VAPAS) introduced by the second author and com-

compares it with some of the infinite theories that can be generated from the six invariant arrays of the Generalized Unified Formulation. All the results are compared against the elasticity solution developed by the first author. A sandwich plate is analyzed. Different aspect ratios are considered. Different Face to Core Stiffness ratios (FCSRs) are adopted. It is demonstrated that VAPAS gives accurate results at least as a fourth-order axiomatic zig-zag theory but with a much smaller number of Degrees of Freedom. The range of applicability of the various theories generated with GUF and VAPAS is discussed.

## 2 Considered Asymptotic Approach: Variational Asymptotic Plate and Shell Analysis

Mathematically, the approximation in the process of constructing a plate theory stems from elimination of the thickness coordinate as an independent variable of the governing equations, a dimensional reduction process. This sort of approximation is inevitable if one wants to take advantage of the relative smallness of the thickness to simplify the analysis. However, other approximations that are not absolutely necessary should be avoided, if at all possible. For example, for geometrically nonlinear analysis of plates, it is reasonable to assume that the thickness,  $h$ , is small compared to the wavelength of deformation of the reference plane,  $l$ . However, it is unnecessary to assume *a priori* some displacement field, although that is the way most plate theories are constructed. As pointed out by Ref. [5], the attraction of *a priori* hypotheses is caused by our inability to extract the necessary information from the 3D energy expression.

According to this line of logic, Yu and his co-workers adopted the variational asymptotic method (VAM)[5], to develop a new approach to modeling composite laminates[38, 39, 37, 36]. These models are implemented in a computer program named VAPAS. In this approach, the original 3D anisotropic elasticity problem is first cast in an intrinsic form, so that the theory can accommodate arbitrarily large displacement and global rotation subject only to the strain being small. An energy functional can be constructed for this nonlinear 3D problem in terms of 2D generalized strain measures and warping functions describing the deformation of the transverse normal:

$$\Pi = \Pi(\epsilon_{11}, \epsilon_{12}, \epsilon_{22}, \kappa_{11}, \kappa_{12}, \kappa_{22}, w_1, w_2, w_3) \quad (1)$$

Here  $\epsilon_{11}, \epsilon_{12}, \epsilon_{22}, \kappa_{11}, \kappa_{12}, \kappa_{22}$  are the so-called 2D generalized strains [19] and  $w_1, w_2, w_3$  are unknown 3D warping functions, which characterize the difference between the deformation represented by the 2D variables and the actual 3D deformation for every material point within the plate. It is emphasized

here that the warping functions are not assumed *a priori* but are unknown 3D functions to be solved using VAM. Then we can employ VAM to asymptotically expand the 3D energy functional into a series of 2D functionals in terms of the small parameter  $h/l$ , such that

$$\Pi = \Pi_0 + \Pi_1 \frac{h}{l} + \Pi_2 \frac{h^2}{l^2} + o\left(\frac{h^2}{l^2}\right) \quad (2)$$

where  $\Pi_0$ ,  $\Pi_1$ ,  $\Pi_2$  are governing functionals for different orders of approximation and are functions of 2D generalized strains and unknown warping functions. The unknown warping functions for each approximation can be obtained in terms of 2D generalized strains corresponding to the stationary points of the functionals, which are one-dimensional (1D) analyses through the thickness. Solutions for the warping functions can be obtained analytically as shown in Ref. [38] and Ref. [36]. After solving for the unknown warping functions, one can substitute them back into the energy functionals in Eq. 1 to obtain 2D energy functionals for 2D plate analysis. For example, for the zeroth-order approximation, the 2D plate model of VAPAS is of the form

$$\Pi_0 = \Pi_0(\epsilon_{11}, \epsilon_{12}, \epsilon_{22}, \kappa_{11}, \kappa_{12}, \kappa_{22}) \quad (3)$$

It should be noted that the energy functional for the zeroth-order approximation,  $\Pi_0$ , coincides to that of CLT but without invoking the Kirchhoff hypothesis and the transverse normal is flexible during deformation.

Higher-order approximations can be used to construct refined models. For example, the approximation through second order ( $h^2/l^2$ ) should be used to handle transverse shear effects. However, there are two challenging issues associated with the second-order approximation:

- The energy functional asymptotically correct up through the second order is in terms of the CLT generalized strains *and their derivatives*. This form is not convenient for plate analysis because the boundary conditions cannot be readily associated with quantities normally specified on the boundary of plates.
- Only part of the second-order energy corresponds to transverse shear deformation, and no physical interpretation is known for the remaining terms.

VAPAS uses exact kinematical relations between derivatives of the generalized strains of CLT and the transverse shear strains along with equilibrium equations to meet these challenges. Minimization techniques are then applied to find the transverse shear energy that is closest to the asymptotically correct second-order energy. In other words, the loss of accuracy between the asymptotically correct model and a generalized Reissner-Mindlin model is minimized mathematically. For the purpose of establishing a direct connection be-

tween 2D Reissner-Mindlin plate finite element analysis, the through-thickness analysis is implemented using a 1D finite element discretization in the computer program VAPAS, which has direct connection with the plate/shell elements in commercial finite element packages and can be conveniently used by application-oriented engineers.

In comparison to most existing composite plate modeling approaches, VAPAS has several unique features:

- VAPAS adopts VAM to rigorously split the original geometrically-exact, nonlinear 3D problem into a linear, 1D, through-the-thickness analysis and a geometrically-exact, nonlinear, 2D, plate analysis. This novel feature allows the global plate analysis to be formulated exactly and intrinsically as a generalized 2D continuum over the reference plane and routes all the approximations into the through-the-thickness analysis, the accuracy of which is guaranteed to be the best by use of the VAM. The optimization procedure minimizes the loss of information in recasting the model to the generalized Reissner-Mindlin form.
- No kinematical assumptions are invoked in the derivation. All deformation of the normal line element is correctly described by the warping functions within the accuracy of the asymptotic approximation.
- VAPAS does not rely on integration of the 3D equilibrium equations through the thickness to obtain accurate distributions of transverse normal and shear strains and stresses.
- VAPAS exactly satisfies all continuity conditions, including those on both displacement and stress, at the interfaces as well as traction conditions on the top and bottom surfaces.
- The resulting plate/shell analysis is geometrically exact, far beyond von-Karman type nonlinearity commonly used in the literature, needed for highly flexible applications.

### **3 Considered Axiomatic Plate Theories: the Generalized Unified Formulation**

#### *3.1 Classification of the Theories*

The main feature of the Generalized Unified Formulation (GUF) is that the descriptions of Layerwise Theories, Higher-order Shear Deformation Theories and Zig-Zag Theories of any combination of orders *do not show any formal differences* and can all be obtained from six invariant kernels. So, with just one theoretical model an infinite number of different approaches can be considered. For example, in the case of moderately thick plates a higher order theory

could be sufficient but for thick plates layerwise models may be required. With GUF the two approaches are formally identical because the kernels are invariant with respect to the type of theory.

In the present work the concepts of *type of theory* and *class of theories* are introduced. The following types of displacement-based theories are discussed. The first type is named as Advanced Higher-order Shear Deformation Theories (AHSDT). These theories are Equivalent Single Layer models because the displacement field is unique and independent of the number of layers. The effects of the transverse normal strain  $\varepsilon_{zz}$  are retained.

The second type of theories is named as Advanced Higher-order Shear Deformation Theories with Zig-Zag effects included (AHSDTZ). These theories are Equivalent Single Layer models and the so called Zig-Zag form of the displacements is taken into account by using Murakami's Zig-Zag Function (MZZF). The effects of the transverse normal strain  $\varepsilon_{zz}$  are included. The third type of theories is named Advanced LayerWise Theories (ALWT). These theories are the most accurate ones because all the displacements have a layerwise description. The effects of the transverse normal strain  $\varepsilon_{zz}$  are included as well. These models are necessary when local effects need to be described. The price is of course (in FEM applications) in higher computational time. An infinite number of theories which have a particular logic in the selection of the used orders of expansion is defined as *class of theories*. For example, the infinite layerwise theories which have the displacements  $u_x$ ,  $u_y$  and  $u_z$  expanded along the thickness with a polynomial of order  $N$  are a class of theories. The infinite theories which have the in-plane displacements  $u_x$  and  $u_y$  expanded along the thickness with order  $N$ , the out of plane displacement expanded along the thickness with order  $N - 1$  are another class of theories.

### 3.2 Basic Idea and Theoretical Formulation

Both layerwise and Equivalent Single Layer models are axiomatic approaches if the unknowns are expanded along the thickness by using *a chosen* series of functions.

When the Principal of Virtual Displacements is used, the unknowns are the displacements  $u_x$ ,  $u_y$  and  $u_z$ . When other variational statements are used the unknowns may also be all or some of the stresses and other quantities as well (multifield case).

The Generalized Unified Formulation is introduced here considering a generic layer  $k$  of a multilayered plate structure. This is the most general approach and the Equivalent Single Layer theories, which consider the displacement unknowns to be layer-independent, can be derived from this formulation with

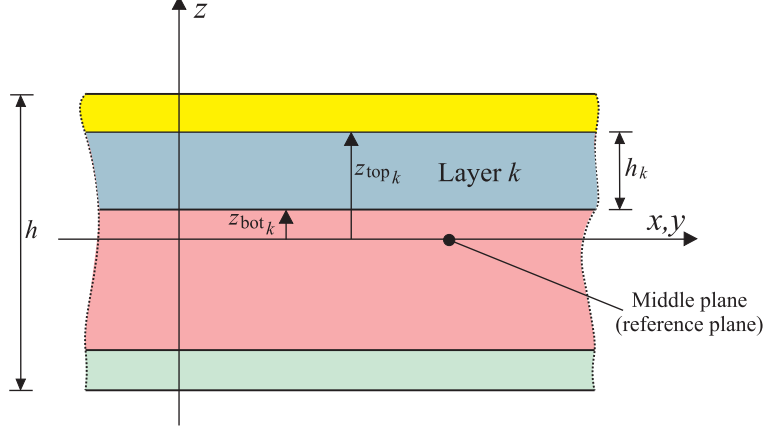


Fig. 1. Multilayered plate: notations and definitions.

some simple formal techniques[15]. Consider a theory denoted as Theory I, in which the displacement in  $x$  direction  $u_x^k$  has four Degrees of Freedom. Here by Degrees of Freedom it is intended the number of unknown quantities that are used to expand a variable. In the case under examination four Degrees of Freedom for the displacement  $u_x^k$  means that four unknowns are considered. Each unknown multiplies a *known function* of the thickness coordinate  $z$ . Where the origin of the coordinate  $z$  is measured is not important. However, from a practical point of view it is convenient to assume that the *middle plane* of the plate is also the plane with  $z = 0$ . This assumption does not imply that there is a symmetry with respect to the plane  $z = 0$ . The formulation is general.

For layer  $k$  the following relation holds:  $z_{\text{bot}_k} \leq z \leq z_{\text{top}_k}$ .  $z_{\text{bot}_k}$  is the global coordinate  $z$  of the bottom surface of layer  $k$  and  $z_{\text{top}_k}$  is the global coordinate  $z$  of the top surface of layer  $k$  (see Figure 1).  $h_k = z_{\text{top}_k} - z_{\text{bot}_k}$  is the thickness of layer  $k$  and  $h$  is the thickness of the plate.

In the case of Theory I,  $u_x^k$  is expressed as follows:

$$\begin{aligned}
 u_x^k(x, y, z) = & \underbrace{f_1^k(z)}_{\text{known}} \cdot \underbrace{u_{x_1}^k(x, y)}_{\text{unknown\#1}} + \underbrace{f_2^k(z)}_{\text{known}} \cdot \underbrace{u_{x_2}^k(x, y)}_{\text{unknown\#2}} \\
 & + \underbrace{f_3^k(z)}_{\text{known}} \cdot \underbrace{u_{x_3}^k(x, y)}_{\text{unknown\#3}} + \underbrace{f_4^k(z)}_{\text{known}} \cdot \underbrace{u_{x_4}^k(x, y)}_{\text{unknown\#4}} \quad z_{\text{bot}_k} \leq z \leq z_{\text{top}_k} \quad (4)
 \end{aligned}$$

The functions  $f_1^k(z)$ ,  $f_2^k(z)$ ,  $f_3^k(z)$  and  $f_4^k(z)$  are *known functions* (axiomatic approach). These functions could be, for example, a series of trigonometric functions of the thickness coordinate  $z$ . Polynomials (or even better orthogonal polynomials) could be selected. In the most general case each layer has different functions. For example,  $f_1^k(z) \neq f_1^{k+1}(z)$ . The next *formal step* is to modify the notation.

The following functions are *defined*:

$$\begin{aligned} {}^x F_t^k(z) &= f_1^k(z) & {}^x F_2^k(z) &= f_2^k(z) \\ {}^x F_3^k(z) &= f_3^k(z) & {}^x F_b^k(z) &= f_4^k(z) \end{aligned} \quad (5)$$

The logic behind these definitions is the following. The *first* function  $f_1^k(z)$  is defined as  ${}^x F_t^k$ . Notice the superscript  $x$ . It was added to clarify that the displacement in  $x$  direction,  $u_x^k$ , is under investigation. The subscript  $t$  identifies the quantities at the “top” of the plate and, therefore, are useful in the assembling of the stiffness matrices in the thickness direction (see Ref. [15]).

The *last* function  $f_4^k(z)$  is defined as  ${}^x F_b^k$ . Notice again the superscript  $x$ . The subscript  $b$  means “bottom” and, again, its utility is discussed in Ref. [15].

The intermediate functions  $f_2^k(z)$  and  $f_3^k(z)$  are defined simply as  ${}^x F_2^k$  and  ${}^x F_3^k$ . To be consistent with the definitions of equation 5, the following unknown quantities are *defined*:

$$u_{x_t}^k(x, y) = u_{x_1}^k(x, y) \quad u_{x_b}^k(x, y) = u_{x_4}^k(x, y) \quad (6)$$

Using the definitions reported in equations 5 and 6, equation 4 can be rewritten as

$$\begin{aligned} u_x^k(x, y, z) &= \underbrace{{}^x F_t^k(z)}_{\text{known}} \cdot \underbrace{u_{x_t}^k(x, y)}_{\text{unknown\#1}} + \underbrace{{}^x F_2^k(z)}_{\text{known}} \cdot \underbrace{u_{x_2}^k(x, y)}_{\text{unknown\#2}} \\ &+ \underbrace{{}^x F_3^k(z)}_{\text{known}} \cdot \underbrace{u_{x_3}^k(x, y)}_{\text{unknown\#3}} + \underbrace{{}^x F_b^k(z)}_{\text{known}} \cdot \underbrace{u_{x_b}^k(x, y)}_{\text{unknown\#4}} \quad z_{\text{bot}_k} \leq z \leq z_{\text{top}_k} \end{aligned} \quad (7)$$

It is supposed that each function of  $z$  is a polynomial. The order of the expansion is then 3 and indicated as  $N_{u_x}^k$ . Each layer has in general a different order. Thus, in general  $N_{u_x}^k \neq N_{u_x}^{k+1}$ . If the functions of  $z$  are not polynomials (for example, this is the case if trigonometric functions are used) then  $N_{u_x}^k$  is just a parameter related to the number of terms or Degrees of Freedom used to describe the displacement  $u_x^k$  in the thickness direction. The expression representing the displacement  $u_x^k$  (see equation 7) can be put in a compact form typical of the Generalized Unified Formulation presented here. In particular it is possible to write:

$$u_x^k(x, y, z) = {}^x F_{\alpha_{u_x}}^k(z) \cdot u_{x\alpha_{u_x}}^k(x, y) \quad \alpha_{u_x} = t, l, b; \quad l = 2, \dots, N_{u_x}^k \quad (8)$$

where, in the example,  $N_{u_x}^k = 3$ . The thickness primary master index  $\alpha$  has the subscript  $u_x$ . This subscript from now on will be called *slave index*. It is introduced to show that the displacement  $u_x$  is considered. An *infinite* number

of theories can be included in equation 8. It is in fact sufficient to change the value of  $N_{u_x}^k$ . It should be observed that *formally* there is no difference between two distinct theories (obtained by changing  $N_{u_x}^k$ ). It is deduced that  $\infty^1$  theories can be represented by equation 8.

The other displacements  $u_y^k$  and  $u_z^k$  can be treated in a similar fashion. The Generalized Unified Formulation for all the displacements is the following:

$$\begin{aligned}
u_x^k &= {}^x F_t u_{x_t}^k + {}^x F_l u_{x_l}^k + {}^x F_b u_{x_b}^k = {}^x F_{\alpha_{u_x}} u_{x\alpha_{u_x}}^k & \alpha_{u_x} &= t, l, b; \quad l = 2, \dots, N_{u_x} \\
u_y^k &= {}^y F_t u_{y_t}^k + {}^y F_m u_{y_m}^k + {}^y F_b u_{y_b}^k = {}^y F_{\alpha_{u_y}} u_{y\alpha_{u_y}}^k & \alpha_{u_y} &= t, m, b; \quad m = 2, \dots, N_{u_y} \quad (9) \\
u_z^k &= {}^z F_t u_{z_t}^k + {}^z F_n u_{z_n}^k + {}^z F_b u_{z_b}^k = {}^z F_{\alpha_{u_z}} u_{z\alpha_{u_z}}^k & \alpha_{u_z} &= t, n, b; \quad n = 2, \dots, N_{u_z}
\end{aligned}$$

In equation 9, for simplicity it is assumed that the type of functions is the same for each layer and that the same number of terms is used for each layer. This assumption will make it possible to adopt the same Generalized Unified Formulation for all types of theories, and layerwise and equivalent single layer theories will *not* show formal differences. This concept means, for example, that if displacement  $u_y$  is approximated with five terms in a particular layer  $k$  then it will be approximated with five terms in *all* layers of the multilayered structure.

Each displacement variable can be expanded in  $\infty^1$  combinations. In fact, it is sufficient to change the number of terms used for each variable. Since there are three variables (the displacements  $u_x$ ,  $u_y$  and  $u_z$ ), it is concluded that equation 9 includes  $\infty^3$  different theories. In equation 9 the quantities are defined in a layerwise sense but it can be shown that the same concept is valid for the Equivalent Single Layer cases too (see Ref. [15]).

It can be shown that when a theory generated by using GUF has the orders of the expansions of all the displacements equal to each other, the results are numerically identical to the ones that can be obtained by using Carrera's Unified Formulation (see Ref. [10]). This is a logical consequence of the fact that GUF can be considered as an extension and generalization of CUF (see more details in Ref. [16]).

### 3.3 Acronyms Used to Identify a Generic Theory Obtained by Using GUF

Three types of displacement-based theories can be obtained. As stated above, the first type is named Advanced Higher-order Shear Deformation Theories (AHS DT). A AHS DT theory with orders of expansion  $N_{u_x}$ ,  $N_{u_y}$  and  $N_{u_z}$  for the displacements  $u_x$ ,  $u_y$  and  $u_z$  respectively, is denoted as  $ED_{N_{u_x}N_{u_y}N_{u_z}}$ . “E” stands for “Equivalent Single Layer” and “D” stands for “Displacement-based” theory.

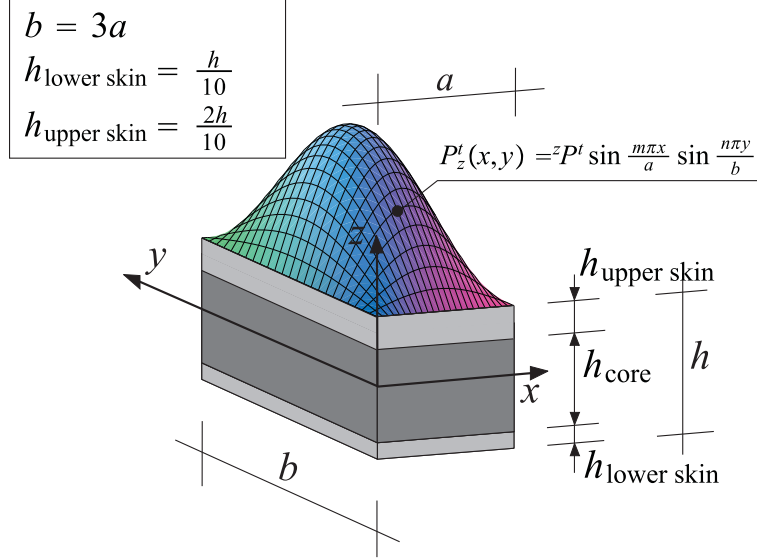


Fig. 2. Test Case 1. Geometry of the plate sandwich structure.

With similar logic, it is possible to define acronyms for the second type (Advanced Higher-order Shear Deformation Theories with Zig-Zag effects included (AHS DTZ)) and for the third type of theories (Advanced LayerWise Theories (ALWT)). The acronyms are  $EDZ_{N_{u_x} N_{u_y} N_{u_z}}$  and  $LD_{N_{u_x} N_{u_y} N_{u_z}}$  (more details can be found in Ref. [15]). For example, a AHS DTZ theory with cubic orders for all the displacements is indicated as  $EDZ_{333}$  whereas a ALWT theory with parabolic orders for all the displacements is indicated as  $LD_{222}$ .

## 4 Results

Two test cases are analyzed in this work.

### 4.1 Description of Test Case 1

Test case 1 is a sandwich plate (see Figure 2) made of two skins and a core [ $h_{\text{lower skin}} = h/10$ ;  $h_{\text{upper skin}} = 2h/10$ ;  $h_{\text{core}} = (7/10)h$ ]. It is also  $\frac{E_{\text{lower skin}}}{E_{\text{upper skin}}} = 5/4$ . The plate is simply supported and the load is a sinusoidal pressure applied at the top surface ( $m = n = 1$ ). Different Face-to-Core Stiffness Ratio (FCSR) are proposed here:

- Face-to-Core Stiffness Ratio =  $FCSR = \frac{E_{\text{lower skin}}}{E_{\text{core}}} = 10^1$ ;  $a/h = 4, 10, 100$
- Face-to-Core Stiffness Ratio =  $FCSR = \frac{E_{\text{lower skin}}}{E_{\text{core}}} = 10^5$ ;  $a/h = 4, 100$

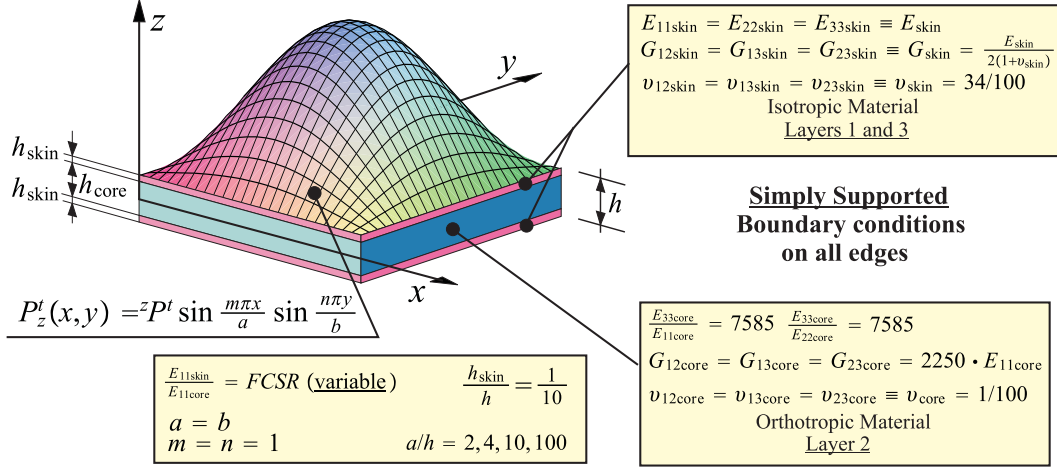


Fig. 3. Test Case 2 (see also [11])

As far as Poisson's ratio is concerned, the following values are used:  $\nu_{\text{lower skin}} = \nu_{\text{upper skin}} = \nu_{\text{core}} = \nu = 0.34$ . The middle plane of the plate is a rectangle with  $b = 3a$ . In this test case there is *no symmetry* with respect the plane  $z = 0$ .

#### 4.2 Description of Test Case 2

This test case is represented by a *symmetric* sandwich structure. The case has been taken from reference [11].

#### 4.3 Test Case 1: Numerical Results and Discussion

The following non-dimensional quantities are introduced:

$$\begin{aligned} \hat{u}_x &= u_x \frac{E_{\text{core}}}{z P^t h \left(\frac{a}{h}\right)^3}; & \hat{u}_y &= u_y \frac{E_{\text{core}}}{z P^t h \left(\frac{a}{h}\right)^3}; & \hat{u}_z &= u_z \frac{100 E_{\text{core}}}{z P^t h \left(\frac{a}{h}\right)^4}; \\ \hat{\sigma}_{zx} &= \frac{\sigma_{zx}}{z P^t \left(\frac{a}{h}\right)}; & \hat{\sigma}_{zy} &= \frac{\sigma_{zy}}{z P^t \left(\frac{a}{h}\right)}; & \hat{\sigma}_{zz} &= \frac{\sigma_{zz}}{z P^t}; \\ \hat{\sigma}_{xx} &= \frac{\sigma_{xx}}{z P^t \left(\frac{a}{h}\right)^2}; & \hat{\sigma}_{yy} &= \frac{\sigma_{yy}}{z P^t \left(\frac{a}{h}\right)^2}; & \hat{\sigma}_{xy} &= \frac{\sigma_{xy}}{z P^t \left(\frac{a}{h}\right)^2}; \end{aligned} \quad (10)$$

All the results have been compared with the solution obtained by solving the “exact” problem[14]. The exact value is indicated with the terminology “elasticity” and is the reference value corresponding to the solution of the differential equations that govern the problem. The details of this elasticity solution are here omitted for brevity. The relative error  $Err\%$  used in the

tables is defined as follows:

$$Err\% = 100 \cdot \frac{\text{Result current theory} - \text{Result elasticity solution}}{\text{Result elasticity solution}} \quad (11)$$

Tables 1 and 2 compare a ALWT, AHS DT, AHS DTZ and VAPAS with VAPAS0 denotes the zeroth-order approximation of VAPAS according to Eq. 3. As shown in Table 1, VAPAS0 has a similar prediction for transverse deflection as  $ED_{111}$  for a thick plate ( $a/h = 4$ ) for both  $FCSR = 10$  and  $FCSR = 10^5$ . It is noted that  $ED_{111}$  is very similar to CLT with a flexible transverse normal. For thin plates with mild modulus contrast, VAPAS0 has an accuracy similar to higher-order theories without zigzag effects ( $ED_{444}$ ,  $ED_{555}$ ,  $ED_{777}$ ). For thin plates with big modulus contrast ( $FCSR = 10^5$ ), VAPAS0 has an accuracy similar to  $ED_{444}$ . VAPAS results for the deflection prediction are generally better than VAPAS0 and has an accuracy comparable to higher-order theories with zig-zag effects such as  $EDZ_{444}$  and higher. The only anomaly case is that for thick plates with the big modulus contrast, VAPAS results are not meaningful. This could be explained that VAPAS is not constructed for such an extreme case. Note in Eq. 2, only the geometrical small parameter  $h/a$  is used for the asymptotical expansion, yet for this extreme case, the modulus contrast is a much smaller parameter than  $h/a$ . Hence, it is suggested that VAPAS is not suitable for thick sandwich plates with huge modulus contrast. Note for the sandwich plate with  $a/h = 100$  and  $FCSR = 10^5$ , VAPAS predicts reasonably well. Later we will use more examples to demonstrate that for moderate modulus contrast, VAPAS actually has a very good prediction. Similar observations can be made about the stress prediction as shown in Table 2. It is worthy to point out that VAPAS plate model only uses three DOFs for its zeroth-order approximation and five DOFs for its first-order approximation. The 2D plate element of VAPAS is the same as a FOSDT and is more efficient than all other theories listed in the tables. In other words, VAPAS presents a great compromise between the accuracy of the results and the number of DOFs. Tables 3-11 present a relatively thick sandwich plate with  $FCSR = 10$ . The out-of-plane stresses are not unknowns of the displaced-based theories based on GUF (this is not the case if a mixed variational theorem is used). Therefore, they can be calculated *a posteriori* by using Hooke's law or by integrating the equilibrium equations. The first approach is usually not satisfactory for ESL theories. Therefore, all the axiomatic results presented in this work report the transverse stresses calculated by integrating the equilibrium equations. In all cases it is possible to see that VAPAS has an accuracy comparable or superior to AHS DTZ. For this particular case we tested, VAPAS has a similar accuracy as, or for most cases better, than  $EDZ_{555}$  for displacement prediction and in-plane stress and transverse normal stress prediction and its accuracy is similar to  $LD_{222}$ . For transverse shear stresses, VAPAS predicts similar values as  $EDZ_{555}$ . However, if integration through the thickness is not used to obtain such values,  $EDZ_{555}$  will be expected to be worse than VAPAS

$a/h$	4	100			
		$\frac{E_{\text{lower skin}}}{E_{\text{core}}} \equiv FCSR = 10^1$			
<i>Elasticity</i>	3.01123	<i>Err.%</i>	1.51021	<i>Err.%</i>	<i>DOF</i>
<i>LD</i> <sub>111</sub>	2.98058	(-1.02)	1.47242	(-2.50)	12
<i>LD</i> <sub>222</sub>	3.00982	(-0.05)	1.51021	(0.00)	21
<i>LD</i> <sub>555</sub>	3.01123	(0.00)	1.51021	(0.00)	48
<i>ED</i> <sub>111</sub>	1.58218	(-47.5)	1.10845	(-26.6)	6
<i>ED</i> <sub>444</sub>	2.79960	(-7.03)	1.50989	(-0.02)	15
<i>ED</i> <sub>555</sub>	2.84978	(-5.36)	1.50996	(-0.02)	18
<i>ED</i> <sub>777</sub>	2.86875	(-4.73)	1.50999	(-0.01)	24
<i>EDZ</i> <sub>111</sub>	2.34412	(-22.2)	1.15866	(-23.3)	9
<i>EDZ</i> <sub>444</sub>	2.97886	(-1.07)	1.51017	(0.00)	18
<i>EDZ</i> <sub>555</sub>	2.98737	(-0.79)	1.51018	(0.00)	21
<i>EDZ</i> <sub>777</sub>	2.99670	(-0.48)	1.51019	(0.00)	27
<i>VAPAS</i> <sub>0</sub>	1.5136	(-49.7)	1.50788	(-0.15)	3
<i>VAPAS</i>	3.0198	(0.28)	1.5102	(0.00)	5
		$\frac{E_{\text{lower skin}}}{E_{\text{core}}} \equiv FCSR = 10^5$			
<i>Elasticity</i>	$1.31593 \cdot 10^{-02}$	<i>Err.%</i>	$2.08948 \cdot 10^{-03}$	<i>Err.%</i>	
<i>LD</i> <sub>111</sub>	$9.79008 \cdot 10^{-03}$	(-25.6)	$1.96509 \cdot 10^{-03}$	(-5.95)	12
<i>LD</i> <sub>222</sub>	$1.31471 \cdot 10^{-02}$	(-0.09)	$2.08948 \cdot 10^{-03}$	(0.00)	21
<i>LD</i> <sub>555</sub>	$1.31593 \cdot 10^{-02}$	(0.00)	$2.08949 \cdot 10^{-03}$	(0.00)	48
<i>ED</i> <sub>111</sub>	$1.79831 \cdot 10^{-04}$	(-98.6)	$1.19941 \cdot 10^{-04}$	(-94.3)	6
<i>ED</i> <sub>444</sub>	$1.16851 \cdot 10^{-03}$	(-91.1)	$1.64835 \cdot 10^{-04}$	(-92.1)	15
<i>ED</i> <sub>555</sub>	$4.29224 \cdot 10^{-03}$	(-67.4)	$1.73120 \cdot 10^{-04}$	(-91.7)	18
<i>ED</i> <sub>777</sub>	$1.08119 \cdot 10^{-02}$	(-17.8)	$2.96304 \cdot 10^{-04}$	(-85.8)	24
<i>EDZ</i> <sub>111</sub>	$8.36735 \cdot 10^{-04}$	(-93.6)	$1.63329 \cdot 10^{-04}$	(-92.2)	9
<i>EDZ</i> <sub>444</sub>	$1.26288 \cdot 10^{-02}$	(-4.03)	$1.16305 \cdot 10^{-03}$	(-44.3)	18
<i>EDZ</i> <sub>555</sub>	$1.30409 \cdot 10^{-02}$	(-0.90)	$1.78411 \cdot 10^{-03}$	(-14.6)	21
<i>EDZ</i> <sub>777</sub>	$1.31363 \cdot 10^{-02}$	(-0.17)	$2.02060 \cdot 10^{-03}$	(-3.30)	27
<i>VAPAS</i> <sub>0</sub>	$1.6421 \cdot 10^{-04}$	(-98.7)	$1.6314 \cdot 10^{-04}$	(-92.2)	3
<i>VAPAS</i>	1.49076	(> 100)	$2.4667 \cdot 10^{-03}$	(18.0)	5

Table 1

Test Case 1. Comparison of various theories to evaluate the transverse displacements amplitude (center plate deflection)  $\hat{u}_z = u_z \frac{100E_{\text{core}}}{zP^t h (\frac{a}{h})^4}$  in  $z = z_{\text{bottom}}^{\text{upper skin}} = \frac{3}{10}h$ ,  $x =$

$a/2$ ,  $y = b/2$ .

$a/h$	4	$Err.$	100	$Err.$	
$\frac{E_{\text{lower skin}}}{E_{\text{core}}} \equiv FCSR = 10^1$					
<i>Elasticity</i>	0.32168	$Err.\%$	0.33176	$Err.\%$	<i>DOF</i>
$LD_{111}$	0.31730	(-1.36)	0.32345	(-2.50)	12
$LD_{222}$	0.32142	(-0.08)	0.33176	(0.00)	21
$LD_{555}$	0.32168	(0.00)	0.33176	(0.00)	48
$ED_{111}$	0.33178	(+3.14)	0.33178	(+0.01)	6
$ED_{444}$	0.33240	(+3.33)	0.33178	(+0.01)	15
$ED_{555}$	0.32884	(+2.23)	0.33178	(+0.01)	18
$ED_{777}$	0.32707	(+1.68)	0.33177	(0.00)	24
$EDZ_{111}$	0.34184	(+6.27)	0.34497	(+3.98)	9
$EDZ_{444}$	0.32913	(+2.32)	0.33178	(+0.01)	18
$EDZ_{555}$	0.32755	(+1.82)	0.33177	(0.00)	21
$EDZ_{777}$	0.32530	(+1.12)	0.33177	(+0.00)	27
$VAPAS_0$	0.33178	(+3.14)	0.33178	(+0.01)	3
$VAPAS$	0.31037	(-3.5)	0.33175	(+0.00)	5
$\frac{E_{\text{lower skin}}}{E_{\text{core}}} \equiv FCSR = 10^5$					
<i>Elasticity</i>	$5.40842 \cdot 10^{-04}$	$Err.\%$	0.27797	$Err.\%$	
$LD_{111}$	$1.05700 \cdot 10^{-04}$	(-80.5)	0.26143	(-5.95)	12
$LD_{222}$	$5.37740 \cdot 10^{-04}$	(-0.57)	0.27797	(0.00)	21
$LD_{555}$	$5.40842 \cdot 10^{-04}$	(0.00)	0.27797	(0.00)	48
$ED_{111}$	0.33242	(> 100)	0.33242	(+19.6)	6
$ED_{444}$	0.30529	(> 100)	0.33238	(+16.6)	15
$ED_{555}$	0.21639	(> 100)	0.33214	(+19.5)	18
$ED_{777}$	$3.96907 \cdot 10^{-02}$	(> 100)	0.32865	(+18.2)	24
$EDZ_{111}$	0.30971	(> 100)	0.33077	(+19.0)	9
$EDZ_{444}$	$6.84336 \cdot 10^{-03}$	(> 100)	0.30392	(+9.34)	18
$EDZ_{555}$	$1.87520 \cdot 10^{-03}$	(> 100)	0.28655	(+3.09)	21
$EDZ_{777}$	$8.02443 \cdot 10^{-04}$	(+48.4)	0.27994	(+0.71)	27
$VAPAS_0$	0.33242	(> 100)	0.33242	(+19.6)	3
$VAPAS$	0.30592	(> 100)	0.33238	(+16.6)	5

Table 2

Test Case 1. Comparison of various theories to evaluate the transverse shear stress  $\hat{\sigma}_{zx} = \frac{\sigma_{zx}}{zPt(\frac{a}{h})}$  in  $z = z_{\text{bottom}}^{\text{upper skin}} = \frac{3}{10}h$ ,  $x = 0$ ,  $y = b/2$ . The indefinite equilibrium equations have been integrated along the thickness.

results. For moderate  $FCSR$  values and thick plates ( $a/h = 4$ , see Figures 4-7, VAPAS presents results that can be comparable of the results obtained by using the axiomatic zig-zag theory  $EDZ_{777}$ . This is particularly evident in Figure 7. However, the VAPAS plate model only requires five DOFs, which is only less than 20% of the computational cost one would need for  $EDZ_{777}$  (27 DOFs). It is also noted, VAPAS plate model remains the same as the well-known Reissner-Mindlin elements universally available in all commercial finite element packages.

The Equivalent Single Layer and Layerwise axiomatic theories presented in this paper and a virtually infinite number of other theories can be implemented in a single FEM code based on the Generalized Unified Formulation. Accuracy and CPU time requirements can be easily met with an appropriate selection of the type of theory and the orders used in the expansions of the displacements.

$a/h$	10		
	$\frac{E_{\text{lower skin}}}{E_{\text{core}}} \equiv FCSR = 10^1$		
<i>Elasticity</i>		<i>Err.%</i>	<i>DOF</i>
$LD_{111}$	$-0.11087 \cdot 10^{-01}$	(-2.59)	12
$LD_{222}$	$-0.11085 \cdot 10^{-01}$	(-0.01)	21
$LD_{333}$	$-0.11087 \cdot 10^{-01}$	(-0.00)	30
$LD_{444}$	$-0.11087 \cdot 10^{-01}$	(-0.00)	39
$ED_{111}$	$-0.08627 \cdot 10^{-01}$	(-22.2)	6
$ED_{222}$	$-0.11736 \cdot 10^{-01}$	(+5.85)	9
$ED_{333}$	$-0.11358 \cdot 10^{-01}$	(+2.45)	12
$ED_{444}$	$-0.11316 \cdot 10^{-01}$	(+2.07)	15
$ED_{555}$	$-0.11242 \cdot 10^{-01}$	(+1.40)	18
$EDZ_{111}$	$-0.08696 \cdot 10^{-01}$	(-21.6)	9
$EDZ_{222}$	$-0.11161 \cdot 10^{-01}$	(+0.67)	12
$EDZ_{333}$	$-0.11166 \cdot 10^{-01}$	(+0.71)	15
$EDZ_{444}$	$-0.11164 \cdot 10^{-01}$	(+0.69)	18
$EDZ_{555}$	$-0.11146 \cdot 10^{-01}$	(+0.53)	21
<i>VAPAS</i>	$-0.111009 \cdot 10^{-01}$	(+0.13)	5

Table 3

Test Case 1. Comparison of various theories to evaluate the in-plane displacement  $\hat{u}_x = u_x \frac{E_{\text{core}}}{z P t h (\frac{a}{h})^3}$  in  $z = z_{\text{bottom}}^{\text{upper skin}} = \frac{3}{10} h$ ,  $x = 0$ ,  $y = b/2$ .

$a/h$	10		
	$\frac{E_{\text{lower skin}}}{E_{\text{core}}} \equiv FCSR = 10^1$		
		<i>Err.%</i>	<i>DOF</i>
<i>Elasticity</i>	$-0.36956 \cdot 10^{-02}$		
<i>LD</i> <sub>111</sub>	$-0.36000 \cdot 10^{-02}$	(-2.59)	12
<i>LD</i> <sub>222</sub>	$-0.36952 \cdot 10^{-02}$	(-0.01)	21
<i>LD</i> <sub>333</sub>	$-0.36956 \cdot 10^{-02}$	(-0.00)	30
<i>LD</i> <sub>444</sub>	$-0.36956 \cdot 10^{-02}$	(-0.00)	39
<i>ED</i> <sub>111</sub>	$-0.28757 \cdot 10^{-02}$	(-22.2)	6
<i>ED</i> <sub>222</sub>	$-0.39120 \cdot 10^{-02}$	(+5.85)	9
<i>ED</i> <sub>333</sub>	$-0.37860 \cdot 10^{-02}$	(+2.45)	12
<i>ED</i> <sub>444</sub>	$-0.37721 \cdot 10^{-02}$	(+2.07)	15
<i>ED</i> <sub>555</sub>	$-0.37473 \cdot 10^{-02}$	(+1.40)	18
<i>EDZ</i> <sub>111</sub>	$-0.28986 \cdot 10^{-02}$	(-21.6)	9
<i>EDZ</i> <sub>222</sub>	$-0.37204 \cdot 10^{-02}$	(+0.67)	12
<i>EDZ</i> <sub>333</sub>	$-0.37220 \cdot 10^{-02}$	(+0.71)	15
<i>EDZ</i> <sub>444</sub>	$-0.37213 \cdot 10^{-02}$	(+0.69)	18
<i>EDZ</i> <sub>555</sub>	$-0.37153 \cdot 10^{-02}$	(+0.53)	21
<i>VAPAS</i>	$-0.37003 \cdot 10^{-02}$	(+0.13)	5

Table 4

Test Case 1. Comparison of various theories to evaluate the in-plane displacement  $\hat{u}_y = u_y \frac{E_{\text{core}}}{zP^t h \left(\frac{a}{h}\right)^3}$  in  $z = z_{\text{bottom}}^{\text{upper skin}} = \frac{3}{10}h$ ,  $x = a/2$ ,  $y = 0$ .

#### 4.4 Test Case 2: Numerical Results and Discussion

The dimensionless displacements used for this study are defined as

$$\hat{u}_x = u_x \frac{E_{\text{skin}}}{zP^t h \left(\frac{a}{h}\right)^3}; \quad \hat{u}_z = u_z \frac{100E_{\text{skin}}}{zP^t h \left(\frac{a}{h}\right)^4} \quad (12)$$

Notice the formal difference with the dimensionless quantities introduced in test case 1: here the elastic modulus used for the non-dimensional quantities is the elastic modulus of the skin and not the one of the core. The results are compared against the elasticity solution (see [14] and [16]). Tables 12, 13, 14, and 15 report some results obtained in reference [11] for thick, moderately thick and thin sandwich structures. The available results have been enriched with the new case of  $a/h = 2$  and with the elasticity solution. The findings

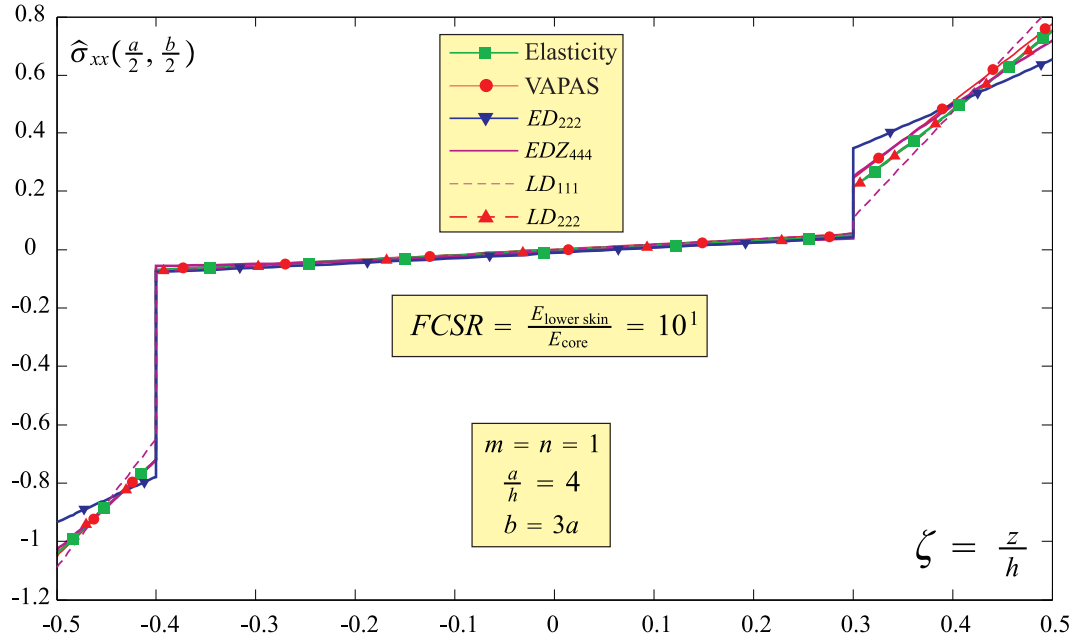


Fig. 4. Test Case 1. Comparison of various theories to evaluate the in-plane normal stress  $\hat{\sigma}_{xx} = \frac{\sigma_{xx}}{zPt(\frac{a}{h})^2}$  in  $x = a/2, y = b/2$ . Note that this stress is not a continuous function on the thickness direction. Hooke's law has been used.

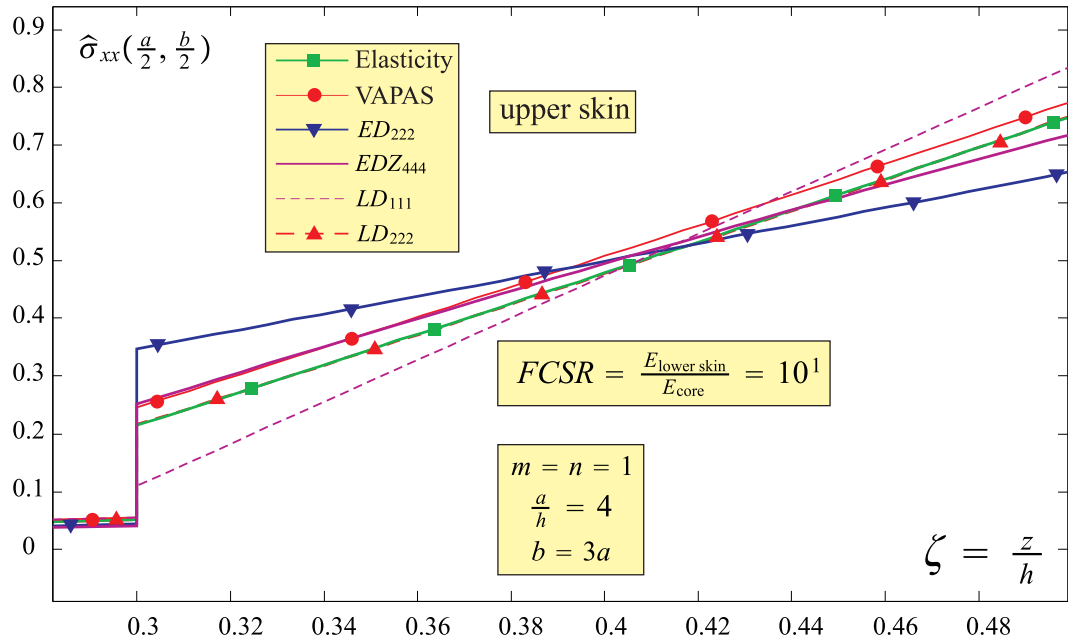


Fig. 5. Test Case 1. Comparison of various theories to evaluate the in-plane normal stress  $\hat{\sigma}_{xx} = \frac{\sigma_{xx}}{zPt(\frac{a}{h})^2}$  in  $x = a/2, y = b/2$  (upper-skin). Hooke's law has been used.

$a/h$	10		
	$\frac{E_{\text{lower skin}}}{E_{\text{core}}} \equiv FCSR = 10^1$		
<i>Elasticity</i>		<i>Err.%</i>	<i>DOF</i>
$LD_{111}$	1.70908	(-1.93)	12
$LD_{222}$	1.74247	(-0.01)	21
$LD_{333}$	1.74265	(-0.00)	30
$LD_{444}$	1.74265	(-0.00)	39
$ED_{111}$	1.18207	(-32.2)	6
$ED_{222}$	1.58561	(-9.01)	9
$ED_{333}$	1.70006	(-2.44)	12
$ED_{444}$	1.71032	(-1.85)	15
$ED_{555}$	1.71796	(-1.42)	18
$EDZ_{111}$	1.34741	(-22.7)	9
$EDZ_{222}$	1.73669	(-0.34)	12
$EDZ_{333}$	1.73805	(-0.26)	15
$EDZ_{444}$	1.73836	(-0.25)	18
$EDZ_{555}$	1.73938	(-0.19)	21
<i>VAPAS</i>	1.74265	(+0.00)	5

Table 5

Test Case 1. Comparison of various theories to evaluate the transverse displacements amplitude (center plate deflection)  $\hat{u}_z = u_z \frac{100E_{\text{core}}}{zP^t h (\frac{a}{h})^4}$  in  $z = z_{\text{bottom}}^{\text{upper skin}} = \frac{3}{10}h$ ,  $x = a/2$ ,  $y = b/2$ .

of reference [11] have been confirmed: the equivalent single layer theories are not indicated to analyze very challenging sandwich structures especially if the face-to-core stiffness ratio is very high and the aspect ratio is small (thick plates). This result is also confirmed in figures 8, 9, and 10. In particular, it is clear from Figure 10 (which presents several AHS DTZ theories) that even zig zag theories with considerably high order for the expansion of the variables present significant error especially in the core region. As previously discussed for Test Case 1, VAPAS provides excellent results for low values of FCSR. If FCSR is increased, the error becomes larger. This suggests that VAPAS presents superior performances with respect to the classical equivalent single layer models (including zig zag effects) only if FCSR is moderate.

$a/h$	10		
	$\frac{E_{\text{lower skin}}}{E_{\text{core}}} \equiv FCSR = 10^1$		
<i>Elasticity</i>		<i>Err.%</i>	<i>DOF</i>
<i>LD</i> <sub>111</sub>	0.26290	(−20.7)	12
<i>LD</i> <sub>222</sub>	0.33169	(+0.07)	21
<i>LD</i> <sub>333</sub>	0.33144	(−0.00)	30
<i>LD</i> <sub>444</sub>	0.33146	(+0.00)	39
<i>ED</i> <sub>111</sub>	0.36049	(+8.76)	6
<i>ED</i> <sub>222</sub>	0.35272	(+6.41)	9
<i>ED</i> <sub>333</sub>	0.34357	(+3.65)	12
<i>ED</i> <sub>444</sub>	0.34649	(+4.54)	15
<i>ED</i> <sub>555</sub>	0.34260	(+3.36)	18
<i>EDZ</i> <sub>111</sub>	0.35807	(+8.03)	9
<i>EDZ</i> <sub>222</sub>	0.32847	(−0.90)	12
<i>EDZ</i> <sub>333</sub>	0.33559	(+1.25)	15
<i>EDZ</i> <sub>444</sub>	0.33753	(+1.83)	18
<i>EDZ</i> <sub>555</sub>	0.33678	(+1.60)	21
<i>VAPAS</i>	0.33364	(+0.66)	5

Table 6

Test Case 1. Comparison of various theories to evaluate the in-plane normal stress  $\hat{\sigma}_{xx} = \frac{\sigma_{xx}}{zPt\left(\frac{a}{h}\right)^2}$  in  $z = z_{\text{bottom}}^{\text{upper skin}} = \frac{3}{10}h$ ,  $x = a/2$ ,  $y = b/2$ . Note that this stress is not a continuous function on the thickness direction. Hooke's law has been used.

$a/h$	10		
	$\frac{E_{\text{lower skin}}}{E_{\text{core}}} \equiv FCSR = 10^1$		
<i>Elasticity</i>		<i>Err.%</i>	<i>DOF</i>
<i>LD</i> <sub>111</sub>	0.08285	(−43.5)	12
<i>LD</i> <sub>222</sub>	0.14688	(+0.17)	21
<i>LD</i> <sub>333</sub>	0.14660	(−0.01)	30
<i>LD</i> <sub>444</sub>	0.14662	(+0.00)	39
<i>ED</i> <sub>111</sub>	0.21666	(+47.8)	6
<i>ED</i> <sub>222</sub>	0.15706	(+7.12)	9
<i>ED</i> <sub>333</sub>	0.15421	(+5.18)	12
<i>ED</i> <sub>444</sub>	0.15783	(+7.64)	15
<i>ED</i> <sub>555</sub>	0.15518	(+5.84)	18
<i>EDZ</i> <sub>111</sub>	0.21309	(+45.3)	9
<i>EDZ</i> <sub>222</sub>	0.14239	(−2.88)	12
<i>EDZ</i> <sub>333</sub>	0.14943	(+1.92)	15
<i>EDZ</i> <sub>444</sub>	0.15141	(+3.27)	18
<i>EDZ</i> <sub>555</sub>	0.15095	(+2.95)	21
<i>VAPAS</i>	0.14758	(+0.65)	5

Table 7

Test Case 1. Comparison of various theories to evaluate the in-plane normal stress  $\hat{\sigma}_{yy} = \frac{\sigma_{yy}}{zPt(\frac{a}{h})^2}$  in  $z = z_{\text{bottom}}^{\text{upper skin}} = \frac{3}{10}h$ ,  $x = a/2$ ,  $y = b/2$ . Note that this stress is not a continuous function on the thickness direction. Hooke's law has been used.

$a/h$	10		
	$\frac{E_{\text{lower skin}}}{E_{\text{core}}} \equiv FCSR = 10^1$		
<i>Elasticity</i>		<i>Err.%</i>	<i>DOF</i>
<i>LD</i> <sub>111</sub>	$-0.67520 \cdot 10^{-01}$	(-2.59)	12
<i>LD</i> <sub>222</sub>	$-0.69305 \cdot 10^{-01}$	(-0.01)	21
<i>LD</i> <sub>333</sub>	$-0.69314 \cdot 10^{-01}$	(-0.00)	30
<i>LD</i> <sub>444</sub>	$-0.69314 \cdot 10^{-01}$	(-0.00)	39
<i>ED</i> <sub>111</sub>	$-0.53936 \cdot 10^{-01}$	(-22.2)	6
<i>ED</i> <sub>222</sub>	$-0.73372 \cdot 10^{-01}$	(+5.85)	9
<i>ED</i> <sub>333</sub>	$-0.71010 \cdot 10^{-01}$	(+2.45)	12
<i>ED</i> <sub>444</sub>	$-0.70749 \cdot 10^{-01}$	(+2.07)	15
<i>ED</i> <sub>555</sub>	$-0.70283 \cdot 10^{-01}$	(+1.40)	18
<i>EDZ</i> <sub>111</sub>	$-0.54366 \cdot 10^{-01}$	(-21.6)	9
<i>EDZ</i> <sub>222</sub>	$-0.69779 \cdot 10^{-01}$	(+0.67)	12
<i>EDZ</i> <sub>333</sub>	$-0.69808 \cdot 10^{-01}$	(+0.71)	15
<i>EDZ</i> <sub>444</sub>	$-0.69795 \cdot 10^{-01}$	(+0.69)	18
<i>EDZ</i> <sub>555</sub>	$-0.69684 \cdot 10^{-01}$	(+0.53)	21
<i>VAPAS</i>	$-0.69775 \cdot 10^{-01}$	(+0.67)	5

Table 8

Test Case 1. Comparison of various theories to evaluate the in-plane shear stress  $\hat{\sigma}_{xy} = \frac{\sigma_{xy}}{z P^i \left(\frac{a}{h}\right)^2}$  in  $z = z_{\text{bottom}}^{\text{upper skin}} = \frac{3}{10}h$ ,  $x = 0$ ,  $y = 0$ . Note that this stress is not a continuous function on the thickness direction. Hooke's law has been used.

$a/h$	10		
	$\frac{E_{\text{lower skin}}}{E_{\text{core}}} \equiv FCSR = 10^1$		
<i>Elasticity</i>		<i>Err.%</i>	<i>DOF</i>
<i>LD</i> <sub>111</sub>	0.32242	(-2.29)	12
<i>LD</i> <sub>222</sub>	0.32994	(-0.01)	21
<i>LD</i> <sub>333</sub>	0.32998	(-0.00)	30
<i>LD</i> <sub>444</sub>	0.32998	(-0.00)	39
<i>ED</i> <sub>111</sub>	0.33178	(+0.55)	6
<i>ED</i> <sub>222</sub>	0.33210	(+0.64)	9
<i>ED</i> <sub>333</sub>	0.33081	(+0.25)	12
<i>ED</i> <sub>444</sub>	0.33178	(+0.54)	15
<i>ED</i> <sub>555</sub>	0.33117	(+0.36)	18
<i>EDZ</i> <sub>111</sub>	0.34444	(+4.38)	9
<i>EDZ</i> <sub>222</sub>	0.33154	(+0.47)	12
<i>EDZ</i> <sub>333</sub>	0.33140	(+0.43)	15
<i>EDZ</i> <sub>444</sub>	0.33124	(+0.38)	18
<i>EDZ</i> <sub>555</sub>	0.33096	(+0.30)	21
<i>VAPAS</i>	0.32836	(-0.50)	5

Table 9

Test Case 1. Comparison of various theories to evaluate the transverse shear stress  $\hat{\sigma}_{zx} = \frac{\sigma_{zx}}{zPt(\frac{a}{h})}$  in  $z = z_{\text{bottom}}^{\text{upper skin}} = \frac{3}{10}h$ ,  $x = 0$ ,  $y = b/2$ . The indefinite equilibrium equations have been integrated along the thickness for all the theories except VAPAS.

$a/h$	10		
	$\frac{E_{\text{lower skin}}}{E_{\text{core}}} \equiv FCSR = 10^1$		
<i>Elasticity</i>		<i>Err.%</i>	<i>DOF</i>
<i>LD</i> <sub>111</sub>	0.10747	(-2.29)	12
<i>LD</i> <sub>222</sub>	0.10998	(-0.01)	21
<i>LD</i> <sub>333</sub>	0.10999	(-0.00)	30
<i>LD</i> <sub>444</sub>	0.10999	(-0.00)	39
<i>ED</i> <sub>111</sub>	0.11059	(+0.55)	6
<i>ED</i> <sub>222</sub>	0.11070	(+0.64)	9
<i>ED</i> <sub>333</sub>	0.11027	(+0.25)	12
<i>ED</i> <sub>444</sub>	0.11059	(+0.54)	15
<i>ED</i> <sub>555</sub>	0.11039	(+0.36)	18
<i>EDZ</i> <sub>111</sub>	0.11481	(+4.38)	9
<i>EDZ</i> <sub>222</sub>	0.11051	(+0.47)	12
<i>EDZ</i> <sub>333</sub>	0.11047	(+0.43)	15
<i>EDZ</i> <sub>444</sub>	0.11041	(+0.38)	18
<i>EDZ</i> <sub>555</sub>	0.11032	(+0.30)	21
<i>VAPAS</i>	0.10945	(-0.49)	5

Table 10

Test Case 1. Comparison of various theories to evaluate the transverse shear stress  $\hat{\sigma}_{zy} = \frac{\sigma_{zy}}{zPl(\frac{a}{h})}$  in  $z = z_{\text{bottom}}^{\text{upper skin}} = \frac{3}{10}h$ ,  $x = a/2$ ,  $y = 0$ . The indefinite equilibrium equations have been integrated along the thickness for all the theories except VAPAS.

$a/h$	10		
	$\frac{E_{\text{lower skin}}}{E_{\text{core}}} \equiv FCSR = 10^1$		
<i>Elasticity</i>		<i>Err.%</i>	<i>DOF</i>
$LD_{111}$	0.87231	(-0.17)	12
$LD_{222}$	0.87233	(+0.00)	21
$LD_{333}$	0.87231	(+0.00)	30
$LD_{444}$	0.87231	(-0.00)	39
$ED_{111}$	0.51236	(-41.3)	6
$ED_{222}$	0.58831	(-32.6)	9
$ED_{333}$	0.77221	(-11.5)	12
$ED_{444}$	0.78478	(-10.0)	15
$ED_{555}$	0.81517	(-6.55)	18
$EDZ_{111}$	0.51803	(-40.6)	9
$EDZ_{222}$	0.83586	(-4.18)	12
$EDZ_{333}$	0.83769	(-3.97)	15
$EDZ_{444}$	0.83847	(-3.88)	18
$EDZ_{555}$	0.84631	(-2.98)	21
<i>VAPAS</i>	0.87354	(+0.14)	5

Table 11

Test Case 1. Comparison of various theories to evaluate the transverse normal stress  $\hat{\sigma}_{zz} = \frac{\sigma_{zz}}{z \rho t}$  in  $z = z_{\text{bottom}}^{\text{upper skin}} = \frac{3}{10}h$ ,  $x = a/2$ ,  $y = b/2$ . The indefinite equilibrium equations have been integrated along the thickness for all the theories except VAPAS.

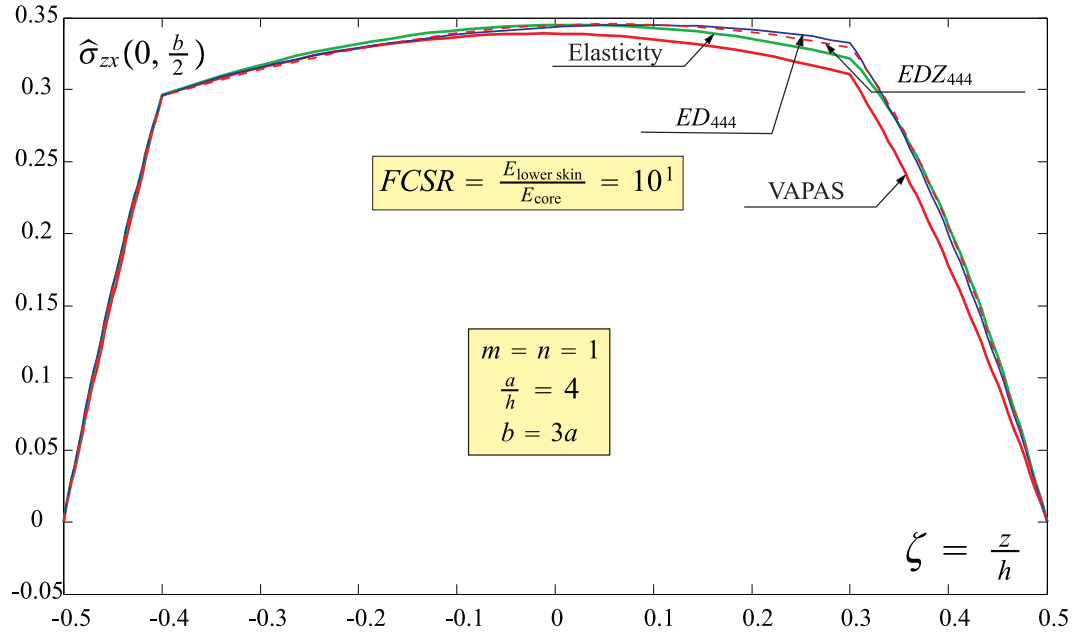


Fig. 6. Test Case 1. Comparison of various theories to evaluate the transverse shear stress  $\hat{\sigma}_{zx} = \frac{\sigma_{zx}}{zPt(\frac{a}{h})}$  in  $x = 0, y = b/2$ . The indefinite equilibrium equations have been integrated along the thickness.

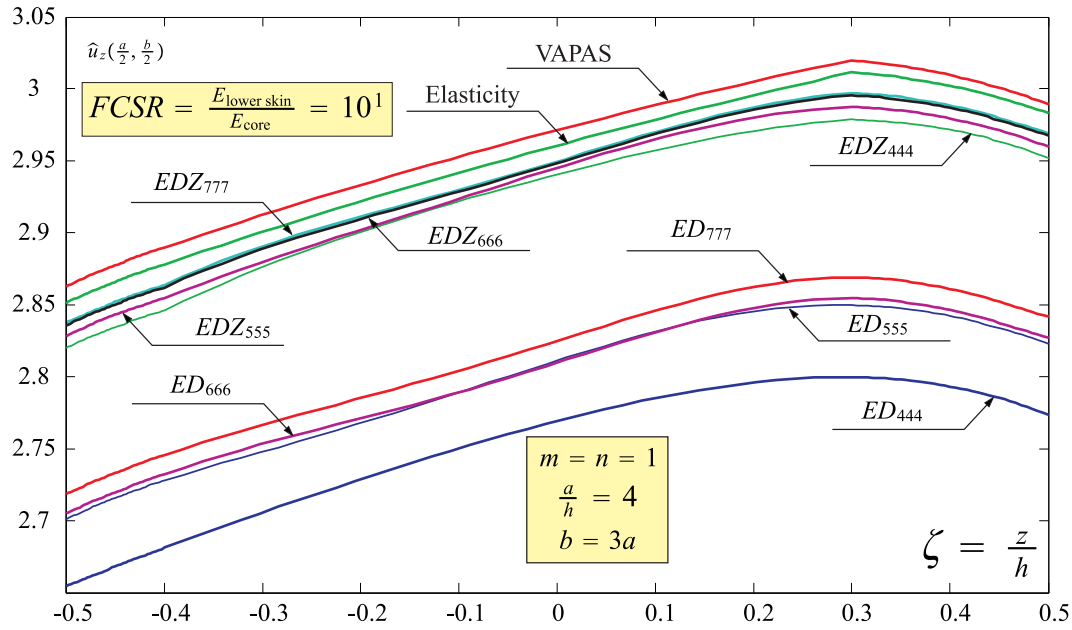


Fig. 7. Test Case 1. Comparison of various theories to evaluate the transverse displacements amplitude (center plate deflection)  $\hat{u}_z = u_z \frac{100E_{\text{core}}}{zPt h(\frac{a}{h})^4}$  in  $x = a/2, y = b/2$ .

$a/h$	2		4		10		100	
	$\frac{E_{11\text{skin}}}{E_{11\text{core}}} \equiv FCSR = 7.3 \times 10^1$							
Elasticity	0.227330	<i>Err%</i>	0.198251	<i>Err%</i>	0.190084	<i>Err%</i>	0.188542	<i>Err%</i>
<i>LM4</i> [11]	<i>NA</i>	<i>NA</i>	0.1982	-0.03	0.1901	+0.01	0.1885	-0.02
<i>ED4</i> [11]	<i>NA</i>	<i>NA</i>	<i>NA</i>	$ 1.61 ^\dagger$	<i>NA</i>	$ 0.79 ^\dagger$	<i>NA</i>	$ 1.22 ^\dagger$
<i>EMZC3</i> [11]	<i>NA</i>	<i>NA</i>	<i>NA</i>	$ 1.66 ^\dagger$	<i>NA</i>	$ 0.74 ^\dagger$	<i>NA</i>	$ 1.17 ^\dagger$
<i>LD1</i> [11]	<i>NA</i>	<i>NA</i>	<i>NA</i>	$ 1.06 ^\dagger$	<i>NA</i>	$ 0.16 ^\dagger$	<i>NA</i>	$ 0.05 ^\dagger$
<i>LD4</i> [11]	<i>NA</i>	<i>NA</i>	<i>NA</i>	$ 0.00 ^\dagger$	<i>NA</i>	$ 0.00 ^\dagger$	<i>NA</i>	$ 0.00 ^\dagger$
<i>EDZ</i> <sub>555</sub>	0.246804	+8.57	0.201527	+1.65	0.188663	-0.75	0.186228	-1.23
<i>LD</i> <sub>222</sub>	0.219334	-3.52	0.195992	-1.14	0.189710	-0.20	0.188538	-0.00
<i>LD</i> <sub>555</sub>	0.227331	+0.00	0.198251	+0.00	0.190084	+0.00	0.188542	+0.00
<i>VAPAS</i>	0.191717	-15.67	0.192759	-2.77	0.189362	-0.38	0.188535	-0.00

Table 12

Test Case 2.  $\frac{E_{11\text{skin}}}{E_{11\text{core}}} \equiv FCSR = 7.3 \times 10^1$ . Comparison of various theories to evaluate the transverse displacements amplitude (center plate deflection)  $\hat{u}_z = u_z \frac{100E_{22\text{skin}}}{zP^t h \left(\frac{a}{h}\right)^4}$

in  $x = a/2$ ,  $y = b/2$ ,  $z = 0$ .

†In Reference [11] the percentage error *Err%* is calculated with respect to the *LM4* theory. In reference [11] it was not specified the formula used for the percentage error. Therefore, in this table the absolute value is used for the errors reported in reference [11]. The present error evaluations are calculated with respect to the present elasticity solution (see equation 11).

$a/h$	2		4		10		100	
	$\frac{E_{11\text{skin}}}{E_{11\text{core}}} \equiv FCSR = 7.3 \times 10^4$							
Elasticity	45.6531	<i>Err%</i>	15.4835	<i>Err%</i>	7.03601	<i>Err%</i>	5.44237	<i>Err%</i>
<i>LM4</i> [11]	<i>NA</i>	<i>NA</i>	15.483	-0.00	7.0360	-0.00	5.4424	+0.00
<i>ED4</i> [11]	<i>NA</i>	<i>NA</i>	<i>NA</i>	7.45  <sup>†</sup>	<i>NA</i>	3.70  <sup>†</sup>	<i>NA</i>	1.58  <sup>†</sup>
<i>EMZC3</i> [11]	<i>NA</i>	<i>NA</i>	<i>NA</i>	0.60  <sup>†</sup>	<i>NA</i>	4.06  <sup>†</sup>	<i>NA</i>	5.56  <sup>†</sup>
<i>LD1</i> [11]	<i>NA</i>	<i>NA</i>	<i>NA</i>	0.91  <sup>†</sup>	<i>NA</i>	0.23  <sup>†</sup>	<i>NA</i>	0.14  <sup>†</sup>
<i>LD4</i> [11]	<i>NA</i>	<i>NA</i>	<i>NA</i>	0.00  <sup>†</sup>	<i>NA</i>	0.00  <sup>†</sup>	<i>NA</i>	0.00  <sup>†</sup>
<i>EDZ</i> <sub>555</sub>	46.3445	+1.51	15.5229	+0.25	6.96904	-0.95	5.35853	-1.54
<i>LD</i> <sub>222</sub>	45.6580	+0.01	15.4824	-0.01	7.03572	-0.00	5.44237	-0.00
<i>LD</i> <sub>555</sub>	45.6531	-0.00	15.4835	+0.00	7.03601	+0.00	5.44237	-0.00
<i>VAPAS</i>	46.0669	+0.91	15.4066	-0.50	7.01576	-0.29	5.44215	-0.00

Table 13

Test Case 2.  $\frac{E_{11\text{skin}}}{E_{11\text{core}}} \equiv FCSR = 7.3 \times 10^4$ . Comparison of various theories to evaluate the transverse displacements amplitude (center plate deflection)  $\hat{u}_z = u_z \frac{100E_{22\text{skin}}}{zP^t h \left(\frac{a}{h}\right)^4}$

in  $x = a/2$ ,  $y = b/2$ ,  $z = 0$ .

†In Reference [11] the percentage error *Err%* is calculated with respect to the *LM4* theory. In reference [11] it was not specified the formula used for the percentage error. Therefore, in this table the absolute value is used for the errors reported in reference [11]. The present error evaluations are calculated with respect to the present elasticity solution (see equation 11).

$a/h$	2		4		10		100	
	$\frac{E_{11\text{skin}}}{E_{11\text{core}}} \equiv FCSR = 7.3 \times 10^6$							
Elasticity	1089.86	<i>Err%</i>	590.538	<i>Err%</i>	149.696	<i>Err%</i>	7.18809	<i>Err%</i>
<i>LM4</i> [11]	<i>NA</i>	<i>NA</i>	590.54	+0.00	149.70	+0.00	7.1881	+0.00
<i>ED4</i> [11]	<i>NA</i>	<i>NA</i>	<i>NA</i>	82.8  <sup>†</sup>	<i>NA</i>	85.2  <sup>†</sup>	<i>NA</i>	20.0  <sup>†</sup>
<i>EMZC3</i> [11]	<i>NA</i>	<i>NA</i>	<i>NA</i>	12.5  <sup>†</sup>	<i>NA</i>	3.22  <sup>†</sup>	<i>NA</i>	0.03  <sup>†</sup>
<i>LD1</i> [11]	<i>NA</i>	<i>NA</i>	<i>NA</i>	14.3  <sup>†</sup>	<i>NA</i>	3.93  <sup>†</sup>	<i>NA</i>	0.19  <sup>†</sup>
<i>LD4</i> [11]	<i>NA</i>	<i>NA</i>	<i>NA</i>	0.00  <sup>†</sup>	<i>NA</i>	0.00  <sup>†</sup>	<i>NA</i>	0.00  <sup>†</sup>
<i>EDZ</i> <sub>555</sub>	980.437	-10.04	581.360	-1.55	149.543	-0.10	7.19023	+0.03
<i>LD</i> <sub>222</sub>	1089.20	-0.06	590.446	-0.02	149.695	-0.00	7.18809	+0.00
<i>LD</i> <sub>555</sub>	1089.86	-0.00	590.538	-0.00	149.696	-0.00	7.18809	+0.00
<i>VAPAS</i>	4125.04	> 100%	1017.25	+72.26	166.073	+10.94	7.18898	+0.00

Table 14

Test Case 2.  $\frac{E_{11\text{skin}}}{E_{11\text{core}}} \equiv FCSR = 7.3 \times 10^6$ . Comparison of various theories to evaluate the transverse displacements amplitude (center plate deflection)  $\hat{u}_z = u_z \frac{100E_{22\text{skin}}}{zP^t h \left(\frac{a}{h}\right)^4}$

in  $x = a/2, y = b/2, z = 0$ .

†In Reference [11] the percentage error *Err%* is calculated with respect to the *LM4* theory. In reference [11] it was not specified the formula used for the percentage error. Therefore, in this table the absolute value is used for the errors reported in reference [11]. The present error evaluations are calculated with respect to the present elasticity solution (see equation 11).

$a/h$	2		4		10		100	
	$\frac{E_{11\text{skin}}}{E_{11\text{core}}} \equiv FCSR = 7.3 \times 10^8$							
Elasticity	1469.50	<i>Err%</i>	1370.58	<i>Err%</i>	1260.31	<i>Err%</i>	149.506	<i>Err%</i>
<i>LM4</i> [11]	<i>NA</i>	<i>NA</i>	1370.6		1260.3		149.51	
<i>ED4</i> [11]	<i>NA</i>	<i>NA</i>	<i>NA</i>	$ 91.8 ^\dagger$	<i>NA</i>	$ 98.1 ^\dagger$	<i>NA</i>	$ 96.1 ^\dagger$
<i>EMZC3</i> [11]	<i>NA</i>	<i>NA</i>	<i>NA</i>	$ 24.7 ^\dagger$	<i>NA</i>	$ 22.5 ^\dagger$	<i>NA</i>	$ 3.10 ^\dagger$
<i>LD1</i> [11]	<i>NA</i>	<i>NA</i>	<i>NA</i>	$ 27.4 ^\dagger$	<i>NA</i>	$ 25.2 ^\dagger$	<i>NA</i>	$ 3.82 ^\dagger$
<i>LD4</i> [11]	<i>NA</i>	<i>NA</i>	<i>NA</i>	$ 0.00 ^\dagger$	<i>NA</i>	$ 0.00 ^\dagger$	<i>NA</i>	$ 0.00 ^\dagger$
<i>EDZ</i> <sub>555</sub>	1283.34	-12.67	1323.09	-3.47	1251.11	-0.73	149.464	-0.03
<i>LD</i> <sub>222</sub>	1468.29	-0.08	1370.09	-0.04	1260.23	-0.01	149.507	+0.00
<i>LD</i> <sub>555</sub>	1469.50	-0.00	1370.58	-0.00	1260.31	+0.00	149.507	+0.00
<i>VAPAS</i>	412009	> 100%	101187	> 100%	16120.2	> 100%	166.591	+11.43

Table 15

Test Case 2.  $\frac{E_{11\text{skin}}}{E_{11\text{core}}} \equiv FCSR = 7.3 \times 10^8$ . Comparison of various theories to evaluate the transverse displacements amplitude (center plate deflection)  $\hat{u}_z = u_z \frac{100E_{22\text{skin}}}{zP^t h \left(\frac{a}{h}\right)^4}$

in  $x = a/2$ ,  $y = b/2$ ,  $z = 0$ .

†In Reference [11] the percentage error *Err%* is calculated with respect to the *LM4* theory. In reference [11] it was not specified the formula used for the percentage error. Therefore, in this table the absolute value is used for the errors reported in reference [11]. The present error evaluations are calculated with respect to the present elasticity solution (see equation 11).

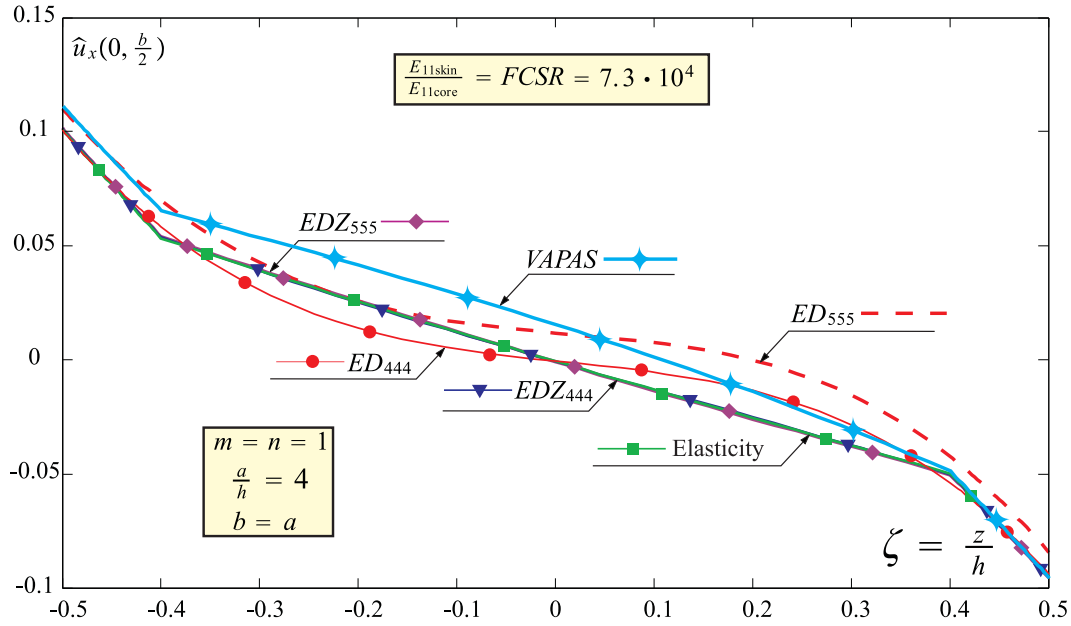


Fig. 8. Test Case 2. Dimension-less displacement  $\hat{u}_x = u_x \frac{E_{\text{skin}}}{z p t h (\frac{a}{h})^3}$ ;  $\frac{E_{11 \text{ skin}}}{E_{11 \text{ core}}} \equiv FCSR = 7.3 \times 10^4$ . Comparison between AHSDT, AHSDTZ, VAPAS, and the elasticity solution.

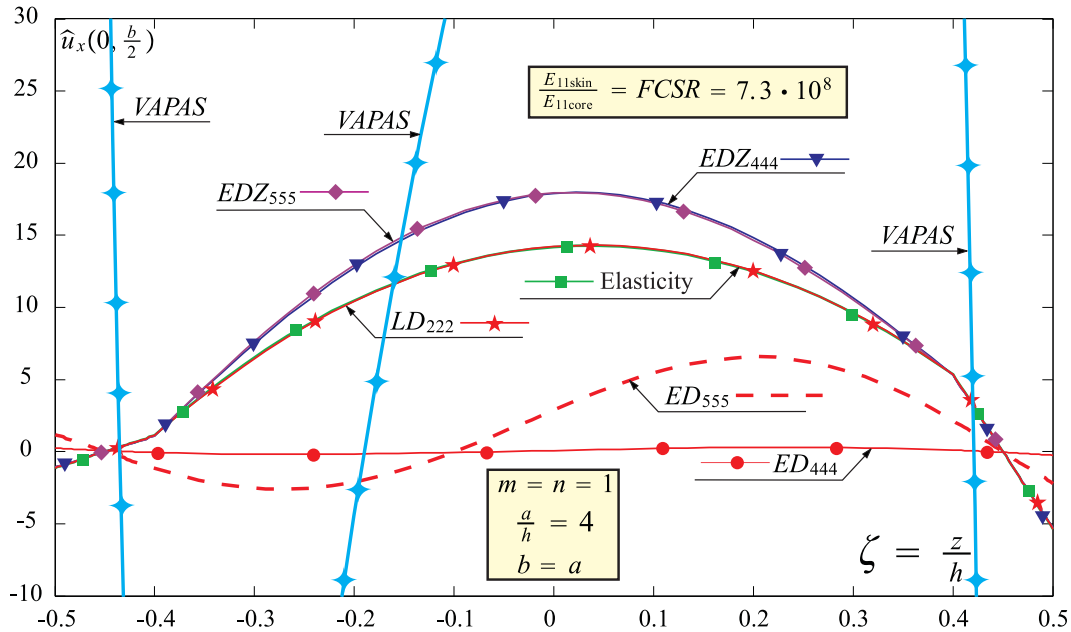


Fig. 9. Test Case 2. Dimension-less displacement  $\hat{u}_x = u_x \frac{E_{\text{skin}}}{z p t h (\frac{a}{h})^3}$ ;  $\frac{E_{11 \text{ skin}}}{E_{11 \text{ core}}} \equiv FCSR = 7.3 \times 10^8$ . Comparison between AHSDT, AHSDTZ, ALWT, VAPAS, and the elasticity solution.

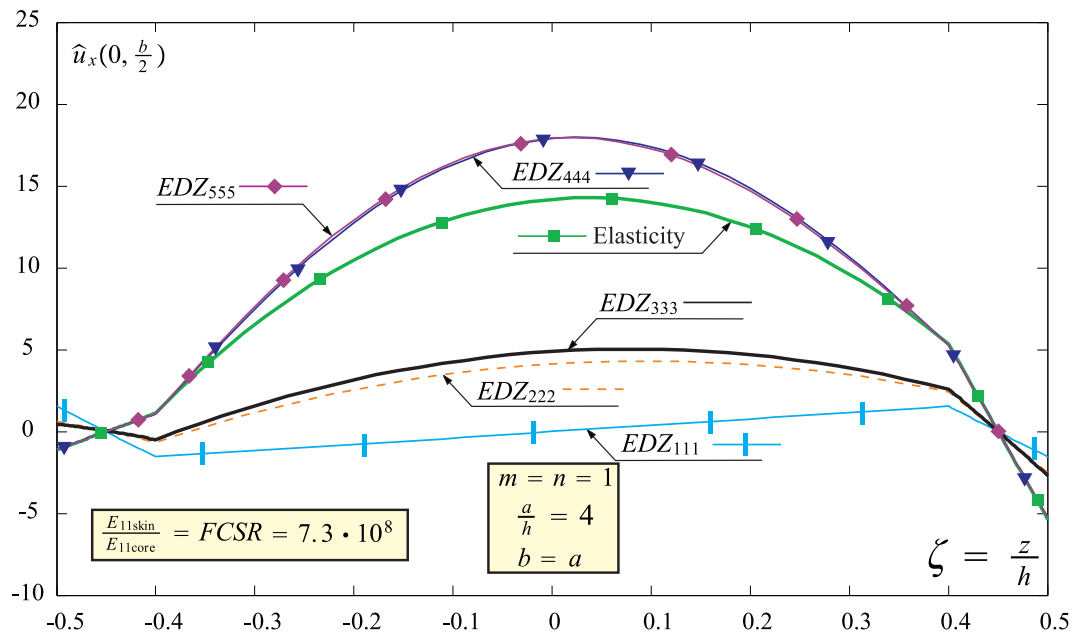


Fig. 10. Test Case 2. Dimension-less displacement  $\hat{u}_x = u_x \frac{E_{\text{skin}}}{z p^t h (\frac{a}{h})^3}$ ;  $\frac{E_{11\text{skin}}}{E_{11\text{core}}} \equiv FCSR = 7.3 \times 10^8$ . Comparison between various zig-zag theories AHSDTZ and the elasticity solution.

## 5 Conclusion

The accuracy of the Variational Asymptotic Plate and Shell Analysis (VAPAS) is assessed against several higher-order, zig-zag and layerwise theories generated by using the invariant axiomatic framework denoted as Generalized Unified Formulation (GUF). Both the axiomatic models generated by GUF and VAPAS are also compared against the elasticity solution developed for the case of a sandwich structure with high Face to Core Stiffness Ratio. It has been shown that the fact that GUF allows to use an infinite number of axiomatic theories (Equivalent Single Layer theories with or without zig-zag effects and Layerwise theories as well) with any combination of orders of the displacements provides an ideal tool to precisely assess the range of applicability of the Variational Asymptotic Plate and Shell Analysis or other theories in general. It is demonstrated that VAPAS achieves accuracy comparable to a fourth (or higher) order zig-zag theory or lower-order layerwise theories, while the plate model uses the least number degrees of freedom. Hence, in comparison to the axiomatic theories, VAPAS has achieved an excellent compromise between accuracy and efficiency. Except for extreme cases of thick sandwich with huge modulus contrast, VAPAS can be used as an effective alternative to avoid expensive 3D finite element analysis for design and analysis of composite laminated plates. This assessment also points out the need that material small parameter needs to be considered to generalize the VAPAS modeling approach to deal with realistic sandwich structures.

GUF can be implemented in a single FEM code and can generate a virtually infinite number of theories with accuracy that range from the low-order equivalent single-layer to the high-order layerwise theories and is the ideal tool for comparisons and assessments of different theories or for the creation of adaptive structural codes in optimization and probabilistic studies.

## Acknowledgements

The first author acknowledges the support by San Diego State University (University Grant Program).

The second author acknowledges the support by the Air Force Office of Scientific Research under Grant FA9550-08-1-0405. The program managers are Dr. Victor Giurgiutiu and Dr. David Stargel. The views and conclusions contained herein are those of the authors and should not be interpreted as necessarily representing the official policies or endorsement, either expressed or implied, of the funding agencies.

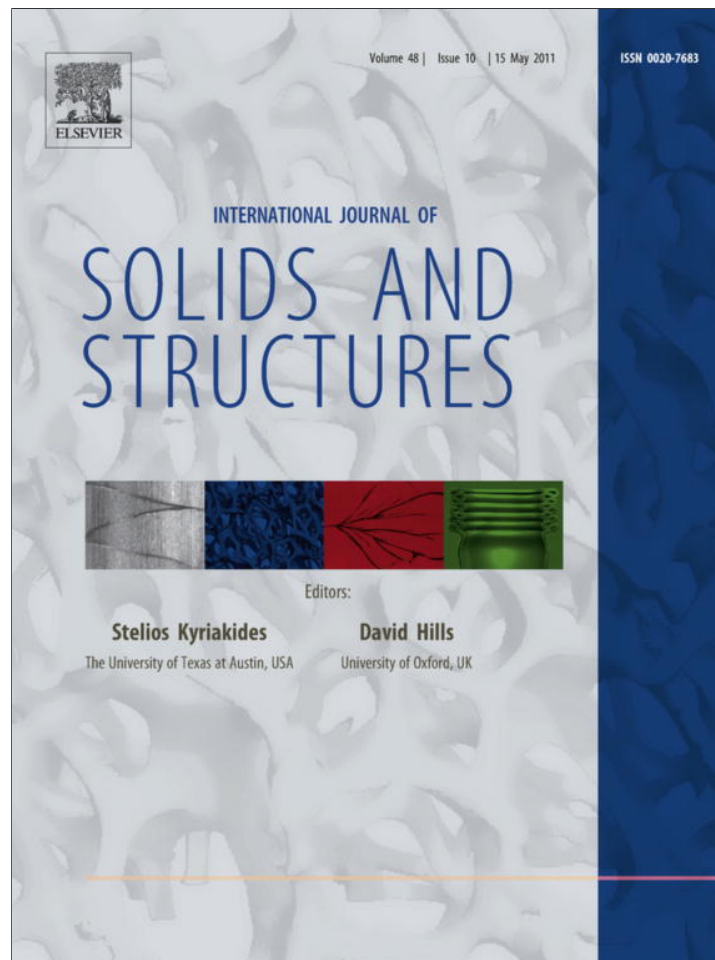
## References

- [1] S. A. Ambartsumian. Analysis of two-layer orthotropic shells. *vestiia Akad Nauk SSSR, Ot Tekh Nauk*, 7, 1957.
- [2] S. A. Ambartsumian. Two analysis method for two-layer orthotropic shells. *Izv An Arm SSR Seiya Fiz-Matem nauk*, X(2), 1957.
- [3] S. A. Ambartsumian. On a general theory of anisotropic shells. *Prikl. Mat. Mekh.*, 22(2):226–237, 1958.
- [4] S. A. Ambartsumian. On a theory of bending of anisotropic plates. *Investiia Akad Nauk SSSR, Ot Tekh Nauk*, 4, 1958.
- [5] V. L. Berdichevsky. Variational-asymptotic method of constructing a theory of shells. *PMM*, 43(4):664 – 687, 1979.
- [6] E. Carrera. Evaluation of layer-wise mixed theories for laminated plates analysis. *American Institute of Aeronautics and Astronautics Journal*, 26(5):830–839, 1998.
- [7] E. Carrera. Layer-wise mixed theories for accurate vibration analysis of multilayered plates. *Journal of Applied Mechanics*, 6(4):820–828, 1998.
- [8] E. Carrera. Mixed layer-wise models for multilayered plates analysis. *Composite Structures*, 43(1):57–70, 1998.
- [9] E. Carrera. Historical review of zig-zag theories for multilayered plates and shells. *App Mech Rev*, 56(3), 2003.
- [10] E. Carrera. Theories and finite elements for multilayered plates and shells: A unified compact formulation with numerical assessment and benchmarking. *Archives of Computational Methods in Engineering*, 10(3):215–296, 2003.
- [11] E. Carrera and S. Brischetto. A survey with numerical assessment of classical and refined theories for the analysis of sandwich plates. *Applied Mechanics Reviews*, 62, 2009.
- [12] KN Cho, CW Bert, and AG. Striz. Free vibrations of laminated rectangular plates analyzed by higher order individual-layer theory. *Journal of Sound and Vibration*, 145:429–442, 1991.
- [13] L. Demasi. Refined multilayered plate elements based on murakami zig-zag functions. *Composite Structures*, 70:308–16, 2005.
- [14] L. Demasi. 2D, quasi 3D and 3D exact solutions for bending of thick and thin sandwich plates. *Journal of Sandwich Structures & Materials*, 10(4):271–310, 2008.
- [15] L. Demasi. Invariant Finite Element Model for Composite Structures: the Generalized Unified Formulation. *AIAA Journal*, 48:1602–1619, 2010.
- [16] L. Demasi. Three-dimensional closed form solutions and  $\infty^3$  theories for orthotropic plates. *Mechanics of Advanced Materials and Structures*, 17:20–39, 2010.
- [17] M. E. Fares and M. Kh. Elmarghany. A refined zigzag nonlinear first-order shear deformation theory of composite laminated plates. *Composite Structures*, 2007. doi: 10.1016/j.compstruct.2006.12.007.
- [18] P. Gaudenzi, R. Barboni, and A. Mannini. A finite element evaluation of

- single-layer and multi-layer theories for the analysis of laminated plates. *Composite Structures*, 30:427–440, 1995.
- [19] D. H. Hodges, A. R. Atilgan, and D. A. Danielson. A geometrically nonlinear theory of elastic plates. *Journal of Applied Mechanics*, 60(1):109 – 116, March 1993.
- [20] T. Kant and K. Swaminathan. Free vibration of isotropic, orthotropic, and multilayer plates based on higher order refined theories. *Journal of Sound and Vibration*, 241(2):319–327, 2001.
- [21] G. Kirchhoff. Über das gleichgewicht und die bewegung einer elastischen schein. *J. Angew. Math.*, 40:51 – 88, 1850.
- [22] S. G. Lekhnitskii. Strength calculation of composite beams. *Vestnik inzhener i tekhnikov*, 9, 1935.
- [23] L. Librescu. Improved linear theory of elastic anisotropic multilayered shells. part i. *Polymer Mechanics (translated from Russian)*, 11(6), 1975.
- [24] L. Kärger, A. Wetzler, R. Rolfes, and K. Rohwer. A three-layered sandwich element with improved transverse shear stiffness and stress based on fsdt. *Computers and Structures*, 84(13-14):843 – 854, 2006.
- [25] R. Mindlin. Influence of rotatory inertia and shear in flexural motion of isotropic elastic plates. *Journal of Applied Mechanics*, 18:1031 – 1036, 1951.
- [26] H. Murakami. Laminated composite plate theory with improved in-plane response. *Journal of Applied Mechanics*, 53:661–666, 1986.
- [27] A. Nosier, RK Kapania, and J. N. Reddy. Free vibration analysis of laminated plates using a layer-wise theory. *AIAA Journal*, pages 2335–2346, 1993.
- [28] J. N. Reddy. An evaluation of equivalent single layer and layerwise theories of composite laminates. *Composite Structures*, 25:21–35, 1993.
- [29] J. N. Reddy. Mechanics of laminated composite plates, theory and analysis. (2nd edn), *CRC Press.: Boca Raton, London, New York, Washington, D. C.*, 2004.
- [30] E. Reissner. The effect of transverse shear deformation on the bending of elastic plates. *Journal of Applied Mechanics*, 12:69 – 76, 1945.
- [31] J. G. Ren. A new theory of laminated plates. *Compos. Sci. Technol.*, 26:225–239, 1986.
- [32] J.G. Ren. Bending theory of laminated plates. *Compos. Sci. Technol.*, 27:225–248, 1986.
- [33] D.H. Robbins and J. N. Reddy. Modelling of thick composites using a layerwise laminate theory. *International Journal for Numerical Methods in Engineering*, 36(4):655–677, 1993.
- [34] K. Swaminathan and S. S. Patil. Analytical solutions using higher order refined computational model with 12 degrees of freedom for the free vibration analysis of antisymmetric angle-ply plates. *Composite Structures*, 2007. doi: 10.1016/j.compstruct.2007.01.001.
- [35] M. Tahani. Analysis of laminated composite beams using layerwise displacement theories. *Composite Structures*, 79:535–547, 2007.

- [36] W. Yu. Mathematical construction of a reissner-mindlin plate theory for composite laminates. *International Journal of Solids and Structures*, 42:6680–6699, 2005.
- [37] W. Yu and D. H. Hodges. An asymptotic approach for thermoelastic analysis of laminated composite plates. *Journal of Engineering Mechanics*, 130(5):531 – 540, 2004.
- [38] W. Yu, D. H. Hodges, and V. V. Volovoi. Asymptotic construction of Reissner-like models for composite plates with accurate strain recovery. *International Journal of Solids and Structures*, 39(20):5185 – 5203, 2002.
- [39] W. Yu, D. H. Hodges, and V. V. Volovoi. Asymptotically accurate 3-D recovery from Reissner-like composite plate finite elements. *Computers and Structures*, 81(7):439 – 454, 2003.
- [40] Wu Zhen, Y. K. Cheung, S. H. Lo, and Chen Wanji. Effects of higher-order global-local shear deformations on bending, vibration and buckling of multilayered plates. *Composite Structures*, 2007. DOI: 10.1016/j.compstruct.2007.01.017.

Provided for non-commercial research and education use.  
Not for reproduction, distribution or commercial use.



This article appeared in a journal published by Elsevier. The attached copy is furnished to the author for internal non-commercial research and education use, including for instruction at the authors institution and sharing with colleagues.

Other uses, including reproduction and distribution, or selling or licensing copies, or posting to personal, institutional or third party websites are prohibited.

In most cases authors are permitted to post their version of the article (e.g. in Word or Tex form) to their personal website or institutional repository. Authors requiring further information regarding Elsevier's archiving and manuscript policies are encouraged to visit:

<http://www.elsevier.com/copyright>



Contents lists available at ScienceDirect

## International Journal of Solids and Structures

journal homepage: [www.elsevier.com/locate/ijsolstr](http://www.elsevier.com/locate/ijsolstr)

# Homogenization and dimensional reduction of composite plates with in-plane heterogeneity

Chang-Yong Lee, Wenbin Yu\*

Department of Mechanical and Aerospace Engineering, Utah State University, Logan, UT 80322-4130, USA

## ARTICLE INFO

## Article history:

Received 21 October 2010

Received in revised form 28 January 2011

Available online 18 February 2011

## Keywords:

Plate

Homogenization

Dimensional reduction

Variational asymptotic method

Heterogeneous plates

## ABSTRACT

The variational asymptotic method is used to construct a new model for composite plates which could have in-plane heterogeneity due to both geometry and material. We first formulate the original three-dimensional problem in an intrinsic form which is suitable for geometrically nonlinear analysis. Taking advantage of smallness of the plate thickness and heterogeneity, we use the variational asymptotic method to rigorously construct an effective plate model unifying a homogenization process and a dimensional reduction process. This approach is implemented in the computer code VAPAS using the finite element technique for the purpose of dealing with realistic heterogeneous plates. A few examples are used to demonstrate the capability of this new model.

© 2011 Elsevier Ltd. All rights reserved.

## 1. Introduction

Along with the rapidly increasing popularity of composite materials and structures, research on accurate and general modeling of structures made of them has remained as a very active field in the last several decades. Moreover the increased knowledge and fabrication techniques of them are possible to manufacture new materials and structures with optimized microstructures to achieve the ever-increasing performance requirements. Although it is logically sound to use the well-established finite element analysis (FEA) to analyze such materials and structures by meshing all the details of constituent microstructures, it is not a practical and efficient way, which requires an inordinate number of degrees of freedom (i.e., computing cost) to capture the micro-scale behavior.

Fortunately, most composite materials exhibit statistical homogeneity (Hashin, 1983) so that we can define a representative volume element (RVE), which is entirely typical of the whole mixture on average and contains a sufficient number of inclusions for the apparent overall properties to be effectively independent of the boundary conditions (Hill, 1963). Although different definitions are given for an RVE in the literature (Nemat-Nasser and Hori, 1993), we give a practice-oriented definition for an RVE as any block of material the analyst wants to use for the micromechanical analysis to find the effective properties and replace it with an equivalent homogeneous material. The term unit cell (UC) is also used extensively in the literature and defined as the building block of the heterogeneous material. In our work, we define UC as the

smallest RVE. In other words, one RVE could contain several UCs. These definitions essentially imply that it is the analyst's judgment to determine what should be contained in an RVE or UC. To be consistent with statistical homogeneity, a well-formulated micromechanics model should not depend on the size of an RVE, which means the effective properties obtained from an RVE containing multiple UCs should be the same as those obtained from a UC. In this sense, we consider the heterogeneous structure as a periodic assembly of many UCs.

If the size of UC ( $d$ ) is much smaller than the size of the structure ( $L$ ) (i.e.,  $\eta = d/L \ll 1$ ), it is possible to homogenize the heterogeneous UC with a set of effective material properties through a micromechanical analysis of the UC. With these effective properties, the analyst can replace the original heterogeneous structure with a homogeneous one and carry out structural analysis for global behavior. In the past several decades, numerous micromechanical approaches have been suggested in the literature, such as the self-consistent model (Hill, 1965; Dvorak and Bahei-El-Din, 1979; Accorsi and Nemat-Nasser, 1986), the variational approach (Hashin and Shtrikman, 1962; Milton, 2001), the method of cells (Aboudi, 1982, 1989; Paley and Aboudi, 1992; Williams, 2005), recursive cell method (Banerjee and Adams, 2004), mathematical homogenization theories (Bensoussan et al., 1978; Sanchez-Palencia, 1980; Murakami and Toledano, 1990), finite element approaches using conventional stress analysis of a representative volume element (Sun and Vaidya, 1996), variational asymptotic method for unit cell homogenization (VAMUCH) (Yu, 2005; Yu and Tang, 2007), and many others (see, e.g. Hollister and Kikuchi (1992), Kalamkarov et al. (2009), Kanouté et al. (2009) for a review).

\* Corresponding author. Tel.: +1 435 7978246; fax: +1 435 7972417.

E-mail address: [wenbin.yu@usu.edu](mailto:wenbin.yu@usu.edu) (W. Yu).

In real applications, many composite structures are dimensionally reducible structures (Yu, 2002) with one or two dimensions much smaller than others. For example, many load bearing components are flat panels with the thickness  $h$  much smaller than the in-plane dimensions (i.e.,  $e = h/L \ll 1$ ) and they can be effectively modeled using plate models. If there are still many unit cells along the thickness direction (i.e.,  $\eta \ll e$ ), we can use the traditional two-step approach that performs homogenization using micromechanics first to obtain effective properties of the heterogeneous material, then performs a dimensional reduction to construct a plate model for structural analysis. Usually, composite plates do not have many unit cells along the thickness direction. For example, for plates made of textiles, the textile microstructure might be as large as the plate thickness. That is, the periodicity is exhibited only in-plane and we have either  $e \ll \eta$  or  $e \sim \eta$ . As pointed out by Kohn and Vogelius (1984), if  $e \ll \eta$ , the order of the aforementioned two-step approach should be reversed. That is, we need to carry out the dimensional reduction to construct plate models first, then homogenize the heterogeneous surface with periodically varying plate properties. If  $e \sim \eta$ , the two steps in the two-step approach should be performed at the same time, that is, both small parameters ( $e$  and  $\eta$ ) should be considered during modeling of such structures. And several studies have shown that models considering  $e$  and  $\eta$  simultaneously also give accurate results for the case  $e \ll \eta$  (Lewiński, 1991; Buannic and Cartraud, 2001).

In recent years, the formal asymptotic method has been used to study this problem (Caillerie, 1984; Kohn and Vogelius, 1984; Lewiński, 1991; Kalamkarov, 1992; Kalamkarov and Kolpakov, 1997). It is a modification to the asymptotic homogenization method which is a direct application of the formalism of two scales to the original three-dimensional (3D) equations governing the plate structure. However, although these models are mathematically elegant and rigorous without introducing *ad hoc* assumptions, it is not easy to relate the equations derived using this method with simple engineering models and extend this approach to geometrical nonlinear problems. Sometimes, the displacement field predicted using this approach is not compatible with the stress field. For example, the displacement field in Eqs. (1.3.5) of Kalamkarov and Kolpakov (1997) implies zero transverse normal strain which further implies nonzero normal stress due to Poisson's effect, which is not compatible with the stress field given in Eq. (1.3.6) of Kalamkarov and Kolpakov (1997). Last but not least, it is difficult to implement these theories numerically.

As a remedy to the shortcomings of formal asymptotic method, we propose to use the variational asymptotic method (VAM) (Berdichevsky, 1979) to carry out simultaneous homogenization and dimensional reduction to construct a model suitable for plates

made of heterogeneous materials. First, the 3D anisotropic elasticity problem is formulated in an intrinsic form suitable for geometrically nonlinear analysis. Then, considering both  $e$  and  $\eta$ , we use VAM to rigorously decouple the original 3D anisotropic, heterogeneous problem into a nonlinear two-dimensional (2D) surface analysis (i.e., plate analysis) on the macroscopic level and a linear micromechanical analysis. The micromechanical analysis is implemented in the computer code VAPAS (Variational Asymptotic Plate and Shell analysis) using the finite element technique for numerically obtaining the effective plate constants for the 2D plate analysis and recovering the local displacement, strain, and stress fields based on the macroscopic behavior. Several examples are used to demonstrate the application and accuracy of this new model and the companion code VAPAS.

### 2. Three-dimensional formulation

A plate may be considered geometrically as a smooth 2D reference plane  $\omega$  surrounded by a layer of matter with thickness  $h$  to form a 3D body with one dimension much smaller than the other two. In general, a point in the plate can be represented mathematically by its Cartesian coordinates  $x_i$ , where  $x_\alpha$  are two orthogonal lines in the reference plane and  $x_3$  is the normal coordinates. (Here and throughout the paper, Greek indices assume values 1 and 2 while Latin indices assume 1, 2, and 3. Repeated indices are summed over their range except where explicitly indicated.) Without loss of generality, we choose the middle of the plate as the origin of  $x_3$ . Let us now consider an heterogeneous plate formed by many UCs ( $\Omega$ ) in the reference plane (see Fig. 1). To describe the rapid change in the material characteristics in the in-plane directions, we need to introduce two so-called 'fast' coordinates  $y_\alpha$  parallel to  $x_\alpha$ . These two sets of coordinates are related as  $y_\alpha = x_\alpha/\eta$ .

If the UC is a cuboid as depicted in Fig. 1, we can describe the domain ( $\Omega$ ) occupied by the UC using  $y_\alpha$  and  $x_3$  as

$$\Omega = \left\{ (y_1, y_2, x_3) \mid -\frac{d_1}{2} < y_1 < \frac{d_1}{2}, -\frac{d_2}{2} < y_2 < \frac{d_2}{2}, -\frac{h}{2} < x_3 < \frac{h}{2} \right\} \quad (1)$$

As our goal is to homogenize the heterogeneous material, we need to assume that the exact solution of the field variables have volume averages over  $\Omega$ . For example, if  $u_i(x_1, x_2, x_3; y_1, y_2)$  are the exact displacements within the UC, there exists  $v_i(x_1, x_2)$  such that

$$v_i = \frac{1}{\Omega} \int_{y_1} \int_{y_2} \int_{x_3} u_i dy_1 dy_2 dx_3 = \frac{1}{\Omega} \int_{\Omega} u_i d\Omega \equiv \langle u_i \rangle \quad (2)$$

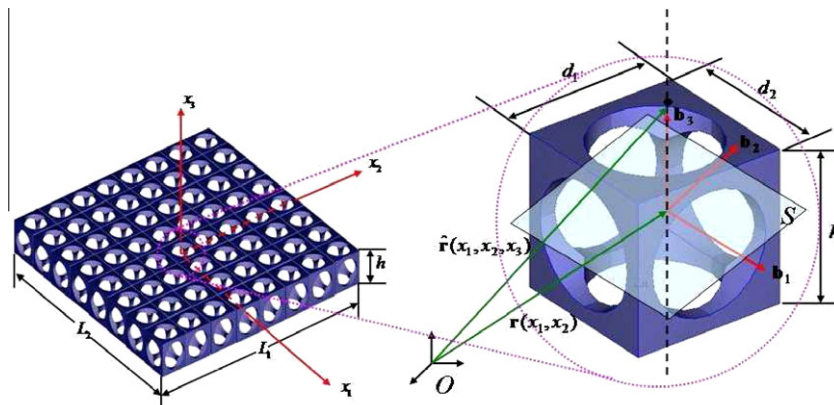


Fig. 1. A heterogeneous plate with representative periodicity cell.

Due to the existence of a distinct scale separation between two types of spatial variations described by  $y_\alpha$  and  $x_\alpha$ , the derivative of a function,  $u_i$ , defined in  $\Omega$  can be evaluated as

$$\frac{\partial u_i(x_1, x_2, x_3; y_1, y_2)}{\partial x_\alpha} = \frac{\partial u_i}{\partial x_\alpha} \Big|_{y_\alpha = \text{const}} + \frac{1}{\eta} \frac{\partial u_i}{\partial y_\alpha} \Big|_{x_i = \text{const}} \equiv u_{i,\alpha} + \frac{1}{\eta} u_{i|\alpha} \quad (3)$$

Note that in real calculation,  $\eta$  is not a number but denoting the order of the term it is associated with.

Letting  $\mathbf{b}_i$  denote a unit vector along  $x_i$  for the undeformed plate, one can then describe the position of any material point in the undeformed configuration by its position vector  $\hat{\mathbf{r}}$  relative to a point  $O$  fixed in an inertial frame, such that

$$\hat{\mathbf{r}}(x_1, x_2, x_3) = \mathbf{r}(x_1, x_2) + x_3 \mathbf{b}_3 \quad (4)$$

where  $\mathbf{r}$  is the position vector from  $O$  to the point located by  $x_\alpha$  on the reference plane.

When the plate deforms, the particle that had position vector  $\hat{\mathbf{r}}$  in the undeformed state now has position vector  $\hat{\mathbf{R}}$  in the deformed configuration. The latter can be uniquely determined by the deformation of the 3D body. To this end, we need to introduce a new triad  $\mathbf{B}_i$  for the deformed plate as unit vectors to express vectors and tensors in their component form during the derivation. The relation between  $\mathbf{B}_i$  and  $\mathbf{b}_i$  can be specified by an arbitrary large rotation in terms of the matrix of direction cosines  $C(x_1, x_2)$  so that

$$\mathbf{B}_i = C_{ij} \mathbf{b}_j \quad \text{with} \quad C_{ij} = \mathbf{B}_i \cdot \mathbf{b}_j \quad (5)$$

subject to the requirement that  $\mathbf{B}_i$  is coincident with  $\mathbf{b}_i$  when the structure is undeformed. Following Hodges et al. (1993) and Yu et al. (2002), the position vector  $\hat{\mathbf{R}}$  can be represented as

$$\hat{\mathbf{R}}(x_i; y_\alpha) = \mathbf{R}(x_1, x_2) + x_3 \mathbf{B}_3(x_1, x_2) + w_i(x_1, x_2, x_3; y_1, y_2) \mathbf{B}_i(x_1, x_2) \quad (6)$$

where  $\mathbf{R}$  denotes the position vector describing the deformed reference surface and  $w_i$  denotes the warping functions describing the deformation not captured by  $\mathbf{R}$  and  $\mathbf{B}_i$ . Because of the way we introduce 'fast' coordinates,  $w_i$  are periodic functions in  $y_\alpha$ , that is

$$\begin{aligned} w_i(x_1, x_2, x_3; d_1/2, y_2) &= w_i(x_1, x_2, x_3; -d_1/2, y_2) \\ w_i(x_1, x_2, x_3; y_1, d_2/2) &= w_i(x_1, x_2, x_3; y_1, -d_2/2) \end{aligned} \quad (7)$$

Eq. (6) can be considered as a change of variable and six constraints are needed to ensure a one-to-one mapping between  $\hat{\mathbf{R}}$  and  $(\mathbf{R}, \mathbf{B}_i, w_i)$ . If we define  $\mathbf{R} = \langle \hat{\mathbf{R}} \rangle$ , then we have the following three constraints

$$\langle w_i \rangle = 0 \quad (8)$$

The other three constraints can be obtained by a proper definition of  $\mathbf{B}_i$ . Two constraints can be specified by defining  $\mathbf{B}_3$  as the normal to the reference surface of the deformed plate. The last constraint can be specified by the rotation of  $\mathbf{B}_\alpha$  around  $\mathbf{B}_3$  such that

$$\mathbf{B}_1 \cdot \frac{\partial \mathbf{R}}{\partial x_2} = \mathbf{B}_2 \cdot \frac{\partial \mathbf{R}}{\partial x_1} \quad (9)$$

Following Atilgan and Hodges (1992), the plate strains can be defined using  $\mathbf{R}$  and  $\mathbf{B}_i$  as

$$\frac{\partial \mathbf{R}}{\partial x_\alpha} = \mathbf{B}_\alpha + \varepsilon_{\alpha\beta} \mathbf{B}_\beta \quad (10)$$

and

$$\frac{\partial \mathbf{B}_i}{\partial x_\alpha} = (-\kappa_{\alpha\beta} \mathbf{B}_\beta \times \mathbf{B}_3 + \kappa_{\alpha 3} \mathbf{B}_3) \times \mathbf{B}_i \quad (11)$$

It can be shown that the last constraint in Eq. (9) actually implies that symmetry of in-plane strains ( $\varepsilon_{\alpha\beta} = \varepsilon_{\beta\alpha}$ ).

Based on the concept of decomposition of rotation tensor (Danielson and Hodges, 1987), the Jauman–Biot–Cauchy strain components for small local rotation are given by

$$\Gamma_{ij} = \frac{1}{2} (F_{ij} + F_{ji}) - \delta_{ij} \quad (12)$$

where  $\delta_{ij}$  is the Kronecker symbol, and  $F_{ij}$  the mixed-basis component of the deformation gradient tensor such that

$$F_{ij} = \mathbf{B}_i \cdot \mathbf{G}_k \mathbf{g}^k \cdot \mathbf{b}_j \quad (13)$$

Here  $\mathbf{g}^i$  are the contravariant base vector of the undeformed configuration and in a plate case,  $\mathbf{g}^i = \mathbf{g}_i = \mathbf{b}_i$ , while  $\mathbf{G}_i$  are the 3D covariant basis vectors of the deformed configuration, which can be obtained in the following way:

$$\mathbf{G}_\alpha = \frac{\partial \hat{\mathbf{R}}}{\partial x_\alpha} = \hat{\mathbf{R}}_{,\alpha} + \frac{1}{\eta} \hat{\mathbf{R}}_{|\alpha} \quad (14)$$

$$\mathbf{G}_3 = \frac{\partial \hat{\mathbf{R}}}{\partial x_3} \equiv \hat{\mathbf{R}}_{|3}$$

With the assumption that the plate strains are small compared to unity which is sufficient for geometrical nonlinear analysis, we can neglect all the terms that are products of the warping and the generalized strains and obtain the 3D strain field as

$$\begin{aligned} \Gamma_{11} &= \varepsilon_{11} + x_3 \kappa_{11} + w_{1,1} + \frac{1}{\eta} w_{1|1} \\ 2\Gamma_{12} &= 2\varepsilon_{12} + x_3 (\kappa_{12} + \kappa_{21}) + w_{1,2} + w_{2,1} + \frac{1}{\eta} (w_{1|2} + w_{2|1}) \\ \Gamma_{22} &= \varepsilon_{22} + x_3 \kappa_{22} + w_{2,2} + \frac{1}{\eta} w_{2|2} \\ 2\Gamma_{13} &= w_{1,3} + w_{3,1} + \frac{1}{\eta} w_{3|1} \\ 2\Gamma_{23} &= w_{2,3} + w_{3,2} + \frac{1}{\eta} w_{3|2} \\ \Gamma_{33} &= w_{3,3} \end{aligned} \quad (15)$$

The strain energy stored in the heterogeneous plates can be obtained as:

$$U = \int_{x_1} \int_{x_2} \langle \Gamma^T D \Gamma \rangle dx_1 dx_2 = \int_{\omega} \langle \Gamma^T D \Gamma \rangle d\omega \quad (16)$$

where  $\Gamma = [\Gamma_{11} 2\Gamma_{12} \Gamma_{22} 2\Gamma_{13} 2\Gamma_{23} \Gamma_{33}]^T$  and  $D(x_3; y_1, y_2)$  is the 3D  $6 \times 6$  material matrix, which consists of elements of the fourth-order elasticity tensor expressed in the local in-plane coordinate system  $y_\alpha$  and the thickness coordinate system  $x_3$ .

To deal with the applied loads, we follow Yu et al. (2002). At first, we will leave open the existence of a potential energy and alternatively develop the virtual work of the applied loads. The virtual displacement is taken as the Lagrangian variation of the displacement field, such that

$$\delta \hat{\mathbf{R}} = \overline{\delta q}_{B_i} \mathbf{B}_i + x_3 \overline{\delta \psi}_{B_i} \mathbf{B}_i \times \mathbf{B}_3 + \delta w_i \mathbf{B}_i + \overline{\delta \psi}_{B_i} \mathbf{B}_i \times w_j \mathbf{B}_j \quad (17)$$

where the virtual displacement of the reference surface is given by

$$\overline{\delta q}_{B_i} = \delta \mathbf{u} \cdot \mathbf{B}_i \quad (18)$$

and the virtual rotation of the reference surface is defined such that

$$\delta \mathbf{B}_i = \overline{\delta \psi}_{B_j} \mathbf{B}_j \times \mathbf{B}_i \quad (19)$$

Because of small strain assumption, we may safely ignore products of the warping and the loading in the virtual rotation term. Then, the work done through a virtual displacement due to the applied loads  $\tau_i \mathbf{B}_i$  at the top surface ( $S^+$ ) and  $\beta_i \mathbf{B}_i$  at the bottom surface ( $S^-$ ) and body force  $\phi_i \mathbf{B}_i$  is

$$\begin{aligned} \overline{\delta W} = & (\bar{\tau}_i + \bar{\beta}_i + \langle \phi_i \rangle) \overline{\delta q_{B_i}} + \overline{\delta \psi_{B_x}} \left[ \frac{h}{2} (\bar{\tau}_x - \bar{\beta}_x) + \langle \chi_3 \phi_x \rangle \right] \\ & + \delta(\bar{\tau}_i w_i^+ + \bar{\beta}_i w_i^- + \langle \phi_i w_i \rangle) \end{aligned} \quad (20)$$

with

$$\bar{\tau} = \frac{1}{S^+} \int_{S^+} \tau_i dS^+ \quad \text{and} \quad \bar{\beta}_i = \frac{1}{S^-} \int_{S^-} \beta_i dS^-$$

Eq. (20) can also be written in a matrix form as:

$$\overline{\delta W} = \overline{\delta q^T} f + \overline{\delta \psi^T} m + \delta(\bar{\tau}^T w^+ + \bar{\beta}^T w^- + \langle \phi^T w \rangle) \quad (21)$$

with

$$\begin{aligned} f &= \bar{\tau} + \bar{\beta} + \langle \phi \rangle \\ m &= \begin{Bmatrix} \frac{h}{2} (\bar{\tau}_1 - \bar{\beta}_1) + \langle \chi_3 \phi_1 \rangle \\ \frac{h}{2} (\bar{\tau}_2 - \bar{\beta}_2) + \langle \chi_3 \phi_2 \rangle \\ 0 \end{Bmatrix} \end{aligned} \quad (22)$$

where  $\tau_i$ ,  $\beta_i$ , and  $\phi_i$  are taken to be independent of the deformation and  $(\cdot)^+ = (\cdot)|_{x_3=h/2}$  and  $(\cdot)^- = (\cdot)|_{x_3=-h/2}$ .

Now, the complete statement of the problem can be presented in terms of the principle of virtual work, such that

$$\delta U - \overline{\delta W} = 0 \quad (23)$$

In spite of the possibility of accounting for nonconservative forces in Eq. (23), the problem that governs the 3D unknown warping functions is conservative. Thus, one can pose the problem that governs the warping as the minimization of a total potential functional

$$\Pi = U + W \quad (24)$$

so that

$$\delta \Pi = 0 \quad (25)$$

in which only the warping displacement is varied, subject to the constraints in Eqs. (7) and (8). This implies that the potential of the applied loads for this portion of the problem is given by

$$W = -\bar{\tau}^T w^+ - \bar{\beta}^T w^- - \langle \phi^T w \rangle \quad (26)$$

Below, for simplicity of terminology, we will refer to  $\Pi$  as the total potential energy, or the total energy.

By principle of minimum total potential energy, one can solve the unknown warping functions by minimizing the functional in Eq. (24) subject to the constraints of Eq. (8) and periodic boundary conditions Eq. (7). Up to this point, this is simply an alternative formulation of the original 3D elasticity problem. If we attempt to solve this problem directly, we will meet the same or even more difficulty as solving any full 3D nonlinear elasticity problem. Fortunately, as shown in Yu et al. (2002), Yu (2005), Yu and Tang (2007), VAM can be used to calculate the 3D unknown functions asymptotically.

### 3. Effective plate model

To rigorously reduce the original 3D problem to a 2D plate model, one must attempt to reproduce the energy stored in the 3D structure in a 2D formulation. The best one can do is to accomplish it asymptotically taking advantage of the small parameters inherent in the structure. As pointed out previously we have two small parameters in our problem:  $e$  denoting the smallness of the thickness and  $\eta$  denoting the smallness of heterogeneity. Following Lewiński (1991) and Buannic and Cartraud (2001), we also assume that two small parameters are of the same order as models constructed based on this assumptions also give accurate results when  $e \ll \eta$ .

In this paper, VAM will be used to mathematically reduce the 3D problem to a 2D plate model. To proceed by this method, first one has to assess and keep track of the orders of all the quantities in the formulation. Following Sutyryn (1997), the quantities of interest have the following orders:

$$\varepsilon_{\alpha\beta} \sim h \kappa_{\alpha\beta} \sim \hat{\varepsilon} \quad f_3 \sim \mu(h/L)^2 \hat{\varepsilon} \quad f_x \sim \mu(h/L) \hat{\varepsilon} \quad m_x \sim \mu h(h/L) \hat{\varepsilon} \quad (27)$$

where  $\hat{\varepsilon}$  is the order of the plate strains and  $\mu$  is the order of the material constants (all of which are assumed to be of the same order).

According to the order analysis in Eq. (27), the applied loads are of higher order, and the work done by the external forces is negligible in the zeroth-order approximation of energy. Thus, the total potential functional can be expressed as:

$$\delta \Pi = 0 \quad \text{with} \quad \delta U = 0 \quad (28)$$

The VAM requires one to find the leading terms of the functional according to the different orders. For the zeroth-order approximation, the corresponding 3D strain field can be expressed in the following matrix in view of Eq. (15)

$$\Gamma = \Gamma_h w + \Gamma_\varepsilon \varepsilon \quad (29)$$

where  $w = [w_1 \ w_2 \ w_3]^T$ ,  $\varepsilon = [\varepsilon_{11} \ 2\varepsilon_{12} \ \varepsilon_{22} \ \kappa_{11} \ \kappa_{12} + \kappa_{21} \ \kappa_{22}]^T$ , and

$$\Gamma_h = \begin{bmatrix} \frac{\partial}{\partial y_1} & 0 & 0 \\ \frac{\partial}{\partial y_2} & \frac{\partial}{\partial y_1} & 0 \\ 0 & \frac{\partial}{\partial y_2} & 0 \\ \frac{\partial}{\partial x_3} & 0 & \frac{\partial}{\partial y_1} \\ 0 & \frac{\partial}{\partial x_3} & \frac{\partial}{\partial y_2} \\ 0 & 0 & \frac{\partial}{\partial x_3} \end{bmatrix} \quad \Gamma_\varepsilon = \begin{bmatrix} 1 & 0 & 0 & x_3 & 0 & 0 \\ 0 & 1 & 0 & 0 & x_3 & 0 \\ 0 & 0 & 1 & 0 & 0 & x_3 \\ 0 & 0 & 0 & 0 & 0 & 0 \\ 0 & 0 & 0 & 0 & 0 & 0 \\ 0 & 0 & 0 & 0 & 0 & 0 \end{bmatrix} \quad (30)$$

For general cases we need to turn to numerical techniques such as FEM for approximate solutions. To this end, we need to express  $w$  using shape functions defined over  $\Omega$  as

$$w(x_1, x_2, x_3; y_1, y_2) = S(y_1, y_2, x_3) V(x_1, x_2) \quad (31)$$

where  $S$  represents the shape functions and  $V$  a column matrix of the nodal values of the warping functions.

Substituting Eq. (31) into Eq. (29) then into Eq. (28), we obtain the leading terms for the zeroth-order approximation in the following discretized form as

$$\Pi_\Omega = \frac{1}{2\Omega} (V^T E V + 2V^T D_{he} \varepsilon + \varepsilon^T D_{ee} \varepsilon) \quad (32)$$

where

$$\begin{aligned} E &= \int_\Omega (\Gamma_h S)^T D (\Gamma_h S) d\Omega \quad D_{he} = \int_\Omega (\Gamma_h S)^T D \Gamma_\varepsilon d\Omega \\ D_{ee} &= \int_\Omega \Gamma_\varepsilon^T D \Gamma_\varepsilon d\Omega \end{aligned} \quad (33)$$

The periodic constraints in Eq. (7) and the average constraints in Eq. (8) can be easily handled as normally done in FEM through assembly for obtaining the functional in Eq. (32). Minimizing  $\Pi_\Omega$  in Eq. (32), gives us the following linear system

$$E V = -D_{he} \varepsilon \quad (34)$$

It is clear that  $V$  will linearly depend on the 2D plate strains  $\varepsilon$ , which means it is unnecessary to assign values to  $\varepsilon$  (even 1's and 0's as in common practice), and they can be treated as symbols without entering the computation. The solution can be symbolically written as

$$V = V_0 \varepsilon \quad (35)$$

Substituting Eq. (35) back into Eq. (32), we can calculate the energy functional storing in the UC, asymptotically correct through the order of  $\mu\hat{\varepsilon}^2$  as

$$\Pi_\Omega = \frac{1}{2\Omega} \varepsilon^T (V_0^T D_{hc} + D_{ec}) \varepsilon \equiv \frac{1}{2} \varepsilon^T \bar{D} \varepsilon \quad (36)$$

$\bar{D}$  is the effective plate stiffness to be used for the classical plate theory (CPT). However, unlike the standard procedure of CPT, the effective plate stiffness are calculated from knowledge of complex geometric and material characteristics in a representative UC at the microscopic level considering the smallness of both thickness and heterogeneity. This microstructurally informed  $\bar{D}$  can be used in CPT to predict the global structural behavior. If the local fields within the UC are of interest, we can recover those fields based on the 2D global displacements  $u_{2d}$ , 2D global strains  $\varepsilon$ , and the 3D local warping functions  $w_i$ .

From Eqs. (4) and (6), we can obtain the 3D displacement field as:

$$\mathbf{U}_{3d} = \hat{\mathbf{R}} - \hat{\mathbf{r}} = \mathbf{R} - \mathbf{r} + x_3(\mathbf{B}_3 - \mathbf{b}_3) + w_i \mathbf{B}_i \quad (37)$$

which can also be expressed in the following matrix form as

$$U_{3d} = u_{2d} + x_3 \begin{bmatrix} C_{31} \\ C_{32} \\ C_{33} - 1 \end{bmatrix} + C^T S V_0 \varepsilon \quad (38)$$

where  $U_{3d}$  is the column matrix containing 3D displacement components in the  $\mathbf{b}_i$  basis and  $u_{2d}$  is the column matrix containing the 2D plate displacements in the  $\mathbf{b}_i$  basis.  $C$  is the direction-cosine matrix relating  $\mathbf{B}_i$  and  $\mathbf{b}_i$ , given in Eq. (5).

From Eq. (29), one can recover the 3D local strain field  $\Gamma$  through the zeroth order as

$$\Gamma = \Gamma_\varepsilon \varepsilon + \Gamma_h S V_0 \varepsilon \quad (39)$$

Finally, the local 3D stress field  $\sigma$  can be recovered straightforwardly using the original 3D constitutive relations as

$$\sigma = D \Gamma \quad (40)$$

We just derived the model for heterogeneous plates with the UC periodically varying along both  $x_1$  and  $x_2$ . It is easy to deduce that it is also applicable to degenerated cases such as the UC is only periodically varying along one direction. For example if it is periodic along  $x_1$ , then the partial derivative with respect to  $y_1$  vanishes in  $\Gamma_h$  operator of Eq. (29). That is, we only need to solve a 2D problem in  $y_2$  and  $x_3$ . If the plate is uniform in plane, then the partial derivatives with respect to  $y_1$  and  $y_2$  both vanish and the theory reduces to a 1D through-the-thickness as that of the classical plate theory derived using VAM as in Yu et al. (2002). The present theory is implemented in the computer code VAPAS (Variational Asymptotic

Plate and Shell Analysis). In the following section, we are going to use a few examples to assess the validity of the present theory and the companion code VAPAS.

#### 4. Validation examples

First, we investigate plates made of binary composites. The effective plate stiffness obtained by the present theory is compared to that obtained from conventional two-step approach. Second, heterogeneous plates having more complex UCs with different geometric and material characteristics at the microscopic level are used to demonstrate the accuracies and capabilities of the new theory and the differences between the conventional two-step approach and the present approach.

##### 4.1. Plates made of binary composites

First, let us consider a plate made of  $N$  binary composites each of which is formed by two different orthotropic layers with the material axes the same as the global coordinates  $x_i$ . Overall, there are  $2N$  layers in the plate. The material is uniform in the  $x_\alpha$  plane and varies along  $x_3$  direction. Let  $\varphi_1$  and  $\varphi_2$  denote the volume fractions of the bottom layer and top layer, respectively, and we have  $\varphi_1 + \varphi_2 = 1$ . The plate structure can be considered periodic along  $x_1$  and/or  $x_2$  directions. Using the present theory, we can model it using three approaches: (1) as a one-dimensional (1D) UC with no periodicity; (2) as a 2D UC with periodicity either in  $x_1$  or  $x_2$ ; (3) as a 3D unit cell with periodicity in both  $x_1$  and  $x_2$ . Each UC will have  $N$  binary composites along the thickness. We have verified that all these three modeling approaches yield the same effective plate stiffness which can be written in the following matrix form:

$$\bar{D} = \begin{bmatrix} \bar{d}_{11} & 0 & \bar{d}_{13} & \bar{d}_{14} & 0 & \bar{d}_{16} \\ 0 & \bar{d}_{22} & 0 & 0 & \bar{d}_{25} & 0 \\ \bar{d}_{13} & 0 & \bar{d}_{33} & \bar{d}_{16} & 0 & \bar{d}_{36} \\ \bar{d}_{14} & 0 & \bar{d}_{16} & \bar{d}_{44} & 0 & \bar{d}_{46} \\ 0 & \bar{d}_{25} & 0 & 0 & \bar{d}_{55} & 0 \\ \bar{d}_{16} & 0 & \bar{d}_{36} & \bar{d}_{46} & 0 & \bar{d}_{66} \end{bmatrix} \quad (41)$$

Particularly, modeling it as a 1D UC with no periodicity can be carried out analytically and the result is the same as classical plate model derived using VAM considering the plate is made of  $2N$  layers (Yu et al., 2002).

To analyze this structure using the two-step approach (TSA), the analyst needs to first homogenize the binary composites to obtain effective 3D material properties which can be expressed in the following matrix

**Table 1**  
Effective plate constants of unidirectional composite plates predicted by different methods.

	SAM	FEM	TSA	VAPAS
$\bar{d}_{11}$	0.443	0.452	0.444	0.443
$\bar{d}_{13}$	0.074	0.062	0.039	0.035
$\bar{d}_{22}$	0.040	0.114	0.045	0.047
$\bar{d}_{33}$	0.261	0.285	0.151	0.145
$\bar{d}_{44}$	2.308	2.256	3.702	2.246
$\bar{d}_{46}$	0.446	0.224	0.328	0.176
$\bar{d}_{55}$	0.195	0.568	0.371	0.547
$\bar{d}_{66}$	1.799	0.873	1.262	0.653

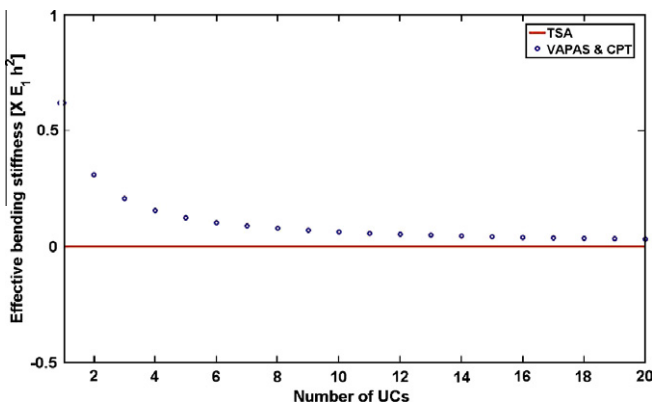


**Fig. 2.** Effective bending stiffness versus number of UCs.

$$\bar{D}^{3D} = \begin{bmatrix} \bar{c}_{11} & 0 & \bar{c}_{13} & 0 & 0 & \bar{c}_{16} \\ 0 & \bar{c}_{22} & 0 & 0 & 0 & 0 \\ \bar{c}_{13} & 0 & \bar{c}_{33} & 0 & 0 & \bar{c}_{36} \\ 0 & 0 & 0 & \bar{c}_{44} & 0 & 0 \\ 0 & 0 & 0 & 0 & \bar{c}_{55} & 0 \\ \bar{c}_{16} & 0 & \bar{c}_{36} & 0 & 0 & \bar{c}_{66} \end{bmatrix} \quad (42)$$

Here for the sake of saving space, the expressions for  $\bar{c}_{ij}$  are not listed here. Interested users can refer to Yu (2005) for analytical expressions of all the terms in Eq. (42) with a rearrangement to be consistent with the ordering of 3D strains used in this paper. Then, the analyst needs to carry out a dimensional reduction to obtain the classical plate model, of which the corresponding stiffness terms based on Eq. (42) are

$$\begin{aligned} \bar{d}_{11} &= \langle c_{11}^* \rangle_{x_3} & \bar{d}_{13} &= \langle c_{13}^* \rangle_{x_3} & \bar{d}_{22} &= \langle \bar{c}_{22} \rangle_{x_3} & \bar{d}_{33} &= \langle c_{33}^* \rangle_{x_3} \\ \bar{d}_{14} &= \langle x_3 c_{11}^* \rangle_{x_3} & \bar{d}_{16} &= \langle x_3 c_{13}^* \rangle_{x_3} & \bar{d}_{25} &= \langle x_3 \bar{c}_{22} \rangle_{x_3} & \bar{d}_{36} &= \langle x_3 c_{33}^* \rangle_{x_3} \\ \bar{d}_{44} &= \langle x_3^2 c_{11}^* \rangle_{x_3} & \bar{d}_{46} &= \langle x_3^2 c_{13}^* \rangle_{x_3} & \bar{d}_{55} &= \langle x_3^2 \bar{c}_{22} \rangle_{x_3} & \bar{d}_{66} &= \langle x_3^2 c_{33}^* \rangle_{x_3} \end{aligned} \quad (43)$$

with  $\langle a \rangle_{x_3} = \int_{-h/2}^{h/2} a dx_3$  and

$$c_{11}^* = \bar{c}_{11} - \frac{\bar{c}_{16}^2}{\bar{c}_{66}} \quad c_{13}^* = \bar{c}_{13} - \frac{\bar{c}_{16}\bar{c}_{36}}{\bar{c}_{66}} \quad c_{33}^* = \bar{c}_{33} - \frac{\bar{c}_{36}^2}{\bar{c}_{66}}$$

We can prove that the present theory and TSA predict the same extensional stiffness,  $\bar{D}_{ij} (i = 1, 2, 3, j = 1, 2, 3)$  (A matrix in CPT). The present theory will predict different coupling stiffness  $\bar{D}_{ij} (i = 1, 2, 3, j = 4, 5, 6)$  (B matrix in CPT) as the coupling stiffness according to TSA always remains zero. The coupling stiffness B predicted by the present theory is:

$$B = \frac{h^2}{2N} \varphi_1 \varphi_2 D^* \quad (44)$$

with

$$D^* = \begin{bmatrix} \hat{c}_{11}^{(2)} - \hat{c}_{11}^{(1)} & 0 & \hat{c}_{13}^{(2)} - \hat{c}_{13}^{(1)} \\ 0 & \hat{c}_{22}^{(2)} - \hat{c}_{22}^{(1)} & 0 \\ \hat{c}_{13}^{(2)} - \hat{c}_{13}^{(1)} & 0 & \hat{c}_{33}^{(2)} - \hat{c}_{33}^{(1)} \end{bmatrix}$$

where the subscripts denote which layer the value evaluated for. For example  $\hat{c}_{11}^{(2)}$  denotes  $\hat{c}_{11}$  evaluated for the top layer of the binary composite. The hatted quantities are calculated as

$$\hat{c}_{11} = c_{11} - \frac{c_{16}^2}{c_{66}} \quad \hat{c}_{13} = c_{13} - \frac{c_{16}c_{36}}{c_{66}} \quad \hat{c}_{33} = c_{33} - \frac{c_{36}^2}{c_{66}} \quad (45)$$

where  $c_{ij}$  are the stiffness components of the stiffness matrix arranged from the fourth-order elasticity for each constituent material of the binary composite. Only if these hatted quantities are the same for both layers, the coupling stiffness B in Eq. (44) predicted by the present theory will vanish as that predicted by TSA.

The present theory will also predict different bending stiffness  $\bar{D}_{ij} (i = 4, 5, 6, j = 4, 5, 6)$  (D matrix in CPT). If we use D and  $D_{TSA}$  to denote the bending stiffness predicted by the present theory and TSA, respectively, we have

$$D - D_{TSA} = \frac{h^3}{6N^2} \varphi_1 \varphi_2 (\varphi_1 - \varphi_2) D^* \quad (46)$$

If the hatted quantities in Eq. (45) are the same for both layers, the present theory will predict the same bending stiffness as TSA. Even if the hatted quantities in Eq. (45) are different for each layer, the present theory will predict the same bending stiffness as TSA if  $\varphi_1 = \varphi_2$  (i.e., the two layers of the binary composites are of equal thickness).

From Eqs. (44) and (46), we observe for a large N, the differences between the present approach and TSA become negligible which is

expected as TSA is only valid when there are many UCs along the thickness. In real situations, this plate can only be made of a finite number of binary composites. For a finite number N, the error caused by TSA for bending stiffness decreases proportional to  $1/N^2$  which is much faster than the coupling stiffness which decreases proportional to  $1/N$ . For example, let us study the binary composite case that Poisson's ratios of both materials are the same, say 0.3, and the second material is 10 times stiffer than the first material. For purposes of comparison between TSA and VAPAS (or CPT), we plot the effective coupling stiffnesses ( $\bar{d}_{14}$ ) with respect to the number of unit cells along the thickness. As one can observe from Fig. 2 for this particular case, there should be at least six UCs along the thickness for the difference between TSA and VAPAS (or CPT) to be below 10% considering each individual layers for plates made of binary composites.

#### 4.2. Plates made of unidirectional composites

The second example is a plate made of a single layer of unidirectional composites as sketched in Fig. 3 with  $d_1 = h = 10 \mu\text{m}$  studied in Sankar and Marrey (1997). The unidirectional composite has a E-glass fiber ( $E_f = 70 \text{ GPa}$ ,  $\nu_f = 0.2$ ), and an epoxy matrix ( $E_m = 3.5 \text{ GPa}$ ,  $\nu_m = 0.35$ ). The volume fraction of matrix is  $\phi_m = 0.4$ . The fiber direction is along  $x_2$  and the plate is periodically varying along  $x_1$ . The effective plate stiffness predicted by different approaches are listed in Table 1, where SAM, FEM, and TSA results are directly taken from Table 6 of Sankar and Marrey (1997) with SAM denoting the results obtained by a selective averaging method, FEM denoting the results obtained by 3D FEA with periodic displacement and traction boundary conditions imposed on opposite surfaces of the unit cell, and TSA denoting the results obtained by the two-step approach with elastic constants obtained using Halpin–Tsai equations.

Significant differences are observed among the results predicted by different approaches. The best way to tell which set of plate constants is accurate is to use these constants to carry out the corresponding plate analysis and compare the global plate behavior with those predict by a direct 3D finite element analysis of the original plate structure. Suppose a square plate composed of 20 UCs is under a uniform pressure and is simply supported at the four edges. Because of symmetry, only 1/4 of the structures needs to be analyzed; see Fig. 4 for sketches for the geometry and finite ele-

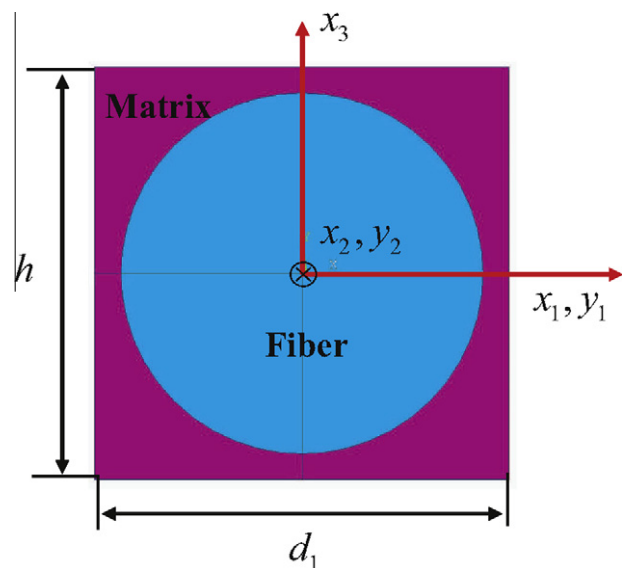


Fig. 3. A unit cell for a unidirectional fiber reinforced composite.

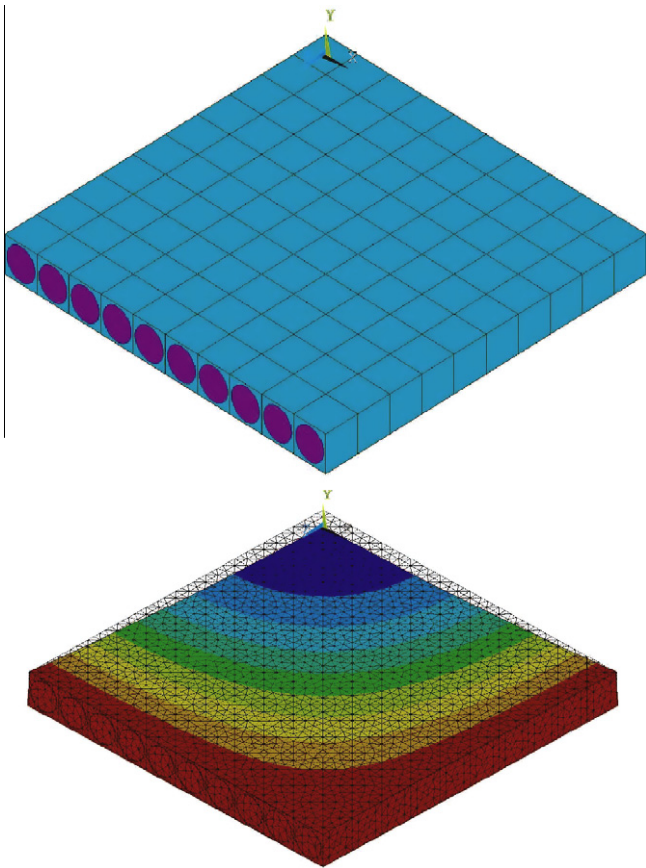


Fig. 4. Direct 3D FEA model of plate made of unidirectional composites.

ment model of this structure. We found out that the max deflection using VAPAS constants is only 0.5% off from the direct 3D FEA analysis, while that using SAM constants is 5% off, and by FEM is 7.0% off, and TSA is 23%. Clearly the plate analysis based on VAPAS can accurately reproduce the original 3D FEA direct analysis.

#### 4.3. A three-layer laminated plate

On the macroscopic level, a *laminated* is a collection of laminae stacked in the same or different fiber directions to achieve the desired stiffness and thickness. Typically, the fundamental building block on the mesoscopic scale is a *lamina* or *layer*, which represents a typical sheet of a composite material. For example, a fiber-reinforced layer commonly consists of many fibers embedded in a matrix material on the microscale level.

This structure is commonly analyzed using TSA. The analyst firsts homogenize a generic layer with specific fiber/matrix configuration to obtain effective 3D material properties using a 2D UC (left) as sketched in Fig. 5 with  $d = 1$  m and  $h = 1$  m. We consider a fiber-reinforced layer made of a transversely isotropic fiber ( $E_L = 58.61$  GPa,  $E_T = 14.49$  GPa,  $G_{LT} = 5.38$  GPa,  $\nu_{LT} = 0.250$ ,  $\nu_{TT} = 0.247$ ) and an isotropic matrix material ( $E = 3.54$  GPa,  $\nu = 0.37$ ). The volume fraction of matrix is  $\phi_m = 0.4$ . The effective 3D material properties were referred to a coordinate system that coincides with the principal material coordinate system. Since composite laminates have several layers, each with different orientation of their material (local) coordinates with respect to the laminate (global) coordinates, we need to transfer the 3D materials properties with different fiber directions (lay-up angles) along the laminate thickness into the global coordinate system. In our problem, a laminate has three layers with different fibers oriented at  $0^\circ$ ,  $45^\circ$  and  $90^\circ$  (top-to-bottom). Then, the analyst carry out a dimensional

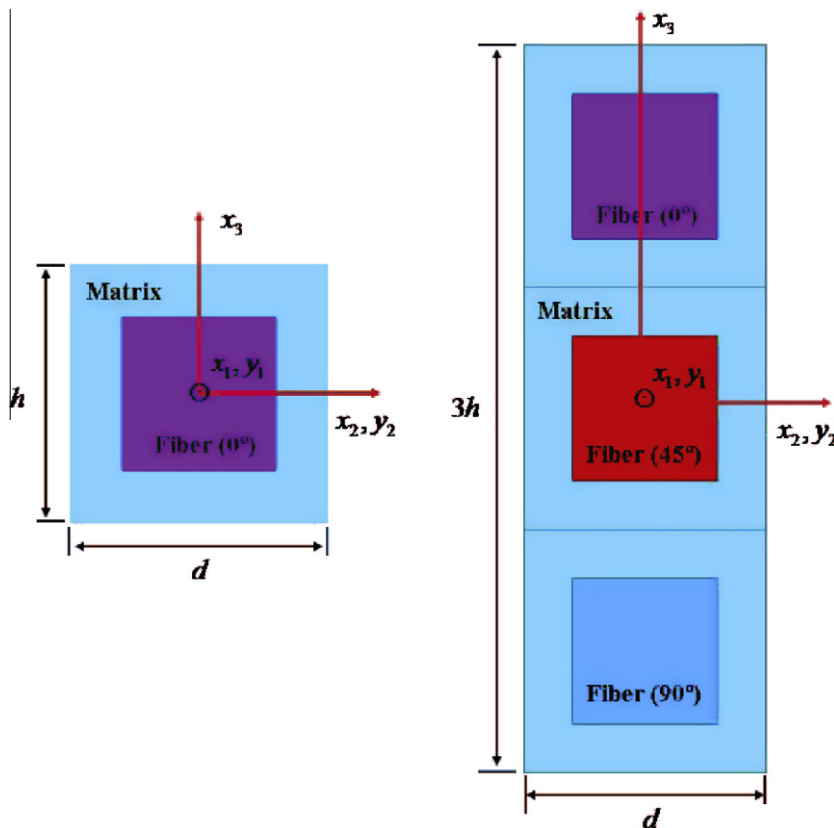


Fig. 5. Unit cells for the two-step and the present approaches.

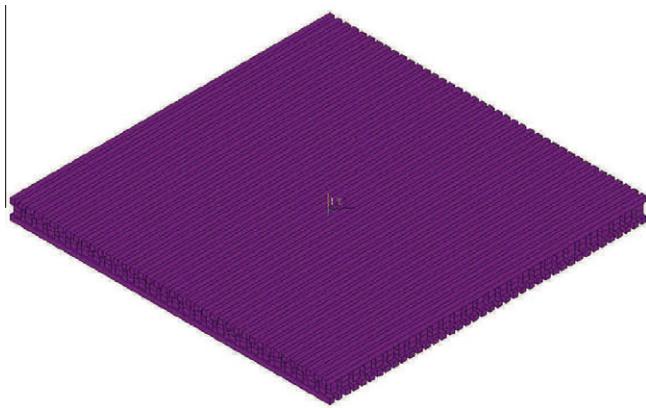


Fig. 6. 3D fiber microstructural configuration with different lay-up angles.

**Table 2**  
Effective extension stiffness of a three-layer composite laminate.

	$\bar{d}_{11}$	$\bar{d}_{12}$	$\bar{d}_{13}$	$\bar{d}_{22}$	$\bar{d}_{23}$	$\bar{d}_{33}$
TSA	4.117	0.438	1.086	1.059	0.438	4.117
VAPAS	4.101	0.069	0.693	0.641	0.046	2.175

**Table 3**  
Effective bending stiffness of a three-layer composite laminate.

	$\bar{d}_{44}$	$\bar{d}_{45}$	$\bar{d}_{46}$	$\bar{d}_{55}$	$\bar{d}_{56}$	$\bar{d}_{66}$
TSA	3.392	0.004	0.510	0.490	0.004	3.392
VAPAS	3.377	0.004	0.433	0.446	0.003	1.585

**Table 4**  
Effective coupling stiffness of a three-layer composite laminate.

	$\bar{d}_{14}$	$\bar{d}_{16}$	$\bar{d}_{34}$	$\bar{d}_{36}$
TSA	1.751	0.0	0.0	-1.751
VAPAS	1.608	0.018	0.020	-0.194

reduction to obtain the effective plate stiffness of the composite laminate based on the transformed 3D effective material properties for each layer. However, as pointed out previously, such a two-step approach (homogenization then dimensional reduction) provides an accurate prediction only if there are many UCs along the thickness. In this three-layer laminated plate, there are three UCs along the thickness and all the UCs are different due to differ-

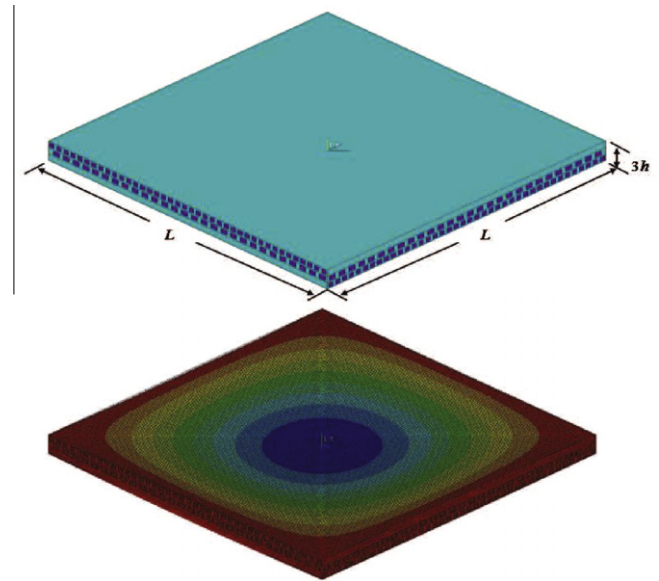


Fig. 7. Direct 3D FEA model of plate made of three-layer with different lay-up angles.

ent layup orientations. We will expect this TSA approach commonly used in analysis of laminated plates will introduce significant errors comparing to a direct 3D FEA of the same structure by meshing details including the microstructural features of the fiber reinforced composites (Fig. 6). Specifically, 10-noded tetrahedral SOLID92 elements are used to mesh the fibers with a total of 120,074 elements and the matrix with a total of 992,695 elements. AESIZE = 0.33 is used to control the element size inside any area or on the face(s) of a volume. To avoid the loss of accuracy of the common two-step approach, we instead can use the present approach to construct an effective plate model using a 2D UC including all the three layers with different layup orientations (see Fig. 5(right)).

The effective plate stiffness predicted by TSA and the present theory implemented in VAPAS are listed in Tables 2–4. Unlike the binary composite case, the present approach and TSA predict significantly different extension, bending, and coupling stiffness. To assess the loss of accuracy of these two modeling approaches, we consider a square plate with  $L = 40$  m under a uniform pressure and simply supported at the four edges; see Fig. 7 for sketches for the geometry and finite element model of this structure. We found out that the max deflection using the present approach is only 0.6% off from the direct 3D FEA analysis, while that using TSA is 14% off

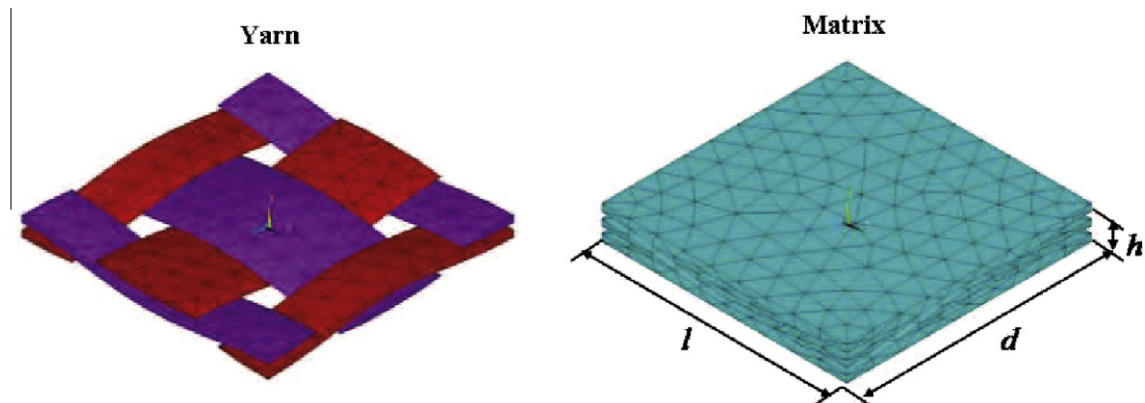


Fig. 8. Unit cell of yarn and matrix for a plain-weave textile composite.

**Table 5**  
Effective plate stiffness of textile composite plate predicted by different methods.

	SAM	FEM	LTCC	VAPAS
$\bar{d}_{11}$	2.667	2.681	2.783	2.171
$\bar{d}_{13}$	0.446	0.565	0.503	0.627
$\bar{d}_{22}$	0.379	0.489	0.490	0.500
$\bar{d}_{33}$	2.667	2.681	2.783	2.201
$\bar{d}_{44}$	6.017	5.687	12.054	5.131
$\bar{d}_{46}$	1.590	1.518	2.177	1.679
$\bar{d}_{55}$	1.360	1.577	2.124	1.478
$\bar{d}_{66}$	6.017	5.687	12.054	5.223

because of unrealistic underlying assumption of periodicity (needed for homogenization) along the thickness coordinate in the TSA approach. This example demonstrates that the plate model constructed using the present approach can accurately reproduce the original 3D FEA direct analysis. To the best knowledge of the authors, such loss of accuracy using the common two-step approach in analyzing composite laminates has not been disclosed in the literature to date.

4.4. Plates made of plain-weave textile composites

The fourth example is a plate made of plain-weave textile composites. The plate along with the details of the unit cell made of a

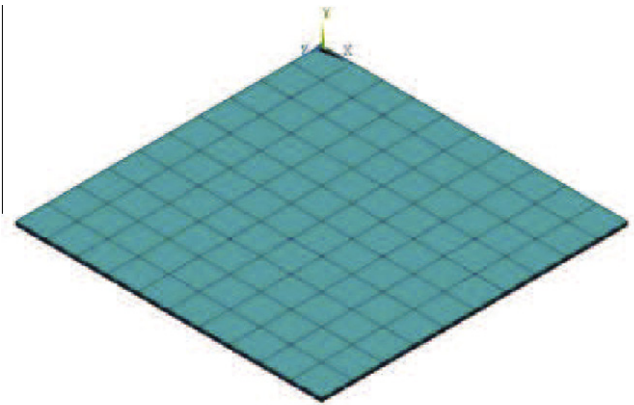


Fig. 9. Direct 3D FEA model of plate made of plain-weave composites.

glass/expoxy yarn (left) and epoxy matrix (right) is sketched in Fig. 8 with  $d = l = 1.680$  mm and  $h = 0.228$  mm studied in Sankar and Marrey (1997). For the textile composite example the yarn was assumed to be transversely isotropic ( $E_L = 58.61$  GPa,  $E_T = 14.49$  GPa,  $G_{LT} = 5.38$  GPa,  $\nu_{LT} = 0.250$ ,  $\nu_{TT} = 0.247$ ) and the matrix material is isotropic ( $E = 3.54$  GPa,  $\nu = 0.37$ ). The volume fraction of yarn is  $\phi_Y = 0.26$ . The effective plate stiffness predicted by different approaches are listed in Table 5 with LTCC denoting the

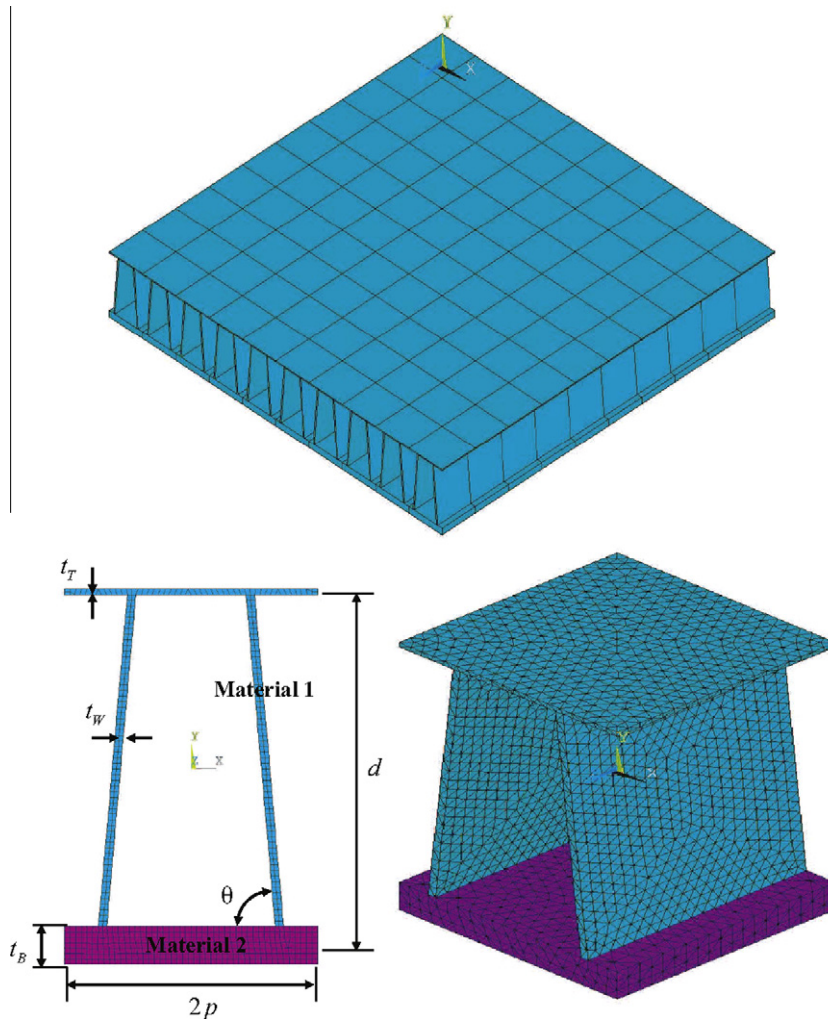


Fig. 10. Sketch of the ITPS panel and its unit cell.

results obtained by the lamination theory using continuum elastic constants (Sankar and Marrey, 1997).

It is clear that there are significant differences among the results predicted by different approaches. Again to assess the loss of accuracy of different approaches, we carry out a direct 3D finite element analysis of the plate structure by meshing all the details of the yarn and matrix. Let us consider a square plate composed of 10 UCs with simply supported and symmetric boundaries and a uniform pressure is applied on the top surface; see Fig. 9 for sketches for the geometry and finite element model of this structure. We found out that the max deflection using VAPAS constants is only 1.3% off from the direct 3D FEA analysis, while that using SAM constants is 3.7% off, and by FEM is 4.0% off, and LTCC is 46%. Clearly, the present approach has a more accurate prediction than other approaches in comparison to the results obtained by the direct 3D FEA.

#### 4.5. Integrated thermal protection system

The last example is to model a corrugated-core sandwich panel, a concept used for Integrated Thermal Protection System (ITPS) studied in Sharma et al. (2010). The ITPS panel along with the details of the unit cell is sketched in Fig. 10. The geometry parameters are  $t_T = 1.2$  mm,  $t_B = 7.49$  mm,  $t_W = 1.63$  mm,  $p = 25$  mm,  $d = 70$  mm, and  $\theta = 85^\circ$ . Both materials are isotropic with  $E_1 = 109.36$  GPa,  $\nu_1 = 0.3$ ,  $E_2 = 209.482$  GPa,  $\nu_2 = 0.063$ . Although a 3D UC is needed for the study in Sharma et al. (2010), only a 2D UC is necessary for VAPAS as it is uniform along one of the in-plane directions. The results obtained in Sharma et al. (2010) are compared with VAPAS in Tables 6–8. VAPAS predictions agree very well with those in Sharma et al. (2010) with the biggest difference (around 1%) appearing for the extension-bending coupling stiffness ( $\bar{d}_{14}$ ). However, the present approach is much more efficient because using the approach in Sharma et al. (2010) one needs to carry out six analyses of a 3D unit cells under six different sets of boundary conditions and load conditions and postprocess the 3D stresses to compute the plate stress resultants, while using the present approach, one only needs to carry out one analysis of a 2D UC without any postprocessing.

We also analyzed a simply supported square panel under uniform pressure with the ITPS microstructure. We find out that with 20 UCs along the width, the max deflection predicted by the plate analysis using the effective plate stiffness is about 55% off the direct 3D FEA analysis. The difference will decrease with increased number of UCs; for example if the plate is composed of 30 UCs,

the difference is 48% and if the plate is composed of 40 UCs, the difference is 42%. The fact that big differences exist even if the plate is very thin (the aspect ratio of the 40 UC plate is around 7:200) is because transverse shear deformation of this type of structure, which is neglected in CPT, is significant. A refined plate theory, such as the Reissner–Mindlin model, which is capable of capturing the shear deformation should be used. Development of such a model is beyond the scope of the present paper and will be presented in a different paper.

#### 5. Conclusions

The variational asymptotic method is used to construct a new model for composite plates with in-plane heterogeneity. This model serves as a rigorous link between the original 3D problem of plate structures made of materials with complex microstructures and the simple classical plate theory. This model not only computes the effective plate stiffness needed for the classical plate theory but also can recover the local displacement, strain, and stress fields based on the global behavior obtained from the plate analysis. The resulting plate model is also suitable for geometrical nonlinear analysis as only small strain assumption is used for obtaining the kinematics. This new model is implemented in the computer code VAPAS using the finite element technique. VAPAS can be used as an alternative of the 3D FEA for efficient yet accurate analysis of composite plates with or without in-plane heterogeneity. The validity and capability of this new model are demonstrated using a few examples.

#### Acknowledgements

The present work is supported, in part, by the Air Force Office of Scientific Research under Grant FA9550-08-1-0405 (the program manager is Dr. David Stargel) and AFRL/RB Summer Faculty Research Program. The views and conclusions contained herein are those of the authors and should not be interpreted as necessarily representing the official policies or endorsement, either expressed or implied, of the funding agency. Technical discussions with Drs. Maxwell Blair, William G. Baron, and Michael A. Falugi of Air Vehicle Direction of Air Force Research Laboratory at Wright-Patterson AFB are greatly appreciated.

#### References

- Aboudi, J., 1982. A continuum theory for fiber-reinforced elastic-viscoplastic composites. *International Journal of Engineering Science* 20 (5), 605–621.
- Aboudi, J., 1989. Micromechanical analysis of composites by the method of cells. *Applied Mechanics Reviews* 42 (7), 193–221.
- Accorsi, M.L., Nemat-Nasser, S., 1986. Bounds on the overall elastic and instantaneous elastoplastic moduli of periodic composites. *Mechanics of Materials* 5 (3), 209–220.
- Atilgan, A., Hodges, D., 1992. On the strain energy of laminated composite plates. *International Journal of Solids and Structures* 29, 2527–2543.
- Banerjee, B., Adams, D., 2004. On predicting the effective elastic properties of polymer bonded explosive using the recursive cell method. *International Journal of Solids and Structures* 41 (2), 481–509.
- Bensoussan, A., Lions, J., Papanicolaou, G., 1978. *Asymptotic Analysis for Periodic Structures*. North-Holland, Amsterdam.
- Berdichevsky, V., 1979. Variational-asymptotic method of constructing a theory of shells. *PMM* 43 (4), 664–687.
- Buannic, N., Cartraud, P., 2001. Higher-order effective modeling of periodic heterogeneous beams. I. Asymptotic expansion method. *International Journal of Solids and Structures* 38, 7139–7161.
- Caillerie, D., 1984. Thin elastic and periodic plates. *Mathematical Methods in the Applied Sciences* 6, 159–191.
- Danielson, D., Hodges, D., 1987. Nonlinear beam kinematics by decomposition of the rotation tensor. *Journal of Applied Mechanics* 54, 258–262.
- Dvorak, G., Bahei-El-Din, Y., 1979. Elastic-plastic behavior of fibrous composites. *Journal of Mechanics and Physics of Solids* 27, 51–72.
- Hashin, Z., 1983. Analysis of composite materials – a survey. *Applied Mechanics Review* 50, 481–505.

**Table 6**  
Effective extension stiffness of ITPS.

	$\bar{d}_{11}$	$\bar{d}_{13}$	$\bar{d}_{22}$	$\bar{d}_{33}$
Sharma et al. (2010)	2.83	0.18	1.07	2.33
VAPAS	2.80	0.18	1.08	2.33

**Table 7**  
Effective bending stiffness of ITPS.

	$\bar{d}_{44}$	$\bar{d}_{46}$	$\bar{d}_{55}$	$\bar{d}_{66}$
Sharma et al. (2010)	3.06	0.22	1.32	2.85
VAPAS	3.03	0.22	1.32	2.87

**Table 8**  
Effective coupling stiffness of ITPS.

	$\bar{d}_{14}$	$\bar{d}_{16}$	$\bar{d}_{25}$	$\bar{d}_{36}$
Sharma et al. (2010)	–71.45	–3.36	–34.05	–71.45
VAPAS	–70.67	–3.31	–34.06	–71.42

- Hashin, Z., Shtrikman, S., 1962. A variational approach to the theory of the elastic behaviour of polycrystals. *Journal of Mechanics and Physics of Solids* 10, 343–352.
- Hill, R., 1963. Elastic properties of reinforced solids: some theoretical principles. *Journal of Mechanics and Physics of Solids* 11, 357–372.
- Hill, R., 1965. Theory of mechanical properties of fibre-strengthened materials-III. Self-consistent model. *Journal of Mechanics and Physics of Solids* 13, 189–198.
- Hodges, D., Atilgan, A., Danielson, D., 1993. A geometrically nonlinear theory of elastic plates. *Journal of Applied Mechanics* 60 (1), 109–116.
- Hollister, S.J., Kikuchi, N., 1992. A comparison of homogenization and standard mechanics analyses for periodic porous composites. *Computational Mechanics*. Kalamkarov, A., 1992. *Composite and Reinforced Elements of Construction*. Wiley Chichester.
- Kalamkarov, A., Kolpakov, A., 1997. *Analysis, Design and Optimization of Composite Structures*. Wiley Chichester.
- Kalamkarov, A.L., Andrianov, I.V., Danishevs'kyy, V.V., 2009. Asymptotic homogenization of composite materials and structures. *Applied Mechanics Reviews* 62, 030802.
- Kanouté, P., Boso, D., Chaboche, J.L., Schrefler, B., 2009. Multiscale methods for composites: a review. *Archives of Computational Methods in Engineering* 16, 31–75.
- Kohn, R., Vogelius, M., 1984. A new model for thin plates with rapidly varying thickness. *International Journal of Solids and Structures* 20 (4), 333–350.
- Lewiński, T., 1991. Effective models of composite periodic plates – Part I. Asymptotic solution. *International Journal of Solids and Structures* 27 (8), 1155–1172.
- Milton, G., 2001. *Theory of Composites*. Cambridge University Press.
- Murakami, H., Toledano, A., 1990. A higher-order mixture homogenization of bilaminated composites. *Journal of Applied Mechanics* 57, 388–396.
- Nemat-Nasser, S., Hori, M., 1993. *Micromechanics: Overall Properties of Heterogeneous Materials*. North-Holland, Amsterdam.
- Paley, M., Aboudi, J., 1992. Micromechanical analysis of composites by the generalized cells model. *Mechanics of Materials* 14, 127–139.
- Sanchez-Palencia, E., 1980. *Non-homogeneous Media and Vibration Theory*. Springer, Berlin.
- Sankar, B.V., Marrey, R.V., 1997. Analytical method for micromechanics of textile composites. *Composites Science and Technology* 57, 703–713.
- Sharma, A., Sankar, B.V., Haftka, R.T., 2010. Homogenization of plates with microstructure and application to corrugated core sandwich panels. In: *Proceedings of the 51st AIAA/ASME/ASCE/AHS/ASC Structures, Structural Dynamics, and Materials Conference*. AIAA, Orlando, Florida.
- Sun, C., Vaidya, R., 1996. Prediction of composite properties from a representative volume element. *Composites Science and Technology* 56, 171–179.
- Sutyurin, V., 1997. Derivation of plate theory accounting asymptotically correct shear deformation. *Journal of Applied Mechanics* 64, 905–915.
- Williams, T., 2005. A two-dimensional, higher-order, elasticity-based micromechanics model. *International Journal of Solids and Structures* 42, 1009–1038.
- Yu, W., 2002. Variational asymptotic modeling of composite dimensionally reducible structures. Ph.D. thesis, Aerospace Engineering, Georgia Institute of Technology.
- Yu, W., 2005. A variational-asymptotic cell method for periodically heterogeneous materials. In: *Proceedings of the 2005 ASME International Mechanical Engineering Congress and Exposition*. ASME, Orlando, Florida.
- Yu, W., Hodges, D., Volovoi, V., 2002. Asymptotic construction of reissner-like models for composite plates with accurate strain recovery. *International Journal of Solids and Structures* 39 (17), 5185–5203.
- Yu, W., Tang, T., 2007. Variational asymptotic method for unit cell homogenization of periodically heterogeneous materials. *International Journal of Solids and Structures* 44, 3738–3755.

# Finite Element Formulation for Dynamics of Moving Plates

Krishnan Chathadi\* and Dewey H. Hodges†

*Georgia Institute of Technology, Atlanta, Georgia 30332-0150*

## 1 Introduction

Plates are flat structures with one dimension much smaller than the other two and are widely used in modeling structures like aircraft wings. A fully intrinsic formulation, i.e. devoid of displacement and rotation variables, for the dynamics of a moving composite plate has been presented by Hodges *et al.* (2009). A variable-order finite element technique is presented and applied to beams by Patil and Hodges (2011). In this paper, the idea from the finite element paper is used to develop a solution methodology for the dynamics of moving plate.

## 2 Nonlinear, Intrinsic Beam Equations

The nonlinear, fully intrinsic governing equations for the dynamics of a moving plate are given as

$$\begin{aligned}
 N_{11,1} + (N_{12} + \mathfrak{N}), 2 - K_{13}(N_{12} - \mathfrak{N}) - K_{23}N_{22} + Q_1K_{11} + Q_2K_{21} + f_1 &= \dot{P}_1 + \Omega_1P_3 - \Omega_3P_2 \\
 N_{22,1} + (N_{12} + \mathfrak{N}), 1 - K_{23}(N_{12} - \mathfrak{N}) - K_{13}N_{11} + Q_1K_{12} + Q_2K_{22} + f_2 &= \dot{P}_2 + \Omega_3P_1 - \Omega_2P_3 \\
 Q_{1,1} + Q_{2,2} - K_{11}N_{11} - K_{22}N_{22} - (K_{12} + K_{21})N_{12} + (K_{12} - K_{21})\mathfrak{N} + f_3 &= \dot{P}_3 + \Omega_2P_2 - \Omega_1P_1 \\
 M_{11,1} + M_{12,2} - Q_1(1 + \epsilon_{11}) - Q_2\epsilon_{12} + 2\gamma_{13}N_{11} + 2\gamma_{23}(N_{12} + \mathfrak{N}) - M_{12}K_{13} - M_{22}K_{23} + m_1 &= \dot{H}_1 - \Omega_3H_2 - V_1P_3 - V_3P_1 \\
 M_{12,1} + M_{22,2} - Q_1\epsilon_{12} - Q_2(1 + \epsilon_{22}) + 2\gamma_{13}(N_{12} - \mathfrak{N}) + 2\gamma_{23}N_{22} + M_{11}K_{13} + M_{12}K_{23} + m_2 &= \dot{H}_2 + \Omega_3H_1 - V_2P_3 - V_3P_2
 \end{aligned} \tag{1}$$

where

$$\begin{aligned}
 (2 + \epsilon_{11} + \epsilon_{22})N &= (N_{22} - N_{11})\epsilon_{12} + N_{12}(\epsilon_{11} - \epsilon_{22}) + M_{22}K_{21} - M_{11}K_{12} \\
 &\quad + M_{12}(K_{11} - K_{22}) - \Omega_1H_2 + \Omega_2H_1 - V_1P_2 + V_2P_1
 \end{aligned} \tag{2}$$

$(\cdot)_{,\alpha}$  denotes the partial derivative with respect to the two coordinates, which describe the reference plane of the plate according to 2D plate theory. (Here and throughout the paper Latin indices assume 1,2,3; and Greek indices assume values 1,2).  $(\dot{\cdot})$  denotes the partial derivative with respect to time.  $V_i$  and  $\Omega_i$  are the velocity and angular velocity measures.  $\epsilon_{\alpha\beta}$  are the in-plane generalized strains,  $\gamma_{\alpha 3}$  are the transverse shear generalized strains, and  $K_{\alpha j}$  are the curvatures of the deformed surface.  $N_{\alpha\beta}$  are generalized in-plane forces,  $Q_\alpha$  are generalized shear forces,  $M_{\alpha\beta}$  are generalized moments,  $P_\alpha$  and  $H_\alpha$  are the linear and angular momenta respectively.  $f_i$  and  $m_\alpha$  are the external forces and moments.  $\mathfrak{N}$  is a Lagrange multiplier to enforce symmetry of in-plane generalized strains.

While solving the above equation, the constitutive equations may be used to replace some of the variables in terms of others. The stress resultants are written in terms of the strains measures and the generalized momenta in terms of the six generalized velocities (i.e. the three velocities and three angular velocities). Thus,

---

\*Graduate Research Assistant, Daniel Guggenheim School of Aerospace Engineering

†Professor, Daniel Guggenheim School of Aerospace Engineering.

we can write the complete formulation in terms of only 18 unknowns (11 generalized strains, three velocities, three angular velocities and  $\mathfrak{N}$ ), which would be solved using 18 equations. Such a set of equations are formed using six of the generalized strainvelocity equations complemented by the six compatibility equations, the five equations of motion and the constraint equation involving  $\mathfrak{N}$ .

As the first step, the plate is assumed to be homogeneous and isotropic, thus eliminating  $K_{\alpha 3}$ ,  $\mathfrak{N}$ ,  $\phi$  and  $\Omega_3$ . This would result in the linear dynamic equations.

## 2.1 Linear dynamic equations

The linear dynamic equations model is derived by removing terms involving  $K_{\alpha 3}$ ,  $\mathfrak{N}$ ,  $\phi$  and  $\Omega_3$  from equations [1 – 5]. There are five equations of motion which are

$$\begin{aligned}
N_{11,1} + N_{12,2} + f_1 &= \mu \dot{V}_1 \\
N_{12,1} + N_{22,2} + f_2 &= \mu \dot{V}_2 \\
Q_{1,1} + Q_{2,2} + f_3 &= \mu \dot{V}_3 \\
M_{11,1} + M_{12,2} + m_1 &= \mu r^2 \dot{\omega}_1 \\
M_{12,1} + M_{22,2} + m_2 &= \mu r^2 \dot{\omega}_2
\end{aligned} \tag{3}$$

Further, we have the strain-velocity relations

$$\begin{aligned}
\epsilon_{11} - V_{1,1} &= 0 & \epsilon_{12} - V_{2,1} + \Omega_3 &= 0 \\
\epsilon_{22} - V_{2,2} &= 0 & \epsilon_{21} - V_{1,2} - \Omega_3 &= 0 \\
\gamma_{13} - V_{3,1} - \Omega_1 &= 0 & \gamma_{23} - V_{3,2} - \Omega_2 &= 0 \\
\Omega_{2,1} - \dot{K}_{12} &= 0 & \Omega_{2,2} - \dot{K}_{22} &= 0 \\
\Omega_{1,1} - \dot{K}_{11} &= 0 & \Omega_{1,1} - \dot{K}_{21} &= 0 \\
\Omega_{3,1} - \dot{K}_{13} &= 0 & \Omega_{3,2} - \dot{K}_{23} &= 0 \\
\dot{K}_{12} + \dot{K}_{21} &= \Omega_{2,1} + \Omega_{1,2}
\end{aligned} \tag{4}$$

The linear and angular momenta are expressed in terms of velocities and angular velocities as

$$\begin{Bmatrix} P \\ H \end{Bmatrix} = \begin{bmatrix} \mu \Delta & -\mu \tilde{\xi} \\ \mu \tilde{\xi} & I \end{bmatrix} \begin{Bmatrix} V \\ \Omega \end{Bmatrix} \tag{5}$$

$\mu, \tilde{\xi}, I$  are, respectively, the mass per unit length, mass center offset (a vector in the cross-section from the beam reference axis to the cross-sectional mass center), and the cross-sectional inertia matrix consisting of mass moments of inertia per unit length on the diagonals.

The sectional constitutive law relates the generalized forces (in-plane, shear and moments) are related to generalized strains using the cross-sectional stiffnesses or flexibilities.

$$\begin{Bmatrix} N \\ M \\ Q \end{Bmatrix} = \begin{bmatrix} R & S & 0 \\ S^T & T & 0 \\ 0 & 0 & U \end{bmatrix} \begin{Bmatrix} \epsilon \\ \kappa \\ 2\gamma \end{Bmatrix} \tag{6}$$

$R, S, T$  and  $U$  are the stiffness parameters governed by the material properties and the geometry of the section.

Usually, the constitutive laws are used to replace some variables in terms of others. Here it was decided to express the generalized strains in terms of the cross-section stress resultants, allowing easy specification of zero flexibility, and the generalized momenta in terms of generalized velocities, allowing easy specification of zero inertia. Thus, the primary variables of interest are  $N_{\alpha\beta}$ ,  $M_{\alpha\beta}$ ,  $Q_\alpha$ ,  $V_i$  and  $\Omega_\alpha$ .

Finally the boundary conditions need to be specified. For the rectangular plate, there will be five boundary conditions along each edge. For the sake of simplicity, the plate is considered to be clamped along one of the edges ( $x_1=0$  edge in this case) and free along the other three edges. Thus, the assumed boundary conditions are

$$\begin{aligned}
x_1 = 0 : \quad & V_i = 0, & \Omega_\alpha = 0 \\
x_1 = a : \quad & N_{1\alpha} = 0, & M_{1\alpha} = 0, & Q_1 = 0 \\
x_2 = 0 : \quad & N_{\alpha 2} = 0, & M_{\alpha 2} = 0, & Q_1 = 0 \\
x_2 = b : \quad & N_{\alpha 2} = 0, & M_{\alpha 2} = 0, & Q_2 = 0
\end{aligned} \tag{7}$$

### 3 Finite Element Formulation

The finite element formulation is based on discretizing the plate into  $m$  elements along  $x_1$  direction and into  $n$  elements  $x_2$  direction respectively so that there is a totally of  $m \times n$  elements. For any element ( $i^{\text{th}}$  element along  $x_1$  and  $j^{\text{th}}$  element along  $x_2$ , denoted by  $ij$ ), the solution is given by  $V_k^{ij}$ ,  $\Omega_\alpha^{ij}$ ,  $N_{\alpha\beta}^{ij}$ ,  $M_{\alpha\beta}^{ij}$ ,  $Q_\alpha^{ij}$ . In addition to satisfying the equations of motion, the kinematic equations and the boundary conditions given above, the solution must also satisfy the continuity equations between adjacent elements along all its edges. Thus,

$$\begin{aligned}
V_1^i(L_i, x_2, t) &= V_1^{i+1}(0, x_2, t) & N_{11}^i(L_i, x_2, t) &= N_{11}^{i+1}(0, x_2, t) \\
V_2^i(L_i, x_2, t) &= V_2^{i+1}(0, x_2, t) & N_{12}^i(L_i, x_2, t) &= N_{12}^{i+1}(0, x_2, t) \\
V_3^i(L_i, x_2, t) &= V_3^{i+1}(0, x_2, t) & M_{11}^i(L_i, x_2, t) &= M_{11}^{i+1}(0, x_2, t) \\
\Omega_1^i(L_i, x_2, t) &= \Omega_1^{i+1}(0, x_2, t) & M_{12}^i(L_i, x_2, t) &= M_{12}^{i+1}(0, x_2, t) \\
\Omega_2^i(L_i, x_2, t) &= \Omega_2^{i+1}(0, x_2, t) & Q_1^i(L_i, x_2, t) &= Q_1^{i+1}(0, x_2, t)
\end{aligned} \tag{8}$$

$$\begin{aligned}
V_1^j(x_1, L_j, t) &= V_1^{j+1}(x_1, 0, t) & N_{12}^j(x_1, L_j, t) &= N_{12}^{j+1}(x_1, 0, t) \\
V_2^j(x_1, L_j, t) &= V_2^{j+1}(x_1, 0, t) & N_{22}^j(x_1, L_j, t) &= N_{22}^{j+1}(x_1, 0, t) \\
V_3^j(x_1, L_j, t) &= V_3^{j+1}(x_1, 0, t) & M_{12}^j(x_1, L_j, t) &= M_{12}^{j+1}(x_1, 0, t) \\
\Omega_1^j(x_1, L_j, t) &= \Omega_1^{j+1}(x_1, 0, t) & M_{22}^j(x_1, L_j, t) &= M_{22}^{j+1}(x_1, 0, t) \\
\Omega_2^j(x_1, L_j, t) &= \Omega_2^{j+1}(x_1, 0, t) & Q_2^j(x_1, L_j, t) &= Q_2^{j+1}(x_1, 0, t)
\end{aligned} \tag{9}$$

The weighting functions are then introduced into the equations of motion, kinematic equations and the boundary conditions in a way similar to Patil and Hodges (2011):

$$\begin{aligned}
& \int \int [\delta V_1(N_{11,1} + N_{12,2} + f_1 - \mu \dot{V}_1) + \delta V_2(N_{12,1} + N_{22,2} + f_2 - \mu \dot{V}_2) + \delta V_3(Q_{1,1} + Q_{2,2} + f_3 - \mu \dot{V}_3) \\
& + \delta \Omega_1(M_{11,1} + M_{12,2} - Q_1 + m_1 - \mu r^2 \dot{\Omega}_1) + \delta \Omega_2(M_{12,1} + M_{22,2} - Q_2 + m_2 - \mu r^2 \dot{\Omega}_2) + \delta N_{11}(\dot{\epsilon}_{11} - V_{1,1}) \\
& + \delta N_{22}(\dot{\epsilon}_{22} - V_{2,2}) + \delta N_{12}(\dot{\epsilon}_{12} - V_{1,2} - V_{2,1}) + \delta M_{11}(\dot{K}_{11} - \Omega_{1,1}) + \delta M_{22}(\dot{K}_{22} - \Omega_{2,2}) \\
& + \delta M_{12}(\dot{K}_{12} - \Omega_{1,2} - \Omega_{2,1}) + \delta Q_1(2\dot{\gamma}_{13} - V_{3,1} - \Omega_1) + \delta Q_2(2\dot{\gamma}_{23} - V_{3,2} - \Omega_2)] dx_2 dx_1
\end{aligned} \tag{10}$$

Finally, each of the 13 variables in the equations is expanded in terms of a trial function. The values of the variables are assumed to be a function of the nodal values. Let there be  $m \times n$  elements ( $i = 1, 2, \dots$ ,

$m; j = 1, 2, \dots, n$ ) and  $p$  nodes ( $k = 1, 2, \dots, p$ ) within each element and  $\mathfrak{F}$  be a shape function. The variables now take the form

$$\begin{aligned}
V_1^i(x^i, x^j, t) &= \mathfrak{F}^k(x^i, x^j)v_1^{k,i}(t) & V_2^i(x^i, x^j, t) &= \mathfrak{F}^k(x^i, x^j)v_2^{k,i}(t) & V_3^i(x^i, x^j, t) &= \mathfrak{F}^k(x^i, x^j)v_3^{k,i}(t) \\
\Omega_1^i(x^i, x^j, t) &= \mathfrak{F}^k(x^i, x^j)\omega_1^{k,i}(t) & \Omega_2^i(x^i, x^j, t) &= \mathfrak{F}^k(x^i, x^j)\omega_2^{k,i}(t) \\
N_{11}^i(x^i, x^j, t) &= \mathfrak{F}^k(x^i, x^j)n_{11}^{k,i}(t) & N_{12}^i(x^i, x^j, t) &= \mathfrak{F}^k(x^i, x^j)n_{12}^{k,i}(t) & N_{22}^i(x^i, x^j, t) &= \mathfrak{F}^k(x^i, x^j)n_{22}^{k,i}(t) \\
M_{11}^i(x^i, x^j, t) &= \mathfrak{F}^k(x^i, x^j)m_{11}^{k,i}(t) & M_{12}^i(x^i, x^j, t) &= \mathfrak{F}^k(x^i, x^j)m_{12}^{k,i}(t) & M_{22}^i(x^i, x^j, t) &= \mathfrak{F}^k(x^i, x^j)m_{22}^{k,i}(t) \\
Q_1^i(x^i, x^j, t) &= \mathfrak{F}^k(x^i, x^j)q_1^{k,i}(t) & Q_2^i(x^i, x^j, t) &= \mathfrak{F}^k(x^i, x^j)q_2^{k,i}(t)
\end{aligned} \tag{11}$$

Thus, the problem reduces to a set of linear algebraic equations of the form

$$\begin{aligned}
[A]_{kji} \{ X \}_{ji} &= [B]_{kji} \{ \dot{X} \}_{ji} \tag{12} \\
[A] &= \begin{bmatrix} \frac{\partial}{\partial x_1} & 0 & \frac{\partial}{\partial x_2} & 0 & 0 & 0 & 0 & 0 & 0 & 0 & 0 & 0 & 0 & 0 \\ 0 & \frac{\partial}{\partial x_2} & \frac{\partial}{\partial x_1} & 0 & 0 & 0 & 0 & 0 & 0 & 0 & 0 & 0 & 0 & 0 \\ 0 & 0 & 0 & 0 & 0 & 0 & \frac{\partial}{\partial x_1} & \frac{\partial}{\partial x_2} & 0 & 0 & 0 & 0 & 0 & 0 \\ 0 & 0 & 0 & \frac{\partial}{\partial x_1} & 0 & \frac{\partial}{\partial x_2} & -1 & 0 & 0 & 0 & 0 & 0 & 0 & 0 \\ 0 & 0 & 0 & 0 & \frac{\partial}{\partial x_2} & \frac{\partial}{\partial x_1} & 0 & -1 & 0 & 0 & 0 & 0 & 0 & 0 \\ 0 & 0 & 0 & 0 & 0 & 0 & 0 & 0 & \frac{\partial}{\partial x_1} & 0 & 0 & 0 & 0 & 0 \\ 0 & 0 & 0 & 0 & 0 & 0 & 0 & 0 & 0 & \frac{\partial}{\partial x_2} & 0 & 0 & 0 & 0 \\ 0 & 0 & 0 & 0 & 0 & 0 & 0 & 0 & \frac{\partial}{\partial x_2} & \frac{\partial}{\partial x_1} & 0 & 0 & 0 & 0 \\ 0 & 0 & 0 & 0 & 0 & 0 & 0 & 0 & 0 & 0 & 0 & \frac{\partial}{\partial x_1} & 0 & 0 \\ 0 & 0 & 0 & 0 & 0 & 0 & 0 & 0 & 0 & 0 & 0 & 0 & \frac{\partial}{\partial x_2} & \frac{\partial}{\partial x_1} \\ 0 & 0 & 0 & 0 & 0 & 0 & 0 & 0 & 0 & 0 & 0 & \frac{\partial}{\partial x_1} & 1 & 0 \\ 0 & 0 & 0 & 0 & 0 & 0 & 0 & 0 & 0 & 0 & \frac{\partial}{\partial x_2} & 0 & 0 & 1 \end{bmatrix} \\
[B] &= \begin{bmatrix} \mu & 0 & 0 & 0 & 0 & 0 & 0 & 0 & 0 \\ 0 & \mu & 0 & 0 & 0 & 0 & 0 & 0 & 0 \\ 0 & 0 & \mu & 0 & 0 & 0 & 0 & 0 & 0 \\ 0 & 0 & 0 & \mu r^2 & 0 & 0 & 0 & 0 & 0 \\ 0 & 0 & 0 & 0 & \mu r^2 & 0 & 0 & 0 & 0 \\ 0 & 0 & 0 & 0 & 0 & R & S & 0 & 0 \\ 0 & 0 & 0 & 0 & 0 & S^T & T & 0 & 0 \\ 0 & 0 & 0 & 0 & 0 & 0 & 0 & U & 0 \end{bmatrix}
\end{aligned}$$

$$\{ X \} = \{ V_1 \ V_2 \ V_3 \ \Omega_1 \ \Omega_2 \ N_{11} \ N_{22} \ N_{12} \ M_{11} \ M_{22} \ M_{12} \ Q_1 \ Q_2 \}^T \tag{13}$$

$[A]$ ,  $[B]$  and  $\{X\}$  are applied to every element ranging from  $i=1,2,\dots,m$  and  $j=1,2,\dots,n$ .

## 4 Results

The equations were solved using the variable-order FEM for a simple cantilevered plate, fixed along the  $x_2 = 0$  edge with the other edges free.

Table 1: Plate Properties

Dimensions	$1 \times 1 \times 0.01$ m
Young's Modulus	70 GPa
Material density	$2700 \text{ kg/m}^3$
Poisson's ratio	0.3

The equations help us to study the bending, stretching and twisting frequencies of a plate. The properties of the plate are given in Table 1, and the results in Table 2. The results for the bending frequencies are compared with those from ABAQUS.

Table 2: Plate Structural Frequencies

Mode	ABAQUS	$1 \times 1$ elements	$2 \times 2$ elements	$3 \times 3$ elements
Bending	8.5209	14.087	13.6618	13.6375
Twisting	–	695.6117	664.4739	613.1459
Stretching	–	5091.7507	5525.2714	5663.2779

Because of the differences in the results, work is being carried out in identifying the reasons and also checking out the alternate Galerkin approach.

## 5 Conclusions

A finite element solution technique, based on a geometrically-exact, fully intrinsic equations is presented and applied to an homogeneous, isotropic cantilevered plate. Right now, the reasons for the deviation of the results compared to the exact solution are being investigated. Future work would involve including the non-linearities and aeroelastic effects and extending the equations to study the dynamics of a flapping wing.

## References

- Hodges, D. H., Yu, W. and Patil, M. J. (2009). Geometrically-exact, intrinsic theory for dynamics of moving composite plates and shells. *International Journal of Solids and Structures* 46, 2036 – 2042.
- Patil, M. J. and Hodges, D. H. (2011). Variable-order finite elements for nonlinear, intrinsic, mixed beam equations. *Journal of Mechanics of Materials and Structures* To appear.